Domain formation and switching kinetics in thin ferroelectric films conditioned by flexoelectricity, surface screening and chemical strains

Domänenbildung und Umschaltungskinetik in ferroelektrischen Dünnschichten unter Einfluss von Flexoelektrizität, chemischen Dehnungen und Oberflächenladungen

Zur Erlangung des Grades eines Doktors der Naturwissenschaften (Dr. rer. nat.) genehmigte Dissertation von M. Sc. Ivan Vorotiahin aus Kiew

Tag der Einreichung: 31.10.2018

Tag der Prüfung: 18.01.2019

Darmstadt — D 17

1. Gutachter: apl. Prof. Dr. Yuri Genenko
2. Gutachter: Prof. Dr. Bai-Xiang Xu
3. Prüfer: Prof. Dr. Wolfgang Donner
4. Prüfer: Prof. Dr. Ralf Müller

TECHNISCHE UNIVERSITÄT DARMSTADT

Fachbereich Material- und Geowissenschaften
Fachgebiet Materialmodellierung

Domain formation and switching kinetics of polarization domains in thin ferroelectric films conditioned by flexoelectricity, surface screening and chemical strains
Domänenbildung und Umschaltungskinetik in ferroelektrischen Dünnschichten unter Einfluss von Flexoelektrizität, chemischen Dehnungen und Oberflächenladungen

Genehmigte Dissertation von M. Sc. Ivan Vorotiahin aus Kiew

1. Gutachter: apl. Prof. Dr. Yuri Genenko
2. Gutachter: Prof. Dr. Bai-Xiang Xu
3. Prüfer: Prof. Dr. Wolfgang Donner
4. Prüfer: Prof. Dr. Ralf Müller

Tag der Einreichung: 31.10.2018

Tag der Prüfung: 18.01.2019

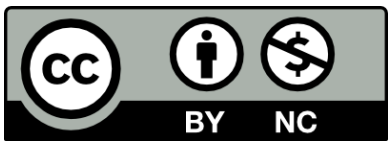

Erklärung zur Dissertation

Hiermit versichere ich, die vorliegende Dissertation ohne Hilfe Dritter und nur mit angegebenen Quellen und Hilfsmitteln angefertigt zu haben. Alle Stellen, die aus Quellen entnommen werden, sind als solche kenntlich gemacht. Diese Arbeit hat in gleicher oder ähnlicher Form noch keiner Prüfungsbehörde vorgelegen.

Darmstadt, den 31.10.2018

Ivan Vorotiahin

Acknowledgements

Working on this project was a challenging, interesting and joyful experience. I would like to thank my supervisors apl. Prof. Dr. Yuri Genenko and, from the Ukrainian side, Dr. Anna Morozovska for their thoroughful and patient guidance through the fields of solid-state physics, profound discussions and moral support.

All the time I worked on the project, the Materialmodellierung group of Prof. Dr. Karsten Albe provided a warm and especially friendly atmosphere. I am honoured to be a part of a dynamic, intellectual and ready for help collective, and my gratitude goes to all colleagues from the group, including the former ones for the wonderful time spent at work and pleasure, intensive discussions and special events. Matters and ideas, productively discussed with Dr. Ruben Khachaturyan, Dr. Kai-Christian Meyer, Dr. Olena Lenchuk, Dr. Ashkan Moradabadi, Arne Klomp, Delwin Perera, Dr. Constanze Kalcher and many others, gave insight, so necessary for a scientist, and helped, at least to certain extent, to shape the work as you see it, for which I am also thankful to them. I gratefully acknowledge the work of Dr. Tobias Brink and Daniel Utt who tirelessly kept the group server up and running. And of course, I wish to thank Prof. Albe for the passionate organization and guidance, and for proofreading this thesis.

I want to specially thank all my co-authors. These people of great competence: Dr. Eugene Eliseev, Prof. Sergei Kalinin, Dr. Qian Li, Prof. Maya Glinchuk, Dr. Maxim Silibin, Dr. Yevhen Fomichov, and Prof. Nicholas Morozovsky, made the tremendous work with their knowledge and skill, and provided useful help when it was desperately needed.

Finally, I wish to respectfully thank the Evaluators and the Examiners of this work, Prof. Dr. Bai-Xiang Xu, Prof. Dr. Ralf Müller, and Prof. Dr. Wolfgang Donner for their time, fruitful discussions of the results and the insight into improvements.

Abstract

Polar and electromechanical properties of ferroelectric thin films including polarization domain formation and switching under the influence of flexoelectric effect, surface charges, and chemical strains have been studied using the phenomenological Landau-Ginzburg-Devonshire theory. The effects are inherent to a thin single-crystalline ferroelectric film containing lattice defects and were studied both separately and in competition with one another to determine their exclusive impacts as well as their interplay in the investigated system.

Ferroelectric films of barium titanate, lead titanate, and lead zirconate-titanate are best characterized, having the predictable behaviour at domain formation and polarization switching and possess the fullest set of measured parametric coefficients to use in phenomenological model in this thesis. Their behaviour is modelled with the inclusion of flexoelectricity, an electromechanical effect connecting polar properties with strain gradient, charges at the film surface, formed from surface states or a non-ideal electrode, and chemical strains resulting from inclusion of defects into the crystal lattice.

The first chapter gives an overview of ferroelectric research, applications, and challenges, as well as explains the origin and working principles of the effects of interest. Ferroelectrics are intensively studied materials that are invisibly omnipresent in modern electronic technology. Their phenomenological study is set to move forward the understanding of processes taking place in these substances. Previous experimental and theoretical works support the statement that the effects of interest indeed have influence upon solid-state substances, and particularly upon ferroelectrics. This study helps to understand how these effects can be represented in phenomenological models and most importantly, how they interact with each other.

The second chapter describes the theoretical background of this study. It is shown how properties of ferroelectrics are expressed through thermodynamic potentials and incorporated into the framework of the Landau-Ginzburg-Devonshire theory. All relevant effects taking place in the ferroelectric film are incorporated into the theoretical model, including ferroelastic properties and semiconductor properties, expressed via electromechanical and electrostatic terms, respectively. Among these properties, the effects of interest are introduced and underlined. A part of the chapter explains the basic principle of the finite-element method used in the modelling software to perform calculations with given precision.

The third chapter is dedicated to the specific problems studied in this thesis. The sections of the chapter follow this division, focusing first on the flexoelectric impact on the static and dynamic characteristics of the samples, then the surface charges influence on domain formation and switching dynamics, and finally the defect-driven chemical strains impacting domain properties of the ferroelectric in a competition with the two other mechanisms. The specific problems are first stated being followed by the publications where the investigations were made.

The fourth chapter discusses the results and makes conclusions on the contributions of each considered effect into the domain formation process and parameters and/or ferroelectric switching dynamics. The tunability of parameters and the prospects of usage and processing of ferroelectric films are discussed.

The final chapter gives an overview of the related scientific problems that may be addressed using methods or results described in the current work.

Zusammenfassung

Polare und elektromechanische Eigenschaften dünner ferroelektrischer Schichten wie Domänenstruktur und Polarisationsumschaltung unter dem Einfluss der Flexoelektrizität, Oberflächenladungen und chemischen Dehnungen, wurden mithilfe der phänomenoligischen Theorie von Landau-Ginzburg-Devonshire erforscht. Die Effekte sind einem System der dünnen ferroelektrischen Einkristallschichte mit Defekten im Kristallgitter charakteristisch, und wurden sowohl getrennt, als auch in Kombination untersucht, um ihre einzelne Einflusse, sowie ihr Zusammenwirken im berücksichtigten System festzustellen.

Untersucht wurden ferroelektrische $BaTiO_3$, $PbTiO_3$ und $Pb(Zr,Ti)O_3$ Schichten, da diese am ausführlichsten charakterisiert sind und sich vorhersagbar bei der Domänenformation und Polarisationsumschaltung verhalten, sowie die größte Anzahl der gemessenen parametrischen Koeffizienten zur Nutzung im phänomenologischen Modell besitzen. Ihr Verhalten wurde unter dem Einfluss von Flexoelektrizität (einem elektromechanischen Effekt, der die Polarisation mit dem Dehnungsgradient verbindet), von elektrischen Oberflächenladungen (die aus Oberflächenenergiezuständen entstehen oder durch eine imperfekte Elektrode verursacht werden) und von chemischen Dehnungen (die ein Resultat von Defekteinfügung sind) modelliert.

Das erste Kapitel gibt eine Übersicht der ferroelektrischen Forschungen, Anwendungen und Herausforderungen und erklärt die Herkunft und Wirkung der berücksichtigten Effekten. Ferroelektrika gehören zu den intensiv erforschten Materialien und befinden sich unscheinbar in vielen modernen elektrotechnischen Geräten. Ihre Phänomenologishe Theorie ist auf die Weiterentwicklung des Verständnisses von Prozessen, die in diesen Stoffen auftreten, gezielt. Vorherige experimentelle und theoretische Werke haben gezeigt, dass die Flexoelektrizität, Oberflächenladungen und die chemishen Dehnungen wesentlich die Festkörpermaterialien, und besonders Ferroelektrika, beeinflussen. Diese Forschung hilft zu verstehen, wie diese Effekte in den phänomenologischen Modellen repräsentiert werden können und, was wichtiger ist, wie sie miteinander wechselwirken.

Das zweite Kapitel beschreibt den theoretischen Hintergrund der Forschung. Es wird gezeigt, wie die Eigenschaften der Ferroelektrika durch thermodynamische Potentiale beschrieben werden können und in die Landau-Ginzburg-Devonshire-Theorie eingeführt sind. Alle relevanten Effekte, die in den ferroelektrischen Schichten stattfinden, sind auch im theoretischen Modell als Erscheinungen von elektromechanischen und Halbleitereigenschaften berücksichtigt. Ein Teil des Kapitels erklärt das Wirkungsprinzip der Finite-Elemente-Methode, die in der Modellierungssoftware benutzt wurde, um die Berechnungen mit der gegebenen Genauigkeit durchzuführen.

Das dritte Kapitel ist den konkreten untergesuchten Problemen gewidmet. Die Abschnitte des Kapitels sind nach den spezifischen Forschungen geteilt, konzentrierend erst auf dem flexoelektrischen Einfluss auf die statischen und dynamischen Schichteigenschaften, dann auf Oberflächenladungen, die Domänenstruktur und Umschaltungsdynamik beeinflussen, und letztens - auf den defektgesteuerten chemischen Dehnungen und ihren Einfluss auf ferroelektrischen Domäneneigenschaften, in Zusammenwirkung mit den zwei anderen Mechanismen. Die formulierten Aufgaben sind von Veröffentlichungen mit den erforschten Ergebnissen gefolgt.

Das vierte Kapitel ist die Schlussfolgerung über die Beiträge jedes untersuchten Effekts in die Domänenstrukturformation und/oder in die Polarisationsumschaltungsdynamik. Diese Ergebnisse werden angesichts der Anwendbarkeit der abstimmbaren Parameter in der Technologie diskutiert.

Das letzte Kapitel gibt einen Überblick von wissenschaftlichen Problemen und Aufgaben, die mit in dieser Arbeit beschriebenen Methoden und Ergebnissen gelöst werden könnten.

„I don't know anything, but I do know that everything is interesting if you go into it deeply enough.“
— Richard P. Feynman

Contents

1. Introduction

Ferroics is a common definition of a vast group of different inorganic and organic materials that at a critical temperature undergo phase transitions which change their physical characteristics, dramatically. In narrow temperature ranges, underneath the critical point, domains appear, which are characterized by a certain order parameter. They lose their centre of inversion symmetry and adopt one of several stable states, corresponding to the minima of the free energy and to a certain value of an order parameter defined as the spontaneous one. Depending on the nature of an order parameter, ferroic materials are split into three main groups: ferromagnetic materials obtain spontaneous magnetization; ferroelectrics have spontaneous electric polarization, whereas ferroelastics possess spontaneous strains.

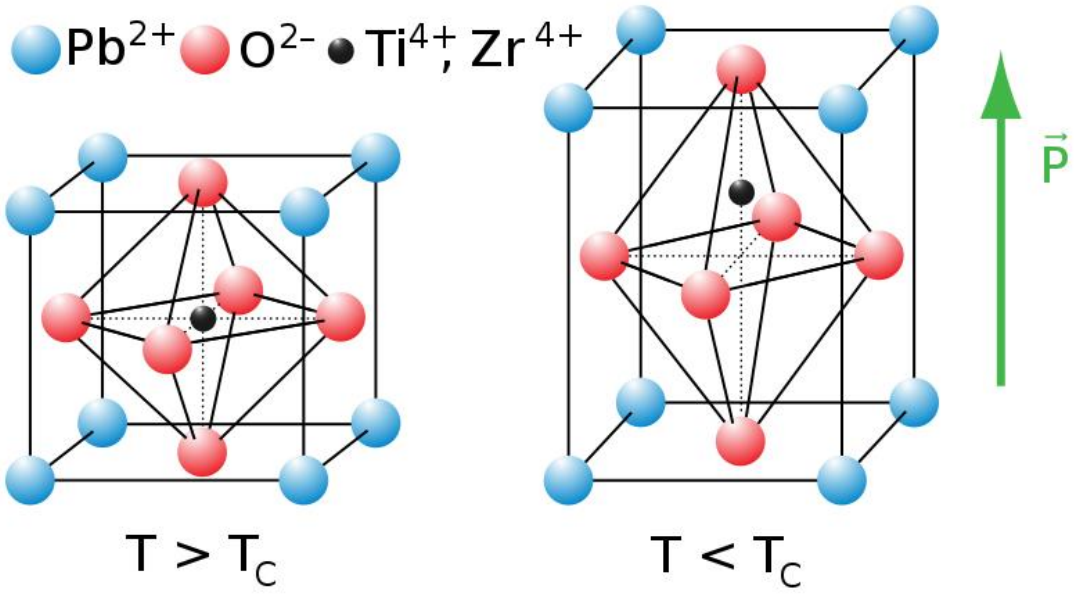

Figure 1.1. Perovskite ferroelectric unit cell in nonpolar (cubic) and polar (tetragonal) phases. Polarization is caused by a displacement of the central ion (titanium or zirconium in the example). The unit cell is elongated to show the spontaneous strain. [1]

If a material belongs to a certain group, it does not preclude, however, that it can also exhibit another type of ferroic properties. Such cases with multiple ferroic propensities found in one substance are called „multiferroics“. They may have multiple phase transitions, each for a single ferroic property, and their properties are interconnected by effects arising from the crystal lattice structure, *e.g.* piezoelectricity.

The emergence of the scanning probe microscopy (SPM) made studies of electromechanical phenomena much easier and, via electromechanical strain microscopy, atomic force microscopy, and piezoresponce force microscopy, as well as related techniques, could reveal that polar and elastic properties are indeed strongly coupled [publication A1].

The combination of ferroelectric and ferroelastic properties makes up a special group of materials where each of the stable states corresponds to spontaneous polarization and spontaneous strain oriented at certain directions. Electromechanical effects bind together polarization components and strains, so that in order to describe a polar phase one needs only to choose a representation (electrical or mechanical) and supply it with required electromechanical tensors.

Though easy at a first glance, the resulting description deals with a whole lot of properties and effects in order to maintain its descriptive precision. It is important to account for effects such as electrostriction,

which can change the order and properties of the phase transition, flexoelectricity, which though being small appears to have a visible impact on the process of polarisation switching, as well as so called chemical strains in films hosting impurities that deform lattice cells around them [2, 3].

Being a defining characteristic feature of ferroelectric materials, polarization reversal has been an object of interest for decades owing to the promising prospects of its use in different types of actuators and in the energy-independent FeRAM memory cells. As it often happens, the study of ferroelectricity produced questions that require investigations on higher levels of complexity. As a result, many mechanisms that govern ferroelectric features like domain nucleation are still obscure and do not have a unified model to explain, although successful attempts to address these points were made and will be discussed below.

Classic models of the polarization reversal were advanced by Rolf Landauer [4] in 1957. There it was shown that reversal occurs via nucleation of a nanosized domain and its growth under a uniform external field. Ferroelectric films were considered to be dielectric, and their spontaneous polarization not influenced by the external field. Domain walls were infinitesimally thin, and the domain itself has been described by electrostatic expressions. It was assumed that surface bound charges were compensated by free charges of metallic electrodes and thus had no impact. This work also gave birth to the so called Landauer Paradox: the nanodomain nucleation would require much more energy than the applied electric field can realistically supply. It is usually answered by assuming a structural defect on the surface that concentrates high electric fields upon itself.

Studies by Molotskii [5, 6] developed the Landauer model. They have shown external field dependencies of domain sizes and considered the case when a domain grows through a thin film. The external field source in this case was not a plane electrode, but a small nanosized conductive spherical tip. Just like in Landauer works, surface bound charges were compensated by electrode charges, even though the surface was not covered with the electrode. With this assumption depolarization fields were studied that oppose the poling process.

Abplanalp obtained different results, studying the nanodomain nucleation directed by an electric field from the tip [7]. In his work, there was a depolarization field created by screening charges located at the domain edges. Unlike in the previous studies, here it was not assumed that surface screening charges are compensated, which resulted in enormously high calculated depolarization fields that did not correspond to experimental results.

It is important to mention the work by Kalinin *et al*. [8] where a critical value of the applied electric field which triggers the nucleation process was found. The tip in this model was presented as a sphere, and the ferroelectric consisted of a surface and an infinite bulk underneath. Surface charges were considered screened, while spontaneous polarization in the bulk was not.

Based on the Molotskii model, Emelyanov [9] considered a ferroelectric film between a bottom electrode and a top cone-shaped electrode. While retaining inconsistent assumptions about the surface screening, the work established a pathway of domain formation consisting of four steps: 1) domain nucleation when the field applied exceeds the critical field; 2) growth at unstable conditions when the lower domain wall approaches the bottom surface; 3) domain taking form of a cylinder and piercing the film from top to bottom electrode; 4) expansion of the domain in the transverse direction.

Recent *ab-initio* studies by Rappe and colleagues [10] have shown a different picture of the domain nucleation. According to them, the domain nucleation can occur even without defects, which offers a solution for the Landauer paradox. The depolarization field energy in their model is smaller than predicted by Miller and Weinreich [11] and could not successfully oppose the domain formation, with the nucleus shape being rectangular rather than triangular as in Miller-Weinreich theory or „droplet-shaped“ as in the Landauer works.

Another topic of interest is, how significant is the influence of effects that are inherent to the ferroic materials but studied so far only separately from the polar properties. The most obvious among them would be the influence of surface charges, bound to the surfaces and interfaces. Needless to say, that any surface can be considered as a defect of the crystalline structure, constituting the bulk, and thus inherently carries a range of imperfections and among them surface states. Another one would be the long time underestimated flexoelectric effect, binding electric charge displacements and mechanic strains via their gradients, that while being inherent to all 32 crystal classes, is noticeable primarily at the nanoscale where it is able to influence macroscopic electrostatic properties of material. The last but not least one would be the influence of defects in the crystal structure that induce elastic dipole tensors which deform the crystal lattice by attracting or repulsing neighbouring ions, the so-called Vegard effect.

1.1. History of Ferroelectrics

Table 1.1. The main important periods of ferroelectric studies and use [12]

1920-1930	Rochelle salt period: discovery of ferroelectricity
1930-1940	KDP age: Thermodynamic and atomistic models of ferroelectricity
1940-1950	Early barium-titanate era: high-K capacitors developed
1950-1960	Period of proliferation: Many new ferroelectrics discovered
1960-1970	Age of high science: Soft modes and order parameters
1970-1980	Age of diversification: Ferroics, electrooptics, thermistors
1980-1990	Age of integration: Packages, composites, and integrated optics
1990-2000	Age of miniaturization: Size effects, manipulated modes and dipoles
2000-present	Age of environmentalism: development of alternative lead-free ferroelectric and relaxor materials [13]

Although its prerequisites reach almost 400 years back, the history of ferroelectricity began in the XX century. It was first recognized by Peter Debye at the University of Zürich [14]. He was interested in outstanding piezoelecric properties of a material known as Rochelle (or Seignette) salt, named after its discoverer: an apothecary Elie Seignette from the French town of La Rochelle, who intended to use this substance as a good purgative, free from the unpleasant side effects of herbs being in use during the XVII century [15]. The Seignette salt by that time was known for its electromechanical properties [16], used among others by Thomas Edison in his phonograph, and was intensely studied by J.A. Anderson [17] and W.G. Cady [18]. It was also known to exhibit pyroelectric properties as was found by David Brewster in 1824 [19]. Studies brought Debye to the idea that there should be electric dipole moments created by certain molecules, which remain permanent, just like magnetic moments in ferromagnets. From the Langevin theory for paramagnetic materials Debye has obtained an equation for dielectric permittivity ε, $\frac{\varepsilon-1}{\varepsilon+2}=a+\frac{b}{T}$, where a is proportional to the material density, b is proportional to the square of the dipole moment, and T is temperature, and established the existence of a certain temperature when this permittivity reaches asymptotic infinity $T_K=\frac{b}{1-a}$. This point was suspiciously similar to the Curie point of ferromagnets, and just like in ferromagnetic case, below the „Curie“ point there ought to be a permanent electric dipole field [20]. Thus, the phenomenon of ferroelectricity has been first predicted, but it was still left to be observed.

In the same year the very term “ferroelectric” has been coined by Erwin Schrödinger [21]. Discussing Debye’s model Schrödinger noticed that if it was applicable to solid-state materials in general, then they could all become “*ferroelektrisch*” at some sufficiently low temperature.

Over the ocean, in the United States, the ferroelectric properties of Seignette salt were experimentally revealed in 1920. W.F.G. Swann, professor of physics at the University of Minnesota was especially interested in using piezoelectrics as a material for seismographs. The outstanding properties of Rochelle salt described in the papers by Anderson and Cady drew his attention, and he began studying the substance, noticing that there were some irreproducible results. Professor Swann could only explain it as some sort of hysteresis and offered his student Joseph Valasek to characterize the material [20].

It was Joseph Valasek who noticed similarities between dielectric response of the Rochelle salt and properties of ferromagnets concluding that there was a direct analogy between the electric displacement (D), electric field intensity (E) and polarization (P) on the one hand and magnetic induction (B), magnetic field intensity (H) and magnetization (M) on the other hand. It was his work [22] where the hysteresis curves for ferroelectrics first appeared.

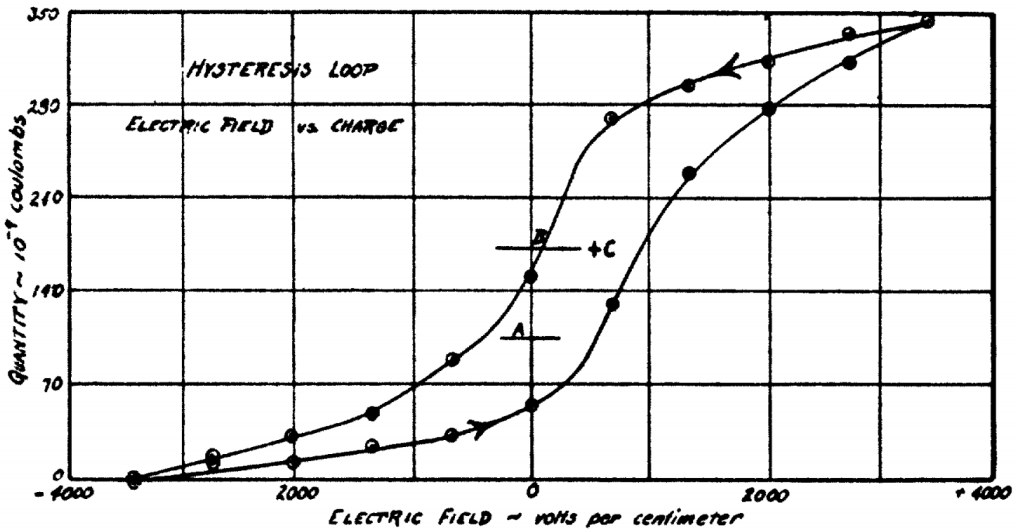

Figure 1.2. The hysteresis curve observed by Valasek (reprinted by permission of APS: Physical Review [22]).

In his later 1922 work Valasek developed this further. He studied piezoelectric properties of Rochelle salt under various conditions [23], including a temperature range where he measured the piezoelectric module. This dependence has shown a narrow range of temperatures where piezoelectricity was the highest. Effectively, this range was confined by two phase transition temperatures which were observed for the first time. Once again, dielectric properties of Rochelle salt were very much similar to ferromagnetism.

As the existence of ferroelectricity has been established, a new question arose. By the time, Seignette salt was the only substance known for its ferroelectric properties, which even gave the name to the effect in Soviet ("*Seignettoelectricity*") as well as in German (*Seignette-Elektrizität*) scientific literature, while use of the similar term in the Western thesaurus slowly faded in favour of the now exclusive "ferroelectricity". But was Seignette salt the only Seignette-electric material? The answer has been given by Swiss physicists Paul Scherrer and Georg Busch who searched for other ferroelectric substances and ultimately - for the mechanism that makes them ferroelectric in the first place.

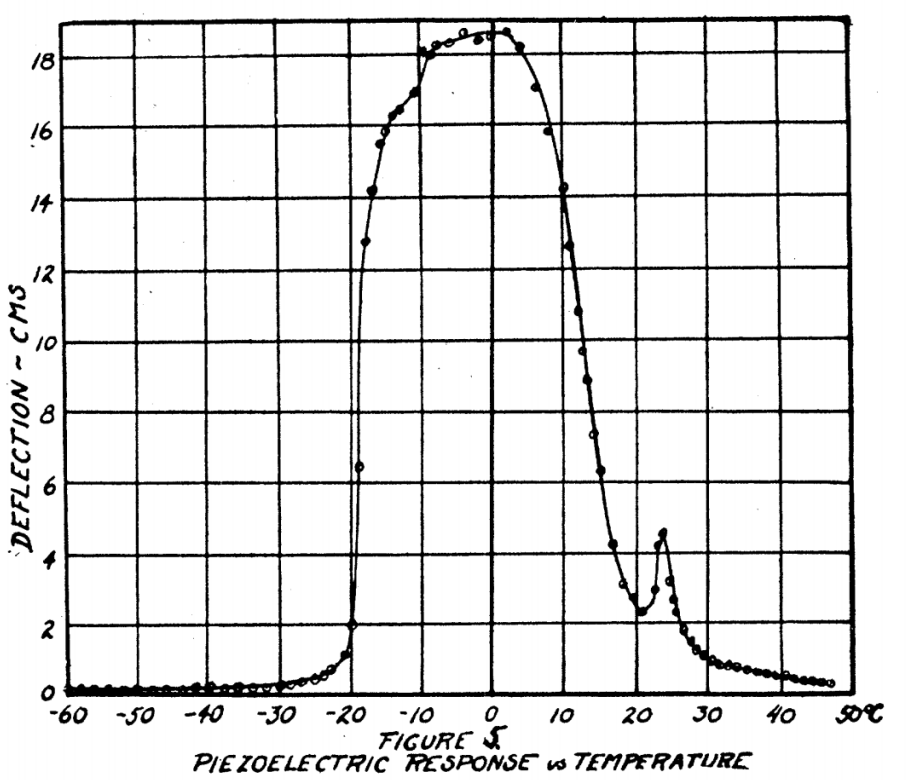

Figure 1.3. Piezoresponse curve versus temperature observed by Valasek (reprinted by permission of APS: Physical Review [23]).

They gathered data for different dielectric compositions, finding them in the work by Gert Steulmann [24] from Technische Hochschule Dresden. Judging by their dielectric permittivity, they have found one compound, KH_2PO_4, with anomalously high constant of 30. X-ray diffraction (XRD) measurements could reveal the types of bonds between atoms, helping to find those crucial for ferroelectricity. Observing a complex structure of the Seignette salt Scherrer believed the movement of water molecules in hydrate crystals was responsible for ferroelectric properties. Busch on the other hand was sure it is mobile hydrogen atoms motion of which contributes to emergence of permanent polarization. Their scientific argument has been resolved by a structural XRD analysis by J. West and Z. Krist from the Bragg laboratory in Manchester [25]. They have found O-H-O bonds, which supported the version of Busch. Scherrer and Busch continued studies of the new material and maintained that it indeed was ferroelectric with the Curie temperature of 123K [26]. Busch underlined it once again in his doctoral thesis [27] that it is hydrogen bonds between oxygen atoms that cause ferroelectricity. Potassium dihydrogen phosphate (KH_2PO_4) became a standard model of ferroelectric materials having less complex structure than Rochelle salt. Busch continued his search for new ferroelectrics, pointing out at the ferroelectricity in dihydrogen arsenate [12] and proposing $NH_4H_3IO_6$ as the next candidate due to the existence of hydrogen bonds within. It is now better known as antiferroelectric, however many other materials with hydrogen bonds were proven to be ferroelectric [20].

The most classical modern perovskite ferroelectric barium titanate ($BaTiO_3$) would most probably not appear so early if not the Second World War started. During the war time there was a special need for good piezoelectrics in sonar systems to prevail in the naval warfare, as well as for high-permittivity dielectrics for capacitors that also functioned inside of war machinery. In the US, most capacitors worked on mica. However, it was almost exclusively shipped to the US from South America, and the constant threat to transport vessels from U-boats shattered this trade lane. With the other combatants seeking to improve their detection systems and radio electronics this led to a secret arm race and resulted in the synthesis of a new material, barium titanate (BT) in the labs of the Japanese Empire, the Soviet Union and the United States between 1941 and 1944. Because of secrecy, it is impossible to establish who among them was the first.

Barium titanate was the first man-made perovskite ferroelectric, analogous to the classical perovskite mineral $CaTiO_3$ that has given its name to the whole newly-discovered group of materials. From the records of the American Lava Corporation made by Thurnmaurer and Deaderick [28], and Gray [29] of Erie Resistor Company, BT was first obtained indirectly, when TiO_2 was doped with BaO. The resulting structure exhibited high dielectric permittivity of hundreds and even thousands and surpassed all known ceramics. This meant that BT was the best to use in supercapacitors. One such supercapacitor was a part of a triggering mechanism in the first atomic bomb thrown onto Hiroshima in 1945.

After the end of World War II, the interest in BT and high-K dielectrics has not gone, and moreover they began to gain new areas of use, above all commercial, as disclosure of secret documents made these findings open to public. High capacitance has proven very useful for domestic and industrial electronics, like TV- and radio-sets, recording devices and sensors. Sonar devices were also based on BT for a long time, even after better sensor and actuator materials were found.

But the competition has not yet ended. Researchers were determined to find out and describe the origins of barium titanate properties, and develop new, more efficient materials. The most important conclusion following from the studies of barium titanate was that ferroelectricity could exist even in simple oxides and was actually not caused exclusively by hydrogen bonds. From XRD measurements [30] it was possible to obtain the exact structure of $BaTiO_3$ and its changes beyond the Curie point. The paraelectric non-polar phase appeared as cubic, whereas the polar ferroelectric phase was tetragonal with a titanium ion displaced along the elongation axis. This was the cause for a persistent electric dipolar moment and for enhanced piezoelectric properties. Moreover, the central ion can take two positions along one axis, which means the dipole moment can point at two opposite directions, and the direction of polarization can be switched by, for instance, applying an electric field. The first switching studies were conducted in 1945-1946 by groups in the US and the USSR independently [31, 32].

While more and more became known about ferroelectrics, a consistent theoretical description still lacked. Because of the similarity of ferroelectricity to ferromagnetism it should have been possible to apply an already established theory of ferromagnets in analogy to electrostatic parameters and variables. The existing ferromagnetic model of Landau [33], Lifshitz [34], and Ginzburg [35] described behaviour of the so-called order parameter in ferromagnetic phase with this parameter in paramagnet phase being equal to zero. In 1950s A.F. Devonshire developed this model further, fitting it to the electromechanical and structural properties of BT with its own phase transition temperature [36, 37, 38]. The Landau-Ginzburg-Devonshire theory proved to be a powerful tool of describing and understanding ferroelectric properties from the phenomenological point of view and, with further developments, continues being used till now.

The use of different perovskite ferroelectrics evolved over the course of time. In 1950 barium titanate was the main perovskite utilized as ceramic. But there was a serious need to improve the material by stabilizing against depoling caused by the tetragonal-rhombohedral phase transition and by low coercive field in the pure titanate ceramics [39].

After the glaring success of BT ceramics, new researches began to examine other perovskite ceramics for piezoelectric and ferroelectric properties. The main point was the search for new compositions that had higher piezomoduli, higher dielectric constants, a higher phase-transition point, or wider phase-transition range where the highest permittivity is available. Studies in Japan by Sawaguchi [40], Shirane [41] and Takeda [42] have found ferroelectric properties of lead titanate ($PbTiO_3$) and its solid solution lead zirconate titanate $PbTiO_3$:$PbZrO_3$ (PZT). They have identified the shape of the phase diagram of PZT and noted its high Curie temperature. Further investigations by Jaffe *et al.* [43, 44] observed the properties of PZT. They have studied a rhombohedral-tetragonal (ferroelectric-ferroelectric) phase transition dependent solely on the composition. This so called morphotropic phase boundary (MPB) existed at approximately 52:48 proportion between Zr and Ti ions in PZT. The poling process at this

point is facilitated, and piezoelectric response of the material is largely enhanced, and as the MPB is temperature independent, the material can remain at the phase transition point in an extremely wide range of temperatures [45]. The poling process, high piezomoduli and high Curie temperature made PZT the best material for piezoelectric applications, and this status PZT retains until now. PZT is integrated into the majority of modern piezoactuators and ultrasonic devices. However, environmental concerns undermined its dominance, as many believe that lead in the composition can be dangerous during synthesis and recycling. For that reason, searches continue for new lead-free compositions and more effective ways of using the old ones.

Several solid solutions have been synthesized with properties close to those of PZT since 1950s and the process continues until now given the new regulations. But they still have not achieved much spread due to reasons like difficult processing, phase instability, undesired phase transition positions or relatively weak piezoelectricity. The closest to PZT compounds are lead-containing as well and cannot be viewed as a substitution.

The main directions of competing for the PZT niche are: (1) revisiting old materials like $BaTiO_3$ as single crystals or textured ceramics, (2) substitution with new perovskite materials like potassium-sodium niobate (KNN) [46] or $(Ba,Ca)TiO_3$-$Ba(Zr,Ti)O_3$ (BCT-BZT) [13], that though not as good as PZT have close properties enhanced near the MPB, (3) introduction of organic polymer ferroelectrics such as polyvinylidene difluoride (PVDF), (4) developing the sub-class of materials known as relaxor ferroelectrics, such as solid solutions BNT-BT, that are known for a blurred phase-transition region with the frequency dependence of its parameters and having big piezocoefficients. All of these approaches have shown success; however, it becomes clear that for modern uses only one single material would be far from enough.

1.2. Applications of Ferroelectrics

As has been already highlighted in the history section, ferroelectric materials play significant roles in modern technological devices and applications, owing to a wide range of properties. The three main branches where ferroelectrics have fit especially good are piezoelectric sensors and actuators, nonvolatile digital memory devices, and nonlinear optic applications. The most important of them will be discussed below.

1.2.1. Piezoelectric Applications

All materials with ferroelectric properties by definition possess piezoeffect, since their crystalline structure belongs to the subclass of piezoelectric non-centrosymmetric crystals. In fact, in most instances ferroelectrics, such as barium titanate ($BaTiO_3$) or lead zirconate-titanate (PZT), are used due to their large piezocoefficients. The history of ferroelectrics usage is indivisibly linked to the history of piezoelectrics.

The first work establishing in 1880 the existence of piezoeffect was a systematic study by Jaques and Pierre Curie [16]. They have described types of crystal lattice symmetry responsible for piezoelectricity and pointed at the materials that already had established linear electromechanical properties. Among them were such materials like quartz, tourmaline, tartrates, boracite and Seignette salt. There was a while until piezoelectric properties have found the way into applications, while remaining a field of scientific interest. Thomas A. Edison was the first to use a piezoelectric device commercially in his phonograph, a bulky and expensive sound-recording machine [15].

When the World War I (WWI) erupted, the threat posed by German U-boats created a demand to develop a way of finding effectively invisible by that time submarines raiding seas all over the world. One of the solutions involved a device, called sonar, capable of tracing an object under water emitting soundwaves

and receiving those reflected from the object's hull. The concept was known earlier, since the idea of sonar came up right after the sinking of "Titanic" in 1912 as a possible way to seek out icebergs. Natural materials for such purpose were piezoelectrics like quartz, but there also was Seignette salt praised for its high piezoelectric coefficient. Walter G. Cady was the one to establish a sonar-aimed piezoelectric programme in the US, after an important meeting with French scientists in 1917, melding together the cutting-edge science and technology of that time [47]. The main developers of sonars during the WWI were an American Alexander M. Nicholson [48] and a Frenchman Paul Langevin [49]. Their inventions were simple, consisting of a piezoelectric matrix between iron plating that by applying an alternate current produced a sound wave under water. The distance to the object detected was measured as a function of time after which an echo from the target would return. The technology allowed the Entente to eventually achieve the strategical superiority on the seas.

Ferroelectrics as materials with strong piezoeffect were once again widely used during the World War II (WWII). At that time and decades after, usage of piezo-materials was prominently for military purposes. Strategic needs also pushed the militant powers to discover the first known ferroelectric perovskite batium titanate, mentioned before, and to throw it into battle. Maritime sonar technology allowed searching for underwater threats and has been extensively used to track submarines during the Cold War and even after, whenever the tensions between military powers rise. Eventually, after the disclosure of classified documents on perovskites to the public, a peaceful application of sonar devices has been found as well, in areas like oceanography allowing to map the ocean floor and observe marine animal species. In the medicine, archaeology and more special civil engineering branches, versions of sonar became a device for ultrasonography. At that time, the best piezomaterial available was lead zirconate-titanate, the properties of which in a wide temperature range has been long unmatched. Close to PZT are competitors like the relaxor ferroelectrics, *e.g.* PMN-PT (lead manganite-niobate-lead titanate), possessing high electromechanical coefficients and a wide phase transition zone, properties of which are frequency-dependent. The origins of these remarkable properties remain enigmatic which impedes their tweaking and narrows a potential range of applications [50].

Since then, the area of the piezomaterial applications has been significantly broadened. Nowadays, piezoelectrics are mostly associated with medical ultrasound detectors and pacemakers, industrial actuators, MEMS, energy harvesting, as well as robotics, with this not being an exhaustive list. The highest performance of piezoelectric devices has been reached and is not a priority any more. The current trends, or rather a roadmap for development in this area are: microminiaturization of devices, their reliability, reduction of energy consumption, environmental friendliness, potential of combining different technological solution, transfer to (disposable) organic materials.

Now that PZT goes out of favour due to the new green policy in the growing number of the world governments, outlawing lead from usage, its niche of a cheap and effective piezoceramic material must be occupied. It is outstanding piezoelectric properties after all that are primarily searched in potential alternatives among semiconductor piezoelectrics (ZnO), perovskite solid solutions (KNN), and relaxor ferroelectrics (PMN-PT). Although they do not possess the whole set of required properties as PZT does, their widespread potential usage is already possible with some infringements.

1.2.2. Ferroelectric Random Access Memory

Functionality of the ferroelectric random access memory (FeRAM) generally resembles the functionality of the dielectric memory (DRAM). The main difference lies in the usage of a ferroelectric layer instead of the linear dielectric to provide energy independence of the device. Different layouts of memory cells can contain either a capacitor with a control transistor or a single transistor with a thin ferroelectric film as a gate oxide (Figure 1.4). Information is stored in the cell as logical „0“ and „1“ according to a spontaneous polarization vector direction in a ferroelectric domain and persists when the device is shut down. The memory cell is written after electric field of a certain sign penetrates the oxide gate and reorients the polarization vector accordingly to attain the corresponding logical value. Reading is

performed by writing „zero“ into the cell. If no reaction is detected „zero“ is displayed. In case of a stored „one“, rewriting causes a short pulse that, when registered, is interpreted and displayed as „one“.

FeRAM reading is a destructive process which makes it necessary to rewrite cells afterwards. However, unlike in DRAM, the polarization does not disappear over time, and hence, no regular rewriting process is needed. This makes up the first advantage of the FeRAM - it requires low energy to operate. When thin films are used, where nanosized domains can be created, writing time reduces, increasing the writing speed, which in combination with small sizes of such cells allows writing of large data volumes on a small area. The nature of the FeRAM makes it possible to use it for all levels of memory in modern computers: cache, main memory and disk memory [51].

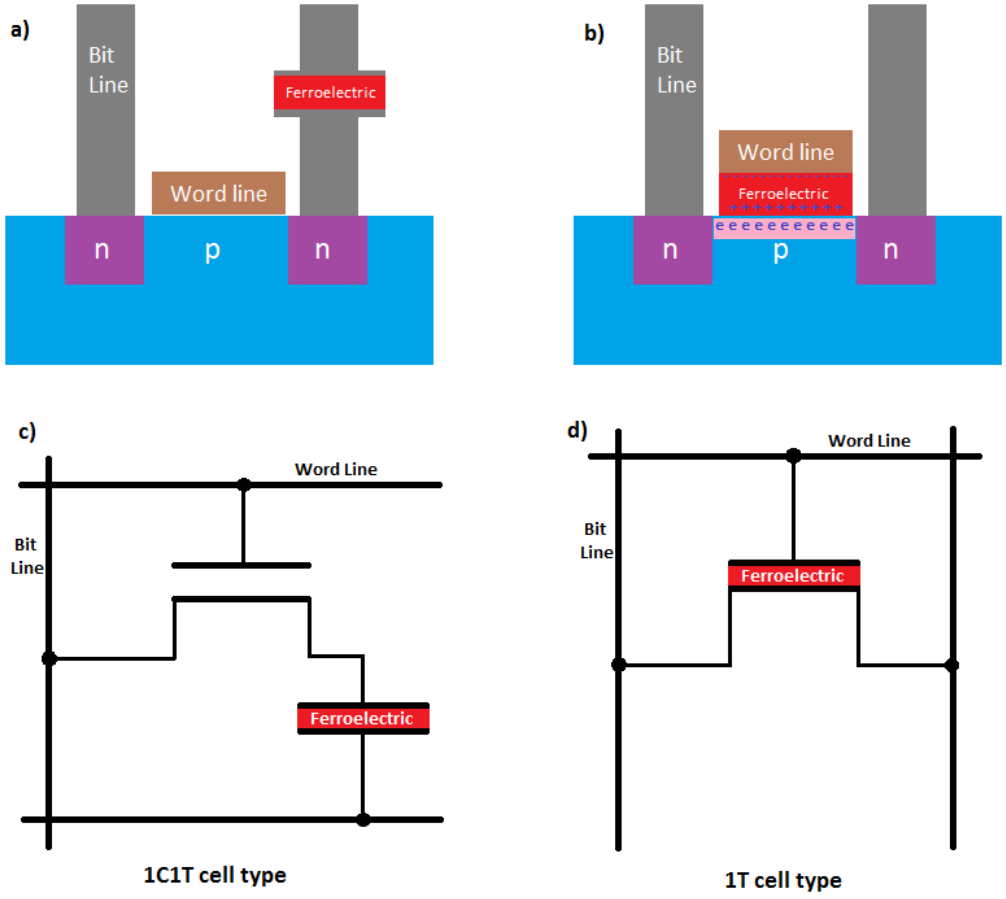

Figure 1.4. Topology (a, b) and corresponding circuits (c, d) of 1-capacitor-1-transistor (a, c) and 1-transistor ferroelectric memory cells.

Nowadays, however, flash-memory dominates the market, and there are several reasons making FeRAM not that much appealing in comparison. First and foremost, flash memory is cheaper than FeRAM and other modern high-efficiency memory types. A modern flash cell can contain up to 3 bits of data, since flash uses transistors with floating gate that allows for extremely reducing sizes, in particular beyond reach of FeRAM, the cell of which consists of either a capacitor and transistor or a transistor with gate oxide. These cells are manufactured with 130 nm and 350 nm technology. The main obstacle for micro-miniaturization are depolarizing fields that at low sizes make the films lose their properties [52]. This must be taken into account when modelling the properties of nanoclusters and nanodomains in ferroelectrics. One of the proposed ways to overcome depolarizing fields influence was a usage of absorbed water molecules [53]. The studies have shown that hydrogen ion adsorption from water

molecules led to increase of the screening charge and established other dependencies of ferroelectric polarization on the adsorbed substances composition [54].

However, one should also note that in a functional sense FeRAM is superior to flash by several parameters. First of all, FeRAM reliability is much higher than that of flash. While flash cells can sustain 10^3-10^5 rewriting cycles, the endurance of FeRAM is in this case up to 10^{12}-10^{14} cycles. FeRAM also performs reading at higher and writing at much higher speeds than flash and requires less energy to operate [55]. Also, FeRAM is free from a problem when charge on the floating gate of flash can leak and tunnel through the oxide, effectively corrupting data when a memory cell is not used for a sufficiently long time.

At the time, FeRAM containing devices include black boxes in aeroplanes, measurement devices, sensors, biomedical equipment, industrial micro-controllers, printers, space exploration probes [56] etc. FeRAM market is much smaller than the flash market, and so far, no signs are seen to change such a power balance. However, energy efficiency and increased operating speed could carry ferroelectric memory cells to a leading position, noting that production technology of FeRAM is more compatible with the modern complementary metal-oxide-semiconductor transistor layout (CMOS) technique.

In 2011, new structures were found in $BiFeO_3$ that *per se* appeared to be ferroelectric dipole vortices, caused by dipole-dipole interactions. The interaction at scales of approximately 5 nm defines the structure of domains and vortices. Depolarizing field appearing on a surface destabilizes domain states, which makes the system transit to the vortex phase to minimize its energy. Dipoles localize parallel to the nanoparticle surface and form a vortex-like structure. This phenomenon was named „vortex nanodomains“. A new type of memory VRAM, resembling the one created on magnetic vortices, is proposed [57].

1.2.3. Electro-optical Applications of Ferroelectrics

As one of the core properties of ferroelectric materials, dielectric nonlinearity makes them useful for applications in photonics. Such devices are widely used in acusto-optics, optical signal processing and computing; the ability to generate second harmonic allows for obtaining a laser with a wide colour spectrum. Thin ferroelectric films are especially useful as their sizes are compatible with micro- and nanoelectronic circuits where they act as waveguides, modulators, second-harmonic generators or other electrooptical devices. Nonlinear optics is used in medicine, solid-state physics, chemistry, aviation, and cybernetics [58].

A special role in electro-optic applications has lithium niobate (LNO) [58]. Its optical transparency for 400-5000 nm waves, refraction coefficient of 2.2-2.3 makes it useful in a wide frequency range. The LNO crystal structure has no centre of symmetry, exhibiting the Pockels effect, nonlinear optic polarizability and photoelasticity. The simplicity of growing and processing has made $LiNbO_3$ the most useful material for nonlinear optics [59]. Waveguides are usually made on an LNO substrate with an active waveguide layer being obtained by ZnO or Ti diffusion into the substrate. Alternatively, $LiTaO_3$, $KNbO_3$, KDP or $LiIO_3$ can also be used for some of the optical applications [60, 61].

The Pockels effect in LNO is a change of its polarizability in response to an external electric field. The effect is non-inertial and can be used for modulators for frequencies up to 110 GHz. Lithium niobate waveguides are used to generate the second harmonics (SHG) in response to incident laser pulse of the wavelength 1053 nm directed under certain angles. As a special case of frequency summation, SHG implies that upon transiting the nonlinear optical medium, two photons of the same frequency combine generating a photon with a doubled frequency. Domain structure parameters directly affect the second harmonic generation, and it is possible to optically investigate ferroelectric domain structure using this effect [62].

LNO waveguides are used in integral optical circuits to encode the data stream transferred via optical fibre. The circuit contains an amplitude modulator that opens or closes the channel depending on the signal in it. The high frequency modulation uses an interference scheme with a constructive interference amplifying the wave (maximum signal) and a destructive interference that dims the wave (no signal). The usage of the modulators can help to save the impulse form when control signal frequencies are high. The data transfer frequency of modern fibres is around 20 GHz which creates demand for modulator schemes [63].

Fibre-optical gyroscopes on optical modulators are used in the air and maritime navigation. A modulator made of planar or channel waveguides is placed upon the single-crystal LNO substrate. The light wave splits and goes through two modulator channels. After that each part of the wave goes further along the closed-loop optical circuit where the two parts meet each other going in the opposite direction and interfere.

Ferroelectric crystals also play role of the nonlinear optical media in parametric amplifiers where their ability to generate harmonics is used for parameter modulation of the input waves when invoked by irradiation of the control wave.

The current challenge in the nonlinear optics is to maintain a stability of the system. While having good electro-optical coefficients and being transparent in a wide frequency range, LNO has also piezoelectric and pyroelectric properties that have its influence on the device functioning. Finding workarounds for these effects is a problem for materials science and microelectronics.

1.3. Phenomena in Ferroelectric Films

Certain physical phenomena inherent to ferroelectric materials can significantly affect the properties of thin films. Below a brief introduction to three effects of interest is given that will be studied scrupulously in this work.

1.3.1. Flexoelectric Effect

Flexoelectricity is an electromechanical property inherent to all solid materials, which can be described as change of electric polarization in response to the mechanical strain gradient or change of the mechanical strain in response to the polarization gradient. This property appears very similar to the piezoelectric effect and was even called „non-local piezoelectricity“ [64] until Indenbom *et al.* [65] coined the term „flexoelectricity“ borrowing it from liquid crystals physics, where it was known for longer time. Nonetheless, it appeared to be not just a simple variation of the piezoeffect, but an additional independent physical property that is able to exist in all 32 structural groups of crystals [66].

From the above definition, it follows that flexoelectricity appears as polarization in response to bending stress or inhomogenious linear strain, and vice versa. If a material has a central symmetry, the flexoelectric interaction essentially breaks it. The top and bottom surfaces of the bulk are not equivalent under the bending strain gradient, and this difference defines a direction of the polarization vector. On the microscopic level, one can see that this inequality between two different sides of an elementary cell squeezes a central ion out of the cell's centre, which is what causes a flexoelectric polarization to appear in structures such as perovskites (see Figure 1.5). The flexoelectric effect is also possible for the case when the lattice is strained uniformly but inhomogeneously (Figure 1.6), when the difference between strains for each unit cell produces strain gradient [67].

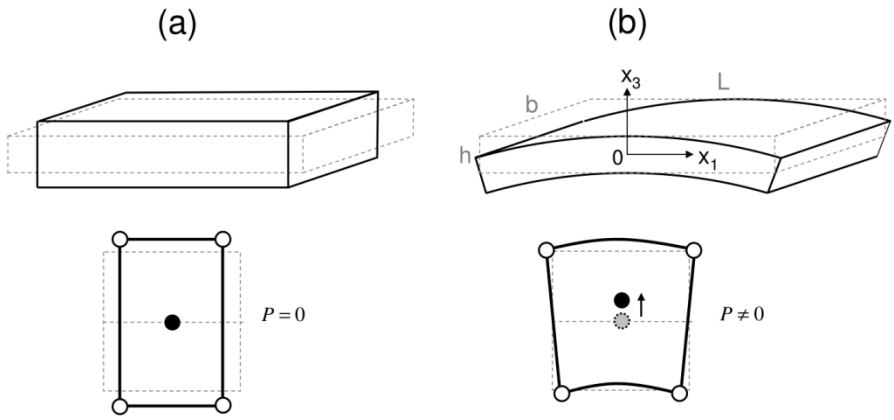

Figure 1.5. Illustration of the microscopic mechanisms of flexoelectricity for the case of bending stress (reprinted by permission of Annual Review of Materials Research [67]).

Another illustration assumes that an acoustic wave going through a solid imposes a time-dependent strain gradient onto the crystal structure making distances between atomic planes unequal and breaking thus central symmetry locally, leading to the same result as the bending stress in the static case. It should be generally treated as a sum of static and dynamic parts.

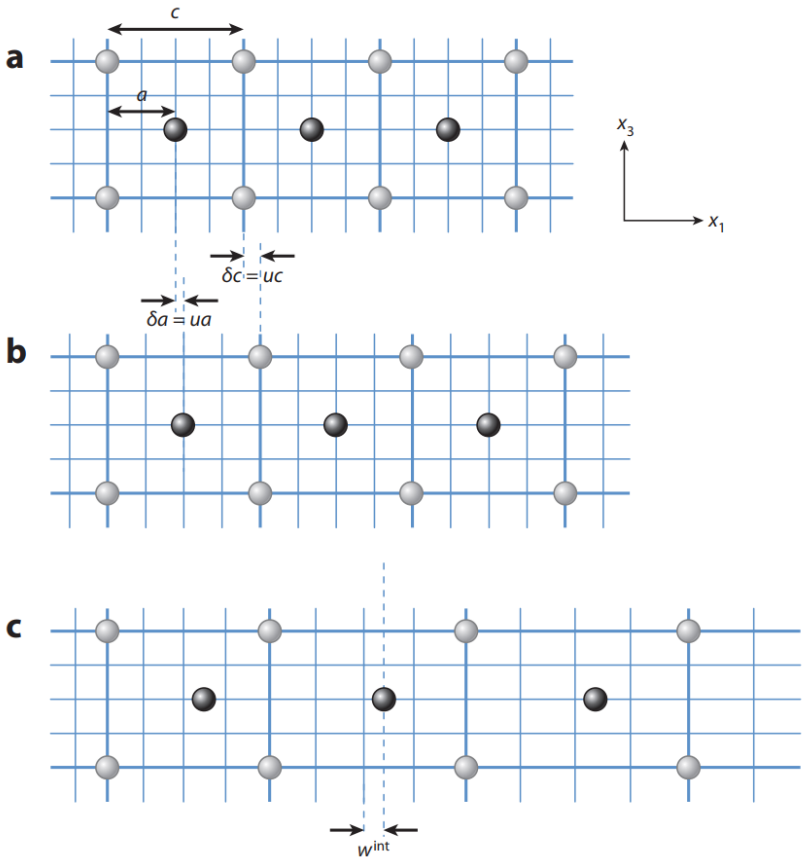

Figure 1.6. Illustration of different cases of uniform strain. A centrosymmetric lattice (a) can deform homogeneously (b). In this case displacement of atoms $\delta a, \delta c$ corresponds to the strain approximation ua, uc in the elastic medium (blue lattice). In case of the inhomogeneous strain (c) there is a difference between actual displacements of central ions δa and elastic medium strain approximation ua which is w^{int} that causes internal strains (reprinted by permission of Annual Review of Material Research [67]).

Strain gradients, however, affect not only ionic, but also electronic subsystems. In response to the gradient of strain, a redistribution of electron density should also take place. The components of flexoelectricity from both subsystems are complementary. Electron density redistribution is a main mechanism of flexoelectricity in graphene [68]. As the ionic picture alone is more simplistic, it is found in a larger number of publications than the full picture [67].

The history of studying flexoelectricity in solids traces back to the 1950ies, when Mashkevich and Tolpygo [69, 70] theoretically derived it from the lattice dynamics in solid materials. Afterwards, in 1964 Kogan [71] studying electron-phonon coupling in crystal lattices with central symmetry formulated the phenomenology of the flexoelectric effect. However, it was not until 1968 that its phenomenology was applied to ferroelectrics, namely by Bursian *et al*. [72, 73] showing the mechanism in BT that can even switch the spontaneous polarization by a strain gradient. At the same time the framework for a phenomenological description has been proposed by Mindlin [74], and two years later, in 1970 the first calculation of flexocoefficients was performed by Ashkar *et al.* [75]. The phenomenology developed by Bursian and colleagues implied that flexoelectricity should be especially stronger in materials with high dielectric permittivity, and thus, in ferroelectrics.

Experiments have also established the existence of the flexoelectric effect in ferroelectric materials by analyzing their phonon spectra [76]. Most importantly, this research has shown that the flexoelectric effect affecting low energy phonon spectra contributes to the formation of modulated incommensurate structures within dielectrics [66].

Finally, in 1981 Indenbom *et al*. [65] has formulated a phenomenological theory for flexoelectricity compatible with the Landau theory for ferroelectrics. At the same time, they were the first to use the very term „flexoelectricity“ for crystalline dielectrics, having taken it from the solid crystal physics where it denoted a similar effect. To draw the line between piezoelectricity and flexoelectricity, first considered to be direct analogues, Tagantsev *et al.* [77, 78] have clearly shown that very different approaches are needed for the phenomenological description of both effects, thus, revealing the flexoelectric effect as a distinct non-trivial phenomenon. The method to calculate flexoelectric coefficients has been also presented.

However, flexoelectricity has for a long time been considered small and exotic and remained poorly studied due to lack of interest. This has changed in the early 2000s with fundamental works by Eric Cross *et al.* [79, 80, 81, 82, 83], who found the flexoelectricity to be much stronger than expected, investigating it in solid solutions like barium-strontium titanate ($(Ba,Sr)TiO_3$, BST). With the effect found also in other materials [84, 85, 86, 87, 88, 89, 90, 91, 92, 93, 94], a deep and comprehensive description of it has become possible. Experimental studies revealed the importance of flexocoupling and were a prerequisite to the new theoretical models.

The main approaches used for an effective description of the flexoelectric effect are divided into phenomenological and *ab-initio* calculations. The former follows Bursian theory [95] and is used to describe finite samples. Studies by Tagantsev and Yurkov [96], Eliseev [97], and Yurkov [98] have established the significance of surface effects in ferroelectric films in the way it modifies electrical and mechanical boundary conditions. The latter uses microscopic theories unfolding the processes on the elementary level in the crystals of most common composites and solid solutions, especially investigating an electronic contribution to the flexoelectric effect. Such works were made, among others, by Sharma *et al*. [99], Hong *et al*. [100], Ponomareva *et al*. [101], Hong and Vanderbildt [102], Dumitrica *et al*. [103], Kalinin and Meunier [104]. The framework for perovskite *ab-initio* calculation comes from the methods described by Tagantsev [105], Stengel [106] and Martin [107].

The newest developments in flexoelectricity studies revolve around a recently discovered combined interaction between flexocoupling and a diverse range of phenomena, most notably in ferroelectrics, including polarization reversal, electromechanical and polar domain properties (Yudin *et al*.,

Morozovska *et al*. [108, 109, 110, 111]), flexoelectric-driven domain imprint and ferroelectric hardening (Abe *et al*., Tagantsev *et al.*, Sharma *et al.*, Chen *et al.* [112, 113, 114, 115, 116, 117, 118]), flexoelectricity-driven dead-layer effect (Majdoub *et al.*, Zhui *et al.* [119, 120]), and many others. So called piezoelectric metamaterials were also found as composites of non-piezoelectrics that exhibit piezoelectric response. This response is conditioned by local strain gradients and therefore has a flexoelectric nature. The importance of piezoelectric metamaterials is that the piezoresponse they show is comparable to that of widely-used commercial piezomaterials. Important steps in discovering, characterizing and describing the metamaterials have been made by groups of Cross, Fousek and Sharma [121, 122, 123, 124, 125, 126, 127].

The studies of the flexoelectric effect continue and new impacts of the effect have been found experimentally. The main interest in flexoelectricity thus arises from its properties that do not have analogues in the common electromechanical effects, such as piezoelectricity and electrostriction. Although being quantitatively weaker than those, the flexoeffect has a high impact at lower scales below micrometers. When it comes to nanosizes, changing strain over a small length results in high strain gradients and thus in higher response. Flexoelectricity, in addition, can play the role of an effective electrical field and can act like it, switching polarization in ferroelectrics, poling them, change domain dimensions, create voltage offsets in hysteresis loops, smear the point of the ferroelectric phase transition or changing conductivity, unlike piezoeffect that can work like this only in a paraelectric-piezoelectric phase, which is a rarity. This property was established in studies of ferroelectric perovskite materials such as BT and PZT done by Gruverman *et al.* [128], Lu *et al.* [129], Lee *et al.* [130], Catalan *et al.* [131], Lubomirsky *et al.* [132]. As it is a universal property of solid materials, the choice of nanosensor and nanoactuator materials spans beyond the traditional piezoelectric scope, allowing for choosing more suitable materials for special needs [67].

However, studies of the flexocoupling experience challenges. First and foremost, there is still a small number of ferroic materials with flexocoefficients measured, estimated or calculated [133, 134, 135, 136, 137]. The second problem deals with the representation of the effect as a main cause for changes in polarization or strains at given conditions, whereas other mechanisms, which are often not sufficiently studied can also contribute. Among them there can be strains caused by defects deforming the crystal lattice - the so-called Vegard effect, or local microscopic polarization caused by a redistribution of charged defect ions. The effects prescribed to the flexoelectricity could also be a result of the processes of domain-wall motion or polarization reversal and this should not be ignored [138].

The above listed publications have shown that the flexoelectric effect manifests itself in a variety of ways affecting the functional properties of materials. Because of the weakness of this effect, modifications caused by it are seen mainly at the nanoscale or occur in thin films. The latter is particularly true because in thin films large strain gradients can exist, as they are inversely proportional to sizes. The best materials to search for high flexoelectric coefficients are ferroelectrics that have high dielectric permittivities. Those ferroelectric films that are grown on rigid substrates experience mismatch stresses between lattice parameters of the film and the substrate. If the film is thick enough, the otherwise homogeneous stresses may be relieved by films via formation of local misfit dislocations [139]. The mechanism is highly inhomogeneous and is itself a prerequisite for a strong flexoeffect.

Further investigations have shown that the mismatch relaxes exponentially throughout the film and is linked to the order-of-magnitude decrease in the dielectric constant and smearing of its peak [140, 141, 142]. The effect is analogous to the impact of external fields that saturate polarization and decrease the permittivity. Surface flexoelectricity can also contribute to the lowering of the permittivity mimicking the dead layer effect [143, 144]. It is also predicted that flexoelectricity increases the critical thickness of ferroelectricity (or decrease the critical temperature) in thin films [145]. As flexoelectricity may act as an external field, it can influence ferroelectrics by displacing the thermodynamic potential and introducing a preferred poling direction that makes hysteresis curves asymmetrical [146, 147, 148, 149, 150]. In the extreme cases strain gradients are even able to switch the polarization actively [151, 152,

153]. Other impacts include flexoelectric influence on the properties of ion conductors [154], appearance of electromechanically-induced polarization in non-centrosymmetric materials [155, 156], polarization-induced bending [157], and modification of phonon dispersion curves [158]. Naturally, flexoelectricity occurs at the ferroelectric and ferroelastic domain walls due to intrinsically large gradients within, inducing flexoelectric polarization [159, 160], and influences domain-wall conductivity via generated depolarization field [161, 162]. The occurring effects received the interest of the scientific community being potentially suitable for a large variety of applications [163].

Given the whole range of effects caused by flexoelectricity, it is important to include it into models of thin-film ferroelectrics. The flexoelectric effect in crystals can be described using the phenomenological approach. There are static and dynamic forms of description that involve different types of differential equations. In the theory part of this thesis, the flexoelectric effect will be presented statically as a term in the Gibbs free energy expression and the subsequent Euler-Lagrange equation, as well as in the expression for the generalized Hooke law.

1.3.2. Surface Screening

Charges in general are recognized as one of the key aspects of the ferroelectric physics. For example, when polarization charges are uncompensated, the energy of the system would diverge with the system's size due to the contributions from these charges. This forms the depolarizing energy, that should be lowered, and there should exist mechanisms for it. One of the mechanisms is the domain formation [164, 165]. Another one is the screening of charges which can be either bulk screening, *i.e.* done by charges inside the ferroelectric bulk [166, 167], or surface screening, *i.e.* done by charges on the surface, opened or covered by an electrode. Surface screening can be provided by an electrode on the surface, which can be ideally conductive or non-ideal, as well as by superficial defects and charges usually adsorbed onto the surface from the ambience to which the sample surface is exposed. There are always charges of one of these types on the surface, and they can only be made small by special experimental treatment of the surface (cleaning in dry atmosphere, high vacuum, dielectric layer etc.) [168]. Surface charges are partially free and are able to distribute along the surface with quasi two-dimensional densities.

Surface charges produce a variety of effects on the electrostatic and mechanical properties of ferroelectrics due to the long-range nature of depolarization effects. There are several different layouts to consider: (i) a perfect conducting electrode at the surface and (ii) a strongly charged defect layer on the surface corresponding to the *ideal* screening; (iii) an imperfect, „real“ electrode characterized by a finite Thomas-Fermi screening length and a finite injection barrier, (iv) an electrode that is separated from the surface by a dead dielectric layer or ambience, and/or (v) a collection of ambient charges on the surface corresponding to the *non-ideal* screening. The *ideal* screening is meant to oppose domain structure formation in the ferroelectric bulk by effectively supporting the single-domain state [169, 170, 171, 172, 173, 174]. A *non-ideal* or defect-driven screening affects polar properties of thin films and most notably domain structure features such as nucleation processes, domain shapes and sizes. It can induce closure domains under the imperfectly screened surface and provide a polarization rotation, domain wall broadening, as well as a crossover between different screening regimes at the moving domain wall-surface junctions [175, 176, 177, 178, 179, 180, 181, 182, 183, 184, 185]. Parameters defining the phase transition, like critical film size or Curie temperature, can also be influenced by surface screening [186, 187, 188].

Though the domain formation process and surface screening as means of minimizing the Gibbs free energy were studied separately, there is a lack of studies where these mechanisms are viewed together in competition with each other. Taking the surface effects into account while studying domain evolution would provide an accurate tool to determine domain periodicity and characteristics of the resulting structure in general.

1.3.3. Vegard Effect

The least studied effect of interest has several names that result from different aspects of observing the phenomenon. It is about deformations in crystal lattice due to ion displacements caused by lattice defects. Vacancies, interstitials, or defect ions *etc.*, occupy a volume in the lattice or represent a volume freed from atoms. In both cases, the usual structure of the unit cell is locally distorted, and neighbouring ions move and rearrange in the lattice. Accordingly, defects can be attractive, *i.e.* those that make neighbouring ions move toward the defect site, repulsive, *i.e.* those that expel neighbouring ions from the defect site, and both. The movements within the lattice are small yet they do contribute to the strains within the system. The more defects are embedded in the film, the greater will be their contribution. Sometimes, structural defects call down a local rearrangement of chemical bounds and composition with the similar results of occurring local strains. In such cases, the effect is called „chemical strain". Below, several studies are listed that illustrate the main properties of the effect.

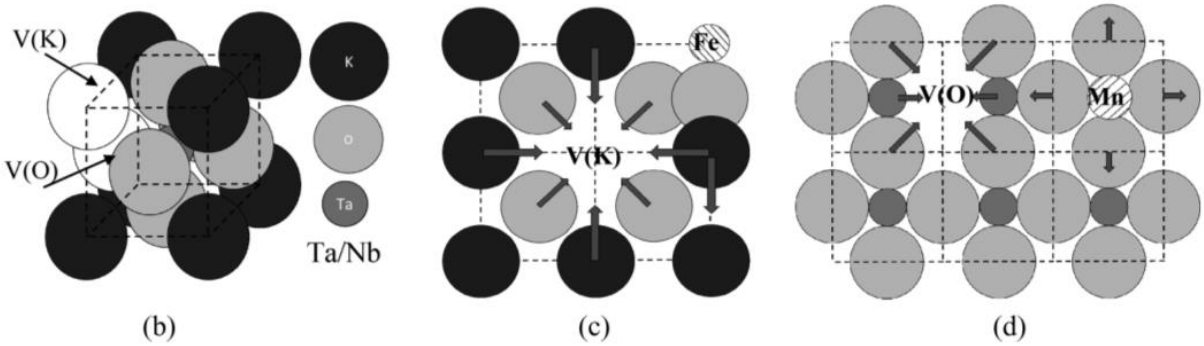

Figure 1.7. Displacement of ions in the unit cells of the crystal lattice caused by vacancies (c, d) and defect ions (d) in K(Ta, Nb)O3 nanoparticles (Reprinted by permission of APS: Physical Review B [189]).

The possibility of creating mechanical forces by point defects that leads to the movement of neighbouring atoms was already known back in 1970s. The mechanical interactions of the lattice with defects were described using elastic dipole tensors varying for each defect type and lattice symmetry [190]. In 2001 Stuart B. Adler studying expansion properties of an electrochemical ceramic (La, Sr)(Co, Fe)O_3 drew the difference between the thermal expansion and the chemical one as those that have different nature and properties[191]. He has found the contribution of oxygen vacancies to the linear expansion of the system and came up with thermodynamic description devising a specific term of „chemical expansivity" as a function of oxygen composition under given temperature and pressure.

The measurements of (La,Sr)CoO_3 by Xiyong Chen *et al.* in 2005 [192] have established that the chemical expansivity actually plays a major role over the thermal expansivity, being controlled by oxygen stoichiometry and Sr content. A secondary expansion effect, also named expansion hysteresis, found in this system was also explained with the chemical expansivity effect.

Effects of doping cerium oxide with Gd have been studied by Bishop *et al.* in 2009 [193]. Gd-doping of the material changes valence of the Ce-ions and turns the structure oxygen-deficient. The formed oxygen vacancies repulse surrounding atoms being source of „chemical expansion".

Local strain effects caused by atomic vacancies in perovskite material $SrTiO_3$ were studied in the same year by Daniel Freedman and colleagues [194]. Vacancies of oxygen, strontium and titanium were characterized by an anisotropic elastic dipole tensor, characterizing mechanical interactions of the vacancy with surrounding atoms causing chemical strain. Alternative forms of representation were also shown, *i.a.* as proportionality coefficients for the Hooke law, with interrelation between these representations devised and stated.

For ferroelectric materials the effect of chemical strains was studied by Morozovska, Golovina *et al.* [189] for K(Ta, Nb)O_3. Here the defect strain tensor has been incorporated into the Landau-Ginzburg-Devonshire theory as the „Vegard strain coefficient“ for defects that accumulate near the surface of a ferroelectric nanoparticle where they influenced polar properties of nanoparticles and the phase transition parameters. To describe it in doped ferroelectrics Vegard's law has been applied, when the source of the defect strain were local changes of defect concentration. Such notation and subsequently the name will be used further in this work.

2. Theoretical Background

The Landau-Ginzburg theory will be used to describe the behaviour of multiferroics. It deals with an expression for the Gibbs free energy that contains terms describing properties of the material, as well as effects that have an impact on the properties.

Theoretical description of the ferroelectrics phenomenon still meets significant difficulties and to this day does not present a general theory that would interpret all experimental facts observed in ferroelectrics. Existing theories can be divided into two essential groups. The first one contains phenomenological theories, which do not assume any specific atomistic model, but are based upon thermodynamic contemplations establishing relations between the physical quantities, characteristic for ferroelectrics. Particularly, the Devonshire theory [38] belongs to this group.

The second group contains theories, which propose a specific atomistic model, suitable only for a particular case, whilst different ferroelectric structures significantly distinguish from each other. The most important models were developed before the ferroelectric phenomenon has been described. The theories given by Slater [195], as well as by Meyer and Vanderbilt [196], Mason and Matthias [197], Rabe and Spaldin [198], especially belong to this group [199]. Here and after we will be considering the phenomenological theory.

2.1. Phase Transitions in Ferroelectrics

In ferroelectrics, at the transition between the polar and nonpolar phases a crystal symmetry change happens. In thermodynamics, phase changes can be described using respective changes of thermodynamic functions. In the thermodynamic contemplations four variables are considered: pressure p, volume V, temperature T as well as entropy S [199].

If a change of the inner energy of the system is denoted as dU, and dW stands for the work done by the system, the first law of thermodynamics can be written as follows:

$$\begin{aligned} dU &= TdS + dW = TdS - pdV, \\ U &= U(S,V). \end{aligned} \tag{2.1.1}$$

The inner energy is a function of two extensive variables S and V. By subtracting the term TS (Legendre transformation) from the inner energy another thermodynamic potential can be introduced, called the Free (or Helmholtz) Energy:

$$\begin{aligned} F &= U - TS; \\ dF &= -SdT - pdV; \\ F &= F(T,V). \end{aligned} \tag{2.1.2}$$

Adding a term pV to the free energy yields the Gibbs free energy of the form:

$$\begin{aligned} &G = F + pV; \\ &dG = -SdT + Vdp; \\ &G = G(T, p). \end{aligned} \tag{2.1.3}$$

The work done by the electric field can be written as

$$dW_e = EdP \tag{2.1.4}$$

The variation of the Gibbs free energy gets the following form:

$$dG = -SdT + Vdp + EdP. \tag{2.1.5}$$

Describing ferroelectric phenomena we assume constant pressure and investigate the expression for a variation of the Gibbs free energy dG linked solely to the temperature change dT, polarization change dP or electric field change dE. We get then:

$$\begin{aligned} &dG = -SdT + EdP, \\ &G = G(T, P). \end{aligned} \tag{2.1.6}$$

At the phase transition temperature $T = T_C$ the Gibbs free energy of the ferroelectric phase A is equal to the free energy of the paraelectric phase B:

$G_A = G_B$.

According to the Ehrenfest classification a phase transition is of n-th order if $G_A = G_B$ and derivatives of (n-1) order of those thermodynamic functions are also equal, whereas n-th derivatives are different from each other. For phase transitions of the 1st order, when n = 1, following relations must be fulfilled:

$$G_A(T_0, P) = G_B(T_0, P) \tag{2.1.7}$$

as well as

$$\frac{\partial G_A}{\partial T} \neq \frac{\partial G_B}{\partial T} \tag{2.1.8}$$

Getting from (2.1.6) while

$$\frac{\partial G_A}{\partial T} = -S_A, \frac{\partial G_B}{\partial T} = -S_B \tag{2.1.9}$$

Using (2.1.8) and (2.1.9) we obtain eventually

$$S_A \neq S_B \tag{2.1.10}$$

and from this

$$S_A - S_B = \Delta S_{AB} = \frac{\Delta Q}{T} \ . \tag{2.1.11}$$

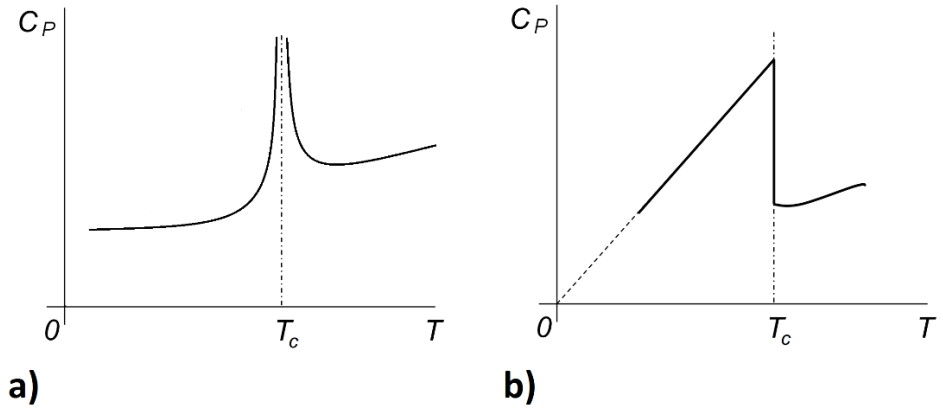

Figure 2.1. Temperature dependency of heat capacity of the crystal for the 1st (a) and the 2nd (b) order phase transitions (adapted from [200]).

Hence it appears, that at the 1st-order phase transitions, an abrupt change of polarization as well as entropy takes place, which is illustrated in Figures. 2.1a and 2.2b. Calculating the second derivative of the Gibbs free energy with respect to the temperature yields

$$\frac{\partial^2 G}{\partial T^2} = \frac{\partial \Delta S_{AB}}{\partial T} = \frac{C_p}{T} \text{ , where } T = T_C \text{ , } C_p \to \infty \qquad (2.1.12)$$

From the equation (2.1.12) it is seen that in case of 1st order phase transitions, the specific heat capacity c_p depending on temperature T shows a discontinuity at the temperature of phase transition and reaches infinitely large values (Figure 2.1a).

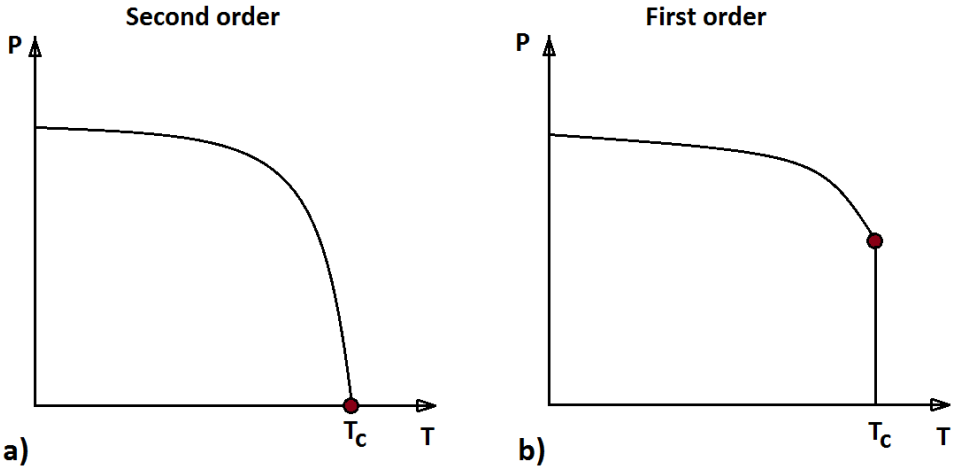

Figure 2.2. Dependence of the spontaneous polarization P_S on temperature for the 2nd (a) and the 1st (b) order phase transitions (adapted from [200]).

For the 2nd order phase transition, when n = 2, at the temperature $T = T_C$ the next relations will be fulfilled:

$$G_A(T,E) = G_B(T,E) = G$$
$$\frac{\partial G_A}{\partial T} = \frac{\partial G_B}{\partial T} \qquad (2.1.13)$$
$$S_A = S_B$$

as well as

$$\frac{\partial^2 G_A}{\partial T^2} \neq \frac{\partial^2 G_B}{\partial T^2}$$
$$\frac{\partial^2 G_A}{\partial T^2} = -\frac{\partial S_A}{\partial T} = -\frac{C_p^A}{T}, \frac{\partial^2 G_B}{\partial T^2} = -\frac{\partial S_B}{\partial T} = -\frac{C_p^B}{T} \qquad (2.1.14)$$
$$C_p^A \neq C_p^B$$

From the equations (2.1.13) and (2.1.14) it appears that in the 2nd order phase transitions entropy and polarization change in continuous way (Figure 2.1b and Figure 2.2a). Heat capacity c_p is a discontinuous function of temperature T, and its course looks similar to the Greek letter lambda λ. Because of this 2nd order phase transitions are also sometimes called λ-transitions.

The majority of ferroelectric crystals show the 2nd order phase transitions at the Curie point. Such transitions occur in Seignette's salt, in the crystals of groups KDP, TGS and others. In barium titanate as well as in isomorphic crystals of this group of ferroelectrics the 1st order phase transition occurs. The Curie point is a special case of the phase transition. Its primary meaning will be discussed in the Elementary thermodynamic theory part. For example, barium titanate has three phase transitions at the temperatures of -90°C, +5°C, and +120°C, but only the last one is the Curie point [199].

2.2. Elementary Thermodynamic Theory

In the thermodynamic theory presented by Devonshire [38], it is postulated that the Gibbs free energy, that does not depend on the polarization direction, can be expressed as

$$G = G_0 + \frac{1}{2}\alpha P^2 + \frac{1}{4}\beta P^4 + \frac{1}{6}\gamma P^6 - PE\,, \qquad (2.2.1)$$

according to the general Landau idea of expansion in terms of the order parameter [33], where α, β and γ are coefficients of the Landau expansion. Assuming that the coefficient α changes sign at temperature T_0 it can be rewritten as $a(T - T_0)$, thus we get

$$G = G_0 + \frac{1}{2}a(T - T_0)P^2 + \frac{1}{4}\beta P^4 + \frac{1}{6}\gamma P^6 - PE\,. \qquad (2.2.2)$$

The first derivative of the Gibbs free energy with respect to polarization defines a value of the electric field E by the relation

$$\frac{\partial G}{\partial P} = a(T - T_0)P + \beta P^3 + \gamma P^5 - E = 0\,, \text{ or}$$
$$E = a(T - T_0)P + \beta P^3 + \gamma P^5 \qquad (2.2.3)$$

being the equation of state of a ferroelectric, whereas the second derivative $\frac{\partial^2 G}{\partial P^2}$ gives us an inverse dielectric susceptibility,

$$\frac{1}{\chi} = \frac{\partial^2 G}{\partial P^2} = a(T - T_0) + 3\beta P^2 + 5\gamma P^4\,. \qquad (2.2.4)$$

Substituting $a = \frac{1}{C}$ and neglecting the terms dependent on polarization we obtain the Curie-Weiss law:

$$\varepsilon_r = \frac{C}{T - T_0}\,. \qquad (2.2.5)$$

According to the Curie-Weiss law, there is a Curie point at the temperature where α changes the sign. It lies in the vicinity of the phase transition temperature, but only at the 2nd order phase transitions the Curie point equals to the transition temperature.

Below the phase transition point, for the electric field $E = 0$, from (2.2.3), we obtain a dependence of square of the spontaneous polarization from temperature as

$$P^2 = \frac{a(T_0 - T)}{\beta} = -\frac{\alpha}{\beta}. \qquad (2.2.6)$$

Depending on the sign of coefficients α, β and γ a first or second order phase transition will occur.

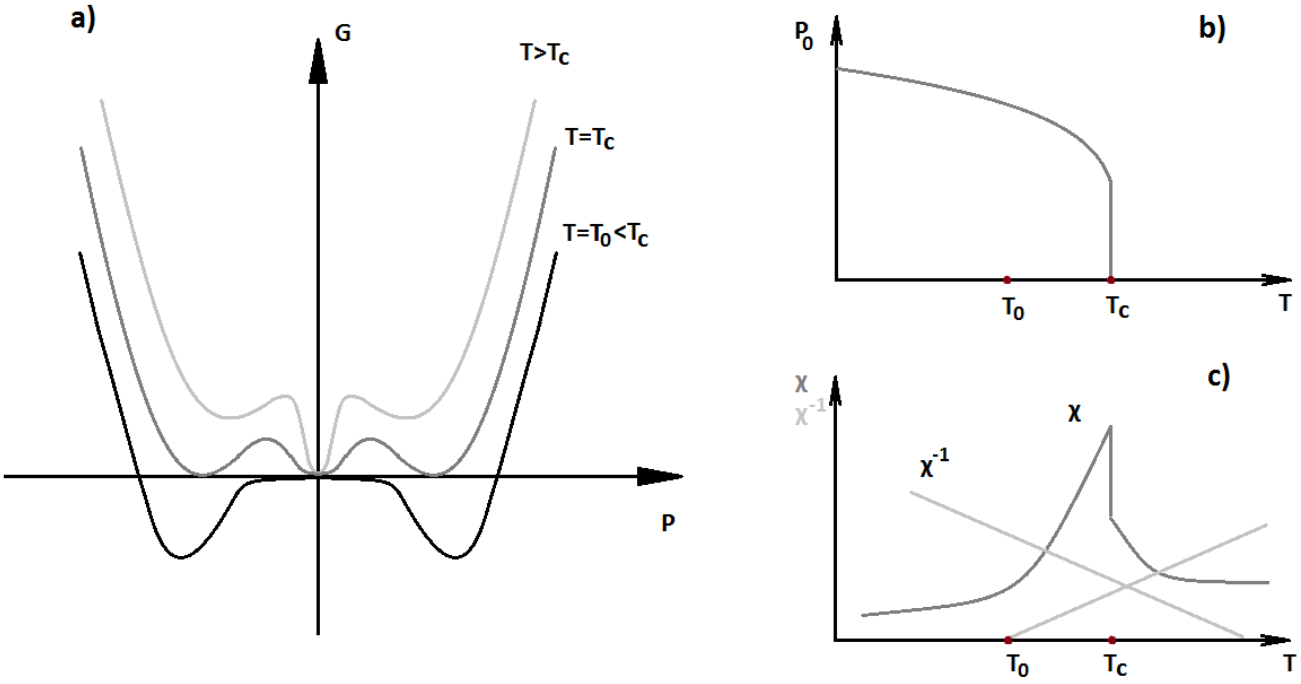

Figure 2.3. a) Dependence of the Gibbs free energy (G) on the polarization, b) of the spontaneous polarization P_S on the temperature, as well as c) of χ and $\chi^{-1} \approx \alpha$ on the temperature for the 1st order phase transition (adapted from [201]).

From the discussion carried out by Devonshire it follows that for the 1st order phase transitions the coefficients of the expansion (2.2.1) must fulfil the following relations at the phase transition point:
$\alpha > 0$, $\gamma > 0$, $\beta < 0$.
Under such an assumption, the Gibbs free energy changes dependent on the polarization P in a way that is presented on the Figure 2.3a. Parameter of the curves on the plot is temperature. In the ferroelectric phase two minima exist correspondent to polarization values of $+P_S$ and $-P_S$. At the phase transition point the curve has three minima characterizing the same energy value. It means that at that temperature the simultaneous existence of two phases is possible: ferroelectric and paraelectric ones. Above the transition point the equilibrium state is paraelectric, for which polarization P_S equals zero. In this case the lowest value of energy corresponds to zero polarization. For the 1st order phase transition, from the equations (2.2.1) and (2.2.3), we obtain relations describing spontaneous polarization and inverse dielectric permittivity (represented from the Curie-Weiss law (2.2.5) by the α coefficient) as functions of coefficients β and γ,

$$P_S^2 = \frac{3}{4}\left(-\frac{\beta}{\gamma}\right) \qquad (2.2.7)$$

as well as

$$\alpha = \frac{3}{16}\frac{\beta^2}{\gamma}. \qquad (2.2.8)$$

Hence, it follows that at the 1st order phase transition, the spontaneous polarization changes in response to the temperature in a discontinuous way (Figure 2.3b).

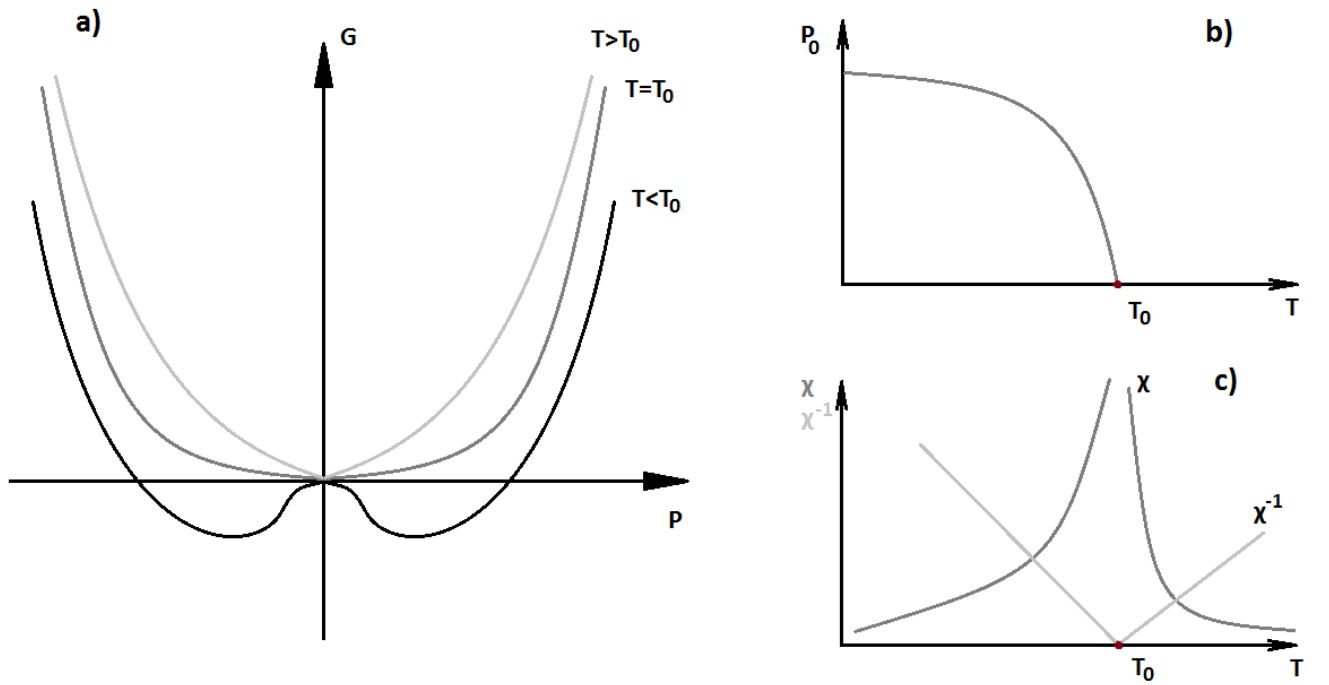

Figure 2.4. a) Dependence of the Gibbs energy on the spontaneous polarization, b) spontaneous polarization P_S on the temperature, as well as c) of χ and $\chi^{-1} \approx \alpha$ on the temperature for the 2nd order phase transition (adapted from [201]).

For the second order phase transitions coefficients in (2.2.1) appear with the next values at the phase transition points:
$\alpha = 0$ (changes sign), $\beta > 0$ and $\gamma > 0$.
Figure 2.4 shows a Gibbs free energy dependence on polarization. In this case at the Curie point, there exists only one free energy value, for which the polarization P_S is equal to zero. Hence, at the 2nd order phase transition we have a continuity of the spontaneous polarization dependency on temperature (Figure 2.4b). Above the Curie point the spontaneous polarization is equal to zero, thus, based on equation (2.2.4) we get the inverse dielectric susceptibility as

$$\frac{1}{\chi} = \left(\frac{\partial^2 G}{\partial P^2} \right)\Bigg|_{P_S=0} = \alpha \ . \tag{2.2.9}$$

Below the Curie point, according to the equations (2.2.4) and (2.2.6) we obtain

$$\left(\frac{\partial^2 G}{\partial P^2} \right)\Bigg|_{P_S\neq 0} = -2\alpha \ . \tag{2.2.10}$$

It follows from this analysis that the ratio of slopes of the function $\frac{1}{\varepsilon} = \frac{1}{\varepsilon}(T)$ above and below the Curie point is equal to -2 (see Figure 2.4c).

On the basis of the Devonshire theory one can predict how the ferroelectric polarization will behave depending on a strength of electric field. From the equation (2.2.3) a dependence $P = P(E)$ can be obtained. Above the Curie point we get a linear dependence, and below the Curie point we have a normal hysteresis loop (Figure 2.5) [199].

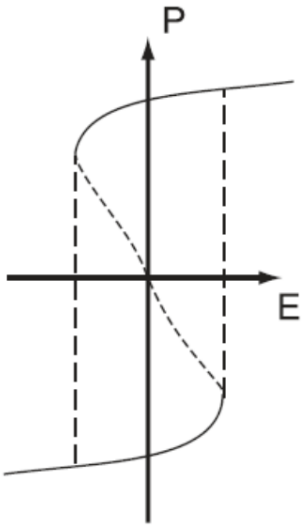

Figure 2.5. Dependence of the spontaneous polarization P_S on the electric field E [200].

2.3. Generalization to Multiaxial Systems

Considered here is a system that consists of a thin ferroelectric film (materials are chosen mainly between barium titanate, lead titanate and PZT) of thickness h ranging between 1 and 200 nm, that is fixed on a metallic electrode (here and after bottom electrode). On the top, a thin film electrode is used to provide a voltage difference (top electrode). This electrode is placed at some distance d_e from the film. If $d_e = 0$, the film is covered by an ideal electrode, its top surface is screened, just as the bottom one. If $d_e > 0$, the top surface is exposed to the ambience, a layer with properties of a linear insulator.

The whole system, thus, can be presented via the subsystem of the bulk, the subsystem of the ambience (dead dielectric layer) and the interface between them. The Gibbs free energy functional for them can be presented as a sum of the bulk G_V, dead layer G_{ext} and surface G_S parts: [publication C1]

$$G = G_V + G_S + G_{ext} \ . \tag{2.3.1}$$

$$G_V = \int_V d^3 r \begin{pmatrix} \frac{\alpha_{ik}}{2} P_i P_k + \frac{\beta_{ijkl}}{4} P_i P_j P_k P_l + \frac{\gamma_{ijklmn}}{6} P_i P_j P_k P_l P_m P_n + \frac{g_{ijkl}}{2} \left(\frac{\partial P_i}{\partial x_j} \frac{\partial P_k}{\partial x_l} \right) - P_i E_i - Q_{ijkl} \sigma_{ij} P_k P_l \\ - \frac{s_{ijkl}}{2} \sigma_{ij} \sigma_{kl} - F_{ijkl} \sigma_{ij} \frac{\partial P_l}{\partial x_k} - \left(W_{ij}^d \delta N_d^+ + W_{ij}^a \delta N_a^- \right) \sigma_{ij} + e\varphi \left(Z_d N_d^+ - Z_a N_a^- - n + p \right) \\ - N_d^+ E_d - N_a^- E_a - T\left(S_d \left[N_d^+ \right] + S_a \left[N_a^- \right] \right) + nE_C + pE_V - T\left(S_{el}[n] + S_h[p] \right) \\ + \frac{3k_B T}{2} \left(N_C F_{3/2} \left(\frac{E_g + e\varphi}{k_B T} \right) + N_V F_{3/2} \left(\frac{E_g - e\varphi}{k_B T} \right) \right) \end{pmatrix}, \tag{2.3.2}$$

$$G_S = \sum_m \int_{Sm} \left(\frac{A_{jk}^m}{2} P_j P_k + d_{jkl}^{Sm} u_{jk}^{Sm} P_l \right) d^2 r \ , \tag{2.3.3}$$

$$G_{ext} = -\int_{\vec{r} \notin V_{FE}} d^3 r \frac{\varepsilon_0 \varepsilon_e}{2} E_i E_i \ . \tag{2.3.4}$$

The designations for the terms in the equations are listed in the Table 2.1. The summation is performed over all repeating indices. Along with coefficients of the Landau expansion and the gradient terms, added are terms describing elastic and semiconductor properties of the material. While the electric part is given

in correspondence to the spontaneous P_i as an order parameter in the Landau expansion, nonzero for the ferroelectric phase and changeable under the applied electric field, the stress variable is responsible for elastic properties, and the concentrations of charge carriers and impurities describe the semiconductor properties. Electromechanical effects relate elastic and polar parts of the potential with correspondent coefficients. Electrostatic part contains terms with electric field $E_i = -\nabla\varphi$ or electrostatic potential φ, with an influence of free electrons and holes with concentrations n and p correspondingly, as well as of donor and acceptor impurities with densities N_d^+ and N_a^-.

Table 2.1. Coefficients, variables and parameters.

Name	Symbol	Units
First Landau coefficient	α_{ik}	mJ/C^2
Second Landau coefficient	β_{ijkl}	$m^5 J/C^4$
Third Landau coefficient	γ_{ijklmn}	$m^9 J/C^6$
Gradient term	g_{ijkl}	$m^3 J/C^2$
Elastic compliance	s_{ijkl}	Pa^{-1}
Elastic stiffness	c_{ijkl}	Pa
Electrostriction tensor	Q_{ijkl}	m^4/C^2
Flexoelectric tensor	F_{ijkl}	m^3/C
Vegard coefficient	W_{ij}	$Å^3$
Electrostatic potential	φ	V
Spontaneous polarization	P_i	C/m^2
Electric field	E_i	V/m
Electron charge	e	C
Elastic stress	σ_{ij}	Pa
Elastic strain	u_{ij}	1
Dielectric permittivity of vacuum	ε_0	F/m
Background dielectric permittivity	ε_b	1
Dead-layer dielectric permittivity	ε_e	1
Electron concentration	n	m^{-3}
Hole concentration	p	m^{-3}
Donor concentration	N_d^+	m^{-3}
Acceptor concentration	N_a^-	m^{-3}
Density of states in conduction band	N_C	m^{-3}
Density of states in valence band	N_V	m^{-3}
Entropy of ionized donors	S_d	J/K
Entropy of ionized acceptors	S_a	J/K
Entropy of electrons	S_{el}	J/K
Entropy of holes	S_h	J/K
Difference between non-equilibrium and equilibrium concentrations.	$\delta N = N - N_0$	m^{-3}
Piezoelectric coefficient	d_{jkl}	m/V

Surface energy coefficient	A_{jk}^m	J/C^2
Temperature	T	K
Band gap	E_g	J
Bottom of conduction band	E_C	J
Valence band maximum	E_V	J
Fermi level	E_f	J
Boltzmann constant	k_B	J/K
Spatial coordinate	x_k	m
Time	t	s
Fermi integral of order k	$F_k(\xi)$	-
Fermi integral of order 1/2	$F_{1/2}(\xi)=\frac{2}{\sqrt{\pi}}\int_0^\infty \frac{\sqrt{\zeta}d\zeta}{1+\exp(\zeta-\xi)}$	
Khalatnikov constant	Γ	Jms/C^2

The problems often deal with the time-development of the order parameter, which is possible to express via kinetic equation [publication A2]. Kinetic equation of state is the Khalatnikov equation $\Gamma\frac{\partial P_i}{\partial t}=-\frac{\partial G}{\partial P_i}$, where the right-hand side results from the first derivative of the Gibbs free energy with respect to polarization (2.2.3) and the left-hand side is the Khalatnikov time-dependent term. The rearranged full form of the equation is named the Landau-Khalatnikov or the time-dependent Landau-Ginzburg-Devonshire equation:

$$\Gamma\frac{\partial}{\partial t}P_k+\alpha_{ik}(T)P_i+\beta_{ijkl}P_i\,P_j\,P_l\,+\gamma_{ijklmn}P_i\,P_j\,P_l\,P_m P_n\,-g_{ijkl}\left(\frac{\partial^2 P_i}{\partial x_j\partial x_l}\right)-2Q_{klij}\sigma_{ij}P_l+F_{ijkl}\frac{\partial\sigma_{ij}}{\partial x_l}=-\frac{\partial\varphi}{\partial x_k}$$

(2.3.5)

The surface part of the Gibbs free energy (2.3.3) turns into boundary conditions for the LGD equation:

$$\left(g_{ijkl}\frac{\partial P_i}{\partial x_j}+A_{jk}^m P_j-F_{ijkl}\sigma_{ij}\right)\Big|_{x_3=h}=0,\ \left(g_{ijkl}\frac{\partial P_i}{\partial x_j}-A_{jk}^m P_j-F_{ijkl}\sigma_{ij}\right)\Big|_{x_3=0}=0 \qquad (2.3.6)$$

The electrostatic part can be expressed via the Poisson equation for the electrostatic potential:

$$\varepsilon_0\varepsilon_{ii}^b\frac{\partial^2\varphi}{\partial x_i^2}=\frac{\partial P_j}{\partial x_j}-e\left(Z_d N_d^+(\varphi)-Z_a N_a^-(\varphi)+p(\varphi)-n(\varphi)\right). \qquad (2.3.7)$$

Here ε_{ii}^b is a part of the dielectric permittivity which is not linked to the spontaneous polarization and represents solely the lattice contribution into the permittivity. When considering a ferroelectric medium, there is the spontaneous polarization present, and the permittivity ε_{ii}^b is assumed to be an isotropic background permittivity ε_b. If the film possesses semiconducting properties, the term of a space charge density is also present. Describing the dead dielectric layer, we must bear in mind the absence of the spontaneous polarization and semiconductor properties, while the permittivity ε_{ii}^b is the isotropic permittivity of a linear dielectric ε_e, which brings us a simpler equation:

$$\varepsilon_0\varepsilon_e\frac{\partial^2\varphi}{\partial x_i^2}=0 \qquad (2.3.8)$$

Boundary conditions for these equations should be:

$$\varphi\big|_{x_3=0}=0,\ \left(D_n^{ext}-D_n^{\text{int}}+\varepsilon_0\frac{\varphi}{\lambda}\right)\Bigg|_{x_3=h}=0,\ \left(\varphi^{ext}-\varphi^{\text{int}}\right)\big|_{x_3=h}=0,\ \varphi\big|_{x_3=h+d_e}=U. \tag{2.3.9}$$

Here D_n is the normal part of the electric displacement, U is voltage applied to the top electrode, and $\frac{\varepsilon_0\varphi}{\lambda}=\Sigma$ is the Bardeen surface screening (BS), characterized by a parameter of the screening length λ. However, the exact form of the expression for the surface screening charge depends on the chosen model. If we choose the Fermi-Dirac model (FD) representing screening by free carriers on the surface, we shall consider this charge being equal to

$$\Sigma_0[\varphi]=e\left(p_{2D}(\varphi)-n_{2D}(\varphi)\right), \tag{2.3.10}$$

where concentrations of holes and electrons on the surface p_{2D} and n_{2D} are given on the right-hand side. If we instead consider that the surface screening is caused by surface ions, the charge can be described with the Stephenson-Highland model (SH):

$$\Sigma_0[\varphi]=\sum_i\frac{eZ_i\theta_i(\varphi)}{A_i}\equiv\sum_i\frac{eZ_i}{A_i}\left(1+q_i\exp\left(\frac{\Delta G_i^{00}+eZ_i\varphi}{k_BT}\right)\right)^{-1}. \tag{2.3.11}$$

This model can operate with different types of surface ions with different charges Z_i, saturation densities $1/A_i$, and the factor $q_i=\left(\frac{p_{atm}}{p_{exc}}\right)^{1/n_i}$ where p_{exc} is a partial pressure of ambient gas relative to the atmospheric pressure p_{atm} and n_i is the number of surface ions created by one gas molecule. ΔG_i^{00} are the standard free energies of the surface ion formation at $p_{exc}=1$ bar and $U=0$.

To deal with elastic properties of the material, we can express them via the generalized Hooke law,

$$u_{ij}=s_{ijkl}\sigma_{kl}+F_{ijkl}\frac{\partial P_k}{\partial x_l}+W_{ij}^d\left(N_d^+-N_{d0}^+\right)+W_{ij}^a\left(N_a^--N_{a0}^-\right)+Q_{ijkl}P_kP_l\ , \tag{2.3.12}$$

where all relevant electromechanical and chemical-pressure effects are taken into account. For ferroelectrics with a cubic parent phase, piezoelectric effect is hidden within the electrostriction term, as $d_{ijk}=2\varepsilon_0\chi_{km}Q_{ijml}P_l$, since $P_k^{total}\approx P_k+\varepsilon_0(\chi_{km})E_m$, where χ_{km} is a full dielectric susceptibility [publication A1]. Note that there is the full stress considered as a variable, rather than spontaneous excessive strain featured in phase-field models such as [202, 203]. The electrostriction term with quadratic dependence of strain on polarization in (2.3.12) contains interrelations between the spontaneous polarization and spontaneous strain/stress in the tetragonal structure [204].

The equilibrium condition for the mechanical subsystem reads:

$$\frac{\partial\sigma_{ij}}{\partial x_i}=0 \tag{2.3.13}$$

with boundary conditions:

$$\left(U_1-x_ju_m\right)\big|_{x_3=0}=0,\ U_3\big|_{x_3=0}=0,\ \sigma_{ij}n_j\big|_{x_3=h}=0, n_j=(0,0,1) \tag{2.3.14}$$

which define the top surface as mechanically free, and the bottom surface having the fixed strain. u_m stands for the misfit strain, appearing as a result of the difference between lattice parameters of the film and the substrate on top of which it is fixed. Strains at the film interfaces can support a certain direction of polarization [publication B1]. Flexoelectric effect is presented as a part of the complex term that has a full form of [2, 205, 206, 207]:

$$\frac{F_{ijkl}}{2}\left(P_k\frac{\partial\sigma_{ij}}{\partial x_l}-\sigma_{ij}\frac{\partial P_k}{\partial x_l}\right)+\frac{\nu_{ijklmn}}{2}\left(\frac{\partial\sigma_{ij}}{\partial x_m}\frac{\partial\sigma_{kl}}{\partial x_n}\right), \quad (2.3.15)$$

where the second part is the elastic gradient, omitted due to the yet undecided and unclear properties and values of the coefficients [publication B1]. The remaining Lifshitz invariant is used in the simplified form of $F_{ijkl}\left(\sigma_{ij}\frac{\partial P_k}{\partial x_l}\right)$ in the free energy expression, since such change does not affect the equation of state while improving the convergence of the modelling calculations.

The Vegard effect is taken into account via corresponding terms in the generalized Hooke law that denote dependency of strain on non-equilibrium concentration of different types of defects.

$$u_{ij} = s_{ijkl}\sigma_{kl}(r) - W_{ij}^{d}\left(N_d(r) - N_{d0}\right) - W_{ij}^{a}\left(N_a(r) - N_{a0}\right). \quad (2.3.16)$$

Here the case with two defect types is considered with one being donors (typically, oxygen vacancies) and another being acceptors (typically, defect ions), although it can be more than two or only one term. Vegard coefficients here denote a proportionality of strain to the difference between the actual local concentration of defects and the intrinsic equilibrium concentration, at which the system is relaxed, and chemical strains are not produced.

2.4. Finite Element Method

The stated problem contains a system of complex partial differential equations that cannot be solved analytically. Thus, numerical methods have to be used to solve them, and namely the finite-element method (FEM) as the most suitable for it. Specialized software which has been used to perform the computer modelling, COMSOL and MatLab, uses this method for obtaining the solutions.

The finite-element method allows numerical calculation of functional variable distributions through a selected domain by splitting it into a number of small finite elements for each of which the differential equation is solved. It is widely used to solve applied physics problems involving fluid dynamics, heat transfer, mechanics of solids, electromagnetic potentials and many more. The mentioned problems all deal with partial differential equations (PDEs) possessing boundary conditions thus making up a variation analysis problem. The complexity of specific equations often does not allow one to solve them analytically, so that only numerical approximated solutions seem viable and attainable. The FEM method was first formulated in 1940-s by Richard Courant [208] and Alexander Hrennikoff [209], however it was not before the advent of modern computers and advanced computing techniques that this method has gained so wide usage. The process of obtaining a set of solutions using FEM is sometimes referred to as Finite Element Analysis (FEA).

The main principle can be illustrated as follows, using a simple 1D case as an example. Consider a function u taking a role of a dependent variable in a PDE, *i.e.* the variable that is changing over the range of some other, independent variables (in the aforementioned problems the independent variables are almost exclusively spatial and/or temporal coordinates). The function u can be approximated by a linear combination of basis functions u_h so that

$$u \approx u_h;$$
$$u_h = \sum_i u_i \psi_i \quad (2.4.1)$$

where ψ_i are basis functions and u_i is the set of coefficients for each function that approximates u_h to u. The basis functions can be chosen differently, for example equal to 1 at their corresponded nodes and equal to 0 elsewhere. For each finite element there is its own basis function. In Figure 2.6(a) an example is shown for an approximated dependent variable distribution over the *x* axis split into seven

elements defined by piecewise linear basis functions. In the engineering this can correspond to heat transfer in a nonuniformly heated rod with the dependent variable being its temperature and the independent being the spatial coordinate. The elements of the solution can be distributed uniformly or nonuniformly with difference between the nodes (Figure 2.6(b)). The latter case is the most commonly used since it provides a great variety of detailing options. Namely, the part of the continuum with the largest gradient receives smaller elements in bigger amounts to show more points at the specified area whereas the areas with the least changes can have more coarse representation with larger elements. In the examples, elements are represented by linear basis functions being nonzero along a narrow interval and overlapping along the *x* axis, however when needed they can be replaced by nonlinear functions. [210] In n-dimensional case basis functions have more complex geometric shape corresponding to problem's dimensionality. In the considered problems, quadratic basis functions were used.

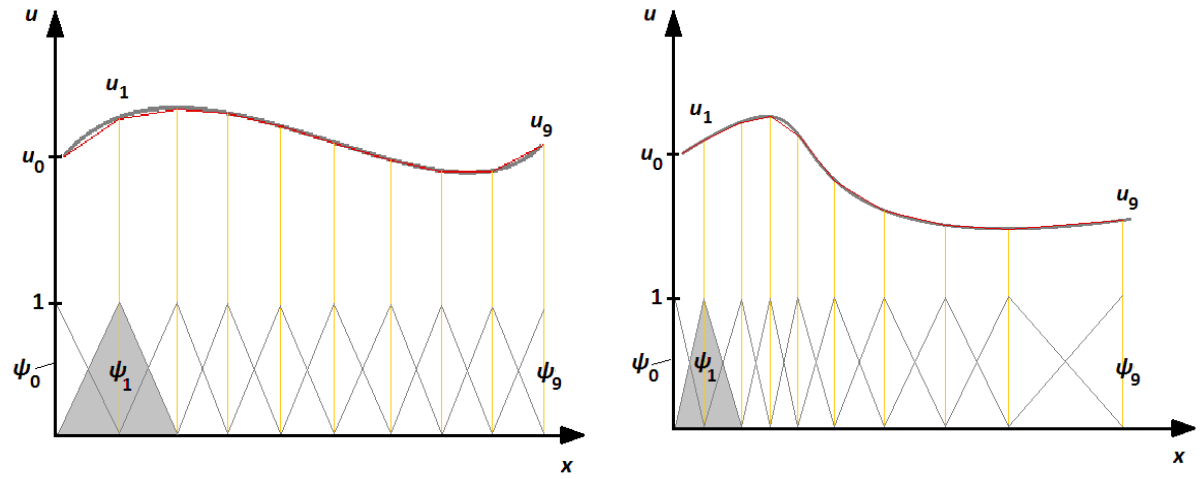

(a) (b)

Figure 2.6. The distribution of the function u (thick grey line) approximated with u_h (red line), which is a combination of the linear basis functions (thin grey lines) with coefficients u_0 through u_9 for each finite element. The distribution of elements can be uniform (a) or nonuniform (b) (adapted from [210]).

A standard and typical sequence of steps using FEM for solving a PDE problem for a certain domain includes:
1) Dividing the problem domain into a set of subdomains and subdomains into a set of finite elements. Each element is described by the element equations for the original problem. These equations are meant to locally approximate the original equations. The approximation is often explained as a process of construction of an integral of the inner product of the residual and the weight functions which is then set to zero, *i.e.* fitting trial functions to the initial equation to minimize the error. The weight functions here are the polynomial approximation functions projecting the residual: the error caused by trial functions. As a result, PDE gets rid of spatial derivatives and locally approximates to element equations in the forms of either ordinary differential equations (ODE) or algebraic equations for cases of the steady state. The element equations are then solved numerically, using methods appropriate to the equation type.
2) Recombination of all sets of element equations to generate a global system of equations. It is done via the transformation of coordinates for local nodes in subdomains into global nodes of the domain with any necessary adjustments by orientation and offset regarding the coordinate systems. The resulting global equation system can be calculated from known initial conditions using chosen computation methods.

3. Results and Publications

In this chapter, the specific problems and challenges from among those listed previously are addressed via phenomenological modelling calculated by means of finite-element method software.

Ferroelectric films can serve as basic model objects for fundamental researches of domain structures and field-induced polarization reversal processes. From the introduction chapter, it follows that there exist surface screening charges, flexocoupling, and defect-driven strains that influence properties of the films. The struggle to optimize and control polar and electrostatic properties of ferroelectrics for their usage in the miniaturized electronic devices dictated the necessity to assess the effects in question and their interaction, as well as provide their high-precision evaluation through the theoretical and numerical description.

Researches comprising this thesis are dedicated to different aspects of the same problem. Considered are static characteristics of a thin film, like domain structure parameters and phase stability, which are important when the films are used in piezoelectric devices, as well as dynamic properties, namely switching kinetics and hysteresis loop dynamics, that are crucial in characterizing ferroelectric materials and for their use in ferroelectric memory devices.

The system described by the equations (2.3.1)-(2.3.4) can be represented as a ferroelectric film, grounded by a conductive electrode from one side (the bottom) and having an interface with ambience from the opposite side (the top). Surface charges are enacted on the top surface, mimicking the surface states or a semiconducting electrode. The perfect electrode can also be applied at the top surface, in which case it can be put either directly on the surface or left above it, creating a gap. When left without the top electrode the system is tuned to study domain properties and phase transition behaviour. When the top electrode is applied, parameters of ferroelectric switching, being reversal kinetics and hysteresis loops properties, are studied.

The Landau-Khalatnikov model described in the theory chapter is the mean of analytical description of the problem. As a result of minimizing the free Gibbs energy a complex Euler-Lagrange equation arises which in our case can only be solved numerically to obtain quantitative results. This approach is sufficient for the scales of interest (10-100 nm) and requires a method to obtain distributions of physical quantities throughout a continuous bulk. Finite element method was chosen as such that allows to make up the whole distribution picture from a set of local values corresponding to characteristics.

3.1. Considered Problems

In the section “Generalization to multiaxial systems” a general case is considered covering the whole range of the problems that will be discussed in the next sections. Before, however, we have to establish the unambiguous problem statements for each studied case. Investigated are primarily the influence of the flexoelectric effect, surface charges and the Vegard strains on the polar state of a ferroelectric, and so all problem statements either consider or disregard each of these effects individually. In the following, all these particular cases will be explained in detail.

A. Flexoelectric Impact

In this set of problems, the effects of flexocoupling are looked into in detail. Static and dynamic characteristics of the ferroelectric film are studied.

A1. Flexocoupling impact on size effects of piezoresponse and conductance in mixed-type ferroelectric semiconductors under applied pressure.

[A.N. Morozovska, E.A. Eliseev, Y.A. Genenko, I.S. Vorotiahin, M.V. Silibin, Y. Cao, Y. Kim, M.D. Glinchuk, and S.V. Kalinin, Flexocoupling impact on the size effects of piezo-response and conductance in mixed-type ferroelectrics-semiconductors under applied pressure, Phys. Rev. B 94 (2016) 174101]

A thin ferroelectric film (1-60 nm) is considered, fixed on the bottom electrode and with the top electrode being a tip of the SPM probe with the radius much larger than the observed film domain (Figure 3.1). Among the effects of interest, flexoelectricity is considered, as well as semiconductor properties of electrons and positively charged donors, and Vegard effect for donors, because the latter are able to move and redistribute. Moreover, the mechanical pressure of the electron gas is also taken into account, so the term $\Sigma_{ij}^{e}\delta n$ with the electron deformation potential tensor and nonequilibrium part of the electron density is added to the Vegard term in (2.3.1) and (2.3.12) instead of the acceptor part. Furthermore, the external stress is applied to the film by the SPM probe, contributing to stresses. Surface screening charges are not studied here.

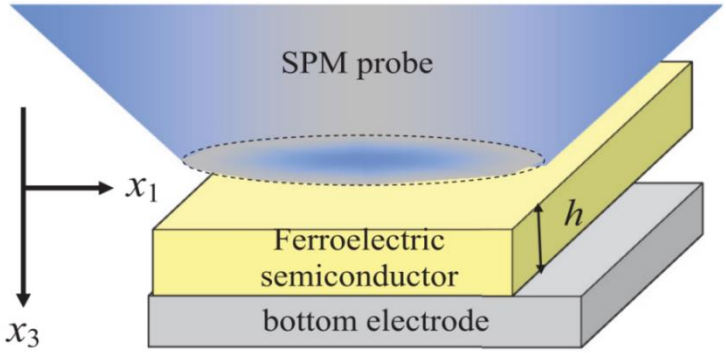

Figure 3.1. Geometry of the problem.

The goal is to find thickness dependencies of the spontaneous polarization, effective piezoresponse, elastic strain and compliance, carrier concentration and piezoconductance and explore their dependence on the pressure applied and on the flexoelectric effect and Vegard effect presence.

A2. Flexocoupling impact on the kinetics of polarization reversal
[I.S. Vorotiahin, A.N. Morozovska, E.A. Eliseev, and Y.A. Genenko, Flexocoupling impact on the kinetics of polarization reversal, Phys. Rev. B 95 (2017) 014104]

A thin ferroelectric film (10-100 nm) is considered, fixed on the bottom conductive electrode and covered with the top film electrode. The presence of the top electrode is assumed as an ideal screening suppressing the multi-domain structure, and thus only an out-of plane polarization remains making this problem effectively one-dimensional. The out-of-plane spontaneous polarization is first relaxed to the self-established equilibrium value and then, by applying voltage upon the top electrode is switched to the field-induced state. Here considered were flexoelectric effect, semiconductor properties of donor ions and electrons with Vegard effect term for donors. As all surfaces are perfectly screened, there were no need to introduce surface charges.

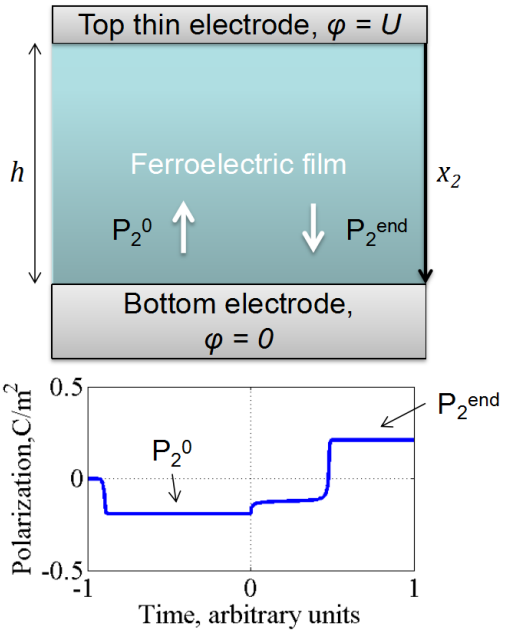

Figure 3.2. Geometry of the problem and an illustration of the switching process.

The objective here is to find distributions of polarization, electric potential and concentrations of donors and electrons as functions of the spatial coordinate and time. Obtained switching curves for polarizations illustrate activation character of the switching process with parameter dependence of the critical switching field and the characteristic switching time on flexoeffect existence and strength.

B. Surface Screening Effect

In this set of problems one of the crucial roles is played by surface screening charges that alone or in the competition with other effects impact the domain formation process or ferroelectric switching.

B1. Tuning the polar states of ferroelectric films via surface charges and flexoelectricity

[I.S. Vorotiahin, E.A. Eliseev, Q. Li, S.V. Kalinin, Y.A. Genenko, and A.N. Morozovska Tuning the Polar States of Ferroelectric Films via Surface Charges and Flexoelectricity, Acta Mater. 137 (2017) 85-92]

A thin ferroelectric film (6-110 nm) is considered, fixed on the bottom ideally-conductive electrode and exposed to the ambience from the top, from which charges are collected on the surface forming an extra-thin surface charge layer with variable screening. Under these conditions, domain structure is formed during the relaxation stage that minimizes the Gibbs free energy. Flexoelectric effect is considered, and its competition with the surface charges in the domain structure formation is the main topic of interest.

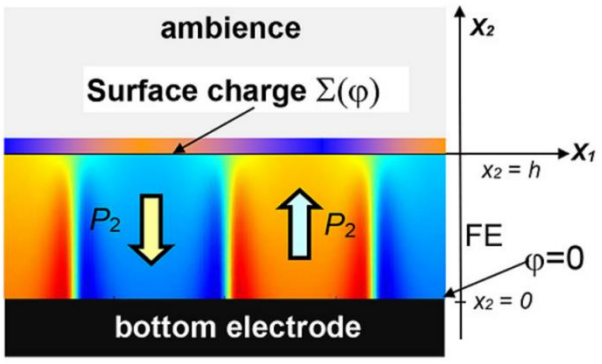

Figure 3.3. Geometry of the problem.

The goal here is to establish the influence of the surface screening and flexoelectric effect on the phase transition parameters (temperature and critical thickness) and on the domain structure judged on by distributions of polarization components, electrostatic and mechanical quantities over the film layer.

B2. Control of polarization hysteresis temperature behaviour by interfacial screening in thin ferroelectric films

[A.N. Morozovska, E.A. Eliseev, I.S. Vorotiahin, M.V. Silibin, S.V. Kalinin and N.V. Morozovsky, Control of Polarization Reversal Temperature Behaviour by Surface Screening in Thin Ferroelectric Films, Acta Mater. 160 (2018) 57-71]

A thin ferroelectric film (3.6-100 nm) is considered, fixed on the conducting bottom electrode, with an electrode over the top surface, separated by a thin dead layer. There is a thin charged layer on the top surface of the film that is considered within the framework of three different screening models: linear Bardeen model, when screening charges are formed from surface impurities, Fermi-Dirac model, when screening is performed by the positive and negative charge carriers distributed over the surface, and Stephenson-Highland (SH) model, when the surface screening is caused by ions on the surface. The mechanical and electromechanical parts of the system are entirely disregarded; considered are only electrostatic properties of the film.

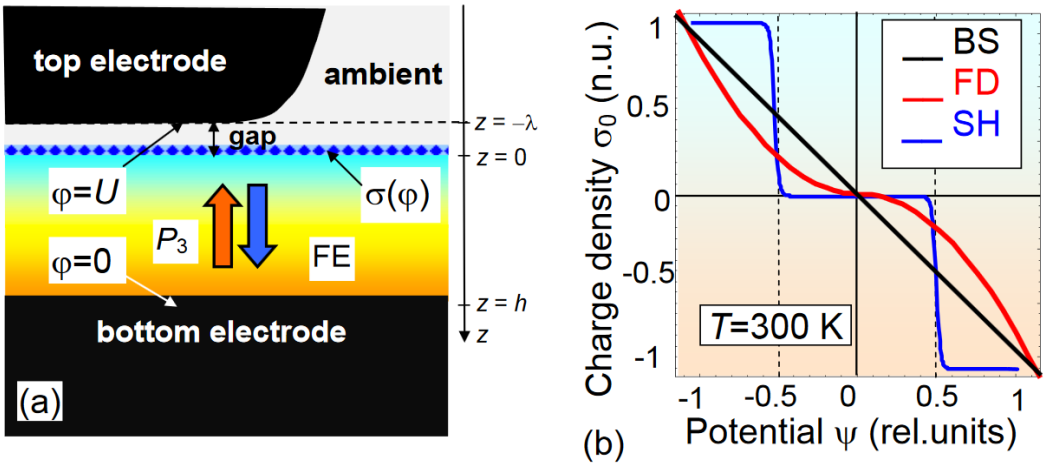

Figure 3.4. Problem geometry and the potential-dependent charge density for three different models of the surface screening.

The objective is to investigate the distortion imposed by the surface screening taking into account according to the three above mentioned models with partially varying parameters on the polarization hysteresis curves for a set of temperatures and thicknesses, as well as on the correspondent free energy profiles.

C. Polar Properties Control via Chemical Strains

The concluding part features the problem where all three effects of interest are included, studying their competing influence on the domain structure properties and phase diagrams of the ferroelectric film.

C1. Defect-driven flexochemical coupling in thin ferroelectric films

[E.A. Eliseev, I.S. Vorotiahin, Y.M. Fomichov, M.D. Glinchuk, S.V. Kalinin, Y.A. Genenko, and A.N. Morozovska. Defect driven flexo-chemical coupling in thin ferroelectric films Phys. Rev. B 97 (2018) 024102]

A thin ferroelectric film (1-170 nm) is considered, fixed on the bottom electrode and exposed to the ambience from the top. Charges are collected from the ambience and form a screening layer on the

surface with a varying charge. Under the top surface a layer of the variable thickness is filled with isovalent defects that form a concentration profile. These are non-charged point elastic defects with no prescribed electric interaction. Flexoelectric effect is considered, however the semiconductor properties of the film are not.

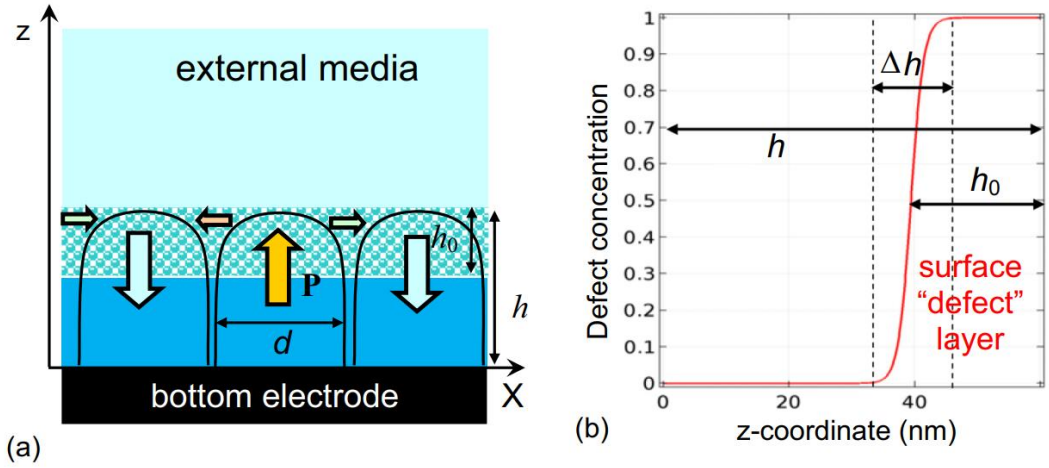

Figure 3.5. Problem geometry and the depth-dependent distribution of the elastic defects with 1 corresponding to the maximum defect concentration in arbitrary units.

The goal here is to find out the influence of the elastic point defects via the Vegard effect and subsequently flexoelectricity and other coupled electromechanical effects on the domain structure properties (distribution of polarization component, electrostatic and mechanical properties, domain dimensions) and phase transition properties (Curie point, critical thickness). Surface screening should play a competing role to the Vegard strains in this study.

3.2. Author's Contributions to the Publications

Publication **A1** is a joint research suggested by Dr. Morozovska and Prof. Dr. Genenko, who also performed analytical calculations. The author (I.S.V.), jointly with Dr. Eliseev, performed all numerical calculations presented in the paper. All other co-authors (Dr. M.V. Silibin, Dr. Y. Cao, Dr. Y. Kim, Prof. M.D. Glinchuk, and Prof. S.V. Kalinin) contributed to the results discussion and manuscript improvement.

In the work **A2,** the numerical calculations and the analysis have been performed by the author, under the supervision of Prof. Dr. Genenko. The idea for the study came from Prof. Dr. Genenko and Dr. Morozovska. Dr. Eliseev, Dr. Morozovska and Prof. Dr. Genenko contributed to the results discussion.

In the publication **B1**, the author performed all FEM modeling and densely contributed to the analysis of its results, supervised by Prof. Dr. Genenko. The idea of the research was given by Prof. Dr. Genenko and Dr. Morozovska, who formulated the theoretical background. The improvements of the FEM-model and its stability were made by Dr. Eliseev and Dr. Li, who are gratefully acknowledged.

The idea for the research in the publication **B2** belongs to Dr. Morozovska, who also has formulated the theory and performed analytical calculations. Dr. Eliseev and the author jointly performed numerical modeling. All other co-authors (Dr. Silibin, Prof. Kalinin and Prof. Morozovsky) contributed to the results discussion and manuscript improvement.

In the publication **C1**, the author performed most for the FEM calculations of the defected film (jointly with Dr. Eliseev and Y. Fomichov) and analysis of the FEM results, prepared illustrations, supervised by Dr. Morozovska and Prof. Dr. Genenko. The problem statement was suggested by Dr. Morozovska.

Results analysis and manuscript improvement was performed by Prof. Dr. Genenko, Prof. Glinchuk, and Prof. Kalinin.

3.3. Publication A1

Flexocoupling impact on size effects of piezoresponse and conductance in mixed-type ferroelectric semiconductors under applied pressure

Anna N. Morozovska, Eugene A. Eliseev, Yuri A, Genenko, Ivan S. Vorotiahin, Maxim V. Silibin, Ye Cao, Yunseok Kim, Maya D. Glinchuk, and Sergei V. Kalinin

Physical Review B 94, 174101 (2016). 10 pages, with Supplementary materials, 10 pages.

Flexocoupling impact on size effects of piezoresponse and conductance in mixed-type ferroelectric semiconductors under applied pressure

Anna N. Morozovska,[1,*] Eugene A. Eliseev,[2] Yuri A. Genenko,[3,†] Ivan S. Vorotiahin,[1,3] Maxim V. Silibin,[4] Ye Cao,[5] Yunseok Kim,[6] Maya D. Glinchuk,[2] and Sergei V. Kalinin[5,‡]

[1]*Institute of Physics, National Academy of Sciences of Ukraine, 46, Prospekt Nauky, 03028 Kyiv, Ukraine*
[2]*Institute for Problems of Materials Science, National Academy of Sciences of Ukraine, Krjijanovskogo 3, 03142 Kyiv, Ukraine*
[3]*Institut für Materialwissenschaft, Technische Universität Darmstadt, Jovanka-Bontschits-Strasse 2, 64287 Darmstadt, Germany*
[4]*National Research University of Electronic Technology "MIET", building 1, Shokin Square, 124498 Moscow, Russia*
[5]*The Center for Nanophase Materials Sciences, Oak Ridge National Laboratory, Oak Ridge, Tennessee 37831, USA*
[6]*School of Advanced Materials Science and Engineering, Sungkyunkwan University (SKKU), Suwon 16419, Republic of Korea*

(Received 18 May 2016; revised manuscript received 31 August 2016; published 2 November 2016)

We explore the role of flexoelectric effect in functional properties of nanoscale ferroelectric films with mixed electronic-ionic conductivity. Using a coupled Ginzburg-Landau model, we calculate spontaneous polarization, effective piezoresponse, elastic strain and compliance, carrier concentration, and piezoconductance as a function of thickness and applied pressure. In the absence of flexoelectric coupling, the studied physical quantities manifest well-explored size-induced phase transitions, including transition to paraelectric phase below critical thickness. Similarly, in the absence of external pressure flexoelectric coupling affects properties of these films only weakly. However, the combined effect of flexoelectric coupling and external pressure induces polarizations at the film surfaces, which cause the electric built-in field that destroys the thickness-induced phase transition to paraelectric phase and induces the electretlike state with irreversible spontaneous polarization below critical thickness. Interestingly, the built-in field leads to noticeable increase of the average strain and elastic compliance in this thickness range. We further illustrate that the changes of the electron concentration by several orders of magnitude under positive or negative pressures can lead to the occurrence of high- or low-conductivity states, i.e., the nonvolatile piezoresistive switching, in which the swing can be controlled by the film thickness and flexoelectric coupling. The obtained theoretical results can be of fundamental interest for ferroic systems, and can provide a theoretical model for explanation of a set of recent experimental results on resistive switching and transient polar states in these systems.

DOI: 10.1103/PhysRevB.94.174101

I. INTRODUCTION

Ferroelectric materials have long remained the focus of theoretical and experimental research due to their unique functional properties. These include strong electromechanical coupling that enables applications in sensors and actuators [1], and the presence of equivalent polar states that enable multiple types of ferroelectric memories [2,3]. In the past 10 years, much attention has been focused on the multiferroic materials combining ferroelectric and magnetic functionalities [4,5]. Finally, in the last several years, the attention of the condensed matter physics and materials community has been riveted to applications combining ferroelectric, ionic, and electronic functionalities of these materials [6–10]. Consequently, investigation of electromechanical, electrochemical, and electrophysical properties of nanosized ferroelectric semiconductors with mixed-type ionic-electronic conductivity (FeMIECs) is of significant interest for both fundamental science and numerous applications. Although FeMIECs in the form of thin films and nanocomposites are among the most promising MIEC materials for the next generation of nonvolatile, resistive and memristive memories, logic devices, ultrasensitive sensors, miniature actuators, and positioners [11–13], the physical principles of the complex interplay between the ferroelectric polarization, elastic strains, and ionic and electronic states at the nanoscale are not clear so far. This lack of physical understanding precludes the successful implementation of FeMIECs in the aforementioned applications.

Furthermore, the emergence of scanning probe microscopy tools has made the studies of coupled electromechanical and conductive phenomena nearly routine. Multiple studies of electromechanical responses (*piezoresponse*) by electrochemical strain microscopy [14–16] and piezoresponse force microscopy (PFM) [17] and local conductivity by current atomic force microscopy (CAFM) [18] and related techniques [19–22] revealed that their electroconductance is strongly coupled with polar and elastic states. Moreover, both scanning probe microscopy (SPM) and interferometric measurements with high subnanometer resolution indicate the important role of the local gradients of polarization, strain, and space charge density in the formation of the aforementioned local response [14–18]. The local gradient of polarization induces elastic strain, and vice versa, the gradient of elastic stress induces an electric field due to flexoelectric coupling (*flexocoupling*) [23,24]. The gradients inevitably cause the space charge redistribution in MIECs and FeMIECs via several mechanisms [25,26], including electromigration and diffusion [27,28], chemical strains and stresses [13,29,30], and deformation potential [31,32]. Generally, these effects are strongly coupled in a ferroelectric and cannot be separated *a priori*. However, the following important aspects should be mentioned.

*anna.n.morozovska@gmail.com
†genenko@mm.tu-darmstadt.de
‡sergei2@ornl.gov

One important aspect of material behavior on the nanoscale is the emergence of flexoelectric coupling [33,34]. The strong strain gradients are inevitably present near the surfaces, in thin films [35–37], nanoparticles [38], and fine-grained ceramics [39,40]. Therefore the role of flexocoupling in the formation of piezoresponse and piezoconductance can essentially increase due to the intrinsic size effects, which become pronounced when the thickness of investigated FeMIEC film becomes less than 50 nm. While the role of flexoeffect in SPM measurements has been discussed as early as 2006 [41,42], recently it has become a mainstream explanation for a broad set of functional observations. While very significant doubts have been raised [43], it remains an important aspect of these systems.

The second important aspect of ferroelectricity in the nanoscale systems is the ferroelectric size effect. The intrinsic size effect in thin ferroelectric films manifests as the disappearance of ferroelectric phase when the film thickness becomes smaller than the critical thickness [44]. The critical thickness depends on the polarization direction, correlation length, surface energy contribution, and electrical and mechanical conditions at the film surfaces [45–48]. Here, the surface energy determines the value of the so-called extrapolation lengths [45]. The depolarization field is originated from nonzero divergence of the polarization vector, as well as from the incomplete screening of the polarization bound charges by the electrodes [45,48]. Elastic strains are caused by, e.g., film and substrate lattice mismatch [46,47]. All these factors, which are closely related to the surface influence, often lead to the appearance of a developed polarization gradient from the film surface towards its center. Note that in the comprehensive description the polarization gradient induces elastic strain due to the flexoelectric coupling, suggesting the potential interplay between the two.

Finally, the third aspect of thin-film behavior is the surface piezoelectric effect caused by inversion symmetry breaking in the direction normal to the surface. The surface piezoeffect coupled with misfit strain leads to the appearance of a built-in electric field that in turn destroys the size-induced phase transition into a paraelectric phase at the critical thickness and induces the electretlike state with irreversible polarization at film thickness less than the critical one [46,47].

These considerations necessitate the theoretical modeling of the flexocoupling impact on the size effects of the spontaneous polarization, effective piezoresponse, elastic strain and compliance, carrier concentration, and piezoconductance in thin films of FeMIECs under applied pressure. Here we analyze these phenomena in the framework of the Landau-Ginzburg-Devonshire (LGD) theory [25–27,38,49,50].

II. PROBLEM STATEMENT AND BASIC EQUATIONS

The generalized expression for the LGD-type Gibbs potential of the spatially confined ferroelectric mixed-type semiconductors, which is the sum of the bulk (G_V) and surface (G_S) parts, has the following form [26,51]:

$$G_V = \int_V d^3r \begin{Bmatrix} \frac{a_{ik}}{2} P_i P_k + \frac{b_{ijkl}}{4} P_i P_j P_k P_l + \frac{g_{ijkl}}{2}\left(\frac{\partial P_i}{\partial x_j}\frac{\partial P_k}{\partial x_l}\right) - P_i E_i - Q_{ijkl}\sigma_{ij} P_k P_l - \frac{s_{ijkl}}{2}\sigma_{ij}\sigma_{kl} \\ -F_{ijkl}\sigma_{ij}\frac{\partial P_l}{\partial x_k} - \left(\Sigma^e_{ij}\delta n + W^d_{ij}\delta N_d^+\right)\sigma_{ij} + e\varphi(Z_d N_d^+ - n) \\ -N_d^+ E_d - T S_d[N_d^+] + nE_C - T S_{el}[n] + \frac{3k_B T}{2} N_C F_{3/2}\left(\frac{E_g + e\varphi}{k_B T}\right) \end{Bmatrix}, \tag{1a}$$

$$G_S = \sum_m \int_{Sm} \left(\frac{A^m_{jk}}{2} P_j P_k + d^{Sm}_{jkl} u^{Sm}_{jk} P_l \right) d^2r. \tag{1b}$$

Here, the summation is performed over all repeating indices; P_i is a ferroelectric polarization, $E_i = -\partial\varphi/\partial x_i$ is a quasistatic electric field, and φ is the electric potential. The coefficients of LGD potential expansion on the polarization powers are $a_{ik} = \alpha^T_{ik}(T - T_c)$ and b_{ijkl}, T is the absolute temperature, and T_c is the Curie temperature. This choice of LGD expansion corresponds to materials with the inversion center in the parent phase (e.g., with cubic parent phase). The elastic stress tensor is σ_{ij}, Q_{ijkl} is the electrostriction tensor, F_{ijkl} is the flexoelectric effect tensor [52], g_{ijkl} is the gradient coefficient tensor, and s_{ijkl} is elastic stiffness.

Variations of the electron density and ionized donor concentration are $\delta n(\mathbf{r}) = n(\mathbf{r}) - n_0$ and $\delta N_d^+(\mathbf{r}) = N_d^+(\mathbf{r}) - N_{d0}^+$. Constant values of n_0 and N_{d0}^+ correspond to a stress-free reference state at zero electric field. e is the electron charge; Z_d is the donor ionization degree. The deformation potential tensor is denoted by Σ^e_{ij} and the Vegard expansion (or elastic dipole) tensor is W^d_{ij} [29,30]. The Vegard tensor W^d_{ij} for donors will be regarded as diagonal. Only ionized donors (e.g., impurity ions or oxygen vacancies) are regarded as mobile [53]. Mobile acceptors can be considered in a similar way. E_d is the donor level; E_C is the bottom of the conduction band.

The entropy of ionized donors is estimated under the approximation of an infinitely thin single donor level, as

$$S_d[N_d^+] = -k_B\left\{ N_d^0\left[\frac{N_d^+}{N_d^0}\ln\left(\frac{N_d^+}{N_d^0}\right) + \left(1 - \frac{N_d^+}{N_d^0}\right)\ln\left(1 - \frac{N_d^+}{N_d^0}\right)\right]\right\}, \tag{2a}$$

where N_d^0 is the concentration of donor atoms. The entropy density of electron Fermi gas, considered in the parabolic or effective mass approximation, is

$$S_{el}[n] = -k_B N_C \int_0^{n/N_C} d\tilde{n} F^{-1}_{1/2}(\tilde{n}), \tag{2b}$$

where $F^{-1}_{1/2}(\xi)$ is the inverse function to the Fermi $\frac{1}{2}$ integral $F_{1/2}(\xi) = \frac{2}{\sqrt{\pi}}\int_0^\infty \frac{\sqrt{\zeta}d\zeta}{1+\exp(\zeta-\xi)}$ (see Appendix A of the

Supplemental Material [54]). $N_C = [m_n k_B T/(2\pi\hbar^2)]^{3/2}$ is the effective density of states in the conduction band; electron effective mass is m_n [55]. The partial derivative is $\partial S_{el}/\partial n = -k_B F_{1/2}^{-1}(n/N_C)$. For analytical estimates, we use approximations for direct and inverse Fermi integrals, $F_{1/2}(\varepsilon) \approx [\exp(-\varepsilon) + (3\sqrt{\pi}/4)(4+\varepsilon^2)^{-3/4}]^{-1}$ and $F_{1/2}^{-1}(\tilde{n}) \approx (3\sqrt{\pi}\tilde{n}/4)^{2/3} + \ln[\tilde{n}/(1+\tilde{n})]$, correspondingly. These are valid in a wide range of ε and $\tilde{n}$ values [56]. The last term, in Eq. (1a), is the electron kinetic energy [51], $F_{3/2}(\xi) = \frac{2}{\sqrt{\pi}}\int_0^\infty \frac{\zeta\sqrt{\zeta}d\zeta}{1+\exp(\zeta-\xi)}$ is the Fermi $\frac{3}{2}$ integral.

The surface properties are described by the constants A_{ij}^{Sm}, the surface dielectric stiffness at the surface S_m, d_{ijk}^S is the surface piezoelectric tensor, and u_{ij}^S is the surface strain field, originated from, e.g., film and substrate lattice mismatch [46]. The surface piezoeffect could be essential at distances of the order of one to five lattice constants from the film surface [57], although for strong enough film-substrate lattice mismatch it can be the source of thin-film self-polarization (see [46,47] and references therein). We will not consider the latter case here and refer it to future studies.

For ferroelectrics with cubic parent phase the term $Q_{ijkl}P_kP_l$ automatically includes the piezoelectric contribution, because the polarization change under electric field E_m can be approximated as [58]

$$P_k^t = P_k(E_m) + \varepsilon_0\left(\varepsilon_{km}^b - \delta_{km}\right)E_m \approx P_k^S + \varepsilon_0\left(\varepsilon_{km}^f - \delta_{km}\right)E_m. \tag{3a}$$

Here P_k^S is a spontaneous polarization component, ε_0 is the dielectric permittivity of vacuum, δ_{km} is a Kronecker symbol, and ε_{ij}^f is the relative dielectric permittivity of ferroelectric that includes a soft-mode related electric-field-dependent contribution ε_{ij}^{sm} and an electric-field-independent lattice background contribution ε_{ij}^b [35]. Consequently, an apparent piezoelectric coefficient becomes [59]

$$d_{ijk} = 2\varepsilon_0\left(\varepsilon_{km}^f - \delta_{km}\right)Q_{ijml}P_l^S. \tag{3b}$$

As a relevant experimental geometry, we consider the case of flattened tip or a thin disk electrode placed in an electric contact with a ferroelectric mixed-type semiconductor film clamped to a rigid bottom electrode. One-component polarization P_3 is normal to the film surface, corresponding to a tetragonal ferroelectric phase in a c-domain film. The problem geometry is shown in Fig. 1**.** One-dimensional (1D) approximation of the capacitor geometry is applicable for the problem solution, if the radius of the top disk electrode is much larger than the film thickness.

For the semiconductor film with mixed ionic-electronic conductivity the electric potential φ can be found self-consistently from the Poisson equation

$$\varepsilon_0\varepsilon_{33}^b\frac{\partial^2\varphi}{\partial x_3^2} = \frac{\partial P_3}{\partial x_3} - e[Z_d N_d^+(\varphi) - n(\varphi)], \tag{4}$$

with boundary conditions corresponding to the fixed potentials at the electrodes, $\varphi(0) = V$, $\varphi(h) = 0$, including the short-circuited case, $\varphi(0) = \varphi(h) = 0$. Here V is the applied voltage. In Eq. (4) we used the relation (3a) between the total and ferroelectric polarization contributions.

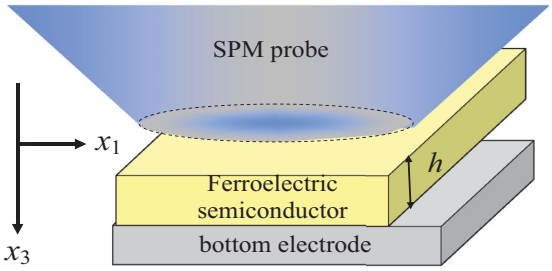

FIG. 1. Geometry of the considered problem. We consider the situation when either the radius of the SPM tip is much larger than the film thickness, or the ambient screening charges play the role of a top electrode.

When the system is in thermodynamic equilibrium, currents are absent and electrochemical potentials are equal to the Fermi level. In the considered case donor concentration is $N_d^+ = N_d^0\{1 - f[(E_d + W_{ij}^d\sigma_{ij} - eZ_d\varphi + E_F)/k_BT]\}$, where the Fermi-Dirac distribution function is introduced as $f(x) = [1+\exp(x)]^{-1}$ and E_F is the Fermi energy level in equilibrium. Electron density is $n = N_C F_{1/2}[(e\varphi + \Sigma_{ij}^e\sigma_{ij} + E_F - E_C)/k_BT]$, where $F_{1/2}(\xi) = \frac{2}{\sqrt{\pi}}\int_0^\infty \frac{\sqrt{\zeta}d\zeta}{1+\exp(\zeta-\xi)}$ is the Fermi $\frac{1}{2}$ integral.

Inhomogeneous spatial distribution of the ferroelectric polarization component(s) is determined self-consistently from the LGD-type Euler-Lagrange equations,

$$\frac{\delta G}{\delta P_i} - \frac{\partial}{\partial x_k}\left[\frac{\delta G}{\delta(\partial P_i/\partial x_k)}\right] = 0, \tag{5a}$$

with boundary conditions at surfaces S_1 at $x_3 = 0$ and S_2 at $x_3 = h$,

$$\left(A_{33}^{S1}P_3 - g_{33}\frac{\partial P_3}{\partial x_3} + F_{kl33}\sigma_{kl}\right)\Big|_{x_3=0} = 0, \tag{5b}$$

and

$$\left(A_{33}^{S2}P_3 + g_{33}\frac{\partial P_3}{\partial x_3} - F_{kl33}\sigma_{kl}\right)\Big|_{x_3=h} = 0, \tag{5c}$$

which follow from the minimization of the Gibbs potential (1). The conditions are of the third kind due to the flexoelectric effect contribution. The explicit form of Euler-Lagrange equations and boundary conditions are listed in Appendix B of the Supplemental Material [54]**.** Note that the product $F_{kl33}\sigma_{kl}/A_{33}^{Si}$ acts as a surface polarization. The coefficients A_{33}^{S1} and A_{33}^{S2} conditioned by the interface chemistry can be very different for the probed surface $x_3 = 0$, where an active chemical environment can exist, and for the electroded surface $x_3 = h$, where the perfect electric contact is present, as will be considered elsewhere [60].

The equation of state for elastic fields, $\delta G/\delta\sigma_{ij} = -u_{ij}$, obtained from the variation of the functional (1), shows that there are four basic contributions to the elastic strain of the spatially confined ferroelectric materials with mobile charge species, namely, purely elastic, flexoelectric, Vegard, and

electrostriction contributions. Hence the local strain is

$$u_{ij} = s_{ijkl}\sigma_{kl} + F_{ijkl}\frac{\partial P_k}{\partial x_l} + W^d_{ij}(N^+_d - N^+_{d0}) + \Sigma^e_{ij}(n - n_0) + Q_{ijkl}P_kP_l. \quad (6)$$

The piezoelectric contribution is automatically included in the relation (6) as linearized electrostriction in the ferroelectric phase according to Eq. (3a), and the apparent piezoelectric coefficient $d^{\rm eff}_{ijk}$ can be introduced according to Eq. (3b).

Generalized Hooke's relations (6) should be supplemented by the mechanical equilibrium equations $\partial\sigma_{ij}/\partial x_j = 0$ in the bulk and equilibrium conditions $\sigma_{ij}n_j|_{S_f} = -p^{\rm ext}_i$ at the free surfaces S_f of the system; n_j is the component of the outer normal $\boldsymbol{n} = (0,0,-1)$ to the surface S_f [61]. Here we suppose that external pressure $p^{\rm ext}_i$ can be applied to the system. Elastic displacement is zero at the clamped surfaces S_c, $u_i(S_c) = 0$. The evident expressions for elastic strains and stresses are listed in Appendix B of the Supplemental Material [54].

The film surface displacement is $u_3 = \int_0^h u_{33}dx_3$ for the considered geometry. The strain u_{33} is listed in Appendix B of the Supplemental Material [54]. The average strain $\langle u_{33}\rangle = \frac{u_3}{h}$ has the following form:

$$\langle u_{33}\rangle = -s^{\rm eff}_{33}p_{\rm ext} + W^{\rm eff}_{33}\langle\delta N^+_d\rangle + \Sigma^{\rm eff}_{33}\langle\delta n\rangle + \frac{F^{\rm eff}_{33}}{h}[P_3(h) - P_3(0)] + Q^{\rm eff}_{33}\langle P^2_3\rangle. \quad (7)$$

Here we introduced the effective coefficients $s^{\rm eff}_{33} = s_{33} - 2s^2_{13}/(s_{11}+s_{12})$, $W^{\rm eff}_{33} = W^d_{33} - 2s_{13}W^d_{11}/(s_{11}+s_{12})$, $\Sigma^{\rm eff}_{33} = \Sigma^e_{33} - 2s_{13}\Sigma^e_{11}/(s_{11}+s_{12})$, $F^{\rm eff}_{33} = F_{33} - 2s_{13}F_{13}/(s_{11}+s_{12})$, and $Q^{\rm eff}_{33} = Q_{33} - 2s_{13}Q_{13}/(s_{11}+s_{12})$. Voigt notations are introduced for the electrostriction Q_{ij}, gradient coefficient g_{ij}, flexoelectric F_{ij}, and elastic compliance s_{ij} tensors, while full matrix notations are retained for all other tensors. The tensor components with subscripts 12, 13, and 23 are equal for materials with cubic parent phase. Corresponding effective elastic compliance can be calculated from the following formula:

$$S^{\rm eff}_{33} = -\frac{1}{h}\frac{du_3}{dp_{\rm ext}}. \quad (8)$$

By definition, effective piezoresponse is given by the expression $R^{\rm eff}_3 = \frac{\partial u_3}{\partial V}$. Since $P_i = -\frac{\delta G}{\delta E_i}$ and $u_{ij} = -\frac{\delta G}{\delta\sigma_{ij}}$, in accordance with Maxwell relations we obtained that

$$R^{\rm eff}_3 = \frac{\partial u_3}{\partial V} = \frac{\partial P_3}{\partial p_{\rm ext}} \equiv \frac{\partial^2 G}{\partial V\,\partial p_{\rm ext}}. \quad (9)$$

Derivation of relation (9) along with approximate analytical expressions of effective piezoresponse is disclosed in Appendixes E and C of the Supplemental Material [54].

In order to study the dependence of the film electroconductance Ω on applied pressure $p_{\rm ext}$, i.e., the effective piezoconductance $\Omega_p \equiv d\Omega/dp_{\rm ext}$, one should solve the dynamic problem and calculate a derivative of the electric current with respect to the applied voltage and study this value in dependence on $p_{\rm ext}$, $\Omega_p \equiv \frac{1}{E_{\rm ext}}\frac{\partial J}{\partial p_{\rm ext}}$; here $E_{\rm ext} = V/h$ (assuming linear approximation on V). The donor current is $J_d = -eZ_d\eta_dN^+_d(\partial\zeta_d/\partial x_3)$, where η_d is the donor mobility coefficient; ζ_d is the electrochemical potential for the donor, $\zeta_d = -(\delta G/\delta N^+_d) \equiv E_d + W^d_{ij}\sigma_{ij} - eZ_d\varphi - k_BT\ln[N^+_d/(N^0_d - N^+_d)]$. The electronic current is $J_e = e\eta_en(\partial\zeta_e/\partial x_3)$, where η_e is the electron mobility coefficient; ζ_e is the electrochemical potential for the electron, $\zeta_e = +(\delta G/\delta n) \equiv E_C - \Sigma^e_{ij}\sigma_{ij} + k_BT\,F^{-1}_{1/2}(n/N_C) - e\varphi$.

Kinetic equations for electrons and donors, $\frac{\partial n}{\partial t} - \frac{1}{e}\frac{\partial J^e_3}{\partial x_3} = 0$ and $\frac{\partial N^+_d}{\partial t} + \frac{1}{eZ_d}\frac{\partial J_d}{\partial x_3} = 0$, are supplemented by ion-blocking boundary conditions $J_d|_{x_3=0,h} = 0$, and fixed electron densities at the electrodes $n(0) = n_0$ and $n(h) = n_1$. For the case of ion-blocking electrodes only electronic current contributes to the conductance Ω. Hence the piezoconductance can be estimated as (see Appendix D of the Supplemental Material [54]):

$$\Omega_p \equiv \frac{1}{E_{\rm ext}}\frac{dJ}{dp_{\rm ext}} \approx e^2\frac{\eta_e}{h}\frac{d}{dp_{\rm ext}}\int_0^h n dx_3 \sim \frac{d\langle n\rangle}{dp_{\rm ext}}. \quad (10)$$

Below we compare approximate analytical expressions derived in the Supplemental Material [54] with self-consistent numerical modeling with and without flexoelectric coupling and pressure application.

III. RESULTS OF SELF-CONSISTENT CALCULATIONS AND DISCUSSION

Size effects of the spontaneous polarization, effective piezoresponse, average elastic strain and compliance, electron concentration, and piezoconductance have been calculated in a self-consistent way for $PbZr_{0.5}Ti_{0.5}O_3$ (PZT) at room temperature (RT)**.** Parameters used are listed in Table I**.**

Corresponding dependences of the spontaneous polarization, effective piezoresponse, average strain and elastic compliance, electron concentration, and piezoconductance on the film thickness h are shown in Figs. 2–4. Calculated curves appeared very slightly sensitive to the Vegard contribution, where the coefficient W was varied in the reasonable range $(0-10)$ Å^3 [62] [compare left (a,c) and right (b,d) columns in Figs. 2–4]. Weak sensitivity to the Vegard strains originated

TABLE I. Material parameters collected and estimated from Refs. [30,67,68].

Coefficient	$PbZr_{0.5}Ti_{0.5}O_3$
ε^b_{33}	10
α^T ($\times 10^5$ C^{-2} J m/K)	2.66
T_C (K)	666
b_{ij} ($\times 10^8$ C^{-4} m^5 J)	$b_{33} = 3.98$
Q_{ij} (C^{-2} m^4)	$Q_{33} = Q_{11} = 0.0812$, $Q_{13} = -0.0295$
s_{ij} ($\times 10^{-12}$ Pa^{-1})	$s_{33} = s_{11} = 8.2$, $s_{13} = -2.6$′
g_{ij} ($\times 10^{-10}$ C^{-2} m^3 J)	$g_{33} = 5.0$
A^{Si} ($\times 10^{-4}$ C^{-2} J)	$A^{S1} = 1$, $A^{S2} = 20000$
F_{ij} ($\times 10^{-11}$ C^{-1} m^3)	$F_{33} = 3$, $F_{13} = 0-3$
W (10^{-30} m^3)	3
E_d (eV)	-0.1
N^0_d (m^{-3})	10^{25}
Σ (eV)	0.1
Universal constants	$e = 1.6\times10^{-19}$ C, $\varepsilon_0 = 8.85\times10^{-12}$ F/m

from the donor-blocking boundary conditions used in the 1D numerical modeling, which means that the full quantity of donors is conserved between the blocking interfaces. The condition minimizes the pure Vegard contribution and does not affect the flexocoupling. Note, however, that the Vegard contribution to FeMIEC response can be very important in two-dimensional (2D) geometry [26].

Dotted and solid curves, calculated at zero and nonzero flexoelectric coupling constants F_{ij}, correspondingly, are very similar at zero external pressure, but become strongly different under external pressure application of $\pm 10^9$ Pa. At that level the difference becomes noticeably stronger for compression ($p_{\text{ext}} > 0$) than for extension ($p_{\text{ext}} < 0$).

Without flexoelectric coupling, the main origin of the response under the application of positive or negative pressure is the linear renormalization of the coefficient a_{33}. Namely, $a_{33}^{\text{eff}} = \alpha_{33}^{T}(T - T_c) + 2Q_{33}^{\text{eff}} p_{\text{ext}}$, where the last term increases or decreases a_{33}^{eff} depending on the p_{ext} sign. The coefficient a_{33}^{eff} defines the critical thickness h_{cr} as

$$h_{cr} = -\frac{g_{33}^{\text{eff}}}{a_{33}^{\text{eff}}}\left(\frac{1}{\lambda_1 + L_C} + \frac{1}{\lambda_2 + L_C}\right), \qquad (11)$$

where the renormalized gradient coefficient $g_{33}^{\text{eff}} = g_{33} + 2F_{13}^2/(s_{11} + s_{13})$; the correlation length [63,64] is $L_C = \sqrt{g_{33}^{\text{eff}}\varepsilon_0\varepsilon_{33}^b}$ and here we introduced extrapolation length as $\lambda_m = g_{33}^{\text{eff}}/A_{33}^{Sm}$ (Appendix B of the Supplemental Material [54]). The approximate expression (11) is valid with high accuracy at small concentration of free carriers.

Thus the flexoelectric coupling renormalizes the gradient coefficient and consequently the extrapolation and correlation lengths [38]. Due to the linear dependence of a_{33}^{eff} on p_{ext} the critical thickness becomes dependent on p_{ext} as $h_{cr} \sim -\frac{1}{\alpha_{33}^{T}(T-T_c)+2Q_{33}^{\text{eff}}p_{\text{ext}}}$. The dependences $h_{cr}(p_{\text{ext}})$ and $a_{33}^{\text{eff}}(p_{\text{ext}})$, which are strongly "asymmetric" functions of p_{ext}, lead to the asymmetry of the spontaneous polarization thickness dependences occurring after the application of positive or negative pressure [see different curves in Figs. 2(a) and 2(b)].

However, the asymmetric form of the effective piezoresponse and average strain is rather complex and not defined only by the asymmetry of $a_{33}^{\text{eff}}(p_{\text{ext}})$ and $h_{cr}(p_{\text{ext}})$. In accordance with Eqs. (6), (7), (B1c), and their solution (B2) [54], the strain is proportional to $s_{33}^{\text{eff}} p_{\text{ext}} + Q_{33}^{\text{eff}} P_3^2$ at zero $F_{33}^{\text{eff}} = 0$, where the pressure dependence is present via the linear contribution $s_{33}^{\text{eff}} p_{\text{ext}}$, and the nonlinear one $Q_{33}^{\text{eff}} P_3^2$, because the polarization is pressure dependent. Hence the influence of the pressure sign on the strain becomes very complex and it causes the complex asymmetric dependence of the effective piezoresponse on applied pressure.

Without flexoelectric coupling all physical quantities depicted in Figs. 2–4 manifest noticeable peculiarities at the critical thickness $h = h_{cr}$. Since $Q_{33}^{\text{eff}} > 0$ for PZT, negative $p_{\text{ext}} < 0$ decreases the critical thickness h_{cr}, while positive $p_{\text{ext}} > 0$ leads to an opposite trend. Therefore $h_{cr}(p_{\text{ext}} < 0) < h_{cr}(p_{\text{ext}} = 0) < h_{cr}(p_{\text{ext}} > 0)$ (compare red, black, and blue dashed curves in Figs. 2–4 corresponding to $p_{\text{ext}} = -1$ GPa, 0, +1 GPa, and $F_{ij} = 0$).

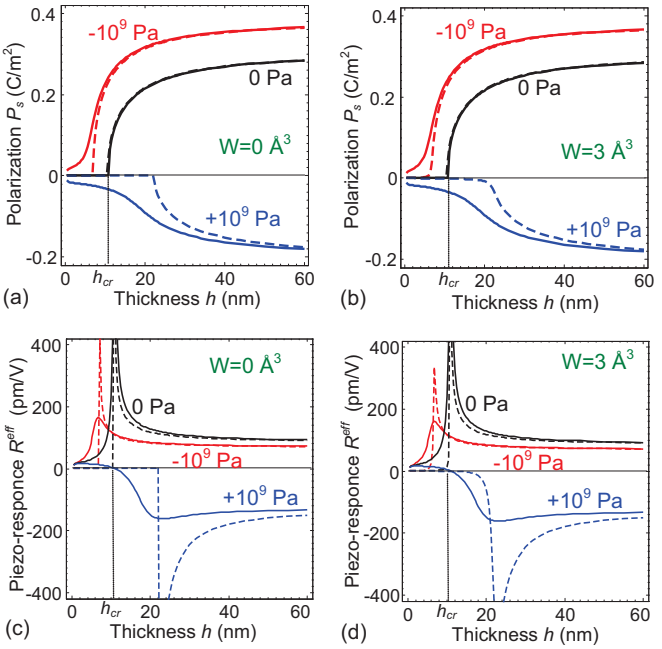

FIG. 2. Thickness dependence of the average spontaneous polarization P_3^S (a,b) and effective piezoresponse R_3^{eff} (c,d) of ferroelectric $PbZr_{0.5}Ti_{0.5}O_3$ calculated at RT for different values of external pressure $p_{\text{ext}} = -10^9$ Pa, 0, $+10^9$ Pa (shown near the curves), and flexoelectric coefficients $F_{13} = F_{33} = 0$ (dashed curves); $F_{13} = 1 \times 10^{-11}$ m^3/C; $F_{33} = 3 \times 10^{-11}$ m^3/C (solid curves). Vegard coefficient is $W = 0$ Å^3 (a,c) and $W = 3$ Å^3 (b,d). Other parameters are listed in Table I.

The spontaneous polarization, calculated at $F_{ij} = 0$, emerges at the critical thickness h_{cr}, and then increases and saturates under the film thickness increasing in a semi-quantitative agreement with the analytical formula $P_3^S = P_S^{\text{bulk}}\sqrt{1 - h_{cr}/h}$ [45] [see dashed curves in Figs. 2(a) and 2(b)]. Effective piezoresponse R_3^{eff} calculated at $F_{ij} = 0$ has a divergence at $h = h_{cr}$ and disappears in a paraelectric phase [see dashed curves in Figs. 2(c) and 2(d)]. The behavior of R_3^{eff} is in agreement with the analytical expression derived in Appendix C of the Supplemental Material [54], $R_3^{\text{piezo}} = d_{33}^{PR}\sqrt{1 - \frac{h_{cr}}{h}}\left(\frac{\theta(h_{cr}/h)}{|1-h_{cr}/h|} + \frac{\varepsilon_{33}^b}{\varepsilon_{33}^{sm}}\right)$, where the piezoresponse amplitude $d_{33}^{PR} \approx 2\varepsilon_0\varepsilon_{33}^{sm} P_S Q_{33}^{\text{eff}}$ and the function $\theta(h_{cr}/h) = 2$ at $h < h_{cr}$ and $\theta(h_{cr}/h) = 1$ at $h \geqslant h_{cr}$.

When the flexoelectric coupling is present, the boundary conditions for polarization [see the Supplemental Material [54], Eq. (B4)] contain the terms proportional to the "surface" polarizations $P_m^{BI} = F_{33}^{\text{eff}} p_{\text{ext}}/A_{33}^{Sm}$, which for the chosen geometry are equivalent to a built-in electric field $E^{BI} \sim (P_1^{BI} - P_2^{BI})/h \sim F_{33}^{\text{eff}} p_{\text{ext}}/h$. The field is inversely proportional to the thickness h, so its influence is significant for thin films. Since the field increases for thinner films, it smears the phase transition with decreasing h. The change of the applied pressure sign leads to the reversal of the surface field. In thin films, the pressure-sensitive surface field causes the situation when only one sign of polarization ($+P_S$ or $-P_S$) is stable for a given pressure sign. Note a quantitative similarity between this effect and polarization reversal and

phase transition smearing due to the adsorption of surface ions under the condition of partial oxygen pressure excess [65,66]. Negative polarization produces negative strain and negative piezoresponse at positive applied pressure [see blue curves in Figs. 2(a) and 2(b)].

The built-in field E^{BI} destroys the thickness-induced phase transition to a paraelectric phase at $h = h_{cr}$ and instead induces an electretlike state with irreversible spontaneous polarization at $h < h_{cr}$ [see solid curves in Figs. 2(a) and 2(b)]. Piezoresponse R_3^{eff} calculated from Eq. (9) appeared nonzero in the electretlike state at $h < h_{cr}$ and monotonically decreases with decreasing h [see solid curves in Figs. 2(c) and 2(d)]. Finally, we observe that the piezoresponse calculated for positive pressure changes its sign at nonzero flexoelectric coupling [see blue curves in Figs. 2(c) and 2(d)]. According to Eq. (7), there are two contributions in piezoresponse, $\Delta\frac{\partial u_3^{\text{piezo}}}{\partial V} \sim \frac{F_{33}^{\text{eff}}}{h}[\chi_3(h) - \chi_3(0)] + Q_{33}^{\text{eff}}\langle 2P_3\chi_3\rangle$, where the linear susceptibility $\chi_3 = \partial P_3/\partial E_3$ is introduced. The first term, which is the direct contribution of the flexoeffect, does not change its sign if the sign of $P_S \sim p_{\text{ext}}$ changes, while the second term being the linearized electrostriction contribution (i.e., piezoelectric term appearing in a ferroelectric phase), changes sign in such a situation. The flexoelectric contribution can dominate for very thin films of thickness less than the critical one, while the piezoelectric contribution becomes the main one with the film thickness increase. Consequently, when the external pressure changes its sign to positive it induces reversal of polarization in thin films, the two contributions of piezoresponse add up, while in the case of zero or negative pressure they are deducted.

The spontaneous average strain $\langle u_{33}\rangle$, calculated for $F_{ij} = 0$ and $p_{\text{ext}} = 0$, emerges at the critical thickness h_{cr}, and then it increases and saturates as $\sqrt{1 - h_{cr}/h}$ as the film thickness increases. Nonzero pressure shifts the strain by a constant value $-s_{33}^{\text{eff}}\, p_{\text{ext}}$ in accordance with Eq. (6) [compare different dashed curves in Figs. 3(a) and 3(b)]. Being the derivative of the strain with respect to the applied pressure, effective compliance S_{33}^{eff}, calculated at $F_{ij} = 0$ from Eq. (8), has a sharp maximum at $h = h_{cr}$ and drops to a constant value s_{33}^{eff} in the paraelectric phase [see dashed curves in Figs. 3(c) and 3(d)].

The built-in field, produced by the joint action of flexocoupling and external pressure, destroys the thickness-induced phase transition at $h = h_{cr}$ and, rather unexpectedly, induces a noticeable increase of the absolute value of strain $|\langle u_{33}\rangle|$ for films of subcritical thickness [see solid curves in Figs. 3(a) and 3(b)]. It appears that the increase is caused by the flexoelectric term $[P_3(h) - P_3(0)]F_{33}^{\text{eff}}/h$ in Eq. (5) that scales as $1/h$ at small thicknesses. The term is conditioned by different built-in surface polarizations and can be estimated as $(P_2^{BI} - P_1^{BI})F_{33}^{\text{eff}}/h$. The flexoeffect leads to the very pronounced increase of the compliance S_{33}^{eff} with thickness decrease at $h < h_{cr}$ [see solid curves in Figs. 3(c) and 3(d)]. In both cases ($p_{\text{ext}} < 0$ and $p_{\text{ext}} > 0$) the sharp fall in compliance with a decrease in film thickness is due to the decrease of polarization. Since the compliance is an even function of polarization, this effect does not depend on the sign of the polarization and therefore on the external pressure sign.

Without flexoelectric coupling the average electron concentration $\langle n\rangle$ starts to differ from the equilibrium bulk value $n_0 = N_C F_{1/2}[(E_F - E_C)/k_B T]$ for film thickness $h > h_{cr}$, because the spontaneous polarization appears above the critical thickness and starts to affect $\langle n\rangle$ via the deformation potential and depolarization field produced by the div$(\vec{P}^S)$. For $p_{\text{ext}} = 1$ GPa concentration $\langle n\rangle$ grows by an order of magnitude compared to base level n_0 at $h > h_{cr}$ and then saturates as the film thickness increases. For $p_{\text{ext}} = 0$ the concentration $\langle n\rangle$ becomes about one order of magnitude smaller than n_0 at $h > h_{cr}$, while it becomes two orders of magnitude smaller than n_0 at $h > h_{cr}$ for $p_{\text{ext}} = -1$ GPa; then it reaches a very flat minimum and subsequently slightly increases as the film thickness increases [see dashed curves in Figs. 4(a) and 4(b)]. Effective piezoconductance Ω_p calculated from Eq. (8) at $F_{ij} = 0$ has a divergence at $h = h_{cr}$ and abruptly disappears in a paraelectric phase at $h < h_{cr}$ [see dashed curves in Figs. 4(c) and 4(d)]. The pressure-induced changes of electron concentration are related with the linear renormalization of the coefficient a_{33}^{eff} by the pressure, $a_{33}^{\text{eff}} = \alpha_{33}^T(T - T_c) + 2Q_{33}^{\text{eff}} p_{\text{ext}}$, since the amplitude of the spontaneous polarization $\vec{P}^S$ depends on a_{33}^{eff} in accordance with the LGD-type Euler-Lagrange equation (B3) listed in Appendix B of the Supplemental Material [54].

When the flexoelectric coupling is present it causes the built-in field $E^{BI} \sim F_{33}^{\text{eff}} p_{\text{ext}}/h$, which in turn induces noticeable deviation of $\langle n\rangle$ from the value n_0 for all film thicknesses h, including the range of small thickness $h \leqslant h_{cr}$. Furthermore, two peculiarities are present with the thickness dependence of $\langle n\rangle$, namely, flat extrema at $h \approx h_{cr}$ followed

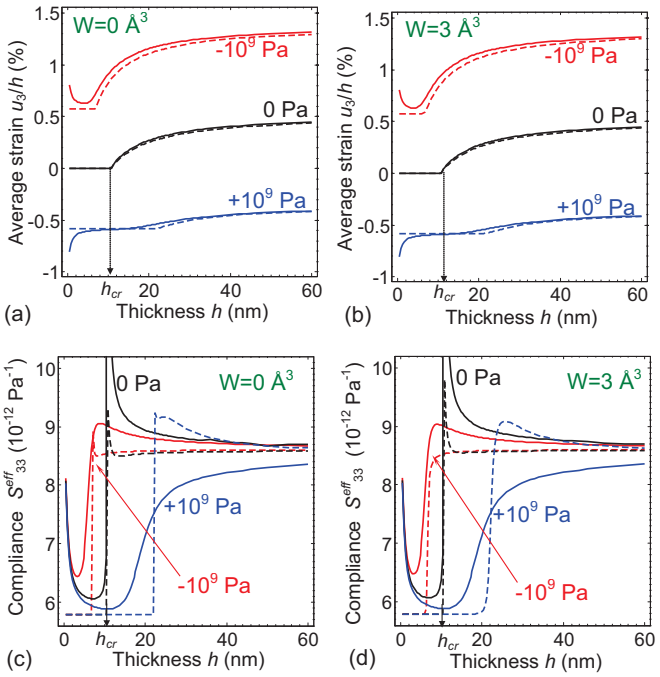

FIG. 3. Thickness dependence of average strain $\langle u_{33}\rangle$ (a,b) and effective elastic compliance S_{33}^{eff} (c,d) of ferroelectric $PbZr_{0.5}Ti_{0.5}O_3$ calculated at RT for different values of external pressure $p_{\text{ext}} = -10^9$ Pa, 0, $+10^9$ Pa (shown near the curves) and flexoelectric coefficients $F_{13} = F_{33} = 0$ (dashed curves); $F_{13} = 1 \times 10^{-11}$ m^3/C; $F_{33} = 3 \times 10^{-11}$ m^3/C (solid curves). Vegard coefficient is $W = 0$ Å^3 (a,c) and $W = 3$ Å^3 (b,d). Other parameters are listed in Table I.

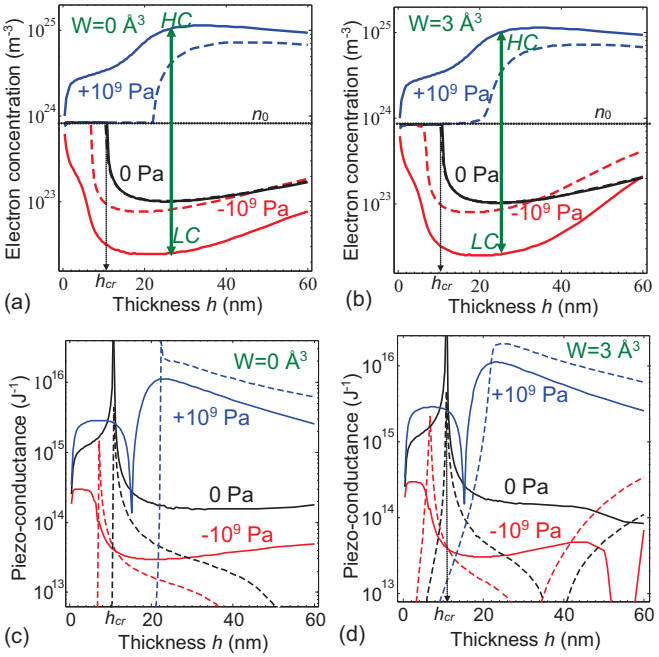

FIG. 4. Thickness dependence of the average electron concentration $\langle n \rangle$ (a,b) and effective piezoconductance Ω_p (c,d) of ferroelectric $PbZr_{0.5}Ti_{0.5}O_3$ calculated at RT for different values of external pressure $p_{ext} = -10^9$ Pa, 0, $+10^9$ Pa (shown near the curves) and flexoelectric coefficients $F_{13} = F_{33} = 0$ (dashed curves); $F_{13} = 1 \times 10^{-11}$ m^3/C; $F_{33} = 3 \times 10^{-11}$ m^3/C (solid curves). Green arrows indicate the difference between high-conductivity (HC) and low-conductivity (LC) states. Vegard coefficient is $W = 0$ Å^3 (a,c) and $W = 3$ Å^3 (b,d). Other parameters are listed in Table I.

by an inflection point and then by a sharp drop to the n_0 value as the film thickness decreases [see solid curves in Figs. 4(a) and 4(b)]. Therefore effective piezoconductance Ω_p, being the pressure derivative of $\langle n \rangle$ in accordance with Eq. (8), is nonzero for all film thicknesses h and reveals nontrivial thickness dependence at $p_{ext} \neq 0$ [see solid curves in Figs. 4(c) and 4(d)]. For $p_{ext} = 1$ GPa the piezoconductance thickness dependence, $\Omega_p(h)$, has two maxima. The first is smeared and located at $h \approx h_{cr}$, whereas the other one is flat and located at $h < h_{cr}$. They are separated by a sharp drop (by an order of magnitude), whose position corresponds to the inflection point of $\langle n \rangle$. For $p_{ext} = 0$ the dependence $\Omega_p(h)$ has one sharp maximum at $h = h_{cr}$ followed by an inflection point; after that the rapid decrease of the dependence $\Omega_p(h)$ occurs with h decrease. For $p_{ext} = -1$ GPa $\Omega_p(h)$ reaches a plateau at $h < h_{cr}$ that continues up to the ultrasmall thickness. The physical origin of the nontrivial peculiarities of the effective piezoconductance thickness dependence is the interplay of the h-dependent built-in field and polarization contributions to the electronic state.

Note that the biggest differences, $\langle n(p_{ext} > 0) - n(p_{ext} < 0) \rangle$ and $\langle \Omega_p(p_{ext} > 0) - \Omega_p(p_{ext} < 0) \rangle$ (more than three orders of magnitude for the pressure difference of 2 GPa), correspond to the film thickness $h \sim h_{cr}$ [see vertical green double arrows in Figs. 4(a) and 4(b)]. The changes of $\langle n \rangle$ by orders of magnitude under application of positive and negative pressures can indicate the appearance of high-conductivity (HC) and low-conductivity (LC) states in a thin film with thickness a bit higher than h_{cr}, in which swing can be ruled by flexoelectric coupling. Using the analogy with mechanical control of electroresistive switching in MIECs (piezochemical effect) [18], the predicted effect makes it possible to control the nonvolatile electroresistive switching in FeMIECs by changing the film thickness, external pressure, and flexoelectric coupling.

The impact of the Vegard mechanism on the size effects is weak in comparison with the flexoelectric coupling, but the thickness dependence of the piezoconductance allows one to see the difference between $W = 0$ and $W = 3$ Å^3 by comparison of Figs. 4(c) and 4(d).

Our theoretical results and predictions can be verified by direct comparison to experimental data obtained in thin ferroelectric-semiconductor films by advanced PFM and CAFM methods. In particular the dependences of the effective piezoresponse and piezoconductance measured simultaneously (i.e., *in situ*) for different film thicknesses at different applied pressures are required. In principle, the current state of the art allows such studies, and we hope that the developed theoretical framework will stimulate further studies. Furthermore, derived expressions for the strain field, effective elastic compliance, piezoresponse, and piezoconductance [see, e.g., Eqs. (7)–(10)], which include the dependence on the film thickness, built-in field, external pressure, and flexoelectric coefficients, can be used for optimization of the thin ferroelectric film parameters to reach better performances and so they can quantitatively rationalize future experimental observations.

IV. CONCLUSION

Flexocoupling impacts on the size effects of the spontaneous polarization, effective piezoresponse, elastic strain and compliance, carrier concentration, and piezoconductance have been calculated in thin films of ferroelectric mixed-type semiconductors within the LGD approach combined with classical electrodynamics and semiconductor properties description. Analysis of the self-consistent calculation results revealed that the thickness dependences of the aforementioned physical quantities, calculated at zero and nonzero flexoelectric coupling, are very similar without applied pressure, but become strongly different under the application of external pressure p_{ext}.

Without flexoelectric coupling the studied physical quantities manifest pronounced peculiarities (disappearance, divergences or sharp maxima, breaks, etc.) if the film thickness h approaches the critical thickness h_{cr} of the ferroelectricity existence. We derived analytically how the value of h_{cr} depends on the flexocoupling constants, applied pressure p_{ext}, surface energy coefficients, and material parameters. Negative pressure $p_{ext} < 0$ decreases the critical thickness h_{cr} while a positive one $p_{ext} > 0$ leads to an opposite trend.

The combined effect of flexoelectric coupling and external pressure induces the polarizations at the film surfaces. The surface polarizations cause the built-in field that destroys the thickness-induced phase transition to the paraelectric phase at $h = h_{cr}$ and induces the electretlike state with irreversible spontaneous polarization at $h < h_{cr}$. The built-in field leads

to the noticeable increase of the average strain and elastic compliance under the film thickness decrease below h_{cr} that scales as $1/h$ at small thicknesses h. The increase is conditioned by different built-in surface polarizations at small enough extrapolation lengths, since the corresponding built-in field $E^{BI} \sim F_{33}^{\text{eff}} p_{\text{ext}}/h$ scales as $1/h$ at small thicknesses h (F_{33}^{eff} is the effective flexocoupling constant).

The built-in field induces nonmonotonic thickness dependence of free-electron density $\langle n \rangle$ for all film thicknesses h including the range of small thickness $h \leqslant h_{cr}$. Corresponding effective piezoconductance Ω_p is nonzero for all film thicknesses h and its thickness dependence is nonmonotonic and nontrivial. The physical origin of the peculiarities of the electron concentration and effective piezoconductance thickness dependences is the interplay of the h-dependent built-in field and polarization impact on the electronic state. The impact of the Vegard mechanism on the size effects is weak as anticipated for the donor-blocking boundary conditions, but its influence on the thickness dependence of the piezoconductance is notable.

The changes of $\langle n \rangle$ and Ω_p by three orders of magnitude under application of positive and negative external pressure of 1 GPa can indicate the appearance of high- and low-conductivity states in a thin film with thickness a bit higher than h_{cr}, in which swing can be ruled by pressure magnitude and flexoelectric coupling. The predicted effect can pave the way for the size effect control of piezoresistive switching in FeMIECs facilitated by flexoelectric coupling.

The obtained theoretical results can be of fundamental and applied interest for the thin ferroic films physics, semiconductor physics, modern interferometry, and scanning probe microscopy development. Predicted nontrivial behavior of the elastic properties and piezoconductance is waiting for experimental verification by modern SPM and precise interferometry methods.

ACKNOWLEDGMENTS

E.A.E. and A.N.M. acknowledge the National Academy of Sciences of Ukraine (Grant No. 07-06-15) and Grant No. CNMS2016-061. S.V.K. acknowledges the Office of Basic Energy Sciences, U.S. Department of Energy. I.S.V. is grateful to the German Research Foundation for support through Grant No. GE 1171/7-1. M.V.S. acknowledges the grant of the President of the Russian Federation for state support of young Russian scientists—Ph.D. (Grant No. 14.Y30.15.2883-MK) and the project part of the state tasks in the field of scientific activity Grant No. 11.2551.2014/K. Y.K. acknowledges that a portion of this work was supported by the Basic Science Research program through the National Research Foundation of Korea funded by the Ministry of Science, ICT and Future Planning (Grant No. NRF-2014R1A4A1008474).

[1] N. Setter, D. Damjanovic, L. Eng, G. Fox, S. Gevorgian, S. Hong, A. Kingon, H. Kohlstedt, N. Y. Park, G. B. Stephenson, I. Stolitchnov, A. K. Tagantsev, D. V. Taylor, T. Yamada, and S. Streiffer, Ferroelectric thin films: Review of materials, properties, and applications, J. Appl. Phys. **100**, 051606 (2006).

[2] R. Waser, *Nanoelectronics and Information Technology* (John Wiley & Sons, Weinheim, 2012).

[3] J. F. Scott, Applications of modern ferroelectrics, Science **315**, 954 (2007).

[4] M. Fiebig, Revival of the magnetoelectric effect, J. Phys. D: Appl. Phys. **38**, R123 (2005).

[5] N. A. Spaldin and M. Fiebig, The renaissance of magnetoelectric multiferroics, Science **309**, 391 (2005).

[6] S. V. Kalinin and N. A. Spaldin, Functional ion defects in transition metal oxides, Science **341**, 858 (2013).

[7] J. Seidel, L. W. Martin, Q. He, Q. Zhan, Y. H. Chu, A. Rother, M. E. Hawkridge, P. Maksymovych, P. Yu, M. Gajek, N. Balke, S. V. Kalinin, S. Gemming, F. Wang, G. Catalan, J. F. Scott, N. A. Spaldin, J. Orenstein, and R. Ramesh, Conduction at domain walls in oxide multiferroics, Nat. Mater. **8**, 229 (2009).

[8] S. V. Kalinin, A. Borisevich, and D. Fong, Beyond condensed matter physics on the nanoscale: the role of ionic and electrochemical phenomena in the physical functionalities of oxide materials, ACS Nano **6**, 10423 (2012).

[9] P. S. Sankara Rama Krishnan, A. N. Morozovska, E. A. Eliseev, Q. M. Ramasse, D. Kepaptsoglou, W.-I. Liang, Y.-H. Chu, P. Munroe, and V. Nagarajan, Misfit strain driven cation interdiffusion across an epitaxial multiferroic thin film interface, J. Appl. Phys. **115**, 054103 (2014).

[10] A. N. Morozovska, E. A. Eliseev, P. S. Sankara Rama Krishnan, A. Tselev, E. Strelkov, A. Borisevich, O. V. Varenyk, N. V. Morozovsky, P. Munroe, S. V. Kalinin, and V. Nagarajan, Defect thermodynamics and kinetics in thin strained ferroelectric films: The interplay of possible mechanisms, Phys. Rev. B **89**, 054102 (2014).

[11] A. Sawa, Resistive switching in transition metal oxides, Mater. Today **11**, 28 (2008).

[12] D. B. Strukov, G. S. Snider, D. R. Stewart, and R. S. Williams, The missing memristor found, Nature **453**, 80 (2008).

[13] G. Catalan and J. F. Scott, Physics and applications of bismuth ferrite, Adv. Mater. **21**, 2463 (2009).

[14] N. Balke, S. Jesse, A. N. Morozovska, E. Eliseev, D. W. Chung, Y. Kim, L. Adamczyk, R. E. Garcıa, N. Dudney, and S. V. Kalinin, Nanoscale mapping of ion diffusion in a lithium-ion battery cathode, Nat. Nanotechnol. **5**, 749 (2010).

[15] H.-Y. Amanieu, H. N. M. Thai, S. Yu. Luchkin, D. Rosato, D. C. Lupascu, M.-A. Keip, J. Schröder, and A. L. Kholkin, Electrochemical strain microscopy time spectroscopy: Model and experiment on $LiMn_2O_4$, J. Appl. Phys. **118**, 055101 (2015).

[16] K. Romanyuk, C. M. Costa, S. Yu. Luchkin, A. L. Kholkin, and S. Lanceros-Méndez, Giant electric field-induced strain in PVDF-based battery separator membranes probed by electrochemical strain microscopy, Langmuir **32**, 5267 (2016).

[17] S. V. Kalinin, S. Jesse, B. J. Rodriguez, J. Shin, A. P. Baddorf, H. N. Lee, A. Borisevich, and S. J. Pennycook, Spatial resolution, information limit, and contrast transfer in piezoresponse force microscopy, Nanotechnology **17**, 3400 (2006).

[18] Y. Kim, S. J. Kelly, A. Morozovska, E. Kabiri Rahani, E. Strelcov, E. Eliseev, S. Jesse, M. D. Biegalski, N. Balke, N. Benedek, D. Strukov, J. Aarts, I. Hwang, S. Oh, J. S. Choi, T. Choi, B. H. Park, V. B. Shenoy, P. Maksymovych, and S. V. Kalinin, Mechanical control of electroresistive switching, Nano Lett. **13**, 4068 (2013).

[19] Y. H. Hsieh, E. Strelcov, J. M. Liou, C. Y. Shen, Y. C. Chen, S. V. Kalinin, and Y. H. Chu, Electrical modulation of the local conduction at oxide tubular interfaces, ACS Nano **7**, 8627 (2013).

[20] Y. Kim, E. Strelcov, I. R. Hwang, T. Choi, B. H. Park, S. Jesse, and S. V. Kalinin, Correlative multimodal probing of ionically-mediated electromechanical phenomena in simple oxides, Sci. Rep. **3**, 2924 (2013).

[21] E. Strelcov, S. Jesse, Y. L. Huang, Y. C. Teng, KravchenkoII, Y. H. Chu, and S. V. Kalinin, Space-and time-resolved mapping of ionic dynamic and electroresistive phenomena in lateral devices, ACS Nano **7**, 6806 (2013).

[22] E. Strelcov, Y. Kim, S. Jesse, Y. Cao, I. N. Ivanov, KravchenkoII, C. H. Wang, Y. C. Teng, L. Q. Chen, Y. H. Chu, and S. V. Kalinin, Probing local ionic dynamics in functional oxides at the nanoscale, Nano Lett. **13**, 3455 (2013).

[23] V. S. Mashkevich and K. B. Tolpygo, Electrical, optical and elastic properties of diamond type crystals. I, Zh. Eksp. Teor. Fiz. **32**, 520 (1957) [Sov. Phys. JETP **5**, 435 (1957)].

[24] Sh. M. Kogan, Piezoelectric effect under an inhomogeneous strain and an acoustic scattering of carriers of current in crystals, Solid State Phys. **5**, 2829 (1963).

[25] A. N. Morozovska, E. A. Eliseev, A. K. Tagantsev, S. L. Bravina, L.-Q. Chen, and S. V. Kalinin. Thermodynamics of electromechanically coupled mixed ionic-electronic conductors: Deformation potential, Vegard strains, and flexoelectric effect, Phys. Rev. B **83**, 195313 (2011).

[26] A. N. Morozovska, E. A. Eliseev, G. S. Svechnikov, and S. V. Kalinin, Nanoscale electromechanics of paraelectric materials with mobile charges: Size effects and nonlinearity of electromechanical response of $SrTiO_3$ films, Phys. Rev. B **84**, 045402 (2011).

[27] A. N. Morozovska, E. A. Eliseev, and S. V. Kalinin. Electromechanical probing of ionic currents in energy storage materials, Appl. Phys. Lett. **96**, 222906 (2010).

[28] A. N. Morozovska, E. A. Eliseev, N. Balke, and S. V. Kalinin, Local probing of ionic diffusion by electrochemical strain microscopy: spatial resolution and signal formation mechanisms, J. Appl. Phys. **108**, 053712(2010).

[29] X. Zhang, A. M. Sastry, and W. Shyy, Intercalation-induced stress and heat generation within single lithium-ion battery cathode particles, J. Electrochem. Soc. **155**, A542 (2008).

[30] D. A. Freedman, D. Roundy, and T. A. Arias, Elastic effects of vacancies in strontium titanate: Short-and long-range strain fields, elastic dipole tensors, and chemical strain, Phys. Rev. B **80**, 064108 (2009).

[31] C. Herring and E. Vogh, Transport and deformation-potential theory for many-valley semiconductors with anisotropic scattering, Phys. Rev. **101**, 944 (1956).

[32] J. Liu, D. D. Cannon, K. Wada, Y. Ishikawa, D. T. Danielson, S. Jongthammanurak, J. Michel, and L. C. Kimerling, Deformation potential constants of biaxially tensile stressed Ge epitaxial films on Si(100), Phys. Rev. B **70**, 155309 (2004).

[33] P. V. Yudin and A. K. Tagantsev, Fundamentals of flexoelectricity in solids, Nanotechnology **24**, 432001 (2013).

[34] S. V. Kalinin and A. N. Morozovska, Multiferroics: focusing the light on flexoelectricity, Nat. Nanotechnol. **10**, 916 (2015).

[35] A. K. Tagantsev, L. E. Cross, and J. Fousek, *Domains in Ferroic Crystals and Thin Films* (Springer, New York, 2010).

[36] G. Catalan, L. J. Sinnamon, and J. M. Gregg, The effect of flexoelectricity on the dielectric properties of inhomogeneously strained ferroelectric thin films, J. Phys.: Condens. Matter **16**, 2253 (2004).

[37] M. S. Majdoub, R. Maranganti, and P. Sharma, Understanding the origins of the intrinsic dead layer effect in nanocapacitors, Phys. Rev. B **79**, 115412 (2009).

[38] E. A. Eliseev, A. N. Morozovska, M. D. Glinchuk, and R. Blinc, Spontaneous flexoelectric/flexomagnetic effect in nanoferroics, Phys. Rev. B. **79**, 165433 (2009).

[39] A. Kholkin, I. Bdikin, T. Ostapchuk, and J. Petzelt, Room temperature surface piezoelectricity in $SrTiO_3$ ceramics via piezoresponse force microscopy, Appl. Phys. Lett. **93**, 222905 (2008).

[40] R. Tararam, I. K. Bdikin, N. Panwar, J. A. Varela, P. R. Bueno, and A. L. Kholkin, Nanoscale electromechanical properties of $CaCu_3Ti_4O_{12}$ ceramics, J. Appl. Phys. **110**, 052019 (2011).

[41] S. V. Kalinin, S. Jesse, W. L. Liu, and A. A. Balandin, Evidence for possible flexoelectricity in tobacco mosaic viruses used as nanotemplates, Appl. Phys. Lett. **88**, 153902 (2006).

[42] S. V. Kalinin, B. J. Rodriguez, J. Shin, S. Jesse, V. Grichko, T. Thundat, A. P. Baddorf, and A. Gruverman, Bioelectromechanical imaging by scanning probe microscopy: Galvani's experiment at the nanoscale, Ultramicroscopy **106**, 334 (2006).

[43] A. Biancoli, C. M. Fancher, J. L. Jones, and D. Damjanovic, Breaking of macroscopic centric symmetry in paraelectric phases of ferroelectric materials and implications for flexoelectricity, Nat. Mater. **14**, 224 (2015).

[44] D. R. Tilley, Finite-size effects on phase transitions in ferroelectrics, in *Ferroelectic Thin Films*, edited by C. Paz de Araujo, J. F. Scott, and G. W. Teylor (Gordon and Breach, Amsterdam, 1996), p. 11-4.

[45] M. D. Glinchuk, E. A. Eliseev, V. A. Stephanovich, and R. Fahri, Ferroelectric thin films properties—depolarization field and renormalization of a "bulk" free energy coefficients, J. Appl. Phys. **93**, 1150 (2003).

[46] M. D. Glinchuk and A. N. Morozovska, The internal electric field originating from the mismatch effect and its influence on ferroelectric thin film properties, J. Phys.: Condens. Matter **16**, 3517 (2004).

[47] M. D. Glinchuk, A. N. Morozovska, and E. A. Eliseev, Ferroelectric thin films phase diagrams with self-polarized phase and electret state, J. Appl. Phys. **99**, 114102 (2006).

[48] A. N. Morozovska, E. A. Eliseev, S. V. Svechnikov, A. D. Krutov, V. Y. Shur, A. Y. Borisevich, P. Maksymovych, and S. V. Kalinin, Finite size and intrinsic field effect on the polar-active properties of ferroelectric semiconductor heterostructures, Phys. Rev. B **81**, 205308 (2010).

[49] D. J. Franzbach, Y. J. Gu, L. Q. Chen, and K. G. Webber, Electric field-induced tetragonal to orthorhombic phase transitions in [110]c-oriented $BaTiO_3$ single crystals, Appl. Phys. Lett. **101**, 232904 (2012).

[50] D. J. Franzbach, B.-X. Xu, R. Mueller, and K. G. Webber, The effects of polarization dynamics and domain switching energies on field induced phase transformations of perovskite ferroelectrics, Appl. Phys. Lett. **99**, 162903 (2011).

[51] M. Y. Gureev, A. K. Tagantsev, and N. Setter, Head-to-head and tail-to-tail 180 domain walls in an isolated ferroelectric, Phys. Rev. B **83**, 184104 (2011).

[52] Note that we did not include the higher elastic gradient term, $\frac{1}{2}v_{ijklmn}(\partial\sigma_{ij}/\partial x_m)(\partial\sigma_{kl}/\partial x_n)$, in the functional (1a), because its value and properties are still under debate. Therefore we must use only one half $[F_{ijkl}P_k(\partial\sigma_{ij}/\partial x_l)]$ of the full Lifshitz invariant $F_{ijkl}[P_k(\partial\sigma_{ij}/\partial x_l) - \sigma_{ij}(\partial P_k/\partial x_l)]/2$. The higher elastic gradient term is required for the stability of the functional with full Lifshitz invariant included. The usage of either the term $F_{ijkl}P_k(\partial\,\sigma_{ij}/\partial x_l)$ or the term $F_{ijkl}[P_k(\partial\sigma_{ij}/\partial x_l) - \sigma_{ij}(\partial P_k/\partial x_l)]/2$ does not affect the equations of state, but influences the elastic boundary conditions.

[53] Y. Gil, O. M. Umurhan, and I. Riess, Properties of a solid state device with mobile dopants: Analytic analysis for the thin film device, J. Appl. Phys. **104**, 084504 (2008).

[54] See Supplemental Material at http://link.aps.org/supplemental/10.1103/PhysRevB.94.174101 for calculation details.

[55] S. M. Sze, *Physics of Semiconductor Devices*, 2nd ed. (Wiley-Interscience, New York, 1981).

[56] A. N. Morozovska, E. A. Eliseev, O. V. Varenyk, Y. Kim, E. Strelcov, A. Tselev, N. V. Morozovsky, and S. V. Kalinin, Space charge dynamics in solid electrolytes with steric effect and Vegard stresses: resistive switching and ferroelectric-like hysteresis of electromechanical response. J. Appl. Phys. **116**, 066808 (2014).

[57] C.-G. Duan, R. F. Sabirianov, W.-N. Mei, S. S. Jaswal, and E. Y. Tsymbal. Interface effect on ferroelectricity at the nanoscale. Nano Lett. **6**, 483 (2006); C.-G. Duan, S. S. Jaswal, and E. Y. Tsymbal, Predicted Magnetoelectric Effect in $Fe/BaTiO_3$ Multilayers: Ferroelectric Control of Magnetism, Phys. Rev. Lett. **97**, 047201 (2006).

[58] Note that the total polarization component $P_k^t(\boldsymbol{r})$ includes both a ferroelectric contribution $P_k(\mathbf{r})$, originated from a soft mode, and a nonferroelectric one, $P_k^b(\mathbf{r})$. For both ferroelectrics and highly polarized paraelectrics the nonferroelectric contribution is typically much smaller than the ferroelectric one, $|P_k(\mathbf{r})| \gg |P_k^b(\mathbf{r})|$, so that we can assume that $P_k^t(\mathbf{r}) \approx P_k(\mathbf{r})$ and hereinafter omit the subscript t in the term $Q_{ijkl}P_kP_l$ in Eq. (1a).

[59] G. A. Smolenskii, V. A. Bokov, V. A. Isupov, N. N Krainik, R. E. Pasynkov, and A. I. Sokolov, *Ferroelectrics and Related Materials* (Gordon and Breach, New York, 1984), p. 421.

[60] S. M. Yang, A. N. Morozovska, R. Kumar, E. A. Eliseev, Y. Cao, L. Mazet, N. Balke, S. Jesse, R. Vasudevan, C. Dubourdieu, and S. V. Kalinin, Mixed electrochemical-ferroelectric states in nanoscale ferroelectrics (unpublished).

[61] A. I. Lurie, *Spatial Problems of the Elasticity Theory* (Gosudarstvennoe Izdatelstvo Techniko-Teoreticheskoy Literatury, Moscow, 1955), in Russian.

[62] M. J. Haun, Z. Q. Zhuang, E. Furman, S. J. Jang, and L. E. Cross, Thermodynamic theory of the lead zirconate-titanate solid solution system, part III: Curie constant and sixth-order polarization interaction dielectric stiffness coefficients, Ferroelectrics **99**, 45 (1989).

[63] N. A. Pertsev, V. G. Kukhar, H. Kohlstedt, and R. Waser, Phase diagrams and physical properties of single-domain epitaxial $Pb(Zr_{1-x}Ti_x)O_3$ thin films, Phys. Rev. B **67**, 054107 (2003).

[64] Zhang *et al.* [29] considered intercalation of Li and used the constant Ω named "the partial molar volume of lithium," determining the strain inserted by the excess concentration of lithium. They used value of Ω that we could recalculate to the value of $W = 1.9\,\text{Å}^3$ (see Eqs. (8) and (9) in Ref. [29]). Freedman *et al.* [30] used a shell potential model to calculate chemical strains or elastic dipole moments for various defects in $SrTiO_3$. They obtained elastic dipole-tensor values in the range $W = (2{-}24)\,\text{Å}^3$ depending on the type of the defect. Hence we concluded that the W within $(0{-}10)\,\text{Å}^3$ can be a reasonable range.

[65] R. Kretschmer and K. Binder, Surface effects on phase transitions in ferroelectrics and dipolar magnets, Phys. Rev. B **20**, 1065 (1979).

[66] C.-L. Jia, V. Nagarajan, J.-Q. He, L. Houben, T. Zhao, R. Ramesh, K. Urban, and R. Waser, Unit-cell scale mapping of ferroelectricity and tetragonality in epitaxial ultrathin ferroelectric films, Nat. Mater. **6**, 64 (2007).

[67] M. J. Highland, T. T. Fister, D. D. Fong, P. H. Fuoss, C. Thompson, J. A. Eastman, S. K. Streiffer, and G. B. Stephenson, Equilibrium Polarization of Ultrathin $PbTiO_3$ with Surface Compensation Controlled by Oxygen Partial Pressure, Phys. Rev. Lett. **107**, 187602 (2011).

[68] G. B. Stephenson and M. J. Highland, Equilibrium and stability of polarization in ultrathin ferroelectric films with ionic surface compensation, Phys. Rev. B **84**, 064107 (2011).

Supplementary Materials to "Flexocoupling impact on the size effects of piezo-response and conductance in mixed-type ferroelectrics-semiconductors under applied pressure"

Anna N. Morozovska[1,1], Eugene A. Eliseev [2], Yuri A. Genenko[32], Ivan S. Vorotiahin[1, 3], Maxim V. Silibin[4], Ye Cao[5], Yunseok Kim[6], Maya D. Glinchuk [2], and Sergei V. Kalinin[53]

[1] Institute of Physics, National Academy of Sciences of Ukraine, 46, pr. Nauky, 03028 Kyiv, Ukraine

[2] Institute for Problems of Materials Science, National Academy of Sciences of Ukraine, Krjijanovskogo 3, 03142 Kyiv, Ukraine

[3]Institut für Materialwissenschaft, Technische Universität Darmstadt, Jovanka-Bontschits-Str. 2, 64287 Darmstadt, Germany

[4]National Research University of Electronic Technology "MIET", Bld. 1, Shokin Square, 124498 Moscow, Russia

[5] The Center for Nanophase Materials Sciences, Oak Ridge National Laboratory, Oak Ridge, TN 37831

[6] School of Advanced Materials Science and Engineering, Sungkyunkwan University (SKKU), Suwon 16419, Republic of Korea

Appendix A. Comment on the form of electron entropy

The electron concentration is

$$n = \int_0^\infty d\varepsilon \cdot g_n(\varepsilon) f\left(\left(\varepsilon - e\varphi - \Sigma_{ij}^e \sigma_{ij} - E_F + E_C\right)/k_B T\right). \qquad (A.1)$$

For the case of parabolic (or effective mass) approximation the density of states $g_n(\varepsilon) \approx \frac{\sqrt{2m_n^3 \varepsilon}}{2\pi^2 \hbar^3}$

and thus one get that

$$n = N_C F_{1/2}\left(\left(e\varphi + \Sigma_{ij}^e \sigma_{ij} + E_F - E_C\right)/k_B T\right), \qquad (A.2)$$

[1] corresponding author 1, e-mail: anna.n.morozovska@gmail.com
[2] corresponding author 2, e-mail: genenko@mm.tu-darmstadt.de
[3] corresponding author 3, e-mail: sergei2@ornl.gov

where $N_C = \left(m_n k_B T/\left(2\pi\hbar^2\right)\right)^{3/2}$ is the effective density of states in the conduction band. Since $E_F = \zeta_e$ in the thermodynamic equilibrium and $\zeta_e = +\left(\delta G/\delta n\right) \equiv E_C - \Sigma_{ij}^e \sigma_{ij} - T\left(\partial S_{el}/\partial n\right) - e\varphi$, one get that the derivative $\partial S_{el}/\partial n = -k_B F_{1/2}^{-1}\left(n/N_C\right)$. Hence the entropy density is $S_{el}[n] = -k_B N_C \int_0^{n/N_C} d\tilde{n} F_{1/2}^{-1}\left(\tilde{n}\right)$. Here $F_{1/2}^{-1}\left(\xi\right)$ is the inverse function to the Fermi ½-integral $F_{1/2}\left(\xi\right) = \frac{2}{\sqrt{\pi}} \int_0^{\infty} \frac{\sqrt{\zeta} d\zeta}{1+\exp(\zeta-\xi)}$. Note, that in the Boltzmann approximation the electron gas entropy is equal to

$$S_{el}[n] = k_B N_C \left(\frac{n_C}{N_C} - \frac{n_C}{N_C} \ln\left(\frac{n_C}{N_C} \right) \right). \tag{A.3}$$

Appendix B. Elastic fields and Euler-Lagrange equations

Hereinafter we consider 1D distributions only and suppose that the tangential external forces are absent and system is only subjected to external pressure p_{ext} along x_3-axis. For the case of mechanical equilibrium, equations with boundary conditions are $\partial\sigma_{i3}/\partial x_3 = 0$, $\sigma_{i3}|_S = 0$ (i=1, 2) and $\sigma_{33}(h)\big|_S = -p_{ext}$. These equations along with boundary conditions have obvious solution: $\sigma_{13} = \sigma_{23} = 0$ and $\sigma_{33} = -p_{ext}$. Elastic displacement u_i is zero at the surface $x_3 = h$, i.e. $u_i\left(h\right) = 0$ (i=1, 2, 3). From the latter conditions one immediately comes to conditions: $u_{11}\left(h\right) = 0$, $u_{22}\left(h\right) = 0$ and $u_{12}\left(h\right) = 0$. Since we suppose that film is attached to a rigid substrate, in 1D approximation these components should be constant, $u_{11} = const$, $u_{22} = const$ and $u_{12} = const$ Therefore, obvious solution is $u_{11} = u_{12} = u_{22} = 0$. Taking these relations into account as well as the fact that we consider only one component of polarization P_3 depending only on x_3, Hooke's law for some components is reduced to the following: $\sigma_{12} s_{66} = 0$, $u_{13} = F_{66} \frac{\partial P_3}{\partial x_1} \equiv 0$ and $u_{23} = F_{66} \frac{\partial P_3}{\partial x_2} \equiv 0$, having only trivial solution. The rest of the elastic equations of state can be written as

$$u_{11} = s_{11}\sigma_{11} + s_{12}\sigma_{22} - s_{13} p_{ext} + W_{11}^d \delta N_d^+ + \Sigma_{11}^e \delta n + Q_{13} P_3^2 + F_{13} \frac{\partial P_3}{\partial x_3} \equiv 0 \tag{B.1a}$$

$$u_{22} = s_{12}\sigma_{11} + s_{11}\sigma_{22} - s_{13} p_{ext} + W_{11}^d \delta N_d^+ + \Sigma_{11}^e \delta n + Q_{13} P_3^2 + F_{13} \frac{\partial P_3}{\partial x_3} \equiv 0 \tag{B.1b}$$

$$u_{33} = s_{13}\sigma_{11} + s_{13}\sigma_{22} - s_{33}p_{ext} + W_{33}^{d}\delta N_{d}^{+} + \Sigma_{33}^{e}\delta n + Q_{33}P_3^2 + F_{33}\frac{\partial P_3}{\partial x_3} \qquad \text{(B.1c)}$$

Solving system of equations (B.1) gives the nonzero elastic field components in the following form

$$\sigma_{33} = -p_{ext}, \qquad \text{(B.2a)}$$

$$\sigma_{11} = \sigma_{22} = \frac{s_{13}p_{ext} - W_{11}^{d}\delta N_{d}^{+} - \Sigma_{11}^{e}\delta n}{s_{11}+s_{12}} - \frac{Q_{13}P_3^2}{s_{11}+s_{12}} - \frac{F_{13}}{s_{11}+s_{12}}\frac{\partial P_3}{\partial x_3}, \qquad \text{(B.2b)}$$

$$u_{33} = s_{33}^{eff}p_{ext} + W_{33}^{eff}\delta N_{d}^{+} + \Sigma_{33}^{eff}\delta n + F_{33}^{eff}\frac{\partial P_3}{\partial x_3} + Q_{33}^{eff}P_3^2. \qquad \text{(B.2c)}$$

Here we used that $\sigma_{11} = \sigma_{22}$ from the symmetry consideration and introduced the effective coefficients $s_{33}^{eff} = s_{33} - \frac{2s_{13}^2}{s_{11}+s_{12}}$, $W_{33}^{eff} = W_{33}^{d} - \frac{2s_{13}W_{11}^{d}}{s_{11}+s_{12}}$, $\Sigma_{33}^{eff} = \Sigma_{33}^{e} - \frac{2s_{13}\Sigma_{11}^{e}}{s_{11}+s_{12}}$, $F_{33}^{eff} = F_{33} - \frac{2s_{13}F_{13}}{s_{11}+s_{12}}$ and $Q_{33}^{eff} = Q_{33} - \frac{2s_{13}Q_{13}}{s_{11}+s_{12}}$. Voigt notations are introduced for the electrostriction Q_{ij}, gradient coefficients g_{ij}, flexoelectric F_{ij} and elastic compliances s_{ij} tensors, while full matrix notations are used for all other tensors. Note, that the piezoelectric contribution is automatically included in the equations (B.2) as linearized electrostriction, since $P_3 \approx P_3^S + \varepsilon_0(\varepsilon_{33}^f - 1)E_3$.

Using Equations (B.2), we excluded the stresses from the equation for polarization P_3 and concentration of donors N_d^+. Remained equations can be solved numerically. Note, that the substitution of expressions (B.2) in the functional (1a) from the main text leads to the appearance of the flexoelectric coupling with Vegard and piezoelectric terms proportional to the products $W_{ii}^{eff}F_{33}^{eff}$, $\Sigma_{ii}^{eff}F_{33}^{eff}$, etc.

Euler-Lagrange equation for determination of the ferroelectric polarization component has an explicit form:

$$\left(a_{33}^{eff} + \frac{4Q_{13}W_{11}^{d}}{s_{11}+s_{12}}\delta N_{d}^{+}\right)P_3 + b_{33}^{eff}P_3^3 - g_{33}^{eff}\frac{\partial^2 P_3}{\partial x_3^2} - \frac{2F_{13}W_{11}^{d}}{s_{11}+s_{12}}\frac{\partial N_{d}^{+}}{\partial x_3} = -\frac{\partial \varphi}{\partial x_3} \qquad \text{(B.3)}$$

The effective coefficients $g_{33}^{eff} = g_{33} + \frac{2F_{13}^2}{s_{11}+s_{12}}$, $a_{33}^{eff} = \alpha_{33}^{T}(T - T_c) + 2Q_{33}^{eff}p_{ext}$ and $b_{33}^{eff} = \left(b_{33} + \frac{4Q_{13}^2}{s_{11}+s_{12}}\right)$ are introduced. Boundary conditions for the out-of-plane polarization component P_3 are of the third kind [i]:

$$\left(P_3 - \lambda_1 \frac{\partial P_3}{\partial x_3} - \frac{2F_{13}W_{11}^d}{s_{11}+s_{12}} \frac{\delta N_d^+}{A_{33}^{S1}} - \frac{2F_{13}Q_{13}}{s_{11}+s_{12}} \frac{P_3^2}{A_{33}^{S1}} - P_1^{BI} \right)\Bigg|_{x_3=0} = 0\,, \qquad \text{(B.4a)}$$

$$\left(P_3 + \lambda_2 \frac{\partial P_3}{\partial x_3} + \frac{2F_{13}W_{11}^d}{s_{11}+s_{12}} \frac{\delta N_d^+}{A_{33}^{S2}} + \frac{2F_{13}Q_{13}}{s_{11}+s_{12}} \frac{P_3^2}{A_{33}^{S2}} + P_2^{BI} \right)\Bigg|_{x_3=h} = 0\,. \qquad \text{(B.4b)}$$

The extrapolation length $\lambda_m = \frac{g_{33}^{eff}}{A_{33}^{Sm}}$ is determined by the surface energy and the surface state. Physically realistic range for λ_m is 0.5 – 2 nm [ii]. Built-in polarizations at the surfaces x_3=0 and x_3=h are, respectively, $P_1^{BI} = \frac{F_{33}^{eff} p_{ext}}{A_{33}^{S1}}$ and $P_2^{BI} = \frac{F_{33}^{eff} p_{ext}}{A_{33}^{S2}}$.

Appendix C. Analytical estimates of effective electromechanical response

Below we will demonstrate that the flexocoupling can impact strongly on size effect of effective piezo-response in a ferroelectric layer with a strong gradient of mobile defects.

Using the linear approximation for the dependence of polarization on electric field in a tetragonal phase of ferroelectric, $P_k \approx P_k^S + \varepsilon_0\left(\varepsilon_{kl}^f - 1\right)E_l$, the piezoelectric strain u_{ij}^{piezo} is proportional to the convolution of the piezoelectric coefficients with electric field, $u_{ij}^{piezo} \approx d_{ijk}^{eff} E_k$ in accordance with Eq.(2b), where the apparent piezoelectric coefficient $d_{ijk}^{eff} = 2\varepsilon_0\left(\varepsilon_{kn}^f - \delta_{kn}\right)Q_{ijnl}P_l^S$ is introduced. Consequently, vertical effective piezoresponse, defined as the derivative of the surface displacement $u_3^{piezo} \approx \int_0^h u_{33}^{piezo} dx_3$ with respect to the applied voltage V, is exactly equal to d_{33}^{eff}, because $\int_0^h E_3\, dx_3 = V$.

When ferroelectric ceramic layer thickness h decreases approaching the critical thickness h_{cr}, the apparent piezoelectric coefficient d_{33}^{eff} becomes thickness-dependent, because the ferroelectric polarization decreases and dielectric permittivity component changes with thickness. Without external pressure the surface polarization are zero ($F_{33}^{eff} p_{ext} / A_{33}^{Si} = 0$) and the following expressions are valid:

$$P_3^S = P_S^{bulk}\sqrt{1 - \frac{h_{cr}}{h}}\,, \qquad \varepsilon_{33}^f(h) = \varepsilon_{33}^b + \frac{\varepsilon_{33}^{sm}\theta(h_{cr}/h)}{\left|1 - h_{cr}/h\right|}\,, \qquad \text{(C.1)}$$

where the function $\theta(h_{cr}/h) = 2$ at $h < h_{cr}$ and $\theta(h_{cr}/h) = 1$ at $h \geq h_{cr}$ in accordance with Curie-Weiss law. According to the expressions (C.1), P_3^S disappears at $h \leq h_{cr}$ and dielectric

permittivity component diverges at $h = h_{cr}$. ε_{33}^{sm} is a soft-mode related relative dielectric permittivity of a bulk ferroelectric material, ε_{33}^{b} is a background contributions (typically $\varepsilon_{33}^{b} << \varepsilon_{33}^{sm}$). The critical thickness depends on the ferroelectric material parameters, temperature, extrapolation length λ_P and flexoelectric coupling coefficients:

$$h_{cr} = -\frac{g_{33}^{eff}}{a_{33}^{eff}}\left(\frac{1}{\lambda_1 + L_C} + \frac{1}{\lambda_2 + L_C}\right), \tag{C.2}$$

where the correlation length $L_C = \sqrt{g_{33}^{eff}\varepsilon_0\varepsilon_{33}^{b}}$ is introduced. Extrapolation length $\lambda_m = g_{33}^{eff} / A_{33}^{Sm}$ is positive or zero. Note that L_C can be much smaller than the lattice constant due to depolarization field influence, so that $\lambda_m + L_C \approx \lambda_m$ for extrapolation lengths more than 1 nm. In this case $h_{cr} \approx -\frac{A_{33}^{S1} + A_{33}^{S2}}{a_{33}^{eff}}$ is dependent on external pressure, but independent on the flexocoupling strength. This happens because we suppose that surface energy coefficients A_{33}^{S1} and A_{33}^{S2} are independent on both pressure and flexoelectric coupling coefficients, therefore extrapolation $\lambda_m = \frac{g_{33}^{eff}}{A_{33}^{Sm}}$ does depend on flexoelectric coupling in accordance with Eqs.(B.4) via $g_{33}^{eff} = g_{33} + \frac{2F_{13}^2}{s_{11} + s_{12}}$. At the same time, since the coefficient a_{33}^{eff} depends only on temperature and pressure (but not on F_{13}), the critical thickness is almost independent on latter, since the expression $h_{cr} \approx -\frac{A_{33}^{S1} + A_{33}^{S2}}{a_{33}^{eff}}$ give rather good approximation for h_{cr} . As for the pressure dependence of the latter, it is solely determined by the pressure dependence of the coefficient $a_{33}^{eff} = \alpha_{33}^{T}(T - T_c) + 2Q_{33}^{eff} p_{ext}$ (see page 9 in the main text).

Allowing for Eqs.(C.1)-(C.2) the thickness dependence of effective piezo-response in a ferroelectric phase has the form:

$$R_3^{piezo} = \frac{\partial u_3^{piezo}}{\partial V} = d_{33}^{PR}\sqrt{1 - \frac{h_{cr}}{h}}\left(\frac{\theta(h_{cr}/h)}{|1 - h_{cr}/h|} + \frac{\varepsilon_{33}^{b}}{\varepsilon_{33}^{sm}}\right). \tag{C.3}$$

In accordance with the expressions $u_3^{piezo} \approx \int_0^h u_{33}^{piezo} dx_3$, $u_{ij}^{piezo} \approx d_{ijk}^{eff} E_k$ and $d_{ijk}^{eff} = 2\varepsilon_0\left(\varepsilon_{kn}^{f} - \delta_{kn}\right)Q_{ijnl}P_l^S$ the piezoresponse amplitude d_{33}^{PR} is a combination of tabulated piezoelectric coefficients of a bulk ferroelectric material, $d_{33}^{PR} \approx 2\varepsilon_0\varepsilon_{33}^{sm}P_S Q_{33}^{eff}$. The piezoresonse

R_3^{piezo} disappears in a paraelectric phase, at $h \le h_{cr}$, because of P_S disappearance accordingly to Eq.(C.1).

Note that the expression (C.3) is valid at zero flexoelectric coupling or/and external pressure, because for this case built-in polarizations in Eqs.(B.4), $P_1^{BI} = \frac{F_{33}^{eff} p_{ext}}{A_{33}^{S1}}$ and $P_2^{BI} = \frac{F_{33}^{eff} p_{ext}}{A_{33}^{S2}}$, are absent.

In accordance with Eq.(5) the Vegard strain u_{ij}^{chemo} is proportional to the convolution of the apparent Vegard coefficients W_{ij}^{eff} with mobile defect concentration spatial variation $\delta N_d^+(\mathbf{x})$, $u_{ij}^{chemo} \approx W_{ij}^{eff} \delta N_d^+(\mathbf{x})$. Deformation potential leads to the strain $u_{ij}^{def} \approx \Sigma_{ij}^{eff} \delta n(\mathbf{x})$. The flexoelectric strain u_{ij}^{flexo} is proportional to the convolution of the apparent flexoelectric coefficients F_{ijkl}^{eff} with polarization gradient, $u_{ij}^{flexo} \approx F_{ijkl}^{eff} \partial P_k / \partial x_l$.

In a paraelectric phase $u_{33}^{flexo} \approx F_{33}^{eff} \varepsilon_0 (\varepsilon_{33}^f - 1) \partial E_3 / \partial x_3$, because $P_3 \approx \varepsilon_0 (\varepsilon_{3n}^f - \delta_{3n}) E_n$ at $h \le h_{cr}$ and small applied voltages. Approximate analytical expressions for the space charges, electric potential and field can be derived within the linear Debye approximation valid at very small applied voltages, $|eZ_d \varphi / k_B T| << 1$, namely

$$\delta N_d^+ \approx n_0 \left(\exp\left(\frac{eZ_d \varphi}{k_B T} \right) - 1 \right) \approx \frac{\varepsilon_0 \varepsilon_{33}^f \varphi}{e h_d^2}, \quad \delta n \approx n_0 \left(\exp\left(\frac{-e\varphi}{k_B T} \right) - 1 \right) \approx -\frac{\varepsilon_0 \varepsilon_{33}^f \varphi}{e h_d^2} \qquad \text{(C.4a)}$$

$$\rho \approx \frac{\varepsilon_0 \varepsilon_{33}^f \varphi}{h_d^2}, \qquad \varphi = -V \frac{\sinh\left((x_3 - h)/h_d\right)}{\sinh\left(h/h_d\right)}, \qquad E_3 = \frac{V}{h_d} \frac{\cosh\left((x_3 - h)/h_d\right)}{\sinh\left(h/h_d\right)} \qquad \text{(C.4b)}$$

The introduced screening length $h_d = \sqrt{k_B T / \left(\varepsilon_0 \varepsilon_{33}^f e^2 (Z_d + 1) n_0\right)}$ is thickness-dependent, because ε_{33}^f is thickness-dependent according to Eq.(C.1).

Using Eqs.(C.4) the flexoelectric and chemical contributions to the longitudinal effective electromechanical response $R_3^{flexo+chemo}$ can be estimated in the paraelectric phase as:

$$R_3^{flexo+chemo} = \frac{\partial}{\partial V} \left(\int_0^h \left(u_{33}^{flexo} + u_{33}^{chemo} + u_{33}^{def} \right) dx_3 \right) \approx R_{33}^{FC} \frac{\varepsilon_{33}^f(h)}{\varepsilon_{33}^{sm}} \frac{1 - \cosh\left(h/h_d\right)}{h_d \sinh\left(h/h_d\right)} \qquad \text{(C.5)}$$

In accordance with Eq.(4) from the main text, the response amplitude R_{33}^{FC} is a sum of three contributions, flexoelectric, Vegard and deformation potential tensors, $R_{33}^{FC} \approx \varepsilon_0 \varepsilon_{33}^{sm} \left(F_{33}^{eff} - \frac{W_{33}^{eff} - \Sigma_{33}^{eff}}{e} \right)$.

In order to calculate the quadratic electrostrictive contribution that can dominate in paraelectric phase, we used the same assumptions as for derivation of Eq.(C.5). The electrostrictive displacement in the paraelectric phase is $u_3^Q(h) = Q_{33}\left(\varepsilon_0\left(\varepsilon_{33}^f - 1\right)\right)^2 \int_0^h E_3^2 dx_3$. The displacement u_3^Q is proportional to V^2, because $E_3^2 \sim V^2$ in accordance with Eq.(C.4b). Hence u_3^Q becomes negligibly small in comparison with the flexoelectric and chemical ones electrostrictive contribution at small enough V.

Appendix D. Analytical estimates of effective piezo-conductance

In order to estimate analytically the effective piezo-conductance, defined as the dependence of electro-conductance on applied pressure, one should perform rigorous calculations of the electric current and its derivatives on applied voltage and pressure. In the considered 1D case of donor-blocking and electron-open electrodes the donor current is zero and the electron current is constant. Namely:

$$-eZ_d\eta_d N_d^+ \frac{\partial \zeta_d}{\partial x_3} = 0, \quad e\eta_e n \frac{\partial \zeta_e}{\partial x_3} = J. \tag{D.1}$$

Let us try to solve Eqs.(D.1) in the Boltzmann-Plank-Nernst (BPN) approximation for donors' and electrons' concentrations. The approximation for donors means that $\ln\left(N_d^+/\left(N_d^0 - N_d^+\right)\right) \approx \ln\left(N_d^+/N_d^0\right)$, $N_d^+ \approx N_d^0 \exp\left(\left(-eZ_d\varphi + E_d + W_{ij}^d\sigma_{ij} - \zeta_d\right)/k_BT\right)$ and $\zeta_d = const$. BPN approximation for electrons means that $n \approx N_C \exp\left(\left(e\varphi + \Sigma_{ij}^e\sigma_{ij} - E_C + \zeta_e\right)/k_BT\right)$ and $\zeta_e = E_C - \Sigma_{ij}^e\sigma_{ij} - e\varphi + k_BT\ln\left(n/N_C\right)$. One can solve the equations for electron concentration $e\eta_e n\left(\frac{k_BT}{n}\frac{\partial n}{\partial x_3} - e\frac{\partial \varphi}{\partial x_3} - \Sigma_{ij}^e\frac{\partial \sigma_{ij}}{\partial x_3}\right) = J$ in the approximation $\frac{\partial n}{\partial x_3} = \frac{J}{e\eta_e k_BT} + \frac{\Sigma_{ij}^e}{k_BT}\overline{n}\frac{\partial \sigma_{ij}}{\partial x_3} + \frac{e\overline{n}}{k_BT}\frac{\partial \varphi}{\partial x_3}$ and obtain the expression $n = \frac{Jx_3}{ek_BT\eta_e} + \frac{\overline{n}}{k_BT}\left(e\varphi + \Sigma_{ij}^e\sigma_{ij}\right) + C$. From here $C = \overline{n}\left(1 - \frac{1}{k_BT}\left(e\overline{\varphi} + \Sigma_{ij}^e\overline{\sigma}_{ij}\right)\right) - \frac{Jh}{2ek_BT\eta_e}$ and so

$$n = \frac{J\left(x_3 - h/2\right)}{ek_BT\eta_e} + \overline{n}\left(1 + \frac{e\left(\varphi - \overline{\varphi}\right) + \Sigma_{ij}^e\left(\sigma_{ij} - \overline{\sigma}_{ij}\right)}{k_BT}\right). \tag{D.2}$$

From the boundary conditions $n(0) = n_0$ and $n(h) = n_1$ one can determine the values of J and $\overline{n}$, namely the solution is

$$\overline{n} = \left(n_1 + n_0\right)\left(2\left(1 - \frac{\overline{\varphi} + \Sigma_{ij}^e \overline{\sigma}_{ij}}{k_B T}\right) + \frac{e\left(\varphi(h) + \varphi(0)\right) + \Sigma_{ij}^e \left(\sigma_{ij}(h) + \sigma_{ij}(0)\right)}{k_B T}\right)^{-1} \tag{D.3a}$$

$$J = \frac{e k_B T \eta_e}{h}\left(n_1 - n_0 - \overline{n}\left(\frac{e\left(\varphi(h) - \varphi(0)\right) + \Sigma_{ij}^e \left(\sigma_{ij}(h) - \sigma_{ij}(0)\right)}{k_B T}\right)\right) \tag{D.3b}$$

Since $\varphi(0) - \varphi(h) = V$ and we can regard that $n_1 = n_0$, so the current $J = e\eta_e \overline{n}\left(\frac{eV + \Sigma_{ij}^e \left(\sigma_{ij}(0) - \sigma_{ij}(h)\right)}{h}\right)$ and $\overline{n} = 2n_0\left(2\left(1 - \frac{\overline{\varphi} + \Sigma_{ij}^e \overline{\sigma}_{ij}}{k_B T}\right) + \frac{eV + \Sigma_{ij}^e \left(\sigma_{ij}(h) + \sigma_{ij}(0)\right)}{k_B T}\right)^{-1}$.

So that the piezo-conductance defined as the derivative of the conductance Ω_p on applied pressure, $\frac{d\Omega_p}{dp_{ext}} \equiv \frac{1}{E_{ext}} \frac{dJ}{dp_{ext}}$, where we regard that $E_{ext} = V/h$, acquires the form:

$$\frac{d\Omega_p}{dp_{ext}} \approx e\eta_e \frac{d}{dp_{ext}}\left(e\overline{n} + \frac{\Sigma_{ij}^e \left(\sigma_{ij}(0) - \sigma_{ij}(h)\right)}{V}\overline{n}\right) \tag{D.4a}$$

Here the convolution $\Sigma_{ij}^e \sigma_{ij} = -\left(\Sigma_{33}^e - \frac{2 s_{13} \Sigma_{11}^e}{s_{11} + s_{13}}\right) p_{ext} - \frac{2\Sigma_{11}^e}{s_{11} + s_{13}}\left(Q_{13} P_3^2 + F_{13} \frac{\partial P_3}{\partial x_3}\right)$ in accordance with Eqs.(B.2), and for small deformation potentials or slowly-varying stress field the second term in brackets can be neglected, resulting in

$$\frac{d\Omega_p}{dp_{ext}} \approx e^2 \eta_e \frac{d\overline{n}}{dp_{ext}}. \tag{D.4b}$$

Let us calculate the concentration derivatives on the applied pressure. When the system is in thermodynamic equilibrium, currents are absent and electrochemical potentials are equal to Fermi level. For the case donor concentration is $N_d^+ = N_d^0\left(1 - f\left(\left(E_d + W_{ij}^d \sigma_{ij} - eZ_d \varphi + E_F\right)/k_B T\right)\right)$, where E_F is the Fermi energy level in equilibrium. Electron density is $n = N_C F_{1/2}\left(\left(e\varphi + \Sigma_{ij}^e \sigma_{ij} + E_F - E_C\right)/k_B T\right)$. Hence the concentration derivatives on the applied pressure are:

$$\frac{\partial n}{\partial p_{ext}} = N_C F'_{1/2}\left(\frac{Y}{k_B T}\right)\frac{1}{k_B T}\frac{\partial Y}{\partial p_{ext}} \tag{D.5a}$$

Where the function $F'_{1/2}(\xi) = \frac{2}{\sqrt{\pi}} \int_0^\infty \frac{\sqrt{\zeta}\exp(\zeta - \xi) d\zeta}{\left(1 + \exp(\zeta - \xi)\right)^2}$. In accordance with expressions (B.2), the arguments

$$Y = -\Sigma_{33}^{eff} p_{ext} - \frac{2\Sigma_{11}^e}{s_{11} + s_{13}}\left(Q_{13} P_3^2 + F_{13} \frac{\partial P_3}{\partial x_3}\right) + e\varphi + E_F - E_C \tag{D.6a}$$

Appendix E. Modified Maxwell relations

In the case of quasy-1D system, thin film or slab of thickness h, it is convenient to introduce free energy per unit area of the slab surface, $G \equiv G_V / S \equiv \int_0^h g\, dx_3$, where g is the free energy density. Considering thermodynamic relation $\partial g / \partial \sigma_{ij} = -u_{ij}$ (see e.g. [iii]) and using the relation (B.2a), $\sigma_{33} = -p_{ext}$, one can get $\partial g / \partial p_{ext} = u_{33}$ and finally

$$\frac{\partial G}{\partial p_{ext}} = \int_0^h \frac{\partial g}{\partial p_{ext}} dx_3 = \int_0^h u_{33}\, dx_3 \equiv -u_3(0) \tag{E.1}$$

since $u_3(h) = 0$.

It is also well-known (see e.g. [iv]) that total electric moment $\wp$ of the body can be determined from the derivative of the bulk thermodynamic potential as follows

$$S \frac{\partial G}{\partial E_{ext}} = -\wp, \tag{E.2}$$

where E_{ext} is the magnitude of external electric field applied along the normal to the slab surface. Since field E_{ext} can be introduced as $E_{ext} = V/h$, the relation (E.2) can be rewritten as

$$\frac{\partial G}{\partial V} = -\overline{P} \tag{E.3}$$

Here $\overline{P} = \wp/(hS)$ is the average polarization.

Considering G as analytical and differentiable function of p_{ext} and V, one has to consider the following relation:

$$\frac{\partial^2 G}{\partial p_{ext} \partial V} \equiv \frac{\partial^2 G}{\partial V \partial p_{ext}} \tag{E.4}$$

Combining Eqs.(E.1), (E.3) and (E.4), one could get the following modified Maxwell relation for linear electromechanical effect:

$$\frac{\partial u_3(0)}{\partial V} = \frac{\partial \overline{P}}{\partial p_{ext}} \tag{E.5}$$

References

[i] R. Kretschmer and K.Binder. " Surface effects on phase transitions in ferroelectrics and dipolar magnets. " Phys. Rev. B **20**, 1065 (1979).

[ii] Chun-Lin Jia, Valanoor Nagarajan, Jia-Qing He, Lothar Houben, Tong Zhao, Ramamoorthy Ramesh, Knut Urban & Rainer Waser. " Unit-cell scale mapping of ferroelectricity and tetragonality in epitaxial ultrathin ferroelectric films." Nature Materials, **6**. 64 (2007).

[iii] L.D. Landau and E.M. Lifshitz, A.M. Kosevich, L. P. Pitaevskii, Theory of Elasticity (Third edition, Butterworth-Heinemann, Oxford, 1986).

[iv] L.D. Landau, E.M. Lifshitz, L. P. Pitaevskii. Electrodynamics of Continuous Media, (Second Edition, Butterworth-Heinemann, Oxford, 1984).

3.4. Publication A2

Flexocoupling impact on the kinetics of polarization reversal
Ivan S. Vorotiahin, Anna N. Morozovska, Eugene A. Eliseev, and Yuri A. Genenko
Physical Review B 95, 014104 (2017). 9 pages, with Supplementary materials, 6 pages.

Flexocoupling impact on the kinetics of polarization reversal

Ivan S. Vorotiahin,[1,2] Anna N. Morozovska,[1] Eugene A. Eliseev,[1,3] and Yuri A. Genenko[2,*]
[1]*Institute of Physics, National Academy of Sciences of Ukraine, 46, Prospekt Nauky, 03028 Kyiv, Ukraine*
[2]*Institut für Materialwissenschaft, Technische Universität Darmstadt, Jovanka-Bontschits-Strasse 2, 64287 Darmstadt, Germany*
[3]*Institute for Problems of Materials Science, National Academy of Sciences of Ukraine, Krjijanovskogo 3, 03142 Kyiv, Ukraine*
(Received 20 July 2016; revised manuscript received 6 November 2016; published 10 January 2017)

The impact of flexoelectric coupling on polarization reversal and space-charge variation in thin films of ferroelectric semiconductors has been studied theoretically. The relaxation-type Landau-Khalatnikov equation together with the Poisson equation and the theory of elasticity equations have been used to calculate in a self-consistent way the spatial-temporal development of ferroelectric polarization, electric potential, space charge, elastic stresses and strains. The analysis of the obtained results reveals a moderate increase in the flexocoupling influence on the polarization, elastic strain, electric potential, and space-charge development with a decrease in the ferroelectric film thickness. In contrast, the dependence of polarization switching time on the applied electric field is remarkably affected by the flexocoupling strength. The polarization reversal process consists typically of two stages; the first stage has no characteristic time, whereas the second one exhibits a switching time strongly dependent on the applied electric field.

DOI: 10.1103/PhysRevB.95.014104

I. INTRODUCTION

The impact of the flexoelectric effect ("flexoeffect"), which appears as an elastic strain in response to the polarization gradient (and vice versa) [1–3], is of great importance for understanding and describing electrophysical and electromechanical properties of ferroics on the nanoscale [4–7], such as ferroelectric thin films [8–11], thin-film-based multilayer structures [12], nanoparticles [13–15], nanograin ceramics [16,17], and nanocomposites [14]. The flexoeffect has an impact on the local electromechanical response [18,19], structure, local symmetry (chirality) and polarity changes at the ferroelectric [20] and ferroelastic [21] domain walls. This dependence is caused by a strong influence of electro-elastic-field gradients on the nanoferroic properties [4–6], in contrast to macroferroics where the gradients are pronounced only near surfaces and domain boundaries [22–27].

This paper is devoted to the theoretical study of the poorly understood influence of the flexoeffect on the polarization switching kinetics in thin ferroelectric films. In contrast to the moderate influence of the flexoeffect on the thermodynamic polarization distribution, increasing monotonously with the film thickness decrease, its influence on the kinetics turns out to be unexpectedly strong with a threshold at certain film thicknesses. These predicted phenomena have nontrivial physical natures and require in-depth experimental verification.

In a number of works the influence of the flexoeffect on phase transitions, thermodynamical equilibrium distributions of polarization, electric and elastic fields, and the domain structures in nanoferroics was theoretically investigated [8–15,22–26], indirectly supported by experimental results [27,28]. These results indicate the significant flexoeffect influence on all thermodynamic characteristics of nanoferroics. Flexocoupling values can directly be extracted from the experiments on bending [29–31] and soft phonon spectra [32–34] or microscopically estimated [2] accounting for an upper limit from energetic considerations [35]. Otherwise the flexoelectric tensor elements can be calculated from the first principles [36–39]. However, experimentally established parameters can differ from each other [29–31] as well as from the calculated values [2,36,37] by several orders of magnitude [40]. The reasons for these discrepancies are still unclear. Dynamic flexoeffect [5,41] has yet been investigated too poorly to speculate about the potential impact on the polarization switching kinetics.

On the other hand, virtually all experimental investigations of electrophysical and electromechanical properties of ferroics were conducted in more or less nonstationary conditions. That is why investigation of the flexoelectric impact on the polarization reversal kinetics, distributions of elastic strains and stresses, electric fields, and space charge is of fundamental interest. Such theoretical research, as it appeared, is still lacking. In this paper, the flexoelectric coupling ("flexocoupling") impact on the kinetics of polarization reversal and space charge in thin films of the ferroelectrics with semiconducting properties is studied.

The impact of the flexoelectric effect on the properties and structure of domain walls in ferroics is rather nontrivial since the high gradients of the polarization and spontaneous strain are always present in these regions [8–15,22–26]. Hence, in thin ferroelectric films with domain structure there can be a complex interference of the polarization gradients caused by the several sources: domain walls, film surfaces, and inhomogeneous strains via electrostriction and flexocoupling. Indeed, it becomes very difficult to establish the role of the flexocoupling due to the cross talk of all aforementioned factors. Thus, in order to analyze the net flexocoupling impact on the polarization reversal kinetics in thin films, occurring from the system spatial confinement (i.e., from the presence of surfaces), we here lay aside the flexoelectric influence on the domain structures formation and growth. Therefore the statistical consideration of the reversed domain nucleation and growth in single-crystalline [42,43] and polycrystalline [44,45] media remains beyond the scope of the current paper. All the results discussed below are valid for the single-domain

*genenko@mm.tu-darmstadt.de

polarization reversal in a thin film of the thickness between 10 and 100 nm. Of course, single domain switching in the 100-nm film is a theoretical abstraction; however, in the case of a 10-nm film, placed between the perfectly conducting electrodes, the stripe or closure domain structures can hardly occur for energy reasons in the case of low defect concentration [46] and in the absence of dislocations [47].

To find the spatial-temporal polarization distribution the relaxation Landau-Ginzburg-Devonshire-Khalatnikov (another name is time-dependent Landau-Ginzburg-Devonshire) equation is used in the actual work. It is solved numerically in a self-consisted manner together with the Poisson equation for electric potential and space-charge distributions and with the elasticity theory equations for the determination of elastic strains and stresses.

The paper is organized as follows: The model is introduced in Sec. II including the closed system of equations for polarization, strain, and electric potential. Static distributions of involved physical quantities are discussed in Sec. III. Section IV presents time development of polarization. The results are summarized and concluded in Sec. V.

II. MODEL DESCRIPTION

Let us consider an epitaxial film of ferroelectric-semiconductor barium titanate with the thickness h sandwiched between parallel plane electrodes. We suppose that all physical quantities depend only on the distance x_3 from the upper electrode (one-dimensional problem). One-component ferroelectric polarization P_3 is normal to the film surface, that corresponds to a tetragonal ferroelectric phase, and electric field E_3 is parallel to P_3 (see Fig. 1). Thus, the polarization vector has the form $\mathbf{P} = [0,0,P_3 + \varepsilon_0(\varepsilon_b - 1)E_3]$, where $\varepsilon_0 = 8.85 \times 10^{-12}$ F/m is the dielectric permittivity of vacuum and ε_b is the "background" dielectric permittivity not related to the ferroelectric polarization [48,49].

The charge-carrier redistribution affects the electric field in the film $E_3 = -\partial\varphi/\partial x_3$ where the corresponding electric potential φ can be determined self-consistently from the Poisson equation resulting from the Gauss equation for the electrical displacement component $D_3 = \varepsilon_0\varepsilon_b E_3 + P_3$,

$$\varepsilon_0\varepsilon_b \frac{\partial^2\varphi}{\partial x_3^2} = \frac{\partial P_3}{\partial x_3^2} - e[Z_d N_d^+(\varphi) - n(\varphi)]. \tag{1}$$

Here the electron density is n, the ionized donor concentration is N_d^+, $e = 1.6 \times 10^{-19}$ C is the electron charge, and Z_d is the donor ionization degree (equal to zero for uncharged vacancies or isovalent impurities). The electric potential satisfies the boundary conditions at the electrodes $\varphi(x_3 = 0,t) = U(t)$ and $\varphi(x_3 = h,t) = 0$. In the considered case the quasiequilibrium donor concentration equals

$$N_d^+ = N_d^0\{1 - f[(E_d + w_{ij}^d u_{ij} - eZ_d\varphi + E_F)/k_BT]\}, \tag{2a}$$

where the Fermi-Dirac distribution function is introduced as $f(x) = [1 + \exp(x)]^{-1}$, E_F is the Fermi energy level in equilibrium, and E_d is the donor level. The Vegard expansion (another name is elastic dipole) tensor is w_{ij}^d [50,51]. The latter tensor will be regarded proportional to the unit tensor hereinafter $w_{ij}^d = W\delta_{ij}$. The strain tensor components are u_{ij}. For the sake of simplicity we will use the quasiequilibrium electron density as in a bulk ferroelectric,

$$n = N_C F_{1/2}[(e\varphi + E_F - E_C)/k_BT], \tag{2b}$$

where $N_C = [m_n k_B T/(2\pi\hbar^2)]^{3/2}$ is the effective density of states in the conduction band, E_C is the bottom of the conduction band, and the electron effective mass is m_n [52]. $F_{1/2}(\xi) = \frac{2}{\sqrt{\pi}}\int_0^\infty \frac{\sqrt{\zeta}d\zeta}{1+\exp(\zeta-\xi)}$ is the Fermi $\frac{1}{2}$ integral that can be approximated [53,54] using the formula given in Appendix B of Ref. [55].

Spatial distribution of the ferroelectric polarization $P_3(x_3)$ can be determined from the time-dependent LGD equation relevant to the energy functional derived in Ref. [56],

$$\Gamma\frac{\partial}{\partial t}P_3 + a_{33}P_3 + b_{33}P_3^3 + \gamma_{333}P_3^5 - g_{33}\frac{\partial^2 P_3}{\partial x_3^2} + f_{kl33}\frac{\partial u_{kl}}{\partial x_3} - 2u_{kl}q_{kl33}P_3 = -\frac{\partial\varphi}{\partial x_3}, \tag{3}$$

where Γ is the Khalatnikov coefficient, determined by the phonon relaxation time. $a_{33}(T) = \alpha_T(T - T_c)$, where T is the absolute temperature and T_c is the Curie temperature of the bulk ferroelectric. The other coefficients of the LGD thermodynamic potential are presented in Table C1 of Appendix C of Ref. [55]. The corresponding boundary conditions read

$$\left(A_S P_3 - g_{33}\frac{\partial P_3}{\partial x_3} + f_{kl33}u_{kl}\right)\Big|_{x_3=0} = 0 \quad \text{and}$$
$$\left(A_S P_3 + g_{33}\frac{\partial P_3}{\partial x_3} - f_{kl33}u_{kl}\right)\Big|_{x_3=h} = 0, \tag{4}$$

where A_S is the surface dielectric stiffness. The initial condition is $P_3(x_3,t = 0) = 0$.

The equations of state, relating strain components u_{ij} to stress components σ_{ij} for a film containing an inhomogeneous distribution of ionized donors with concentration $\delta N_d^+ = N_d^+ - \bar{N}_d^+$ are

$$\sigma_{ij} = c_{ijkl}u_{kl} + w_{ij}\delta N_d^+ + f_{ijkl}\frac{\partial P_k}{\partial x_l} - q_{ijkl}P_kP_l. \tag{5}$$

Here $\bar{N}_d^+$ is the distribution of ionized donors in the absence of the applied voltage, and c_{ijkl}, f_{ijkl}, and q_{ijkl} are tensors of elastic stiffness, flexoelectric, and electrostriction effects, respectively.

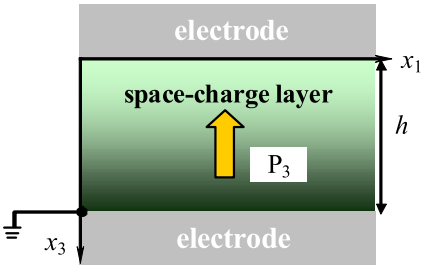

FIG. 1. Schematics of the single-domain ferroelectric-semiconductor film with electrodes in the flat capacitor geometry. Polarization direction is shown by the arrow.

Equation (5) should be supplemented by the equilibrium conditions of bulk and surface forces, namely, $\partial\sigma_{ij}/\partial x_j = 0$ in the bulk and $\sigma_{ij}n_j|_S = 0$ at the free surface of the system. The static equation is valid under the realistic assumption that the propagation of the polarization front is much slower than sound velocity. This leads to the equation for mechanical displacement vector u_i inside the film,

$$c_{ijkl}\frac{\partial^2 u_k}{\partial x_i \partial x_j} - w_{kl}\frac{\partial \delta N_d^+}{\partial x_k} - f_{klmn}\frac{\partial^2 P_m}{\partial x_k x_n} - q_{klst}\frac{\partial (P_s P_t)}{\partial x_k} = 0. \tag{6}$$

The boundary condition on the free surface of the film ($x_3 = 0$) is the absence of normal stresses $\sigma_{3j}(x_3 = 0,t) = 0$. The surface $x_3 = h$ is assumed to be clamped to a rigid substrate so that the displacement components are zero $u_k|_{x_3=h} = 0$.

The latter condition is particularly meaningful since it prevents polarization rotation in contrast to the mechanically free bulk case [57–59]. A detailed analysis presented in the Appendix allows justification of the assumed one-dimensional treatment of one-component polarization switching in the case of a thin film as opposed to the three-dimensional problems in the bulk. Three-dimensional polarization rotation is a phenomenon widely discussed in literature which becomes particularly important, for example, in materials at the morphotropic boundary separating two phases [60,61]. The physical reason for such a behavior is a flattened free-energy profile providing instability of both involved phases. Another factor facilitating polarization rotation within the same crystal phase is compressive stress [59]. Rotational behavior of the polarization is promoted also by the application of the electric field in a direction compromising polarization directions of different possible ferroelectric phases [62,63]. Neither of the above-mentioned cases applies to this paper dealing with a collinear field-polarization configuration deep in the thermodynamically stable tetragonal phase. Nevertheless, even in the latter case polarization rotation may occur in a single crystal during the polarization switching as was shown by Budimir *et al.* [59], who demonstrated flattening of the Gibbs energy profile in the tetragonal phase of $BaTiO_3$ subject to an antiparallel electric field at room temperature, i.e., exactly under conditions considered in our paper. However, a very significant difference to the aforementioned work consists in the fact that we consider a thin film tightly bound to a rigid substrate. Strong clamping of the ferroelectric film at the bottom surface $x_3 = h$ forbids 90° switching at this surface related to the in-plane strain. Because the in-plane strain and stress are virtually constant across the thickness of the film [see Eq. (A1) in the Appendix] the clamping extends over the whole film volume and thus prevents polarization rotation everywhere. To make this argument quantitative we estimated the contribution of the in-plane stress into the Gibbs energy accounting for possible rotation from the initial $(0,0,P_s)$ state to the $(0,P_s,0)$ state. According to Eqs. (A1a) and (A2a) of the Appendix evaluated for $P_3 = P_s$ this contribution is of the same magnitude as the energy ΔG in Fig. 4(b) of the paper by Budimir *et al.* [59] on the same polarization scale. Therefore, accounting for the clamping stress at the bottom surface superimposes the flat profile in the cited Fig. 4(b) of Ref. [59] with the positive parabolic one, thus eliminating the rotation instability in the case of a thin film. This warrants consideration of the polarization switching in terms of the polarization component P_3 alone.

III. STATIC DISTRIBUTIONS OF PHYSICAL QUANTITIES WITH AND WITHOUT AN APPLIED FIELD

The coupled systems of Eqs. (1), (3), and (6) with appropriate boundary conditions were solved numerically for thin ferroelectric films of thicknesses of 10–100 nm with and without taking into account the flexoeffect (see Appendix D of Ref. [55] for details), and results are presented below.

Typical static distributions of the polarization and electric potential inside 100- and 10-nm films as well as the corresponding donor and electron distributions with and without the flexoelectric effect are displayed in Figs. 2–5, where the relative strength of the flexoelectric effect is characterized by a dimensionless factor FA varying between 0 and 1. With the decrease in film thickness a moderate increase in the flexocoupling influence on the polarization distribution is observed. The Vegard effect contribution turns out to be negligible.

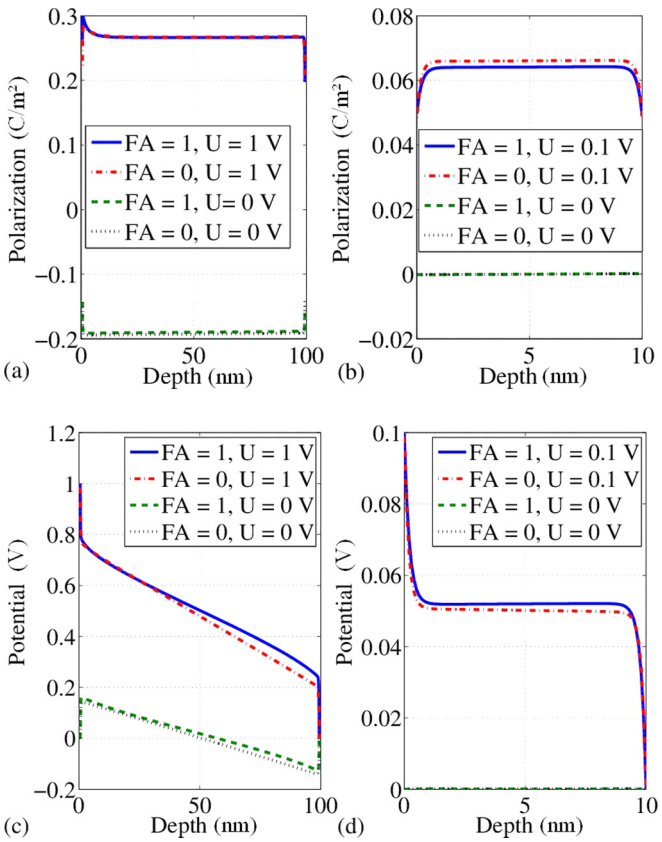

FIG. 2. (a) and (b) Spatial distributions of polarization, as well as (c) and (d) electric potential calculated for the films of 100-nm ((a) and (c)) and 10-nm ((b) and (d)) thicknesses. Different curves are calculated with (FA = 1) and without (FA = 0) flexocoupling, as well as with ($U = 1$ or $U = 0.1$ V) and without ($U = 0$) applied electric voltage. Material parameters are listed in Table C1 in Appendix C of Ref. [55].

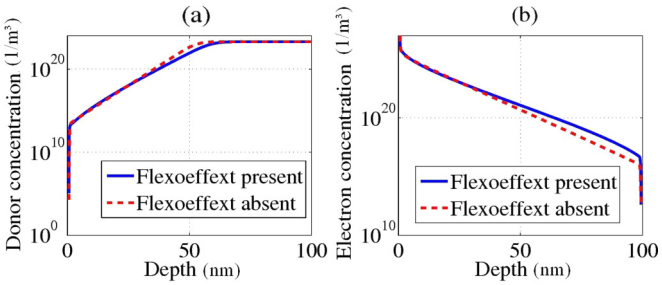

FIG. 3. (a) Donor and (b) electron concentrations for the film with a thickness of 100 nm with (blue solid curve) and without (red dashed curve) the flexoelectric effect [compare with Figs. 2(a) and 2(c)]. The voltage applied to the film is 1 V. Material parameters are listed in Table C1 in Appendix C of Ref. [55].

The asymmetry of the polarization distribution in the 100-nm film [Fig. 2(a)] is caused by the applied field when its amplitude is high enough (10 MV/m and higher) and is affected by asymmetric mechanical boundary conditions. The space-charge distribution in Fig. 3 is also asymmetric since it follows the distribution of the electric potential mainly determined by the voltage applied to the film. The difference of the latter distribution to that in the thin film (Fig. 4) is due to the fact that, in the thicker film, the Fermi level crosses the donor level position in the band gap because of the spatial variation of the potential.

When the applied electric field is absent, the mentioned asymmetry is much weaker as Figs. 2(a) and 2(b) demonstrate. The system becomes stable in the energetically favorable state with the spontaneous polarization value in the bulk region of the film. The amplitude of polarization drops rapidly from its maximum in the bulk towards zero near the film boundaries, driven by the boundary conditions. The electric potential drops to zero at both film surfaces as demanded by boundary conditions (see Appendix D of Ref. [55]). Two regions with the different signs of potential are created within the film [Figs. 2(c) and 2(d)]. The potential in the bulk obtains maximal absolute values near the surfaces, just before the film boundaries and linearly goes to the opposite maximum at the other surface, crossing zero [see Fig. 2(b)]. Flexocoupling makes these distributions slightly asymmetric.

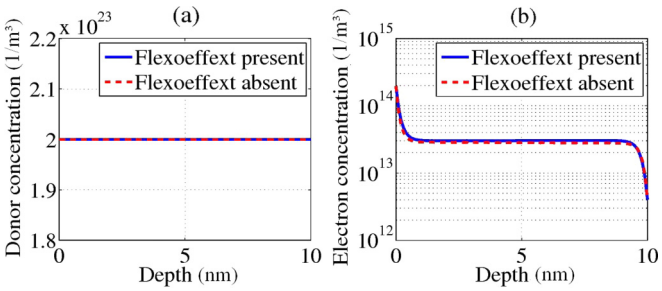

FIG. 4. (a) Donor and (b) electron concentrations for the film with a thickness of 10 nm with (blue solid curve) and without (red dashed curve) the flexoelectric effect [compare with Figs. 2(b) and 2(d)]. The voltage applied to the film is 0.1 V. Material parameters are listed in Table C1 in Appendix C of Ref. [55].

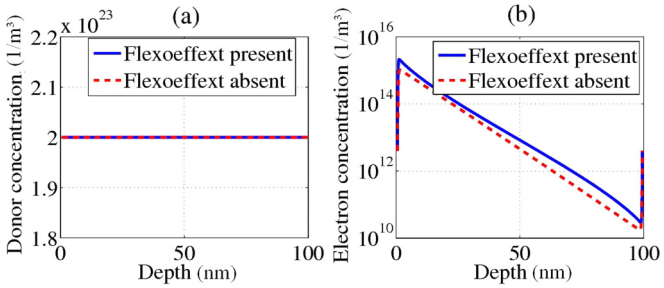

FIG. 5. (a) Donor and (b) electron concentration distributions in the 100-nm film without an applied electric field, $U = 0$ [compare with Fig. 2(c)]. Material parameters are listed in Table C1 in Appendix C of Ref. [55]. The blue solid line represents the distribution calculated with an account of the flexoelectric effect, and the red dashed line represents the distribution without the flexoelectric effect.

Space-charge distribution largely follows the electric potential profile (Fig. 5).

The distributions similar to those shown in Figs. 2–5 can also be obtained for the films of various thicknesses between 100 and 10 nm. One can observe thereby the changes in the distribution behavior when changing the film thickness. With the decrease in the film thickness the flexocoupling influence on the static distributions increases, and amplitudes of the spontaneous and field-induced polarizations decrease moderately. In the film with the thickness of 47 nm the spontaneous polarization amplitude becomes negligibly small in comparison with the value of 0.19 C/m² for the 100-nm film. As will be discussed in the next section, the polarization reversal process also changes below 47 nm as the spontaneous polarization distribution allows the film to switch in one step because the spontaneous polarization distribution is close to the homogeneous one in the equilibrium state.

IV. POLARIZATION SWITCHING KINETICS

When considering kinetics of polarization switching the following scenario is studied. By a tiny voltage pulse the system is first allowed to polarize spontaneously in the negative direction. Then, after a while, the system is pulled out of the negative equilibrium state to the field-induced polarization in the positive direction by applying an external electric field of the opposite sign. Corresponding polarization switching occurs generally in two steps: At first the system polarization insignificantly changes its value in the direction of the applied field and tries to become homogeneous across the film depth. As soon as it happens, the film rapidly and coherently switches to the state with the stable field-induced polarization. The first stage does not exhibit a characteristic time in the time dependence of the polarization (Fig. 6). The second stage clearly reveals a characteristic switching time identified by the inflection point in the time dependence of the polarization (or by the peak in its time derivative) and denoted by τ.

A homogeneous polarization distribution is much easier to achieve in the films of smaller thicknesses so that the switching process occurs much faster there. A stable state of the system is close to the homogeneous distribution without an applied field for the film thickness of $h_{cr} = 47$ nm and

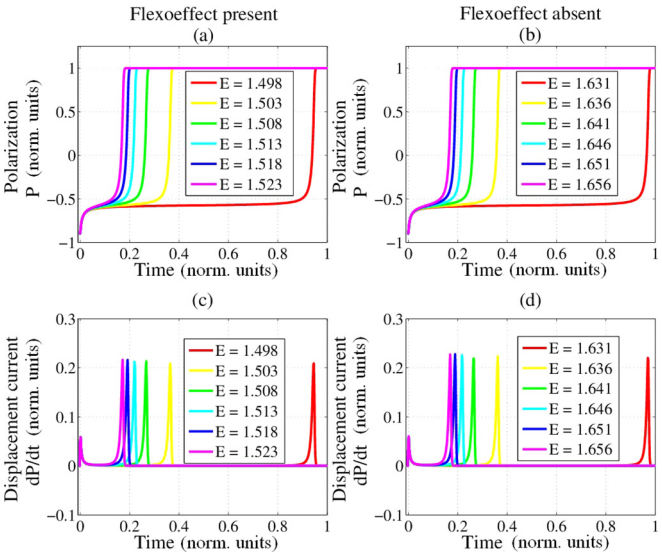

FIG. 6. (a) and (b) Single-domain polarization reversal kinetics together with (c) and (d) correspondent displacement currents calculated for the 100-nm films with ((a) and (c)) and without ((b) and (d)) the flexoelectric effect. The applied electric field is measured in megavolts per meter and increases from right to left in all plots. Parameters used in the modeling are listed in Table C1 in Appendix C of Ref. [55].

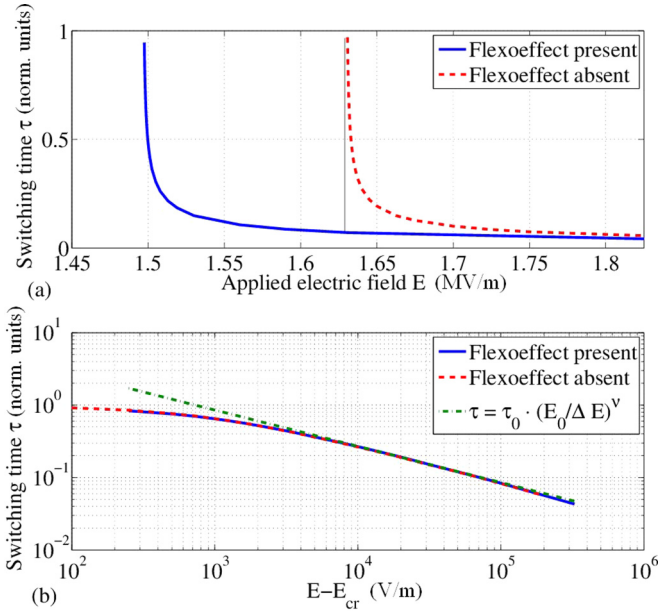

FIG. 7. (a) Dependence of the polarization switching time τ on the strength of the applied electric field. The solid line denotes the dependences calculated with the flexocoupling ($E_{cr}^{fl} = 1.50\,MV/m$), and the dashed line shows the one calculated without it ($E_{cr}^{nofl} = 1.63\,MV/m$). (b) The dashed-dotted line shows the asymptotic power behavior of both dependences on the logarithmic scale. Film thickness is 100 nm. Material parameters are listed in Table C1 in Appendix C of Ref. [55].

smaller with flexocoupling (and for 46 nm without it) so that the homogenization takes a negligibly short time. In the films of bigger thicknesses the polarization reversal process exhibits two stages as is seen in Fig. 6, whereas the process occurs in one stage in the films of smaller thicknesses as no further relaxation is required for the system to reach quasihomogeneous reversed polarization distribution.

A well-known nontrivial difference in the single-domain switching from the multidomain scenario is the existence of the critical field E_{cr} below which the switching does not occur [64]. E_{cr} and τ drop down dramatically with the decrease in film thickness accompanied by a gradual reduction of spontaneous and field-induced polarization amplitudes. This trend can be explained by the analytical expressions for the thermodynamic coercive field for a defect-free film (see Eqs. (3) in Ref. [65] and Eq. (12) in Ref. [66]): $E_c = \frac{2}{5}(2b_{33} + \sqrt{9b_{33}^2 - 20\alpha\gamma_{333}})\left(\frac{2\alpha}{-3b_{33} - \sqrt{9b_{33}^2 - 20\alpha\gamma_{333}}}\right)^{3/2}$ where the coefficient $\alpha(T,h) \cong \alpha_T[T - T_c(1 - h_{cr}/h)]$ is renormalized by the finite-size effects and screening conditions in thin films and h_{cr} is the critical thickness of the size-induced film transition into a paraelectric phase at absolute zero $T = 0\,K$ [67]. Note that the lattice pinning phenomena, defects, and elastic stresses can lead to the crossover from the idealized "intrinsic" thermodynamic switching scenario to the realistic "extrinsic" one, based on domain nucleation on favorable defects at the field $E_{th} \ll E_c$ and hence to the actual thickness independence of the observable E_c for ultrathin films [64,65].

Another nontrivial modeling result is the dependence of the characteristic time τ on the applied electric field which is strongly influenced by the flexoeffect (Fig. 7). There is a narrow range in the electric-field strengths where the switching time τ goes down from infinity to the values tending towards zero, the critical field E_{cr} indicating the vertical asymptote of this dependence. For instance, in order to switch the 100-nm film during the one normalized time unit (which corresponds to the time span of about 10^{-8} s, see Appendix D of Ref. [55]) one needs to apply a critical field E_{cr} of 1.5 MV/m to the film with an account of the flexocoupling contribution or 1.6 MV/m without flexocoupling (see for details Appendix C of Ref. [55]). The difference is about 10%, but the switching times of the process with and without the flexocoupling contribution can be different by one order of the magnitude [see the vertical line in Fig. 7(a)]. Hence the flexoelectric effect facilitates the polarization switching and reduces E_{cr}. The difference between the critical fields calculated with and without flexocoupling is $\Delta E_{cr} \approx 1.3 \times 10^5\,V/m$. Figure 7(b) demonstrates that, in a wide range of the relative field strength variation $(E - E_{cr})/\Delta E_{cr}$, the approximation $\tau(E) \sim (E - E_{cr})^{-1/2}$ [68] for the field dependence of the switching time is valid with and without the flexoeffect.

Acceleration of polarization switching due to the flexoeffect is, in fact, paradoxical. Indeed, the direct flexoelectric contribution to the free energy is negative [20], and thus it is expected to reduce the energy of the ground state of either polarization direction. Therefore its difference from the energy at the saddle point at $P_3 = 0$, which does not depend on the flexoeffect and defines the energy barrier for switching, should increase in the presence of flexoelectricity and retard the switching. Contrary to the expectations, the evaluation of the free energy shows an increase in the ground-state energy due to the flexoeffect which can indirectly result from the modified polarization and strain profiles as well as from the flexoeffect term in the boundary

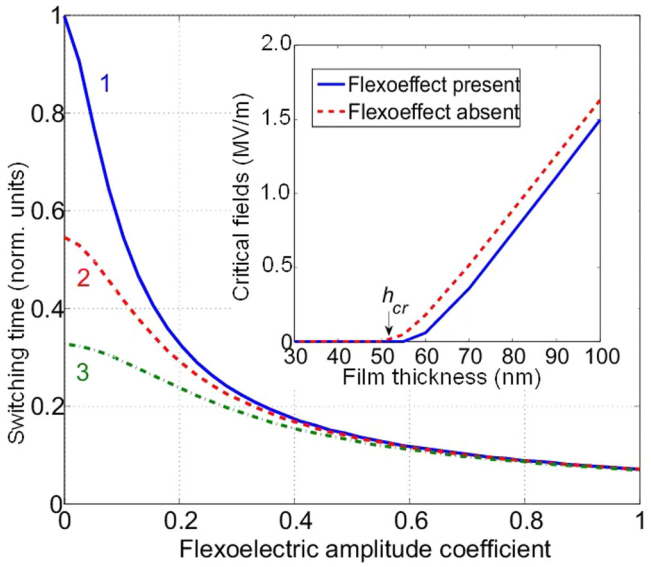

FIG. 8. Switching time dependence on the relative FA coefficient under the applied electric fields of about 1.631 MV/m (curve 1), 1.633 MV/m (curve 2), and 1.637 MV/m (curve 3). Material parameters are listed in Table C1 in Appendix C of Ref. [55]. FA = 1 corresponds to the flexocoefficient of 2.46×10^{-11} m^3/C, and the other FA values are the corresponding parts of this value. The inset: thickness dependence of the critical field in films with (solid lines) and without (dashed lines) the flexoelectric effect.

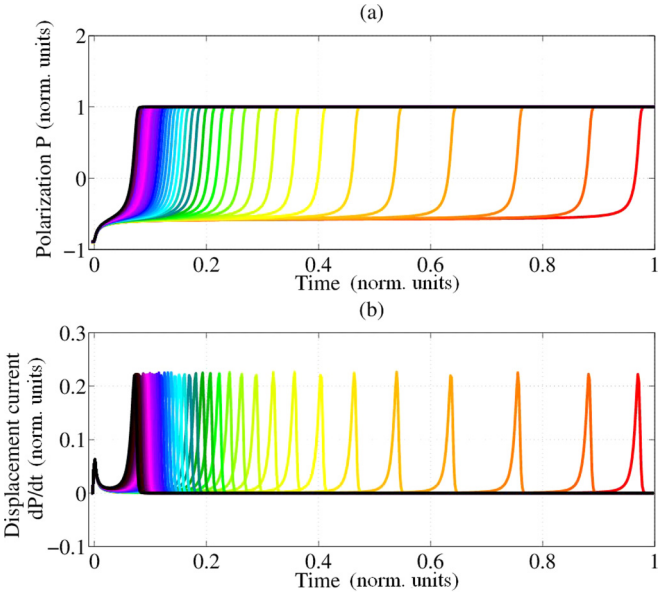

FIG. 9. (a) Single-domain polarization reversal kinetics and (b) correspondent displacement current calculated for the 100-nm film under the applied electric field of 1.631 MV/m. Each curve corresponds to different values of the flexocoupling coefficient defined as FA $\times$ F_{33}, where F_{33} is the flexoelectric tensor component (see Table C1 in Appendix C of Ref. [55]) and FA is a relative amplitude coefficient that increases from 0 (the right curve in the plot) to 1 (the left curve) adopting 40 equidistant values. The switching time of the system is maximal at FA = 0 (no flexoeffect) and minimal at FA = 1 (full flexoeffect present).

conditions (4). This results finally in the reduction of the barrier and the critical field E_{cr}.

Dependence of the switching time on the relative amplitude of the flexoelectric amplitude (FA) coefficient is shown in Fig. 8. Thickness dependence of the critical field is presented in the inset of Fig. 8 where the thickness threshold (h_{cr}) clearly is seen. The physical nature of this phenomenon is related with the strong flexocoupling influence on the polarization dynamics and elastic strain gradient distribution near the film surfaces. After all an explicit dependence of the polarization kinetics on the strength of the flexoeffect is displayed in Fig. 9 for the 100-nm film subject to a fixed external field of 1.631 MV/m.

V. CONCLUSIONS

The impact of flexoelectric coupling on the kinetics of polarization reversal and space-charge variation in thin films of ferroelectric semiconductors was theoretically studied. The Landau-Ginzburg-Devonshire-Khalatnikov relaxation equation was used to define a spatial-temporal polarization evolution together with the Poisson equation for self-consistent determination of electric potential and space-charge distribution as well as the elasticity theory equations to determine mechanical stresses and strains.

The polarization reversal process consists of two stages for thicker films, whereas it is reduced to one stage for the thinner films with thicknesses below the critical value of h_{cr}. The analysis of the obtained results reveals a moderate increase in the flexocoupling influence on the polarization, elastic strain, electric potential, and space-charge distribution with the decrease in a ferroelectric film thickness. In contrast, the dependence of polarization switching time on the applied electric field is strongly affected by the flexocoupling strength. Therefore we can conclude that the flexocoupling can affect the dynamic properties of ferroelectric thin films drastically without a significant impact on static distributions. The physical nature of this effect turned out to be related to the strong flexocoupling effect on the distribution dynamics of a polarization gradient and elastic deformation near the film surfaces.

ACKNOWLEDGMENTS

A.N.M. and E.A.E. acknowledge the National Academy of Sciences of Ukraine (Grant No. 07-06-15). I.S.V. gratefully acknowledges support from the Deutsche Forschungsgemeinschaft (DFG) through Grant No. GE 1171/7-1.

APPENDIX: ELASTIC FIELDS AND EULER-LAGRANGE EQUATIONS

For the case of mechanical equilibrium, corresponding equations read $\partial\sigma_{i3}/\partial x_3 = 0$. Boundary conditions describe a mechanically free upper surface of the film $\sigma_{i3}(0)|_S = 0$ and a fixed bottom surface $x_3 = h$ where the elastic displacement u_i is zero, i.e., $u_i(h) = 0$. In the presence of the film-substrate lattice mismatch, in-plane strains are fixed at the film-substrate interface $u_{11}(h) = u_{22}(h) = u_m$.

Elastic field components are quasihomogeneous [69] for an ultrathin ferroelectric film ($h < h_d$, where $h_d \sim 10$ nm is a characteristic thickness due to misfit dislocations) with a constant polarization in the absence of the Vegard and flexoelectric effects. In the presence of these effects, the approximate expressions for the nonzero components in a very thin film have the following form:

$$\sigma_{11}(x_3) = \sigma_{22}(x_3) = \frac{u_m - Q_{13}P_3^2}{s_{11}+s_{13}} - \frac{W_{11}^d \delta N_d^+}{s_{11}+s_{13}} - \frac{F_{13}}{s_{11}+s_{13}}\frac{\partial P_3}{\partial x_3}, \tag{A1a}$$

$$u_{11}(x_3) = u_{22}(x_3) = u_m,$$

$$u_{33}(x_3) = \frac{2s_{13}u_m}{s_{11}+s_{13}} + Q_{33}^{\text{eff}}P_3^2 + W_{33}^{\text{eff}}\delta N_d^+ + F_{33}^{\text{eff}}\frac{\partial P_3}{\partial x_3}. \tag{A1b}$$

The apparent coefficients were introduced as $W_{33}^{\text{eff}} = W_{33}^d - \frac{2s_{13}W_{11}^d}{s_{11}+s_{13}}$, $F_{33}^{\text{eff}} = F_{33} - \frac{2s_{13}F_{13}}{s_{11}+s_{13}}$, and $Q_{33}^{\text{eff}} = Q_{33} - \frac{2s_{13}Q_{13}}{s_{11}+s_{13}}$. Voigt notations are used for the electrostriction Q_{ij}, gradient coefficients g_{ij}, flexoelectric F_{ij} and elastic compliance s_{ij} tensors, whereas full matrix notations are retained for all other tensors. The tensor components with subscripts 12, 13, and 23 are equal for materials with cubic parent phases.

Misfit dislocations, the defect concentration gradient, and other factors lead to the misfit strain and spontaneous stresses vanishing in thicker films. This becomes clear from the simple energy considerations because thick strained/stressed films have much higher energy than relaxed ones.

Following Speck and Pompe [47], we modify the solutions (A1) for a thicker film ($h > h_d$) in the following way:

$$\sigma_{11} = \sigma_{22} = \frac{u_m - Q_{13}P_3^2}{s_{11}+s_{13}}\frac{h_d}{h} - \frac{W_{11}^d\delta N_d^+}{s_{11}+s_{13}} - \frac{F_{13}}{s_{11}+s_{13}}\frac{\partial P_3}{\partial x_3}, \tag{A2a}$$

$$u_{11} = u_{22} = u_m\frac{h_d}{h}$$

$$u_{33} = \left(\frac{2s_{13}u_m}{s_{11}+s_{13}} + Q_{33}^{\text{eff}}P_3^2\right)\frac{h_d}{h} + W_{33}^{\text{eff}}\delta N_d^+ + F_{33}^{\text{eff}}\frac{\partial P_3}{\partial x_3}. \tag{A2b}$$

Here h_d has the sense of some characteristic thickness defined by several factors, such as the critical thickness of misfit dislocation appearance, the film thickness-to-width ratio, the film-substrate thickness ratios, etc.

Actually, it is a well-known fact that misfit dislocations emerge in epitaxial films when their thicknesses exceed the critical thicknesses of dislocation appearance h_d. These thicknesses decrease with the increase in the interface misfit strain u_m. In accordance with the Matthews-Blakeslee theory and the Speck and Pompe model for perovskites [47], $h_d \approx \frac{b}{u_m}\frac{\sqrt{2}\ln(4h_d/b)}{8\pi(1+\nu)} \sim u_m^{-1}$ in a wide range of u_m, which is in good agreement with experiments (the Burgers vector of dislocation b is on the order of the lattice constant a, $\nu \sim 0.3$ is Poisson's ratio). For typical misfit strains $|u_m| \sim 10^{-2}$ the thickness is $h_d \sim 10 - 0.5$ nm, i.e., it is not more than several tens of lattice constants [47]. Hence we can regard that $h_d \leqslant (5-10)$ nm. More rigorously, Eqs. (A2) can be a good approximation in the average sense (as Saint-Venant conditions).

Note that the piezoelectric contribution is automatically included in Eq. (A1) as linearized electrostriction since $P_3 \approx P_3^S + \varepsilon_0(\varepsilon_{33}^f - 1)E_3$.

Using Eqs. (A1) and (A2), we exclude the stresses from the equations for polarization P_3 and concentration of donors N_d^+. The remaining equations can be solved numerically. Note that the substitution of expressions (A1) and (A2) in the Gibbs functional leads to the appearance of the flexoelectric coupling with Vegard and piezoelectric terms proportional to the products $W_{ii}^{\text{eff}}F_{33}^{\text{eff}}$, $\Sigma_{ii}^{\text{eff}}F_{33}^{\text{eff}}$, etc.

The Euler-Lagrange equation for determination of the ferroelectric polarization component has an explicit form

$$a_{33}^{\text{eff}}P_3 + b_{33}^{\text{eff}}P_3^3 + \gamma_{333}P_3^5 - g_{33}^{\text{eff}}\frac{\partial^2 P_3}{\partial x_3^2} - \frac{2F_{13}W_{11}^d}{s_{11}+s_{13}}\frac{\partial N_d^+}{\partial x_3} = -\frac{\partial\varphi}{\partial x_3}. \tag{A3}$$

The effective coefficients were introduced as $g_{33}^{\text{eff}} = g_{33} + \frac{2F_{13}^2}{s_{11}+s_{13}}$, $b_{33}^{\text{eff}} = (b_{33} + \frac{4Q_{13}^2}{s_{11}+s_{13}})$, and $a_{33}^{\text{eff}} = \alpha_{33}^T(T-T_c) - \frac{2u_mQ_{13}}{s_{11}+s_{13}} + \frac{4Q_{13}W_{11}^d}{s_{11}+s_{13}}\delta N_d^+$ for the case of $h \leqslant h_d$. For the case of $h > h_d$ the coefficients are $b_{33}^{\text{eff}} = (b_{33} + \frac{4Q_{13}^2}{s_{11}+s_{13}}\frac{h_d}{h})$ and $a_{33}^{\text{eff}} = \alpha_{33}^T(T-T_c) - \frac{2u_mQ_{13}}{s_{11}+s_{13}}\frac{h_d}{h} + \frac{4Q_{13}W_{11}^d}{s_{11}+s_{13}}\delta N_d^+$.

Boundary conditions for the out-of-plane polarization component P_3 are of the third kind [70],

$$\left(P_3 - \lambda_1\frac{\partial P_3}{\partial x_3} - \frac{2F_{13}W_{11}^d}{s_{11}+s_{12}}\frac{\delta N_d^+}{A_{33}^{S1}} - \frac{2F_{13}Q_{13}}{s_{11}+s_{13}}\frac{P_3^2}{A_{33}^{S1}}\right)\Big|_{x_3=0} = 0, \tag{A4a}$$

$$\left(P_3 + \lambda_2\frac{\partial P_3}{\partial x_3} + \frac{2F_{13}W_{11}^d}{s_{11}+s_{13}}\frac{\delta N_d^+}{A_{33}^{S2}} + \frac{2F_{13}Q_{13}}{s_{11}+s_{13}}\frac{P_3^2}{A_{33}^{S2}}\right)\Big|_{x_3=h} = 0. \tag{A4b}$$

The extrapolation length $\lambda_m = \frac{g_{33}^{\text{eff}}}{A_{33}^{Sm}}$ is determined by the surface energy and the surface state. Physically the realistic range for λ_m is 0.5–2 nm [71].

[1] V. S. Mashkevich and K. B. Tolpygo, Zh. Eksp. Teor. Fiz. **32**, 520 (1957) [Sov. Phys. JETP **5**, 435 (1957)].

[2] S. M. Kogan, Solid State Phys. **5**, 2829 (1963) [Sov. Phys.-Solid State **5**, 2069 (1964)].

[3] A. K. Tagantsev, Phys. Rev B **34**, 5883 (1986).

[4] P. Zubko, G. Catalan, and A. K. Tagantsev, Annu. Rev. Mater. Res. **43**, 387 (2013).

[5] P. V. Yudin and A. K. Tagantsev, Nanotechnology **24**, 432001 (2013).

[6] S. V. Kalinin and A. N. Morozovska, Nat. Nanotechnol. **10**, 916 (2015).

[7] *Flexoelectricity in Solids: From Theory to Applications*, edited by A. K. Tagantsev and P. V. Yudin (World Scientific, Singapore, 2016).

[8] G. Catalan, L. J. Sinnamon, and J. M. Gregg, J. Phys.: Condens. Matter **16**, 2253 (2004).
[9] M. S. Majdoub, R. Maranganti, and P. Sharma, Phys. Rev. B **79**, 115412 (2009).
[10] A. S. Yurkov and A. K. Tagantsev, Appl. Phys. Lett. **108**, 022904 (2016).
[11] A. S. Starkov and I. A. Starkov, Int. J. Solids Struct. **82**, 65 (2016).
[12] C. Zhang, L. Zhang, X. D. Shen, and W. Chen, J. Appl. Phys. **119**, 134102 (2016).
[13] E. A. Eliseev, A. N. Morozovska, M. D. Glinchuk, and R. Blinc, Phys. Rev. B **79**, 165433 (2009).
[14] A. N. Morozovska and M. D. Glinchuk, J. Appl. Phys. **119**, 094109 (2016).
[15] E. A. Eliseev, A. V. Semchenko, Y. M. Fomichov, V. V. Sidsky, V. V. Kolos, Y. M. Pleskachevsky, M. V. Silibin, N. V. Morozovsky, and A. N. Morozovska, J. Appl. Phys. **119**, 204104 (2016).
[16] A. Kholkin, I. Bdikin, T. Ostapchuk, and J. Petzelt, Appl. Phys. Lett. **93**, 222905 (2008).
[17] R. Tararam, I. K. Bdikin, N. Panwar, J. A. Varela, P. R. Bueno, and A. L. Kholkin, J. Appl. Phys. **110**, 052019 (2011).
[18] U. K. Bhaskar, N. Banerjee, A. Abdollahi, Z. Wang, D. G. Schlom, G. Rijnders, and G. Catalan, Nat. Nanotechnol. **11**, 263 (2016).
[19] J. Narvaez, F. Vasquez-Sancho, and G. Catalan, Nature (London) **538**, 219 (2016).
[20] E. A. Eliseev, P. V. Yudin, S. V. Kalinin, N. Setter, A. K. Tagantsev, and A. N. Morozovska, Phys. Rev. B **87**, 054111 (2013).
[21] E. K. H. Salje, S. Li, M. Stengel, P. Gumbsch, and X. D. Ding, Phys. Rev. B **94**, 024114 (2016).
[22] E. A. Eliseev, A. N. Morozovska, G. S. Svechnikov, P. Maksymovych, and S. V. Kalinin, Phys. Rev. B **85**, 045312 (2012).
[23] A. N. Morozovska, E. A. Eliseev, M. D. Glinchuk, L. Q. Chen, and V. Gopalan, Phys. Rev. B **85**, 094107 (2012).
[24] A. N. Morozovska, E. A. Eliseev, S. V. Kalinin, L. Q. Chen, and V. Gopalan, Appl. Phys. Lett. **100**, 142902 (2012).
[25] E. A. Eliseev, A. N. Morozovska, Y. J. Gu, A. Y. Borisevich, L. Q. Chen, V. Gopalan, and S. V. Kalinin, Phys. Rev. B **86**, 085416 (2012).
[26] Y. J. Gu, M. L. Li, A. N. Morozovska, Y. Wang, E. A. Eliseev, V. Gopalan, and L.-Q. Chen, Phys. Rev. B **89**, 174111 (2014).
[27] A. Y. Borisevich, E. A. Eliseev, A. N. Morozovska, C. J. Cheng, J. Y. Lin, Y. H. Chu, D. Kan, I. Takeuchi, V. Nagarajan, and S. V. Kalinin, Nat. Commun. **3**, 775 (2012).
[28] P. Maksymovych, A. N. Morozovska, P. Yu, E. A. Eliseev, Y. H. Chu, R. Ramesh, A. P. Baddorf, and S. V. Kalinin, Nano Lett. **12**, 209 (2012).
[29] W. Ma and L. E. Cross, Appl. Phys. Lett. **82**, 3293 (2003).
[30] P. Zubko, G. Catalan, A. Buckley, P. R. L. Welche, and J. F. Scott, Phys. Rev. Lett. **99**, 167601 (2007).
[31] W. Ma and L. E. Cross, Appl. Phys. Lett. **88**, 232902 (2006).
[32] A. N. Morozovska, Y. M. Vysochanskii, O. V. Varenyk, M. V. Silibin, S.V. Kalinin, and E. A. Eliseev, Phys. Rev. B **92**, 094308 (2015).
[33] M. Stengel, Phys. Rev. B **93**, 245107 (2016).
[34] A. N. Morozovska, E. A. Eliseev, C. M. Scherbakov, and Y. M. Vysochanskii, Phys. Rev. B **94**, 174112 (2016).
[35] P. V. Yudin, R. Ahluwalia, and A. K. Tagantsev, Appl. Phys. Lett. **104**, 082913 (2014).
[36] J. W. Hong and D. Vanderbilt, Phys. Rev. B **84**, 180101 (2011).
[37] I. Ponomareva, A. K. Tagantsev, and L. Bellaiche, Phys. Rev. B **85**, 104101 (2012).
[38] J. W. Hong and D. Vanderbilt, Phys. Rev. B **88**, 174107 (2013).
[39] M. Stengel, Phys. Rev. B **88**, 174106 (2013).
[40] A. Biancoli, C. M. Fancher, J. L. Jones, and D. Damjanovic, Nat. Mater. **14**, 224 (2015).
[41] A. Kvasov and A. K. Tagantsev, Phys. Rev. B **92**, 054104 (2015).
[42] Y. Ishibashi and Y. Takagi, J. Phys. Soc. Jpn. **31**, 506 (1971).
[43] S. Liu, I. Grinberg, and A. M. Rappe, Nature (London) **534**, 360 (2016).
[44] A. K. Tagantsev, I. Stolichnov, N. Setter, J. S. Cross, and M. Tsukada, Phys. Rev. B **66**, 214109 (2002).
[45] Y. A. Genenko, S. Zhukov, S. V. Yampolskii, J. Schütrumpf, R. Dittmer, W. Jo, H. Kungl, M. J. Hoffmann, and H. von Seggern, Adv. Funct. Mater. **22**, 2058 (2012).
[46] J. F. Scott, Adv. Mater. **22**, 5315 (2011).
[47] J. S. Speck and W. Pompe, J. Appl. Phys. **76**, 466 (1994).
[48] A. K. Tagantsev, L. E. Cross, and J. Fousek, *Domains in Ferroic Crystals and Thin Films* (Springer, New York, 2010).
[49] A. K. Tagantsev and G. Gerra, J. Appl. Phys. **100**, 051607 (2006).
[50] X. Zhang, A. M. Sastry, and W. Shyy, J. Electrochem. Soc. **155**, A542 (2008).
[51] D. A. Freedman, D. Roundy, and T. A. Arias, Phys. Rev. B **80**, 064108 (2009).
[52] S. M. Sze, *Physics of Semiconductor Devices* (Wiley-Interscience, New York, 1981).
[53] O. Hirsch, Master's thesis, Technische Universität Darmstadt, 2012.
[54] X. Aymerich-Humet, F. Serra-Mestres, and J. Milán, J. Appl. Phys. **54**, 2850 (1983).
[55] See Supplemental Material at http://link.aps.org/supplemental/10.1103/PhysRevB.95.014104 for details on calculations and used parameter values.
[56] A. N. Morozovska, E. A. Eliseev, Y. A. Genenko, I. S. Vorotiahin, M. V. Silibin, Y. Cao, Y. Kim, M. D. Glinchuk, and S. V. Kalinin, Phys. Rev. B **94**, 174101 (2016).
[57] W. Cao and L. E. Cross, Phys. Rev. B **44**, 5 (1991).
[58] J. Hlinka and P. Marton, Phys. Rev. B **74**, 104104 (2006).
[59] M. Budimir, D. Damjanovic, and N. Setter, Phys. Rev. B. **73**, 174106 (2006).
[60] D. Damjanovic, Appl. Phys. Lett. **97**, 062906 (2010).
[61] G. A. Rossetti, A. G. Khachaturyan, G. Akcay, and Y. Ni, J. Appl. Phys. **103**, 114113 (2008).
[62] D. J. Franzbach, B. X. Xu, R. Mueller, and K. G. Webber, Appl. Phys. Lett. **99**, 162903 (2011).
[63] D. J. Franzbach, Y. J. Gu, L. Q. Chen, and K. G. Webber, Appl. Phys. Lett. **101**, 232904 (2012).
[64] V. M. Fridkin and S. Ducharme, Phys.-Usp. **57**, 597 (2014).
[65] S. Ducharme, V. M. Fridkin, A. V. Bune, S. P. Palto, L. M. Blinov, N. N. Petukhova, and S. G. Yudin, Phys. Rev. Lett. **84**, 175 (2000).

[66] A. N. Morozovska, E. A. Eliseev, S. V. Svechnikov, A. D. Krutov, V. Y. Shur, A. Y. Borisevich, P. Maksymovych, and S. V. Kalinin. Phys. Rev. B **81**, 205308 (2010).
[67] M. D. Glinchuk, E. A. Eliseev, V. A. Stephanovich, and R. Fahri, J. Appl. Phys. **93**, 1150 (2003).
[68] G. Vizdrik, S. Ducharme, V. M. Fridkin, and S. G. Yudin, Phys. Rev. B **68**, 094113 (2003).
[69] N. A. Pertsev, A. G. Zembilgotov, and A. K. Tagantsev, Phys. Rev. Lett. **80**, 1988 (1998).
[70] R. Kretschmer and K. Binder, Phys. Rev. B **20**, 1065 (1979).
[71] C. L. Jia, V. Nagarajan, J. Q. He, L. Houben, T. Zhao, R. Ramesh, K. Urban, and R. Waser, Nat. Mater. **6**, 64 (2007).

Supplementary Materials to
"Flexocoupling impact on the kinetics of polarization reversal"

Ivan S. Vorotiahin[1, 2], Anna N. Morozovska[1], Eugene A. Eliseev[1, 3], Yuri A. Genenko[2],

[1] Institute of Physics, National Academy of Sciences of Ukraine,

46, pr. Nauky, 03028 Kyiv, Ukraine

[2]Institut für Materialwissenschaft, Technische Universität Darmstadt,

Jovanka-Bontschits-Str. 2, 64287 Darmstadt, Germany

[3] Institute for Problems of Materials Science, National Academy of Sciences of Ukraine,

Krjijanovskogo 3, 03142 Kyiv, Ukraine

Appendix B. Fermi integral and its Approximation

To solve Poisson's equation for electrostatic potential the numerical calculation of the space charge concentration is required. The electron concentration is strongly dependent on the potential itself and positions of the energy levels in bulk, i.e. bottom of the conduction band in relation to the Fermi level. For calculation the Fermi integral $F_{1/2}(\xi)=\frac{2}{\sqrt{\pi}}\int_0^{\infty}\frac{\sqrt{\zeta}d\zeta}{1+\exp(\zeta-\xi)}$ should be used as the reflection of Fermi-Dirac statistics for the electron distribution.

The above integral is a form of a polylogarithm, so that no explicit analytical solution can be shown. Instead, we need to calculate this integral numerically, using an approximation. A useful expression for the approximate Fermi integral was presented by X. Aymerich-Humet et al. [1,2], having the following form:

$$\widetilde{F}_j(x)=\frac{1}{\Gamma(j+1)}\left(\frac{(j+1)\cdot 2^{j+1}}{\left[b+x+\left(|x-b|^c+a^c\right)^{1/c}\right]^{j+1}}+\frac{e^{-x}}{\Gamma(j+1)}\right)^{-1},$$

where j is the order of integral, $\Gamma(n)$ is the Gamma-Euler-function, a factorial function with the following properties: $\Gamma(n)=(n-1)!$, $\Gamma(1/2)=\sqrt{\pi}$, $\Gamma(p+1)=p\Gamma(p)$. a, b, c denote the short forms of the polynomial expressions $a=\left[1+\frac{15}{4}(j+1)+\frac{1}{40}(j+1)^2\right]^{\frac{1}{2}}$, $b=1.8+0.61\cdot j$, $c=2+(2+\sqrt{2})\cdot 2^j$.

Appendix C. Listing of the Material Parameters

TABLE C1. Known material properties and experimental parameters [3, 4]

Material			***$BaTiO_3$***
Structure			***Tetragonal***
Property	**Symbol**	**Units**	**Value**
Temperature	T	°K	300
Curie Temperature	T_C	°K	400
Film thickness	h	nm	100; 75; 60; 45; 30; 10
Background dielectric permittivity	ε_b		7
Vegard expansion tensor	w	Å³	10
Effective electron mass	m_n		$0.3m_e$
Electron mass	m_e	kg J eV	$9.11\cdot10^{-31}$ $8.19\cdot10^{-14}$ $0.511\cdot10^{6}$
Gap between donor level and the bottom of conduction band	E_c - E_d	eV	0.1
Bottom of conduction band	E_c	eV	0.85
Donor level	E_d	eV	0.75
Fermi energy	E_F	eV	0
Predicted spontaneous polarization	P_S	C/m²	0.27
Donor concentration	N_d^0	1/m³	10^{23}
LGD and elastic tensors:			
Temperature independent P² expansion coefficient	α_{33}^T	$mJC^{-2}K^{-1}$	$3.34\ 10^5$
P⁴ expansion coefficient	b_{33}	m^5JC^{-4}	$-6.71\cdot10^8$
P⁴ expansion coefficient	b_{12}	m^5JC^{-4}	$3.23\cdot10^8$
P⁶ expansion coefficient	γ_{333}	$C^{-6}m^9J$	8.004×10^9
P⁶ expansion coefficient	γ_{112}	$C^{-6}m^9J$	4.47×10^9
P⁶ expansion coefficient	γ_{123}	$C^{-6}m^9J$	4.91×10^9
Gradient tensor	g_{33}	m^3J/C^2	$5.1\cdot10^{-10}$
Gradient tensor	g_{12}	m^3J/C^2	$-0.2\cdot10^{-10}$
Gradient tensor	g_{44}	m^3J/C^2	$0.2\cdot10^{-10}$
Elastic stiffness tensor	s_{11}	1/Pa	$8.3\cdot10^{-12}$
Elastic stiffness tensor	s_{13}	1/Pa	$-2.7\cdot10^{-12}$
Elastic stiffness tensor	s_{44}	1/Pa	$9.24\cdot10^{-12}$
Elastic compliance tensor	c_{11}	Pa	$0.12\cdot10^{12}$
Elastic compliance tensor	c_{13}	Pa	$-0.37\cdot10^{12}$

Elastic compliance tensor	c_{44}	Pa	$0.108\cdot10^{12}$
Electrostriction tensor	Q_{33}	m^4/C^2	0.11
Electrostriction tensor	Q_{13}	m^4/C^2	-0.043
Electrostriction tensor	Q_{44}	m^4/C^2	0.059
Flexoelectric coefficient	F_{33}	m^3/C	$2.46\cdot10^{-11}$
Flexoelectric coefficient	F_{13}	m^3/C	$0.48\cdot10^{-11}$
Flexoelectric coefficient	F_{44}	m^3/C	$0.05\cdot10^{-11}$
Recalculated values	($F_{ij} = f_{ik}\cdot s_{jk}$; $Q_{ij} = q_{ik}\cdot s_{jk}$)		
Flexoelectric coefficient	f_{33}	J/C	2.96
Flexoelectric coefficient	f_{44}	J/C	0.054
Electrostriction tensor	q_{33}	$J\cdot m/C^2$	$13.2\cdot10^9$
Electrostriction tensor	q_{44}	$J\cdot m/C^2$	$6.372\cdot10^9$
Additional parameters			
Donor charge Z_d			2
Electrochemical potential of electrons	ζ_e	eV	Equal to Fermi level
Electrochemical potential of donors	ζ_d	eV	Equal to Fermi level
Landau-Khalatnikov coefficient	Γ	sec	1.336×10^6
Evaluation of the Khalatnikov term	$\Gamma/(\alpha_t T_c)$		10^{-3}
Inhomogeneous mobile species concentration	δN_d^+		Coordinate-dependent
Depolarization distance	h_d	nm	10
Extrapolation length	λ	nm	0.5
Misfit strain	u_m		0

Appendix D. Coupled equations in dimensionless variables

Poisson equation (S.1) for electric potential $\tilde{\varphi} = e\varphi/k_B T$ in dimensionless variables acquires the form:

$$\frac{\partial^2\tilde{\varphi}}{\partial\tilde{z}^2} = \frac{eP_{s0}L_P}{\varepsilon_0\varepsilon_b k_B T}\frac{\partial\tilde{P}}{\partial\tilde{z}} - \frac{L_P^2}{L_D^2}\left(\tilde{N}(\varphi) - \tilde{n}(\varphi)\right). \tag{D.1}$$

Here we introduced characteristic length scale as a gradient length $L_P = \sqrt{\left(g_{33} + \frac{2F_{13}^2}{s_{11}+s_{12}}\right)\Big/\alpha_{33}^T T_c}$ along with the Debye screening length $L_D = \sqrt{\varepsilon_0\varepsilon_b k_B T/\left(e^2 N_s\right)}$, where the equilibrium concentration of ionized donors is $N_s = N_d^0\left(1 - f\left(\left(E_d - E_F\right)/k_B T\right)\right)$. Equation for dimensionless polarization $\tilde{P} = P_3/P_{s0}$ can be found from Eq.(A.3) in the following form

$$\begin{aligned}&\frac{\Gamma}{\alpha_{33}^T T_C}\frac{\partial\tilde{P}}{\partial t} + \left(\frac{T}{T_C} - 1 + \frac{4Q_{13}W_{11}^d N_s}{\alpha_{33}^T T_C\left(s_{11}+s_{12}\right)}\delta\tilde{N}\right)\tilde{P} + \frac{P_{s0}^2}{\alpha_{33}^T T_C}b_{33}^{eff}\tilde{P}^3 + \frac{\gamma_{333}P_{s0}^4}{\alpha_{33}^T T_C}\tilde{P}^5 - \\ &- \frac{g_{33} + 2F_{13}^2/(s_{11}+s_{12})}{\alpha_{33}^T T_C L_P^2}\frac{\partial^2\tilde{P}}{\partial\tilde{z}^2} + \frac{1}{\alpha_{33}^T T_C P_{s0}}\frac{k_B T}{L_P e}\frac{\partial\tilde{\varphi}}{\partial\tilde{z}} - \frac{2F_{13}W_{11}^d N_s}{\alpha_{33}^T T_C P_{s0}\left(s_{11}+s_{12}\right)L_P}\frac{\partial\tilde{N}}{\partial\tilde{z}} = 0\end{aligned} \tag{D.2a}$$

Here we introduced characteristic value of polarization $P_{s0} = \sqrt{\left[\sqrt{\left(b_{33}^{eff}\right)^2 - 4\gamma_{333}\alpha_{33}^T(T-T_c)} - b_{33}^{eff}\right] \Big/ 2\gamma_{333}}$.

In the dimensionless variables, polarization boundary conditions (4) are transformed to

$$\left(\frac{\tilde{P}}{\tilde{\lambda}} \pm \left(\frac{\partial \tilde{P}}{\partial \tilde{z}} + \frac{2F_{13}W_{11}^d N_s}{P_{s0}\left(s_{11}+s_{12}\right)\alpha_{33}^T T_c L_P}\delta\tilde{N} + \frac{P_{s0}}{\alpha_{33}^T T_c L_P}\frac{2F_{13}Q_{13}}{s_{11}+s_{12}}\tilde{P}^2\right)\right)\Bigg|_{x_3=0,h} = 0 \qquad \text{(D.2b)}$$

Here we introduced a dimensionless extrapolation length as $\tilde{\lambda} = \frac{1}{L_P A_{33}^S}\left(g_{33} + \frac{2F_{13}^2}{s_{11}+s_{12}}\right)$.

Dimensionless concentration of donors is

$$\tilde{N} = \frac{N_d^0}{N_s}\tilde{f}\left(\tilde{\varphi} + \tilde{E}_F - \tilde{E}_d + \frac{2W_{11}^d}{k_B T\left(s_{11}+s_{12}\right)}\left(W_{11}^d N_s \delta\tilde{N} + \frac{F_{13}P_{s0}}{L_P}\frac{\partial\tilde{P}}{\partial\tilde{z}} + Q_{13}P_{s0}^2\tilde{P}^2\right)\right). \qquad \text{(D.3)}$$

Also we will need a dimensionless concentration of electrons, which can be expressed as:

$$\tilde{n} = \frac{N_C}{N_s}F_{1/2}\left(\tilde{\varphi} + \tilde{E}_F - \tilde{E}_C\right) \qquad \text{(D.4)}$$

Boundary conditions for electric potential are

$$\tilde{\varphi}\big|_{\tilde{z}=0} = \tilde{V}, \quad \tilde{\varphi}\big|_{\tilde{z}=\tilde{h}} = 0. \qquad \text{(D.5)}$$

Dimensionless out-of-plane displacement at the surface is

$$\frac{u_3}{L_P}\bigg|_{\tilde{z}=\tilde{h}} = \left(\tilde{F}_{33} - \frac{2s_{13}\tilde{F}_{13}}{s_{11}+s_{12}}\right)\left(\tilde{P}\big|_{\tilde{z}=\tilde{h}} - \tilde{P}\big|_{\tilde{z}=0}\right) + \left(\tilde{Q}_{33} - \frac{2s_{13}\tilde{Q}_{13}}{s_{11}+s_{12}}\right)\int_0^{\tilde{h}}\tilde{P}^2 d\tilde{z} \quad (\text{at } h \le h_d) \qquad \text{(D.6a)}$$

$$\frac{u_3}{L_P}\bigg|_{\tilde{z}=\tilde{h}} = \left(\tilde{F}_{33} - \frac{2s_{13}\tilde{F}_{13}}{s_{11}+s_{12}}\right)\left(\tilde{P}\big|_{\tilde{z}=\tilde{h}} - \tilde{P}\big|_{\tilde{z}=0}\right) + \frac{h_d}{h}\left(\tilde{Q}_{33} - \frac{2s_{13}\tilde{Q}_{13}}{s_{11}+s_{12}}\right)\int_0^{\tilde{h}}\tilde{P}^2 d\tilde{z} \quad (\text{at } h > h_d) \qquad \text{(D.6b)}$$

Dimensionless variables and parameters involved in Eqs.(D.1)-(D.6) are listed in the **Table D1.**

In the dimensionless LGD equation Landau-Khalatnikov coefficient Γ becomes $\tilde{\Gamma}$. Standing in front of the time derivative this coefficient is measured in the time units. The factor $\frac{1}{\alpha_{33}^T T_C}$ determines the unit on time scale, which in this case is equal to ~10^{-8} s. $\tilde{\Gamma}$ is assigned a value of 10^{-3} s to observe the whole switching process within the given time interval (~10 ns), which corresponds to the characteristic order of $\Gamma \sim 10^6$ s.

TABLE D1. Dimensionless variables and parameters

Quantity	**Definition/designation**
Gradient length – characteristic value of length	$L_P = \sqrt{\left(g_{33} + \frac{2F_{13}^2}{s_{11}+s_{12}}\right) \Big/ \alpha_{33}^T T_c}$

Debye screening length	$L_D = \sqrt{\varepsilon_0 \varepsilon_b k_B T / \left(e^2 N_s\right)}$
coordinate and thickness	$\tilde{z} = x_3 / L_P$, $\tilde{h} = h / L_P$
donor concentration	$\tilde{N} = \frac{N_d^0}{N_s} \tilde{f} \left(\begin{array}{l} \tilde{\varphi} + \tilde{E}_F - \tilde{E}_d + \\ + \frac{2W_{11}^d}{k_B T (s_{11} + s_{12})} \left(\begin{array}{l} W_{11}^d N_s \delta\tilde{N} + \tilde{F}_{13} \frac{\partial \tilde{P}}{\partial \tilde{z}} + \\ + \tilde{Q}_{13} \tilde{P}^2 \end{array} \right) \end{array} \right)$
electron density	$\tilde{n} = \frac{N_C}{N_s} F_{1/2} \left(\tilde{\varphi} + \tilde{E}_F - \tilde{E}_C \right)$
Equilibrium concentration of ionized donors at zero potential and stress	$N_s = N_d^0 \left(1 - f\left(\left(E_d - E_F\right) / k_B T \right)\right)$
electric potential	$\tilde{\varphi} = e\varphi / k_B T$ or $\varphi = \tilde{\varphi} k_B T / e$
electric field	$\tilde{E}_3 = L_P e E_3 / k_B T$ or $E_3 = \tilde{E} k_B T / L_P e$
Applied voltage	$\tilde{V} = eU / k_B T$
chemical potential of electrons	$\tilde{\zeta}_d = \zeta_d / k_B T$
donor level and conduction band	$\tilde{E}_d = E_d / k_B T$ $\quad$ $\tilde{E}_C = E_C / k_B T$
Fermi level	$\tilde{E}_F = E_F / k_B T$
polarization	$\tilde{P} = P_3 / P_{s0}$ or $P_3 = P_{s0} \tilde{P}$
Characteristic value of polarization	$P_{s0} = \sqrt{\left[\sqrt{\left(b_{33}^{eff}\right)^2 - 4\gamma_{333} \alpha_{33}^T (T - T_c)} - b_{33}^{eff} \right] / 2\gamma_{333}}$
Vegard coefficient	$\tilde{W} = W_{11}^d N_s$
Dimensionless concentration	$\tilde{n}_b = \frac{n_b}{N_s}$
Electrostriction coefficient	$\tilde{Q}_{13} = Q_{13} P_{s0}^2$, $\tilde{Q}_{33} = Q_{33} P_{s0}^2$
flexoelectric coefficient	$\tilde{F}_{13} = F_{13} \frac{P_{s0}}{L_P}$, $\tilde{F}_{33} = F_{33} \frac{P_{s0}}{L_P}$
Extrapolation length	$\tilde{\lambda} = \frac{1}{L_P A_{33}^S} \left(g_{33} + \frac{2F_{13}^2}{s_{11} + s_{12}} \right)$
Landau-Khalatnikov coefficient	$\tilde{\Gamma} = \frac{\Gamma}{\alpha_{33}^T T_C}$

References

[1] O. Hirsch, Master Thesis, Technische Universität Darmstadt, 2012.

[2] X. Aymerich-Humet, F. Serra-Mestres, and J. Milán, J. Appl. Phys. 54, 2850 (1983).

[3] J. Hlinka, P. Márton, Phys. Rev. B **74**, 104104 (2006).

[4] A. J. Bell, L. E. Cross, Ferroelectrics, **59**, 197-203 (1984).

3.5. Publication B1

Tuning the polar states of ferroelectric films via surface charges and flexoelectricity
Ivan S. Vorotiahin, Eugene A. Eliseev, Qian Li, Sergei V. Kalinin, Yuri A. Genenko, Anna N. Morozovska
Acta Materialia 137 (2017) 85-92. 8 pages, with Supplementary materials, 15 pages.

Acta Materialia 137 (2017) 85–92

Contents lists available at ScienceDirect

Acta Materialia

journal homepage: www.elsevier.com/locate/actamat

Full length article

Tuning the polar states of ferroelectric films via surface charges and flexoelectricity☆

Ivan S. Vorotiahin [a, b], Eugene A. Eliseev [c], Qian Li [d], Sergei V. Kalinin [d, *], Yuri A. Genenko [a, **], Anna N. Morozovska [b, ***]

[a] Institut für Materialwissenschaft, Technische Universität Darmstadt, Jovanka-Bontschits-Str. 2, 64287 Darmstadt, Germany
[b] Institute of Physics, National Academy of Sciences of Ukraine, 46, Pr. Nauky, 03028 Kyiv, Ukraine
[c] Institute for Problems of Materials Science, National Academy of Sciences of Ukraine, Krjijanovskogo 3, 03142 Kyiv, Ukraine
[d] The Center for Nanophase Materials Sciences, Oak Ridge National Laboratory, Oak Ridge, TN 37831, USA

ARTICLE INFO

Article history:
Received 3 April 2017
Received in revised form
13 July 2017
Accepted 14 July 2017
Available online 14 July 2017

Keywords:
Ferroelectric film
Domain structure
Flexoelectric effect
Surface screening charges

ABSTRACT

Using the self-consistent Landau-Ginzburg-Devonshire approach we simulate and analyze the spontaneous formation of the domain structure in thin ferroelectric films covered with the surface screening charge represented by the Bardeen-type surface states. Hence we consider the competition between the screening and the domain formation as alternative ways to reduce the electrostatic energy and reveal unusual peculiarities of distributions of polarization, electric and elastic fields conditioned by the surface screening length and the flexocoupling strength. We have established that the critical thickness of the film and its transition temperature to a paraelectric phase strongly depend on the Bardeen screening length, while the flexocoupling affects the polarization rotation and closure domain structure. Furthermore the flexocoupling induces ribbon-like nano-scale domains in the film depth far from the top open surface, which might be related to the enigmatic polar nanoregions in relaxor ferroelectrics. Thus the joint action of the surface screening (originating from e.g. the adsorption of ambient ions or surface states) and flexocoupling may remarkably modify polar and electromechanical properties of thin ferroelectric films.

1. Introduction

Ferroelectric materials remain the object of endless fascination for applied and fundamental science alike. The fundamental aspect of these materials is the presence of surface and interface bound charges due to the discontinuity of the spontaneous polarization. Since the early days of ferroelectricity, these charges were recognized as the key aspect of the physics of ferroelectric surfaces and interfaces. Indeed, if the polarization charge were uncompensated, it would provide bulk-like contributions to the free energy of materials, *i.e.* the corresponding energy would diverge with the system size. These considerations stimulated the search for mechanisms for lowering of this depolarization energy. One such mechanism is formation of ferroelectric domains, extensively analyzed in classical textbooks [1,2]. The second is charge screening, either internal "bulk" screening by free charges inside a ferroelecric [3,4] or external "surface" screening by the free charges in the case of the open or electroded ferroelectric film surface. Surprisingly, until now the domain formation and surface screening mechanisms were considered separately, and the competition between these effects almost escaped the attention of scientific community, despite the fact that these processes are intertwined in thin films.

Surface screening of the bound charges is typically provided by the mobile charges adsorbed from the ambience in the case of high or normal humidity [5–9] or by internal mobile charges of defect

☆ This manuscript has been authored by UT-Battelle, LLC, under Contract No. DE-AC0500OR22725 with the U.S. Department of Energy. The United States Government retains and the publisher, by accepting the article for publication, acknowledges that the United States Government retains a non-exclusive, paid-up, irrevocable, world-wide license to publish or reproduce the published form of this manuscript, or allow others to do so, for the United States Government purposes. The Department of Energy will provide public access to these results of federally sponsored research in accordance with the DOE Public Access Plan (http://energy.gov/downloads/doe-public-access-plan).

* Corresponding author.
** Corresponding author.
*** Corresponding author.
E-mail addresses: sergei2@ornl.gov (S.V. Kalinin), genenko@mm.tu-darmstadt.de (Y.A. Genenko), anna.n.morozovska@gmail.com (A.N. Morozovska).

http://dx.doi.org/10.1016/j.actamat.2017.07.033
1359-6454/

nature [10,11]. In a specific case of the very weak screening, or its artificial absence due to the experimental treatment (cleaned surface in dry atmosphere, ultra-high vacuum or thick dielectric layer at the surface) the screening charges can be localized at surface states caused by the strong band-bending by depolarization field [12–17]. For both aforementioned cases the screening charges are at least partially free (i.e. mobile) and the spatial distribution of their quasi two-dimensional density is determined by the polarization distribution near the surface.

Due to the long-range nature of the depolarization effects, the incomplete surface screening of ferroelectric polarization strongly influences the domain structure and leads to pronounced effects both near and relatively far from the surface. The incomplete screening strongly affects domain nucleation dynamics, domain shape and period control in thin film under the open-circuit conditions [2,18], polar properties of the films placed between imperfect "real" electrodes with the finite Tomas-Fermi screening length [19] or separated from the electrodes by ultra-thin dead layers [20] and spatial gaps [21]. The screening deficiency can induce the appearance of the closure domains near free surfaces in ferroelectrics [2,22,23], polarization rotation [24], domain wall broadening in both uniaxial and multiaxial ferroelectrics [25,26], and crossover between different screening regimes of the moving domain wall - surface junctions [27,28]. Sometimes the screening charges of electrochemical nature can stabilize the single-domain state in the open-circuited thin films [29–34]. However, more often the multidomain phase stability region on phase diagrams is between the paraelectric and homogeneous ferroelectric phases. Thus the critical thickness of the size-induced phase transition into a paraelectric phase can vary in a wide range from several lattice constants [35,36] to tens or hundreds of nanometers [18] or even to micrometers [1,13], depending on the geometry (e.g. the gap or dead layer thickness), ferroelectric material parameters, temperature, bulk and surface screening charges concentration and mobility.

Note that it is relatively easy to determine the period of the domain structure analytically only in the framework of the simplest Kittel model that considers 180-degree domain stripes with infinitely thin domain walls and does not consider any of screening mechanism at the free surface [37]. In this case the equilibrium period of the domain stripes corresponds to the free energy minimum that consists of the depolarization field energy and the wall surface energy. Polarization gradient, bulk and surface screening make the analytical solution of the problem impossible, and even the numerical solution becomes rather complicated.

Notably, the domain formation offers several possible pathways, including development of classical antiparallel domain arrays and emerging of closure domains. The competition between the two is controlled by the mechanisms for strain accommodation, in turn closely linked to coupling between polarization and strain. This behaviour is described by flexoelectric coupling [38] that can lead to unusual changes of the ferroelastic and ferroelectric domain structure, such as interfacial polarization [39], bichirality [40] and non-Ising features [41]. Sometimes, depending on temperature and flexoelectric coupling strength, relative conductivity of the ferroelectric and ferroelastic domain walls becomes at least one order of magnitude higher than in the single-domain regime [42–45]. The joint action of flexoelectricity and incomplete surface screening facilitates surprisingly versatile changes of the domain structure (including emerging of polarization rotation, closure domains, etc.) near the surfaces of ferroic films [46–50] and has a noticeable impact on the thermodynamics [51] and kinetics [52] of polarization reversal.

Here for the first time we explore the competition between domain formation and surface screening in a thin ferroelectric film covered with the surface screening charge of specific nature (Bardeen-type surface states). Special attention is paid to the influence of the Bardeen screening length Λ [12] and flexoelectric coupling [38,53,54] on the film critical thickness, its transition temperature to a paraelectric phase and domain wall structure. Obtained results show that a nontrivial interplay between the surface screening efficiency, stripe domain period, domain wall broadening and closure domains appearance at the open surface occurs to minimize the electro-elastic energy of the ferroelectric film.

2. Problem statement and basic equations

We consider a ferroelectric film with thickness h placed in a perfect electric contact with conducting bottom electrode that mechanically clamps the film. The top surface of the film is mechanically free and electrically open-circuited, but covered with the surface screening charge due to surface states, or electrochemically active ions [see Fig. 1].

The Landau-Ginzburg-Devonshire (LGD)-type Gibbs thermodynamic potential of the ferroelectric film is the sum of the bulk (G_V) and surface (G_S) contributions [44,48]:

$$G_V = \int\limits_{0<x_2<h} d^3r \left(\begin{array}{l} a_{ik}P_iP_k + a_{ijkl}P_iP_jP_kP_l + a_{ijklmn}P_iP_jP_kP_lP_mP_n + \frac{g_{ijkl}}{2}\left(\frac{\partial P_i}{\partial x_j}\frac{\partial P_k}{\partial x_l}\right) \\ -P_iE_i - \frac{\varepsilon_0\varepsilon_b}{2}E_iE_i + Q_{ijkl}\sigma_{ij}P_kP_l - \frac{s_{ijkl}}{2}\sigma_{ij}\sigma_{kl} - F_{ijkl}\sigma_{ij}\frac{\partial P_l}{\partial x_k} \end{array} \right) - \int\limits_{x_2>h} \frac{\varepsilon_0\varepsilon_e}{2}E_iE_id^3r \quad (1)$$

The former and the latter integrals represent contributions of a ferroelectric film and an ambient medium, respectively. Summation is performed over all repeating indexes; P_i is a ferroelectric polarization, $E_i = -\partial\varphi/\partial x_i$ is a quasi-static electric field, φ is an electric potential. Here we introduced background dielectric permittivity ε_b [2] and dielectric permittivity of the ambient

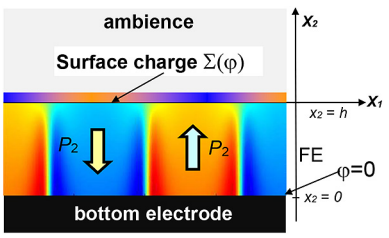

Fig. 1. Considered system, consisting of electrically conducting bottom electrode, ferroelectric (FE) film of thickness h with a domain structure (if any exists), surface screening charge with density $\Sigma(\varphi)$ (a model for imperfect screening) and ambient media (from bottom to the top).

medium, ε_e. The coefficients of the LGD potential expansion in powers of the polarization are $a_{ik} = \delta_{ik}\alpha_T(T - T_c)$ with the positive constant α_T, a_{ijkl} and a_{ijklmn}; T is absolute temperature, T_c is the Curie temperature. The elastic stress tensor is σ_{ij}, Q_{ijkl} is the electrostriction coefficients tensor, F_{ijkl} is the flexoelectric effect tensor, g_{ijkl} is the gradient coefficients tensor, s_{ijkl} is the elastic compliances tensor.

Note that we did not include the higher elastic gradient term, $^1/_2 v_{ijklmn}(\partial\,\sigma_{ij}/\partial x_m)(\partial\,\sigma_{kl}/\partial x_n)$, in the functional (1), because its value and properties are still under debate. Therefore we use only one half $(F_{ijkl}P_k(\partial\,\sigma_{ij}/\partial x_l))$ of the full Lifshitz invariant $F_{ijkl}(P_k(\partial\,\sigma_{ij}/\partial x_l) - \sigma_{ij}(\partial\,P_k/\partial x_l))/2$. The higher elastic gradient term is required for the stability of the functional with the full Lifshitz invariant included. The usage of either the term $F_{ijkl}P_k(\partial\,\sigma_{ij}/\partial x_l)$ or the term $F_{ijkl}(P_k(\partial\,\sigma_{ij}/\partial x_l) - \sigma_{ij}(\partial\,P_k/\partial x_l))/2$ does not affect the equations of state. We recognize that the usage of the full Lifshitz invariant along with the higher gradient term, whose forms in polarization-stress and polarization-strain representations are $\frac{F_{ijkl}}{2}\left(P_k\frac{\partial\sigma_{ij}}{\partial x_l} - \sigma_{ij}\frac{\partial P_k}{\partial x_l}\right) + \frac{v_{ijklmn}}{2}\left(\frac{\partial\sigma_{ij}}{\partial x_m}\frac{\partial\sigma_{kl}}{\partial x_n}\right)$ and $-\frac{f_{ijkl}}{2}\left(P_k\frac{\partial u_{ij}}{\partial x_l} - u_{ij}\frac{\partial P_k}{\partial x_l}\right) + \frac{w_{ijklmn}}{2}\left(\frac{\partial u_{ij}}{\partial x_m}\frac{\partial u_{kl}}{\partial x_n}\right)$, respectively, is the most consistent way for the description of the gradient coupling of polarization and elastic fields in spatially confined systems (see Yurkov and Tagantsev et al. works [55–58]). However, the full form leads to the higher order of elastic equations and, as it should be, it changes the existing boundary conditions for polarization and strains by producing a new form of elastic boundary conditions [55,56]. Hereinafter we use the part of the Lifshitz invariant in Eq. (1), because the implementation of the full form entails the poor convergence of the numerical code and impairs the quality and reliability of the obtained results. Thus we postpone the rigorous study of the full form influence on the system behaviour for further studies. A possible physical background of using the truncated form in Eq. (1) as an approximation is the smallness of the flexoelectric coupling strength in comparison with the polarization gradient term. By following the results of Refs. [59,60] we assume that the approximation can work if $f^2_{klmn} << g_{ijkl}c_{ijmn}$, where f_{ijkl} is the static flexoelectric stress tensor coefficients and c_{ijmn} are the components of elastic stiffness tensor.

The surface energy contains short-range non-electrostatic [61] polarization-dependent contributions from the film surfaces, which have the form

$$G_S = \int\limits_{x_2=0}\left(\frac{\alpha_{S0}}{2}P_iP_j\right)d^2r + \int\limits_{x_2=h}\left(\frac{\alpha_{Sh}}{2}P_iP_j\right)d^2r. \tag{2}$$

The surface energy parameters α_{S0} and α_{Sh} are positive or zero.

The electric potential φ obeys the Poisson equation in the film and the Laplace equation in the ambient medium:

$$\varepsilon_0\varepsilon_b\frac{\partial^2\varphi}{\partial x_j\partial x_j} = \frac{\partial P_i}{\partial x_i}, \quad 0 < x_2 < h, \tag{3a}$$

$$\varepsilon_0\varepsilon_e\frac{\partial^2\varphi}{\partial x_j\partial x_j} = 0, \quad x_2 \geq h. \tag{3b}$$

The boundary conditions **(BCs)** for Eq. (3) assume the vanishing electric potential at the bottom of the film contacting the conducting substrate, and its continuity at the interface between the ferroelectric film and the ambient medium. Another boundary condition at the latter interface requires the equivalence of a discontinuity in the normal component of the electric displacement to the surface free charge:

$$\varphi|_{x_2=0} = 0,\ \varphi|_{x_2=h-0} - \varphi|_{x_2=h+0} = 0, \tag{4a}$$

$$\left(P_2 - \varepsilon_0\varepsilon_b\frac{\partial\varphi}{\partial x_2}\right)\Big|_{x_2=h-0} + \varepsilon_0\varepsilon_e\frac{\partial\varphi}{\partial x_2}\Big|_{x_2=h+0} + \Sigma(\varphi)|_{x_2=h} = 0. \tag{4b}$$

Note that the BC (4b) results directly from the Gauss equation and cannot be obtained from the variation of the Gibbs energy (1)–(2) [62]. Periodic BCs are imposed on the polarization and the electric potential in transverse x_1-direction.

Here, we consider the special case of the surface screening charge with the density given by $\Sigma(\varphi) = -\varepsilon_0\varphi/\Lambda$, where Λ is the Bardeen screening length [12,63]. The period of domain stripes depends on the film thickness h and the length Λ in a self-consistent way. Besides the Bardeen model [see Fig. 3 and Eq. (17) in Ref. [12]], the expression for $\Sigma(\varphi)$ is relevant for all physical situations assuming that a linear relation between the screening charge density and the electric potential is valid (Tomas-Fermi and Debye-Hückel approximations, physical gaps, etc). For instance, the mathematical form of $\Sigma(\varphi)$ coincides with the Stephenson and Highland model for ionic charge density after a linearization over electric potential at equal ion formation energies [31,32].

Below we consider a two dimensional (2D) case with polarization components P_1 and P_2 [see Fig. 1], and suppose the cubic symmetry m3m of the parent phase. Minimization of the functional (1) with respect to P_2 brings about the Euler-Lagrange equation

$$\begin{aligned}&(2a_1 - 2Q_{12}(\sigma_{11}+\sigma_{33}) - 2Q_{11}\sigma_{22})P_2 - Q_{44}\sigma_{12}P_1\\ &+4a_{11}P_2^3 + 2a_{12}P_2P_1^2 + 6a_{111}P_2^5 + a_{112}\left(2P_2P_1^4 + 4P_2^3P_1^2\right) - -g_{11}\frac{\partial^2P_2}{\partial x_2^2} - g_{44}\frac{\partial^2P_2}{\partial x_1^2}\\ &-(g'_{44} + g_{12})\frac{\partial^2P_1}{\partial x_1\partial x_2} + F_{44}\frac{\partial\sigma_{12}}{\partial x_1} + F_{12}\left(\frac{\partial\sigma_{11}}{\partial x_2} + \frac{\partial\sigma_{33}}{\partial x_2}\right) + F_{11}\frac{\partial\sigma_{22}}{\partial x_2} = E_2\end{aligned} \tag{5}$$

Minimization with respect to P_1 results in the same form as Eq. (5) with the interchange of subscripts $1 \leftrightarrow 2$. Subscripts 1, 2 and 3, which denote Cartesian coordinates x_1, x_2, x_3 and the Voigt's (matrix) notations are used [64]. BCs for polarization components are the consequence of minimization of the functional (1)–(2):

$$\begin{aligned}&\left(\alpha_{S0}P_2 - g_{11}\frac{\partial P_2}{\partial x_2} - g_{12}\frac{\partial P_1}{\partial x_1} + F_{12}(\sigma_{11}+\sigma_{33}) + F_{11}\sigma_{22}\right)\Big|_{x_2=0} = 0,\\ &\left(-\alpha_{Sh}P_2 - g_{11}\frac{\partial P_2}{\partial x_2} - g_{12}\frac{\partial P_1}{\partial x_1} + F_{12}(\sigma_{11}+\sigma_{33}) + F_{11}\sigma_{22}\right)\Big|_{x_2=h} = 0.\end{aligned} \tag{6a}$$

$$\left(F_{44}\sigma_{12} - g_{44}\frac{\partial P_1}{\partial x_2} - g'_{44}\frac{\partial P_2}{\partial x_1}\right)\Big|_{x_2=0} = 0, \quad \left(F_{44}\sigma_{12} - g_{44}\frac{\partial P_1}{\partial x_2} - g'_{44}\frac{\partial P_2}{\partial x_1}\right)\Big|_{x_2=h} = 0 \tag{6b}$$

The generalized fluxes are continuous in x_1-direction.

To determine the ***domain period***, we developed the following procedure. We impose periodic boundary conditions on the simulation box along x_1 direction, thus closing a bulk on itself. The main problem of this approach is that there can only be even number of domains created in the box, so that a period of simulated domain structures is commensurate with the box size. However, it is still possible to seek for the real size of the domain period, calculating total energy of the system via the energy functional G from Eqs. (1)–(2). In stable states (unlike metastable ones) the system energy is minimal. By varying the box width one can find a value at which the total energy of the given system is minimum while the number of domains is also minimal (i.e. two), unlike any metastable states splitting the structure into several domains or irregularly polarized regions ("band" or "diamond" structures) [see Fig. S1 in Ref. [65]].

Elastic problem formulation is based on the modified Hooke law obtained using the thermodynamic relation $u_{ij} = -\delta G/\delta\sigma_{kl}$:

$$Q_{ijkl}P_kP_l + F_{ijkl}\frac{\partial P_k}{\partial x_l} + s_{ijkl}\sigma_{kl} = u_{ij}, \tag{7}$$

where u_{ij} are elastic strain tensor components. Mechanical equilibrium conditions $\partial\sigma_{ij}/\partial x_j = 0$ [66] could be rewritten for the considered 2D case as follows:

$$\frac{\partial\sigma_{11}}{\partial x_1} + \frac{\partial\sigma_{12}}{\partial x_2} = 0, \quad \frac{\partial\sigma_{12}}{\partial x_1} + \frac{\partial\sigma_{22}}{\partial x_2} = 0, \quad \frac{\partial\sigma_{31}}{\partial x_1} + \frac{\partial\sigma_{32}}{\partial x_2} = 0 \tag{8}$$

Conditions of a mechanically free boundary for the mechanical sub-system are imposed at the ferroelectric-outer medium interface ($x_2 = h$) and a fixed mechanical displacement $\vec{U}$ is applied at the ferroelectric-substrate interface $\sigma_{12}|_{x_2=h} = 0$, $\sigma_{22}|_{x_2=h} = 0$, $\sigma_{32}|_{x_2=h} = 0$, $U_1|_{x_2=0} = x_1u_m$, $U_2|_{x_2=0} = 0$, $U_3|_{x_2=0} = 0$. At the box side fictional boundaries we used the conditions $U_2|_{x_1=-w} = U_2|_{x_1=w}$ and $U_1|_{x_1=+w} - U_1|_{x_1=-w} = 2wu_m$ Note that a compressive misfit strain u_m was applied at the film-substrate interface $u_{11} = u_{22} = u_m$ to support vertical direction of polarization (see e.g. Refs. [67, 68, 69]).

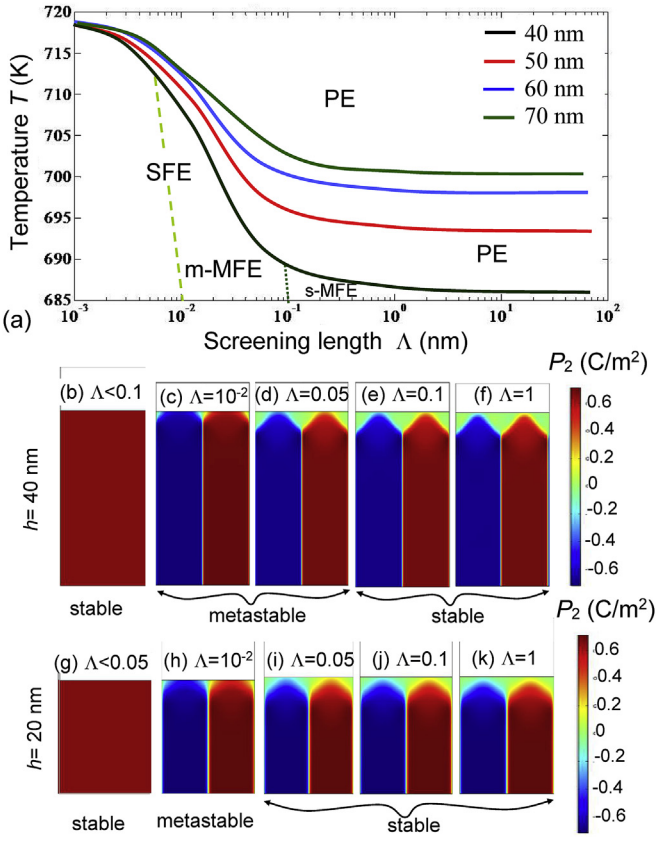

Fig. 2. **(a)** Phase diagrams in coordinates "temperature – screening length" calculated for different film thickness h = 40, 50, 60 and 70 nm (black, red, blue and green curves). There are regions of paraelectric phase (**PE**), stable single-domain ferroelectric phase (**SFE**), metastable (**m-MFE**) and stable (**s-MFE**) multi-domain ferroelectric phases with and/or without broadened domain walls and closure domains near the top surface of the film. **(b)–(k)** Distributions of the vertical component of the spontaneous polarization P_2 throughout a 40-nm [**(b)–(f)**] and 20-nm [**(g)–(k)**] PTO films calculated at FA = 0 for different values of the screening length Λ: 0.005 nm, 0.01 nm, 0.05 nm, 0.1 nm, and 1 nm. Note that the transition temperature (shown in Fig. 2(a)) saturates when the closure domains merge together, since the merging creates an ultra-thin layer with very high relative dielectric permittivity acting as an additional screening layer in addition to the surface charge Σ. As a matter of fact, Fig. 2 illustrates the key result of this work exhibiting how the interplay between the surface screening and domain formation gives rise to complex domain structures (stripe domains, broadened stripes, closure domains, domain splitting, etc.). (For interpretation of the references to colour in this figure legend, the reader is referred to the web version of this article.)

3. Numerical results and discussion

The coupled system of Eqs. (3)–(8) along with relevant boundary conditions was analyzed numerically for $PbTiO_3$ (PTO) films. Parameters used in the numerical calculations are listed in Table 1. We use the so-called "natural case", α_{S0}=0 and α_{Sh}=0, in numerical calculations, which corresponds to the minimal critical thickness of the film [48,49]. We estimate in the end of Appendix A

Table 1
Material parameters of ferroelectrics collected and estimated from the Refs.

Parameter of the functional (1)–(2)	Designation and units	Numerical value or interval used in the calculations for ferroelectric $PbTiO_3$	
background permittivity	ε_b	7	N/A
Inverse CW constant	α^T ($\times 10^5 C^{-2}\cdot Jm/K$)	3.8	[70]
Curie temperature	T_C (K)	479 + 273	[64,65]
LGD coefficient	a_{ij} ($\times 10^8 C^{-4}\cdot m^5 J$)	$a_{11} = -0.73$, $a_{12} = 7.5$	[61,64]
LGD coefficient	a_{ijk} ($\times 10^8 C^{-6}\cdot m^9 J$)	$a_{111} = 2.6$, $a_{112} = 6.1$, $a_{123} = -37.0$	[64]
electrostriction	Q_{ij} ($C^{-2}\cdot m^4$)	$Q_{11} = 0.089$, $Q_{12} = -0.026$, $Q_{44} = 0.0675$	[71, 61]
compliance	s_{ij} ($\times 10^{-12}$ Pa^{-1})	$s_{11} = 8.0$, $s_{12} = -2.5$, $s_{44} = 9.0$	[61]
gradient coefficients	g_{ij} ($\times 10^{-10} C^{-2} m^3 J$)	$g_{11} = 5.1$, $g_{12} = -0.2$, $g'_{44} = 0.2$	N/A
surface energy coefficient	α_{Si} ($\times 10^{-4} C^{-2}$ J)	$\alpha_{S0} = \alpha_{Sh} = 0$	N/A
flexoelectric coefficient	F_{ij} ($\times 10^{-11} C^{-1} m^3$)	$F_{11} = 3$, $F_{12} = 1$, $F_{44} = 0.5$ ($F_{44} = 5$ for insets in Fig. 3)	N/A
misfit strain	u_m	− 0.01	N/A

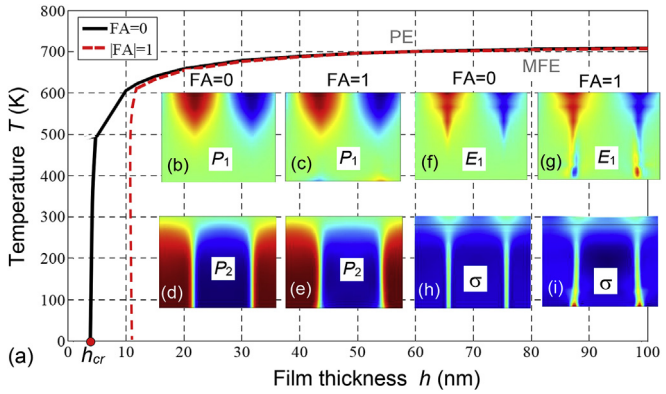

Fig. 3. Phase diagrams in coordinates "PTO film thickness – temperature" calculated for $\Lambda = 0.1$ nm and flexocoupling amplitudes FA = 0 (solid curve) and FA = ±1 (dashed curve). There are regions of paraelectric phase (PE) for thin films and multidomain ferroelectric phase (MFE) with or without closure domains and broadened domain walls near the top surface for thicker films. Spatial distributions of the lateral P_1 **(b, c)** and vertical P_2 **(d, e)** polarization components, electric field component E_1 **(f, g)** and von Mises elastic stress invariant σ **(h, i)** calculated for film thickness $h = 12$ nm, $T = 611$ K, $\Lambda = 0.1$ nm, with ($FA = 1$) and without ($FA = 0$) flexocoupling are shown in insets. Notable features near the free top surface and bottom interface with the rigid electrode may be observed.

[65] that the truncated form of the Lifshitz invariant in Eq. (1) can be a reasonable approximation for chosen ferroelectric parameters.

To get insight into the interplay between domain formation and surface screening, we analyze the phase diagram of the film in coordinates "temperature T – screening length Λ" for several values of the film thickness varying in the range (40–70) nm [Fig. 2(a)]. The transition temperature to the paraelectric phase monotonically decreases with the reduction of the film thickness (compare top and bottom curves). Similarly, the transition temperature monotonically decreases and then saturates with the increase of Λ. This happens because a very small $\Lambda < 10^{-2}$ nm provides an almost perfect screening and so supports the single domain ferroelectric phase stability. The increase of Λ up to 0.1 nm strongly mitigates the screening effectiveness, and $\Lambda \sim 1$ nm or more results in the almost open-circuit boundary conditions at the top surface. Domain stripes with broadened domain walls as well as the appearance of the closure domains near the top surface of the film reduce the depolarization field energy at intermediate Λ values but cannot prevent the film transition to a paraelectric phase with the temperature increase and/or Λ increase. Therefore the temperature region of paraelectric phase expands with the Λ increase and temperature increase, while the multi-domain ferroelectric phase with broadened domain walls and closure domains near the open surface becomes energetically favorable at smaller temperatures and intermediate Λ values, respectively. As has been stated by Kittel in Ref. [37], "the domain structure always has its origin in the possibility of lowering the energy of a system by going from a saturated configuration with high energy to a domain configuration with a lower energy". Accordingly, an emergence of the closure domain structure at the top surface of the film is a result of striving for charge neutrality in the absence of a significant compensating surface charge, just as non-emergence of the large closure domains at the bottom is a result of the presence of the bottom electrode which compensates electric charges at the bottom film surface.

We have further obtained that the phase boundary between the paraelectric and ferroelectric phases is slightly dependent on the flexocoupling strength $F^*_{ij} = FA \cdot F_{ij}$, where the realistic coefficients F_{ij} are listed in Table 1. The amplitude FA was varied in the range from −1 to +1, since the coefficients F_{ij} were not measured experimentally for PTO, but some components were calculated from the first principles for different perovskites [72,73] and their thin films [74]. At the same time the values of $F_{11} = 3$, $F_{12} = 1$ and $F_{44} = 0.5$ (in $10^{-11}C^{-1}m^3$ units) are of the same order as the microscopic estimations (F~10^{-11} m^3/C) made by Kogan [54], as well as with the values measured experimentally for $SrTiO_3$ by Zubko et al. [75,76]. The value $F_{44} = 5 \times 10^{-11}C^{-1}m^3$ (that we used sometimes) is higher than usual, but its influence appeared noticeable only for the fine details of polarization and elastic field distributions near the bottom electrode. At the same time all the values we used are essentially smaller than the ones (F~(5–10) $\times$ 10^{-10} m^3/C) measured for $PbZrTiO_3$ by Ma and Cross [77].

Changes in the distribution of the vertical component of the spontaneous polarization, P_2, throughout the 40-nm and 20-nm PTO films occurring with the increase of Λ values are shown in Fig. 2(b)-(f) and (g)-(k), respectively. At very small Λ the screening is almost perfect and the single domain state is not perturbed by the top surface [Fig. 2(b) and (g)]. Metastable domain stripes occur with the Λ increase [Fig. 2(c)-(d) and 2(h)]. A small broadening of the domain walls near the top surface appears and increases with the Λ increase [Fig. 2(c)-(d) and 2(h)-(i)]. Further increase of Λ leads to the formation of stable domain stripes and lateral growth of the closure domains [Fig. 2(e) and (j)], which eventually merge together at the surface, and then form an ultra-thin layer with almost zero vertical polarization [Fig. 2(f) and (k)].

Dependencies of the electric potential, the vertical components of the electric field and polarization at $x_2 = h$ on the length Λ are shown in Figs. S2-S3 in Ref. [65]. They are monotonic with saturation at high Λ. As anticipated, surface electric potential and field tend to zero at $\Lambda \to 0$. The expressions derived in this limit for a homogeneous polarization, $\varphi = \frac{P_2}{\varepsilon_0}\frac{\Lambda h}{\varepsilon_b \Lambda + h}$ and $E_2 = -\frac{P_2}{\varepsilon_0}\frac{\Lambda}{\varepsilon_b \Lambda + h}$, are valid subject to the absence of applied voltage. Moreover, we should recognize that, in accordance with our numerical calculations, the energy of a single-domain state in films thicker than 40 nm is the lowest, but very close to the multi-domain ones for $\Lambda <$ 0.1 nm. Thus the periodic domain structures shown in Fig. 2 (c)-(d) and 2(h) are metastable configurations with a very long life-time, at that their period depends on the surface screening length, film thickness and temperature [see Fig. S4 in Ref. [65]].

To get insight into the impact of surface screening on a finite size effect, we further analyze the phase diagram of the film in coordinates "temperature T - film thickness h" for the fixed screening length $\Lambda = 0.1$ nm and different flexocoupling amplitude [Fig. 3(a)]. The transition temperature could be affected by the flexoelectricity

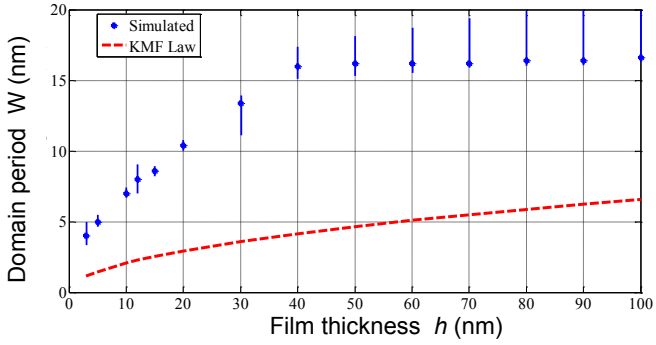

Fig. 4. Period of the domain structure W vs. the thickness h of PTO film calculated for considered screening model (points with error bars) and the Kittel-Mitsui-Furuichi law (dashed curve). The data simulated at $\Lambda = 0.1$ nm exhibit saturation at around 17 nm at big thicknesses (40–100 nm) and thus does not fit into the KMF law, defined as $W = 2\sqrt{h_M h}$ where h_M is a characteristic length equal to ≈ 0.11 nm in the PTO case.

via the changes in the total energy of the system. However, we have obtained that the phase boundary between the paraelectric and multi-domain ferroelectric phases only slightly depends on the absolute value of *FA* for the films thicker than 20 nm, while the critical thickness h_{cr} of the transition into a paraelectric phase is about 3 nm for FA = 0 and h_{cr} = 12 nm for FA = ±1 [compare the solid and dotted curves in Fig. 3(a)]. Since the flexoeffect makes the **homogeneous** ferroelectric state less energetically favorable, the transition temperature becomes slightly lower. By creating additional structures (e.g. nanodomains of lateral polarization at the bottom of films) and deforming polarization profiles (see Fig. 3 (b–i)), the flexocoupling increases the total energy of the system, making the zero-point of the temperature-dependent total energy circa 1 K lower for each film thickness. Spatial distributions of the polarization, electric field and elastic stress [shown in the color maps in Fig. 3(b)-(i) and in Figs. S5-S7 in Ref. [65]] slightly yet remarkably depend on the flexocoupling strength in thin films. In particular, the closure domains at the top surface are conditioned by the imperfect screening, while their profile near the bottom electrode is affected by the flexoeffect. It appears that the flexoelectricity creates and stabilizes tiny closure nanodomains near the bottom film-electrode interface, increases the mechanical stresses and wall bending in these areas.

The domain period appears to be almost independent of the flexocoupling amplitude *FA*, while its dependence on the screening length Λ is a bit stronger with a smooth minima [see Fig. S4 in Ref. [65]]. Notably, the expected Kittel-Mitsui-Furuichi (**KMF**) relation connecting the period *W* of the stripe domain structure with infinitely thin walls and the film thickness *h*, $W \sim \sqrt{h}$, appears invalid in our model, that naturally accounts for domain wall broadening near electrically-open surfaces (via the polarization gradient) and closure domains (via polarization rotation). Instead, a weak dependence of the domain period *W* on the film thickness *h* is observed, becoming stronger only with reduction of *h*. Other film properties, including screening length Λ or dead layer thickness, also do not show much influence on the equilibrium period of the system. In particular, we carefully checked that the KMF law does not describe our results in the limit $\Lambda \to \infty$ that is the situation most close to the one considered by Mitsui and Furuichi [78]. One of the possible explanations of our result can be a rapid reduction of the electric field under the surface at the distances far below the structure period *W* values (see Figs. S2–7 in Ref. [65]), which can breach a KMF-type balance between the domain wall and electrostatic energies, each of which is dependent on the period [2]. Different relation between these energies can cause different dependencies of the period that is a parameter essentially resulting from the energy minimization. In general, the calculated domain structure periods are greater than those predicted by the KMF law (see in Fig. 4) and wane differently from KMF behaviour with the decrease of the film thickness, with an enhanced slope at small thicknesses below 40 nm.

Finally, we note that though the flexoelectricity affects the system energy and phase diagram relatively weakly it can cause unusual features in the domain morphology. In particular, we have found several cases when the flexocoupling impact facilitates interesting formations in the depth of a thicker film. Exemplarily, Fig. 5 shows the appearance of ribbon-like nanodomains with domain dimensions ($\approx 10 \times 20$ nm) in the depth of the film caused and stabilized by the flexocoupling. The nanodomains are reminiscent of polar nanoregions known in ferroelectric relaxors [79]. Ribbon-like domains far from the top open surface (rather closer to the bottom electroded surface) are critically conditioned by the flexoeffect [Fig. 5(a)-(b)], they are absent at FA = 0 [Fig. 5(c)-(d)]. The film thickness h = 110 nm is chosen to show the difference of the distributions near the top and bottom surfaces from those in the central part of the film.

The physical origin of the ribbon-like nanodomains is a metastability dependent on ferroelectric material parameters, film thickness and external conditions. The appearance of such structures is insensitive to the initial seeding (multi-domain, or single-domain, or any other), slightly sensitive to the computation box in lateral direction, and critically sensitive to the flexocoupling. The increase of the flexocoupling strength enhances the probability of appearance of unusual inhomogeneous structures. Note that the emergence of the metastable ribbon-like nanodomains does not affect significantly the domain period, which remains close to its equilibrium value. It is particularly important that a film in which they form is thick enough to contain such structures deep in the bulk, so that they cannot reach any of the surfaces and “annihilate”. Thus, in relatively thick ferroelectric films, the regions with horizontal polarization component can emerge deep in the bulk, enlarging energy of the system and creating “ribbon” or “diamond” structures that split vertical domains in parts.

During the numerical calculations, along with minimum-energy two-domain states [see the note on the domain period definition] also other, less energetically favorable multidomain states, occur. Typically, such states exhibit few (usually 2 or 3) pairs of narrow domains, however they might form structures with regions of ribbon or diamond shapes as well. Such metastable states have different sources. One of them is numerical and means that the box

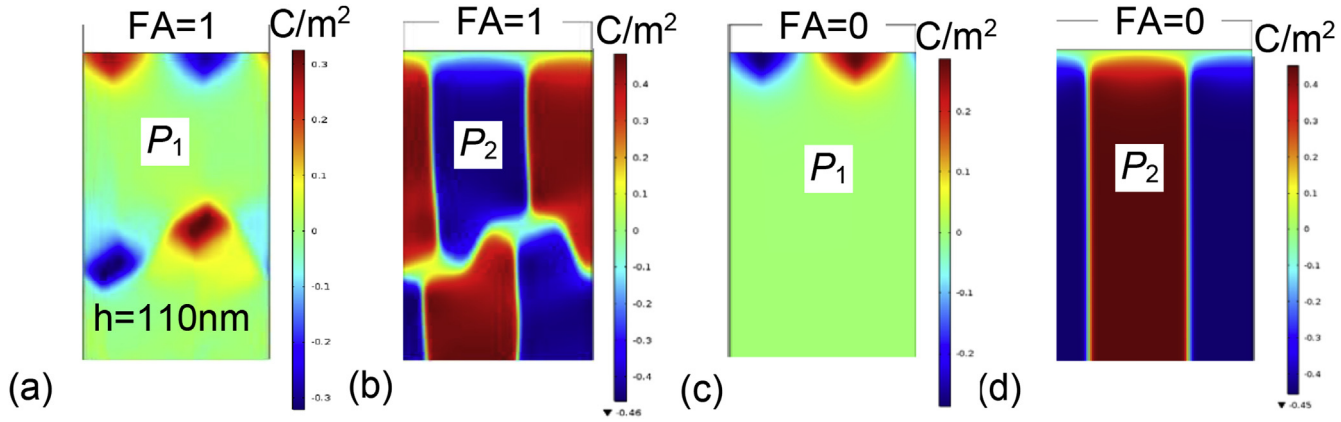

Fig. 5. Plots **(a–d)** show spatial distributions of the lateral P_1 **(a, c)** and vertical P_2 **(b, d)** components of the spontaneous polarization in the 110 nm thick PTO film calculated for Λ = 0.1 nm, positive, FA = 1 **(a,b),** and zero, FA = 0 **(c,d),** flexocoupling amplitudes.

width is incommensurate with the domain period. By choosing a correct box size these states can be avoided. Without flexoelectric coupling (at FA = 0) another reason can be initial conditions, when a structure is formed, but then it can only relax into a long-living metastable state other than the stable one, although the latter case is extremely rare. After introducing the flexocoupling into the system (FA = 1), the metastability (if it occurred) becomes independent on the initial conditions, though not entailing significant changes in the period of the domain structure.

4. Conclusions

Using a self-consistent Landau-Ginzburg-Devonshire approach we simulated the formation of the domain structure in thin ferroelectric films covered with the surface screening charge of the specific nature (Bardeen-type surface states) and analyzed unusual features of the polarization distribution, the electric and elastic fields conditioned by the surface screening length and the flexocoupling strength.

Paying special attention to the flexoelectric coupling we explored the competition between the domain formation and the surface screening, as alternative ways to reduce the electrostatic energy, and constructed the phase diagrams showing dominance of the domain splitting for weak screening. We established that the film critical thickness and its transition temperature to a paraelectric phase strongly depend on the Bardeen screening length and very weakly depend on the flexocoupling, while the flexocoupling influences the polarization rotation and closure domain structure. Particularly, the screening length increase leads to the essential reduction of the transition temperature to the paraelectric phase. Flexoelectric coupling also leads to a slight decrease of the transition temperature, has a small yet remarkable effect on the domain structure near the film surfaces and causes nanoscopic closure domains at the rigid contact with the bottom conducting electrode.

Surprisingly, ribbon-like nanodomains emerge due to the flexoeffect also in the film depth far from the surfaces at specific boundary conditions. This principal observation might be related to a still highly disputable formation mechanism of the so-called polar nanoregions in relaxor ferroelectrics. Being exotic metastable formations boosted by flexoelectricity in the conventional ferroelectric PTO such structures could be stabilized in relaxor ferroelectrics by chemical or structural disorder. It is interesting that recent studies [80,81] revealed the enhancement of the flexoelectric effect due to polar nanoregions. The actual work has disclosed a converse effect of the stabilization of metastable nanosize polar regions due to the flexoeffect that advances understanding of the nature of relaxor behaviour.

Dependence of the period of the stripe domain structure on the screening length and on the flexoelectric coupling appears to be weak. Its monotonically increasing dependence on the film thickness is, in contrast, pronounced but clearly distinct from the classical Kittel-Mitsui-Furuichi square root law. The latter disagreement must not be surprising since the classical model neglects both the structure of the domain walls and the formation of the closure domains near the free surface. Nevertheless, a virtually constant domain width for large film thicknesses above some characteristic value (in our simulations, above h~40 nm) could hardly be expected. This behaviour might disclose the fact that the domain wall energy in thick films is not proportional to the domain wall length.

Acknowledgements

I.S.V. gratefully acknowledges support from the Deutsche Forschungsgemeinschaft (DFG) through the grant GE 1171/7–1. E.A.E. and A.N.M. acknowledge the Center for Nanophase Materials Sciences, which is a DOE Office of Science User Facility, CNMS2016-061. S.V.K. research is sponsored by the Division of Materials Sciences and Engineering, BES, US DOE. A portion of this research (S.V.K.) was conducted at the Center for Nanophase Materials Sciences, which is a DOE Office of Science User Facility.

Appendix A. Supplementary data

Supplementary data related to this article can be found at http://dx.doi.org/10.1016/j.actamat.2017.07.033

References

[1] A.S. Sidorkin, Domain Structure in Ferroelectrics and Related Materials, Cambridge international science publishing, Cambridge, 2006.
[2] A.K. Tagantsev, L.E. Cross, J. Fousek, Domains in Ferroic Crystals and Thin Films, Springer, New York, 2010. ISBN 978-1-4419-1416-3, e-ISBN 978-1-4419-1417-0.
[3] B.V. Selyuk, Charged domain boundaries in ferroelectric crystals, Ferroelectrics 6 (1973) 37.
[4] E.A. Eliseev, A.N. Morozovska, G.S. Svechnikov, V. Gopalan, V.Ya Shur, Static conductivity of charged domain walls in uniaxial ferroelectric semiconductors, Phys. Rev. B 83 (2011), 235313.
[5] S.V. Kalinin, D.A. Bonnell, Screening phenomena on oxide surfaces and its implications for local electrostatic and transport measurements, Nano Lett. 4 (2004) 555.
[6] S. Jesse, A.P. Baddorf, S.V. Kalinin, Switching spectroscopy piezoresponse force microscopy of ferroelectric materials, Appl. Phys. Lett. 88 (2006), 062908.
[7] A.N. Morozovska, S.V. Svechnikov, E.A. Eliseev, S. Jesse, B.J. Rodriguez, S.V. Kalinin, Piezoresponse force spectroscopy of ferroelectric-semiconductor materials, J. Appl. Phys. 102 (2007), 114108.
[8] A.V. Ievlev, S. Jesse, A.N. Morozovska, E. Strelcov, E.A. Eliseev, Y.V. Pershin, A. Kumar, V.Y. Shur, S.V. Kalinin, Intermittency, quasiperiodicity and chaos in probe-induced ferroelectric domain switching, Nat. Phys. 10 (2014) 59.
[9] A.V. Ievlev, A.N. Morozovska, V.Ya Shur, S.V. Kalinin, Humidity effects on tip-induced polarization switching in lithium niobate, Appl. Phys. Lett. 104 (2014), 092908.
[10] Y.A. Genenko, Space-charge mechanism of aging in ferroelectrics: an analytically solvable two-dimensional model, Phys. Rev. B 78 (2008), 214103.
[11] Y.A. Genenko, J. Glaum, O. Hirsch, H. Kungl, M.J. Hoffmann, T. Granzow, Aging of poled ferroelectric ceramics due to relaxation of random depolarization fields by space-charge accumulation near grain boundaries, Phys. Rev. B 80 (2009), 224109.
[12] J. Bardeen, Surface states and rectification at a metal semi-conductor contact, Phys. Rev. 71 (1947) 717.
[13] V.M. Fridkin, Ferroelectrics Semiconductors, Consultant Bureau, New-York and London, 1980, p. 119.
[14] M.A. Itskovsky, Some peculiarities of phase transition in thin layer ferroelectric, Fiz. Tv. Tela 16 (1974) 2065.
[15] P.W.M. Blom, R.M. Wolf, J.F.M. Cillessen, M.P.C.M. Krijn, Ferroelectric Schottky diode, Phys. Rev. Lett. 73 (1994) 2107.
[16] A.N. Morozovska, E.A. Eliseev, S.V. Svechnikov, A.D. Krutov, V.Y. Shur, A.Y. Borisevich, P. Maksymovych, S.V. Kalinin, Finite size and intrinsic field effect on the polar-active properties of ferroelectric semiconductor heterostructures, Phys. Rev. B 81 (2010), 205308.
[17] Y.A. Genenko, O. Hirsch, P. Erhart, Surface potential at a ferroelectric grain due to asymmetric screening of depolarization fields, J. Appl. Phys. 115 (2014), 104102.
[18] E.A. Eliseev, S.V. Kalinin, A.N. Morozovska, Finite size effects in ferroelectric-semiconductor thin films under open-circuit electric boundary conditions, J. Appl. Phys. 117 (2015), 034102.
[19] A.M. Bratkovsky, A.P. Levanyuk, Continuous theory of ferroelectric states in ultrathin films with real electrodes, J. Comput. Theor. Nanosci. 6 (2009) 465.
[20] A.M. Bratkovsky, A.P. Levanyuk, "Effects of anisotropic elasticity in the problem of domain formation and stability of monodomain state in ferroelectric films, Phys. Rev. B 84 (2011), 045401.
[21] E.V. Chensky, V.V. Tarasenko, Theory of phase transitions to inhomogeneous states in finite ferroelectrics in an external electric field, Sov. Phys. JETP 56 (1982) 618 [Zh. Eksp. Teor. Fiz. 83 (1982) 1089].
[22] C.-L. Jia, K.W. Urban, M. Alexe, D. Hesse, I. Vrejoiu, Direct observation of continuous electric dipole rotation in flux-closure domains in ferroelectric Pb(Zr,Ti)O3, Science 331 (2011) 1420.
[23] Y.L. Tang, Y.L. Zhu, X.L. Ma, A.Y. Borisevich, A.N. Morozovska, E.A. Eliseev, W.Y. Wang, Y.J. Wang, Y.B. Xu, Z.D. Zhang, S.J. Pennycook, Observation of a periodic array of flux-closure quadrants in strained ferroelectric PbTiO3 films, Science 348 (2015) 547.
[24] G. Catalan, A. Lubk, A.H.G. Vlooswijk, E. Snoeck, C. Magen, A. Janssens, G. Rispens, G. Rijnders, D.H.A. Blank, B. Noheda, Flexoelectric rotation of

polarization in ferroelectric thin films, Nat. Mater 10 (2011) 963.
[25] B.M. Darinskii, A.P. Lazarev, A.S. Sidorkin, Domain-wall structure near the surface of a ferroelectric, Fiz. Tverd. Tela. 31 (1989) 287 [Sov. Phys. Solid State, 31 (1989) 2003].
[26] E.A. Eliseev, A.N. Morozovska, S.V. Kalinin, Y.L. Li, J. Shen, M.D. Glinchuk, L.Q. Chen, V. Gopalan, Surface effect on domain wall width in ferroelectrics, J. Appl. Phys. 106 (2009), 084102.
[27] V.Ya Shur, A.L. Gruverman, V.P. Kuminov, N.A. Tonkachyova, Dynamics of plane domain-walls in lead germanite and gadolinium molybdate, Ferroelectrics 111 (1990) 197.
[28] E.A. Eliseev, A.N. Morozovska, G.S. Svechnikov, E.L. Rumyantsev, E.I. Shishkin, V.Y. Shur, S.V. Kalinin, Screening and retardation effects on 180°-domain wall motion in ferroelectrics: wall velocity and nonlinear dynamics due to polarization-screening charge interaction, Phys. Rev. B 78 (2008), 245409.
[29] D.D. Fong, A.M. Kolpak, J.A. Eastman, S.K. Streiffer, P.H. Fuoss, G.B. Stephenson, C. Thompson, D.M. Kim, K.J. Choi, C.B. Eom, I. Grinberg, A.M. Rappe, Stabilization of monodomain polarization in ultrathin PbTiO3 films, Phys. Rev. Lett. 96 (2006), 127601.
[30] R.V. Wang, D.D. Fong, F. Jiang, M.J. Highland, P.H. Fuoss, C. Tompson, A.M. Kolpak, J.A. Eastman, S.K. Streiffer, A.M. Rappe, G.B. Stephenson, Reversible chemical switching of a ferroelectric film, Phys. Rev. Lett. 102 (2009), 047601.
[31] G.B. Stephenson, M.J. Highland, Equilibrium and stability of polarization in ultrathin ferroelectric films with ionic surface compensation, Phys. Rev. B 84 (2011), 064107.
[32] M.J. Highland, T.T. Fister, D.D. Fong, P.H. Fuoss, C. Thompson, J.A. Eastman, S.K. Streiffer, G.B. Stephenson, Equilibrium polarization of ultrathin PbTiO3 with surface compensation controlled by oxygen partial pressure, Phys. Rev. Lett. 107 (2011), 187602.
[33] S.M. Yang, A.N. Morozovska, R. Kumar, E.A. Eliseev, Y. Cao, L. Mazet, N. Balke, S. Jesse, R. Vasudevan, C. Dubourdieu, and S.V. Kalinin. Mixed Electrochemical-ferroelectric States in Nanoscale Ferroelectrics. (Accepted to NaturePhysics).
[34] A.N. Morozovska, E.A. Eliseev, N.V. Morozovsky, and S.V. Kalinin. Ferroionic states in ferroelectric thin films. (Submitted to Phys. Rev. B).
[35] S.K. Streiffer, J.A. Eastman, D.D. Fong, C. Thompson, A. Munkholm, M.V. Ramana Murty, O. Auciello, G.R. Bai, G.B. Stephenson, Observation of Nanoscale 180° stripe domains in ferroelectric PbTiO3 thin films, Phys. Rev. Let. 89 (2002), 067601.
[36] D.D. Fong, G.B. Stephenson, S.K. Streiffer, J.A. Eastman, O. Auciello, P.H. Fuoss, C. Thompson, Ferroelectricity in ultrathin perovskite films, Science 304 (2004) 1650.
[37] C. Kittel, Introduction to Solid State Physics, Chapmen & Hall, London, 1956.
[38] A.K. Tagantsev, Piezoelectricity and flexoelectricity in crystalline dielectrics, Phys. Rev. B 34 (1986) 5883.
[39] A.N. Morozovska, E.A. Eliseev, M.D. Glinchuk, L.-Q. Chen, V. Gopalan, Interfacial polarization and pyroelectricity in antiferrodistortive structures induced by a flexoelectric effect and rotostriction, Phys. Rev. B 85 (2012), 094107.
[40] P.V. Yudin, A.K. Tagantsev, E.A. Eliseev, A.N. Morozovska, N. Setter, Bichiral structure of ferroelectric domain walls driven by flexoelectricity, Phys. Rev. B 86 (2012), 134102.
[41] Y. Gu, M. Li, A.N. Morozovska, Y. Wang, E.A. Eliseev, V. Gopalan, L.-Q. Chen, Non-ising character of a ferroelectric wall arises from a flexoelectric effect, Phys. Rev. B 89 (2014), 174111.
[42] E.A. Eliseev, A.N. Morozovska, G.S. Svechnikov, P. Maksymovych, S.V. Kalinin, Domain wall conduction in multiaxial ferroelectrics: impact of the wall tilt, curvature, flexoelectric coupling, electrostriction, proximity and finite size effects, Phys. Rev.B 85 (2012), 045312.
[43] A.N. Morozovska, R.K. Vasudevan, P. Maksymovych, S.V. Kalinin, E.A. Eliseev, Anisotropic conductivity of uncharged domain walls in $BiFeO_3$, Phys. Rev. B 86 (2012), 085315.
[44] E.A. Eliseev, P.V. Yudin, S.V. Kalinin, N. Setter, A.K. Tagantsev, A.N. Morozovska, Structural phase transitions and electronic phenomena at 180-degree domain walls in rhombohedral BaTiO3, Phys. Rev. B 87 (2013), 054111.
[45] E.A. Eliseev, A.N. Morozovska, Y. Gu, A.Y. Borisevich, L.-Q. Chen, V. Gopalan, S.V. Kalinin, Conductivity of twin walls - surface junctions in ferroelastics: interplay of deformation potential, octahedral rotations, improper ferroelectricity and flexoelectric coupling, Phys. Rev. B 86 (2012), 085416.
[46] R. Maranganti, P. Sharma, Atomistic determination of flexoelectric properties of crystalline dielectrics, Phys. Rev. B 80 (2009), 054109.
[47] N.D. Sharma, C.M. Landis, P. Sharma, Piezoelectric thin-film superlattices without using piezoelectric materials, J. Appl. Phys. 108 (2010), 024304.
[48] P. Zubko, G. Catalan, A.K. Tagantsev, Flexoelectric effect in solids, Ann. Rev. Mater. Res. 43 (2013) 387.
[49] P.V. Yudin, A.K. Tagantsev, Fundamentals of flexoelectricity in solids, Nanotechnology 24 (2013), 432001.
[50] S.V. Kalinin, A.N. Morozovska, Multiferroics: focusing light on flexoelectricity, Nat. Nanotechnol. 10 (2015) 916.
[51] A.N. Morozovska, E.A. Eliseev, Y.A. Genenko, I.S. Vorotiahin, M.V. Silibin, Y. Cao, Y. Kim, M.D. Glinchuk, S.V. Kalinin, Flexocoupling impact on the size effects of piezo- response and conductance in mixed-type ferroelectrics-semiconductors under applied pressure, Phys. Rev. B 94 (2016), 174101.
[52] I.S. Vorotiahin, A.N. Morozovska, E.A. Eliseev, Y.A. Genenko, Flexocoupling impact on the kinetics of polarization reversal, Phys. Rev. B 95 (2017), 014104.
[53] V.S. Mashkevich, K.B. Tolpygo, Electrical, optical and elastic properties of diamond type crystals. 1, Zh. Eksp. Teor. Fiz. 32 (1957) 520 [Sov. Phys. JETP 5, (1957) 435].
[54] S.M. Kogan, Piezoelectric effect during inhomogeneous deformation and acoustic scattering of carriers in crystals, Solid State Phys. 5 (1964) 2069.
[55] A.S. Yurkov, Elastic boundary conditions in the presence of the flexoelectric effect, JETP Lett. 94 (6) (2011) 455.
[56] A.K. Tagantsev, P.V. Yudin (Eds.), Flexoelectricity in Solids: from Theory to Applications, World Scientific, 2016 (and Refs. Therein).
[57] P.V. Yudin, A.K. Tagantsev, E.A. Eliseev, A.N. Morozovska, N. Setter, Bichiral structure of ferroelectric domain walls driven by flexoelectricity, Phys. Rev. B 86 (2012), 134102.
[58] E.A. Eliseev, P.V. Yudin, S.V. Kalinin, N. Setter, A.K. Tagantsev, A.N. Morozovska, Structural phase transitions and electronic phenomena at 180-degree domain walls in rhombohedral BaTiO3, Phys. Rev. B 87 (054111) (2013).
[59] P.V. Yudin, R. Ahluwalia, A.K. Tagantsev, Upper bounds for flexocoupling coefficients in ferroelectrics, Appl. Phys. Lett. 104 (082913) (2014).
[60] A.N. Morozovska, E.A. Eliseev, C.M. Scherbakov, Y.M. Vysochanskii, The influence of elastic strain gradient on the upper limit of flexocoupling strength, spatially-modulated phases and soft phonon dispersion in ferroics, Phys. Rev. B 94 (2016), 174112.
[61] J. Wang, A.K. Tagantsev, N. Setter, Size effect in ferroelectrics: competition between geometrical and crystalline symmetries, Phys. Rev. B 83 (2011), 014104.
[62] It is impossible to obtain the boundary conditions (4b) from the variation of the energy Eq. (2). One can construct a functional whose variation allows obtaining both electrostatic Eqs. (3) with the boundary conditions (4b) and equations of state (5) with the boundary conditions (6), but there are no grounds to assume that this functional has a minimum for solutions of the equations of state. It has Extrem. fact.
[63] E.A. Eliseev, A.V. Semchenko, Y.M. Fomichov, M.D. Glinchuk, V.V. Sidsky, V.V. Kolos, YuM. Pleskachevsky, M.V. Silibin, N.V. Morozovsky, A.N. Morozovska, Surface and finite size effects impact on the phase diagrams, polar and dielectric properties of $(Sr,Bi)Ta_2O_9$ ferroelectric nanoparticles, J. Appl. Phys. 119 (2016), 204104.
[64] In the notations $a_{11}\equiv a_1$, $a_{1111}\equiv a_{11}$, $6a_{1122}\equiv a_{12}$, $6a_{111111}=a_{111}$, $6a_{111122}=a_{112}$, $g_{1111}\equiv g_{11}$, $g_{1122}\equiv g_{12}$, $g_{1212}\equiv g_{44}$, $Q_{1111}\equiv Q_{11}$, $Q_{1122}\equiv Q_{12}$, $4Q_{1212}\equiv Q_{44}$, $s_{1111}\equiv s_{11}$, $s_{1122}\equiv s_{12}$, $4s_{1212}\equiv s_{44}$, $F_{1111}\equiv F_{11}$, $F_{1122}\equiv F_{12}$, $2F_{1212}\equiv F_{44}$. Note that different factors (either "4", "2" or "1") in the definition of matrix notations with indices "44" are determined by the internal symmetry of tensors as well as by the symmetry of the corresponding physical property tensors. See e.g. J.F. Nye. Physical Properties of Crystals: Their Representation by Tensors and Matrices (Oxford: Clarendon Press, 1985).
[65] See supplementary Materials [URL will be provided by Publisher].
[66] L.D. Landau, E.M. Lifshitz, Theory of Elasticity. Theoretical Physics, vol. 7, Butterworth-Heinemann, Oxford, 1976.
[67] N.A. Pertsev, A.G. Zembilgotov, A.K. Tagantsev, Effect of mechanical boundary conditions on phase diagrams of epitaxial ferroelectric thin films, Phys. Rev. Lett. 80 (1998) 1988.
[68] N.A. Pertsev, V.G. Kukhar, H. Kohlstedt, R. Waser, Phase diagrams and physical properties of single-domain epitaxial Pb.Zr1AxTix.O3 thin films, Phys. Rev. B 67 (2003), 054107.
[69] V.G. Kukhar, N.A. Pertsev, H. Kohlstedt, R. Waser, Polarization states of polydomain epitaxial Pb(Zr1-xTix)O3 thin films and their dielectric properties, Phys. Rev. B 73 (2006), 214103.
[70] K. Rabe, Ch.H. Ahn, J.-M. Triscone (Eds.), Physics of Ferroelectrics: a Modern Perspective, Springer, 2007 (L.-Q. Chen, Appendix A. Landau Free-Energy Coefficients).
[71] M.J. Haun, E. Furman, S.J. Jang, H.A. McKinstry, L.E. Cross, Thermodynamic theory of PbTiO3, J. Appl. Phys. 62 (1987) 3331.
[72] J.W. Hong, D. Vanderbilt, First-principles theory and calculation of flexoelectricity, Phys. Rev. B 88 (2013), 174107.
[73] M. Stengel, Unified ab initio formulation of flexoelectricity and strain-gradient elasticity, Phys. Rev. B 93 (2016), 245107.
[74] I. Ponomareva, A.K. Tagantsev, L. Bellaiche, Finite-temperature flexoelectricity in ferroelectric thin films from first principles, Phys. Rev. B 85 (2012), 104101.
[75] P. Zubko, G. Catalan, A. Buckley, P.R.L. Welche, J.F. Scott, Strain-gradient-induced polarization in SrTiO3 single crystals, Phys. Rev. Lett. 99 (2007), 167601.
[76] P. Zubko, G. Catalan, A. Buckley, P.R.L. Welche, J.F. Scott, Erratum: "Strain-Gradient-Induced polarization in SrTiO3 single crystals, Phys. Rev. Lett. 99 (2007), 167601. Phys. Rev. Lett. 100 (2008) 199906.
[77] W. Ma, L.E. Cross, Flexoelectric effect in ceramic lead zirconate titanate, Appl. Phys. Lett. 86 (072905) (2005).
[78] T. Mitsui, J. Furuichi, Domain structure of rochelle salt and KH_2PO_4, Phys. Rev. 90 (1953) 193.
[79] L.E. Cross, Relaxor ferroelectrics, in: W. Heywang, K. Lubitz, W. Wersing (Eds.), Piezoelectricity, Springer, 2008.
[80] J. Narvaez, G. Catalan, Origin of the enhanced flexoelectricity of relaxor ferroelectrics, Appl. Phys. Lett. 104 (2014), 162903.
[81] L.M. Garten, S. Trolier-McKinstry, Enhanced flexoelectricity through residual ferroelectricity in barium strontium titanate, J. Appl. Phys. 117 (094102) (2015).

Supplementary Materials to the manuscript "Tuning the Polar States of Ferroelectric Films via Surface Charges and Flexoelectricity"

Ivan S. Vorotiahin[1,2], Eugene A. Eliseev,[3] Qian Li[4],

Sergei V. Kalinin[4¯], Yuri A. Genenko[1¯] and Anna N. Morozovska[2,¯¯],

[1]Institut für Materialwissenschaft, Technische Universität Darmstadt, Jovanka-Bontschits-Str. 2, 64287 Darmstadt, Germany

[2] Institute of Physics, National Academy of Sciences of Ukraine, 46, pr. Nauky, 03028 Kyiv, Ukraine

[3] Institute for Problems of Materials Science, National Academy of Sciences of Ukraine, Krjijanovskogo 3, 03142 Kyiv, Ukraine

[4] The Center for Nanophase Materials Sciences, Oak Ridge National Laboratory, Oak Ridge, TN 37831

¯ Corresponding author E-mail: sergei2@ornl.gov (S.V.K.)

¯ Corresponding author E-mail: genenko@mm.tu-darmstadt.de (Y.A.G.)

¯¯ Corresponding author E-mail: anna.n.morozovska@gmail.com (A.N.M.)

APPENDIX A.

Here we consider only 2D case with two polarization components. For the sake of clarity let us denote "x_1" as "x", "x_2" as "y", and "x_3" as "z", therefore one could reduce free energy (1) to the following form (see e.g. [i]). The bulk contribution is (G_V)

$$G_V = \int\limits_{0<y<h} d^3r \left(\begin{array}{l} a_1\left(P_x^2 + P_y^2\right) + a_{11}\left(P_x^4 + P_y^4\right) + a_{12}P_x^2P_y^2 + a_{111}\left(P_x^6 + P_y^6\right) + +a_{112}\left(P_x^2P_y^4 + P_x^4P_y^2\right) \\ \frac{g_{11}}{2}\left(\left(\frac{\partial P_x}{\partial x}\right)^2 + \left(\frac{\partial P_y}{\partial y}\right)^2\right) + \frac{g_{44}}{2}\left(\left(\frac{\partial P_x}{\partial y}\right)^2 + \left(\frac{\partial P_y}{\partial x}\right)^2\right) + g'_{44}\frac{\partial P_x}{\partial y}\frac{\partial P_y}{\partial x} + g_{12}\frac{\partial P_x}{\partial x}\frac{\partial P_y}{\partial y} \\ -P_xE_x - P_yE_y - \frac{\varepsilon_0\varepsilon_b}{2}\left(E_x^2 + E_y^2\right) \\ -\left(Q_{12}\left(\sigma_{yy} + \sigma_{zz}\right) + Q_{11}\sigma_{xx}\right)P_x^2 - \left(Q_{12}\left(\sigma_{xx} + \sigma_{zz}\right) + Q_{11}\sigma_{yy}\right)P_y^2 - Q_{44}\sigma_{xy}P_xP_y \\ -\left(F_{44}\sigma_{xy}\frac{\partial}{\partial y} + F_{12}\left(\sigma_{yy}\frac{\partial}{\partial x} + \sigma_{zz}\frac{\partial}{\partial x}\right) + F_{11}\sigma_{xx}\frac{\partial}{\partial x}\right)P_x \\ -\left(F_{44}\sigma_{xy}\frac{\partial}{\partial x} + F_{12}\left(\sigma_{xx}\frac{\partial}{\partial y} + \sigma_{zz}\frac{\partial}{\partial y}\right) + F_{11}\sigma_{yy}\frac{\partial}{\partial y}\right)P_y \\ -\frac{s_{11}}{2}\left(\sigma_{xx}^2 + \sigma_{yy}^2 + \sigma_{zz}^2\right) - s_{12}\left(\sigma_{xx}\sigma_{yy} + \sigma_{yy}\sigma_{zz} + \sigma_{xx}\sigma_{zz}\right) - \frac{s_{44}}{2}\left(\sigma_{xy}^2 + \sigma_{yz}^2 + \sigma_{xz}^2\right) \end{array} \right)$$

$$- \int\limits_{y>h} d^3r \frac{\varepsilon_0\varepsilon_e}{2}\left(E_x^2 + E_y^2\right) \qquad \text{(S1.1a)}$$

The first and the last integrals represent the contributions of ferroelectric film and external media, respectively. The surface contribution (G_S) has the following form

$$G_S = \int\limits_{x_2=h} \left(\frac{\alpha_{Sx}}{2}P_x^2 + \frac{\alpha_{Sy}}{2}P_y^2\right)d^2r \qquad \text{(S1.1b)}$$

Surface contribution (S1.1b) contains only polarization dependent term. P_i is a ferroelectric polarization, $E_i = -\partial\varphi/\partial x_i$ is a quasi-static electric field, φ is the electric potential. Here we introduced background dielectric permittivity ε_b and dielectric permittivity of outer media, ε_e. The coefficients of LGD potential expansion on the polarization powers are $a_{ik} = \delta_{ik}\alpha_T(T - T_c)$, a_{ijkl} and a_{ijklmn}, T is the absolute temperature, T_c is the Curie temperature. This choice of LGD expansion corresponds to materials with inversion center in the parent phase (e.g. with cubic parent phase). Elastic stress tensor is σ_{ij}, Q_{ijkl} is electrostriction tensor, F_{ijkl} is the flexoelectric effect tensor [ii], g_{ijkl} is gradient coefficient tensor, s_{ijkl} is elastic compliance tensor.

Subscripts 1, 2 and 3 denote Cartesian coordinates *x*, *y*, *z* and Voigt's (matrix) notations are used:

$$a_{11} \equiv a_1, \quad a_{1111} \equiv a_{11}, \quad 6a_{1122} \equiv a_{12}, \tag{S1.2a}$$

$$g_{1111} \equiv g_{11}, \quad g_{1122} \equiv g_{12}, \tag{S1.2b}$$

$$g_{1212} \equiv g_{44}, \quad g'_{44} = g_{1221}, \quad \text{(at that it is possible } g_{44} \neq g'_{44}\text{)}, \tag{S1.2c}$$

$$Q_{1111} \equiv Q_{11}, \quad Q_{1122} \equiv Q_{12}, \quad 4Q_{1212} \equiv Q_{44}, \tag{S1.2d}$$

$$s_{1111} \equiv s_{11}, \quad s_{1122} \equiv s_{12}, \quad 4s_{1212} \equiv s_{44}, \tag{S1.2e}$$

$$F_{1111} \equiv F_{11}, \quad F_{1122} \equiv F_{12}, \quad 2F_{1212} \equiv F_{44}. \tag{S1.2f}$$

Note that different factors (either "4", "2" or "1") in the definition of matrix notations with indices "44" are determined by the internal symmetry of tensors as well as by the symmetry of the corresponding physical properties tensors (see e.g. [iii]). Here we suppose cubic symmetry m3m of the parent phase.

Let us consider a ferroelectric film with thickness *h* on the rigid conductive substrate. The minimization of free energy (S1.1) with respect to the electric potential φ gives the Poisson equation

$$\varepsilon_0 \varepsilon_b \frac{\partial^2 \varphi}{\partial x_j \partial x_j} = \frac{\partial P_i}{\partial x_i} \quad 0 < x_2 < h \tag{S1.3a}$$

$$\varepsilon_0 \varepsilon_e \frac{\partial^2 \varphi}{\partial x_j \partial x_j} = 0 \quad x_2 \geq h \tag{S1.3b}$$

Here the summation is performed over all repeating indexes. The following conditions should be met at the interface between ferroelectric and outer media:

$$\left(-\varepsilon_0 \varepsilon_e \frac{\partial \varphi}{\partial x_2} \right)\Bigg|_{x_2 = h+0} - \left(-\varepsilon_0 \varepsilon_b \frac{\partial \varphi}{\partial x_2} + P_2 \right)\Bigg|_{x_2 = h-0} = \Sigma \tag{S1.4a}$$

$$\varphi\big|_{x_2 = h-0} - \varphi\big|_{x_2 = h+0} = 0 \tag{S1.4b}$$

Here we introduced surface screening charge with density

$$\Sigma = -\varepsilon_0 \varphi / \Lambda. \tag{S1.4c}$$

where Λ is the surface screening length [iv].The boundary condition at the conducting substrate corresponds to the fixed potential, namely:

$$\varphi\big|_{x_2 = 0} = 0 \tag{S1.5}$$

Since in numerical computations most of the calculations are restricted to finite "calculation domain", we have to consider "fictious boundaries" $x_2 = \pm w$, at which additional boundary conditions should be applied. Periodic boundary conditions for polarization, potential and mechanics are set to the side boundaries, with $A_{src} = A_{dst}$, where A is a correspondent value of the aforementioned physical quantities (P_1, P_2, V, σ_{ijkl}) on "source" and "destination" boundaries.

The Euler-Lagrange equations of LGD theory for polarization components P_x and P_y of multiaxial ferroelectric can be obtained from Eq. (S1.1a) as follows

$$\left(2a_1 - 2Q_{12}\left(\sigma_{yy} + \sigma_{zz}\right) - 2Q_{11}\sigma_{xx}\right)P_x - Q_{44}\sigma_{xy}P_y + 4a_{11}P_x^3 + 2a_{12}P_y P_x^2 + 6a_{111}P_x^5 + a_{112}\left(2P_x P_y^4 + 4P_x^3 P_y^2\right) -$$
$$- g_{11}\frac{\partial^2 P_x}{\partial x^2} - g_{44}\frac{\partial^2 P_x}{\partial y^2} - \left(g'_{44} + g_{12}\right)\frac{\partial^2 P_y}{\partial y \partial x} + F_{44}\frac{\partial \sigma_{xy}}{\partial y} + F_{12}\left(\frac{\partial \sigma_{yy}}{\partial x} + \frac{\partial \sigma_{zz}}{\partial x}\right) + F_{11}\frac{\partial \sigma_{xx}}{\partial x} = E_x \tag{S1.6a}$$

$$\left(2a_1 - 2Q_{12}\left(\sigma_{xx} + \sigma_{zz}\right) - 2Q_{11}\sigma_{yy}\right)P_y - Q_{44}\sigma_{xy}P_x + 4a_{11}P_y^3 + 2a_{12}P_y P_x^2 + 6a_{111}P_y^5 + a_{112}\left(2P_y P_x^4 + 4P_y^3 P_x^2\right) -$$
$$- g_{11}\frac{\partial^2 P_y}{\partial y^2} - g_{44}\frac{\partial^2 P_y}{\partial x^2} - \left(g'_{44} + g_{12}\right)\frac{\partial^2 P_x}{\partial y \partial x} + F_{44}\frac{\partial \sigma_{xy}}{\partial x} + F_{12}\left(\frac{\partial \sigma_{xx}}{\partial y} + \frac{\partial \sigma_{zz}}{\partial y}\right) + F_{11}\frac{\partial \sigma_{yy}}{\partial y} = E_y \tag{S1.6b}$$

Boundary conditions for polarization are the consequence of the functional (S1.1a) minimization:

$$\left(-g_{44}\frac{\partial P_x}{\partial y} - g'_{44}\frac{\partial P_y}{\partial x} + F_{44}\sigma_{xy}\right)\Big|_{y=0} = 0, \quad \left(+g_{44}\frac{\partial P_x}{\partial y} + g'_{44}\frac{\partial P_y}{\partial x} - F_{44}\sigma_{xy}\right)\Big|_{y=h} = 0 \tag{S1.7a}$$

$$\left(+g_{11}\frac{\partial P_x}{\partial x} + g_{12}\frac{\partial P_y}{\partial y} - F_{12}\left(\sigma_{yy} + \sigma_{zz}\right) - F_{11}\sigma_{xy}\right)\Big|_{x=w} = 0,$$
$$\left(-g_{11}\frac{\partial P_x}{\partial x} - g_{12}\frac{\partial P_y}{\partial y} + F_{12}\left(\sigma_{yy} + \sigma_{zz}\right) + F_{11}\sigma_{xx}\right)\Big|_{x=-w} = 0. \tag{S1.7b}$$

$$\left(\alpha_{S0}P_y - g_{11}\frac{\partial P_y}{\partial y} - g_{12}\frac{\partial P_x}{\partial x} + F_{12}\left(\sigma_{xx} + \sigma_{zz}\right) + F_{11}\sigma_{yy}\right)\Big|_{y=0} = 0,$$
$$\left(\alpha_{Sh}P_y + g_{11}\frac{\partial P_y}{\partial y} + g_{12}\frac{\partial P_x}{\partial x} - F_{12}\left(\sigma_{xx} + \sigma_{zz}\right) - F_{11}\sigma_{yy}\right)\Big|_{y=h} = 0 \tag{S1.7c}$$

$$\left(-g_{44}\frac{\partial P_y}{\partial x} - g'_{44}\frac{\partial P_x}{\partial y} + F_{44}\sigma_{xy}\right)\Big|_{x=-w} = 0, \quad \left(+g_{44}\frac{\partial P_y}{\partial x} + g'_{44}\frac{\partial P_x}{\partial y} - F_{44}\sigma_{xy}\right)\Big|_{x=w} = 0. \tag{S1.7d}$$

It is seen that one can introduce the generalized polarization flux matrix $\hat{\Gamma}$ with following components

$$\Gamma_{xx} = -g_{11}\frac{\partial P_x}{\partial x} - g_{12}\frac{\partial P_y}{\partial y} + F_{12}\left(\sigma_{yy} + \sigma_{zz}\right) + F_{11}\sigma_{xx},\ \ \Gamma_{yx} = -g_{44}\frac{\partial P_x}{\partial y} - g'_{44}\frac{\partial P_y}{\partial x} + F_{44}\sigma_{xy} \qquad \text{S1.8a)}$$

$$\Gamma_{xy} = -g_{44}\frac{\partial P_y}{\partial x} - g'_{44}\frac{\partial P_x}{\partial y} + F_{44}\sigma_{xy},\ \ \Gamma_{yy} = -g_{11}\frac{\partial P_y}{\partial y} - g_{12}\frac{\partial P_x}{\partial x} + F_{12}\left(\sigma_{xx} + \sigma_{zz}\right) + F_{11}\sigma_{yy} \qquad \text{(S1.8b)}$$

With this designation the LGD equations (S1.6) can be rewritten as

$$\left(2a_1 - 2Q_{12}\left(\sigma_{yy} + \sigma_{zz}\right) - 2Q_{11}\sigma_{xx}\right)P_x - Q_{44}\sigma_{xy}P_y + 4a_{11}P_x^3 + 2a_{12}P_y^2P_x + 6a_{111}P_x^5 + a_{112}\left(2P_xP_y^4 + 4P_x^3P_y^2\right) + \frac{\partial\Gamma_{xx}}{\partial x} + \frac{\partial\Gamma_{yx}}{\partial y} - E_x = 0 \qquad \text{(S1.9a)}$$

$$\left(2a_1 - 2Q_{12}\left(\sigma_{xx} + \sigma_{zz}\right) - 2Q_{11}\sigma_{yy}\right)P_y - Q_{44}\sigma_{xy}P_x + 4a_{11}P_y^3 + 2a_{12}P_yP_x^2 + 6a_{111}P_y^5 + a_{112}\left(2P_yP_x^4 + 4P_y^3P_x^2\right) + \frac{\partial\Gamma_{xy}}{\partial x} + \frac{\partial\Gamma_{yy}}{\partial y} - E_y = 0 \qquad \text{(S1.9b)}$$

along with the boundary conditions (S1.7) in the form

$$\left(\alpha_{S0}P_y + \Gamma_{yy}\right)\Big|_{y=0} = 0, \quad \left(\alpha_{Sh}P_y - \Gamma_{yy}\right)\Big|_{y=h} = 0. \qquad \text{(S1.10a)}$$

$$\Gamma_{xy}\Big|_{x=-w} = 0, \quad -\Gamma_{xy}\Big|_{x=w} = 0. \qquad \text{(S1.10b)}$$

$$\Gamma_{yx}\Big|_{y=0} = 0, \quad -\Gamma_{yx}\Big|_{y=h} = 0. \qquad \text{(S1.10c)}$$

$$\Gamma_{xx}\Big|_{x=-w} = 0, \quad -\Gamma_{xx}\Big|_{x=w} = 0. \qquad \text{(S1.10d)}$$

Elastic subproblem formulation is based on the modified Hooke law in the following form, which can be obtained using the thermodynamic relation $u_{ij} = -\delta G_V / \delta\sigma_{kl}$:

$$Q_{ijkl}P_kP_l + F_{ijkl}\frac{\partial P_k}{\partial x_l} + s_{ijkl}\sigma_{kl} = u_{ij} \qquad \text{(S1.11)}$$

where u_{ij} are elastic strain tensor components. Mechanical equilibrium conditions are[v]

$$\frac{\partial\sigma_{ij}}{\partial x_j} = 0 \qquad \text{(S1.12a)}$$

which can be rewritten for the considered 2D case as follows:

$$\frac{\partial\sigma_{xx}}{\partial x} + \frac{\partial\sigma_{xy}}{\partial y} = 0,\ \ \frac{\partial\sigma_{yx}}{\partial x} + \frac{\partial\sigma_{yy}}{\partial y} = 0,\ \ \frac{\partial\sigma_{zx}}{\partial x} + \frac{\partial\sigma_{zy}}{\partial y} = 0 \qquad \text{(S1.12b)}$$

Boundary conditions for the mechanical part are the following. At the mechanically free interface ferroelectric / outer media one has

$$\sigma_{xy}\Big|_{y=h}=0,\quad \sigma_{yy}\Big|_{y=h}=0,\quad \sigma_{zy}\Big|_{y=h}=0 \tag{S1.13}$$

We suppose that mechanical displacement $\vec{U}$ is fixed at the interface ferroelectric/substrate

$$U_x\big|_{y=0}=x\,u_m,\quad U_y\big|_{y=0}=0,\quad U_z\big|_{y=0}=0. \tag{S1.14}$$

At the side boundaries one could use periodic condition, modified with respect to misfit strain:

$$U_x\big|_{x=+w}-U_x\big|_{x=-w}=2wu_m,\qquad U_y\big|_{x=+w}-U_y\big|_{x=-w}=0 \tag{S1.15}$$

Taking into account Eqs. (S1.2), Eqs. (S1.11) for cubic symmetry ferroelectrics with the components of polarization P_x, P_y can be rewritten as:

$$u_{xx}=s_{11}\sigma_{xx}+s_{12}\left(\sigma_{yy}+\sigma_{zz}\right)+Q_{11}P_x^2+Q_{12}P_y^2+F_{11}\frac{\partial P_x}{\partial x}+F_{12}\frac{\partial P_y}{\partial y}, \tag{S1.16a}$$

$$u_{yy}=s_{11}\sigma_{yy}+s_{12}\left(\sigma_{xx}+\sigma_{zz}\right)+Q_{12}P_x^2+Q_{11}P_y^2+F_{11}\frac{\partial P_y}{\partial y}, \tag{S1.16b}$$

$$u_{zz}=s_{11}\sigma_{zz}+s_{12}\left(\sigma_{yy}+\sigma_{xx}\right)+Q_{12}P_x^2+Q_{12}P_y^2+F_{12}\frac{\partial P_y}{\partial y} \tag{S1.16c}$$

$$u_{xy}=\frac{s_{44}}{2}\sigma_{xy}+\frac{Q_{44}}{2}P_xP_y+\frac{F_{44}}{2}\frac{\partial P_y}{\partial x}+\frac{F_{44}}{2}\frac{\partial P_x}{\partial y} \tag{S1.16d}$$

$$u_{xz}=\frac{s_{44}}{2}\sigma_{xz} \tag{S1.16e}$$

$$u_{yz}=\frac{s_{44}}{2}\sigma_{yz} \tag{S1.16f}$$

Note that denominator "2" appearance in Eqs. (S1.16d)-(S1.16f) is related to the fact, that we use tensor notation for strain and stress components, and matrix notations for compliances.
Parameters to be used are listed in Table 1.

A conceivable physical background of using the truncated form as an approximation is the smallness of the flexoelectric coupling strength in comparison to the polarization gradient term. Namely, using results of [vi] and [vii] we estimated that the approximation (1) can be used when

$$f_{44}^2 << g_{44}c_{44}, \tag{S1.17a}$$

$$\left(f_{11}-f_{12}\right)^2 << \left(c_{11}-c_{12}\right)\left(g_{11}-g_{12}\right), \tag{S1.17b}$$

$$\left(f_{44}+f_{11}-f_{12}\right)^2 << \left(c_{44}+c_{11}-c_{12}\right)\left(g_{44}+g_{11}-g_{12}\right) \tag{S1.17c}$$

wherein f_{ijkl} is the static flexoelectric stress tensor coefficients, c_{ijmn} are the components of elastic stiffness tensor and g_{ijkl} are the components of polarization gradient tensor. To check the inequality validity for the chosen coefficients of PTO, we should make the transition from the polarization-stress representation of the free energy flexoelectric coefficients F_{11}= 3, F_{12}= 1, F_{44}= 0.5 (in $10^{-11}C^{-1}m^3$ units) and elastic compliances s_{11}=8.0, s_{12}= –2.5, s_{44}=9.0 (in 10^{-12} Pa^{-1} units) to polarization-strain representation of the coefficients and get that flexoelectric stress coefficients f_{11}=6.8, f_{12}=4.9, f_{44}=0.56 (in Volts) and elastic stiffness c_{11}=17, c_{12}=8, c_{44}=11 (in 10^{10} Pa units), and gradient coefficients g_{11}=5.1, g_{12}= – 0.2, g_{44}=0.2 (in $10^{-10}C^{-2}m^3$ J units). Thus we estimated that 0.31<<2.22 (so (S1.17a) is valid), 3.63<<46.67 (so (S1.17b) is valid) and 6.05<<105.24 (so (S1.17c) is valid).

APPENDIX B

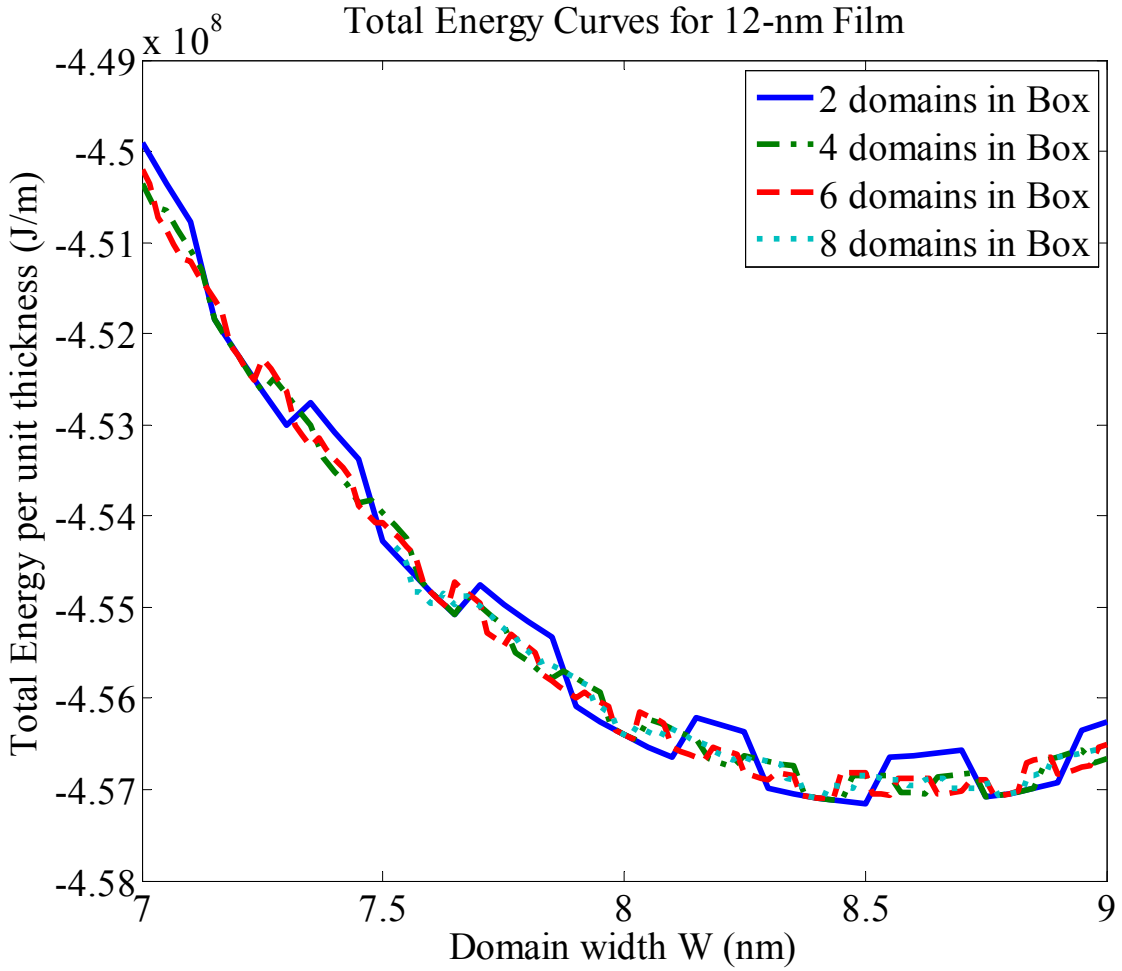

FIG. S1. Evaluation of the equilibrium domain width for 12-nm film through the minimum of total energy of the system at room temperature and Λ=0.1 nm. Different curves correspond to the different size orders of the simulation box that can contain 2, 4, 6, and 8 domains, having minimized energy. It can be seen that the domain width with minimum energy for this film is estimated as ≈8.5.

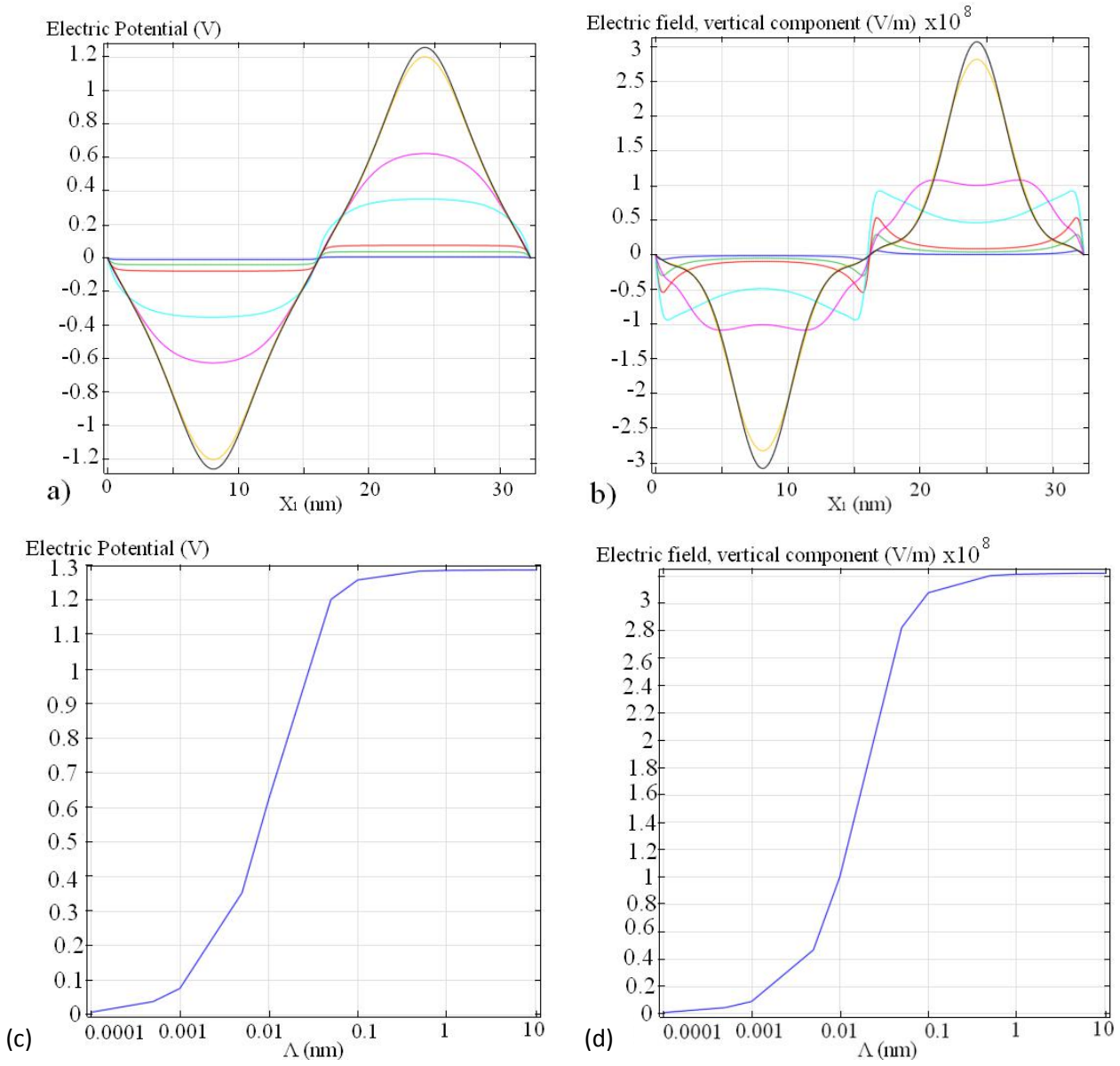

FIG. S2. The electric potential (a, c), the vertical component of the electric field (b, d) at the top surface dependencies of on the parameter of Λ. (a, b) Distribution along the surface at different Λ (0.0001 nm - blue curve, 0.0005 - green, 0.001 - red, 0.005 - cyan, 0.01 - magenta, 0.05 - yellow, 0.1 - black); (c, d) the values in the middle of the domain.

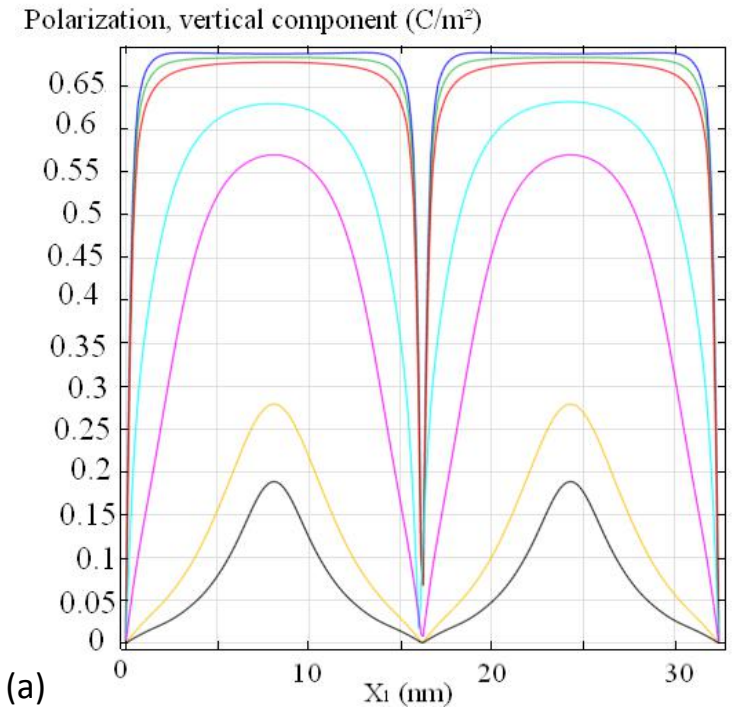

(a)

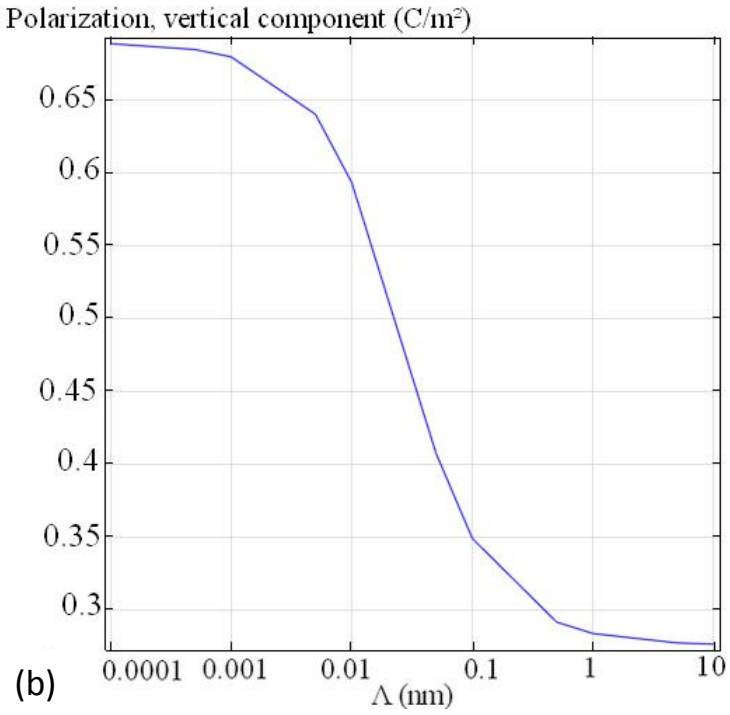

(b)

FIG. S3. (a) Distribution of the polarization along the surface at different Λ (0.0001 nm - blue curve, 0.0005 - green, 0.001 - red, 0.005 - cyan, 0.01 - magenta, 0.05 - yellow, 0.1 - black). (b) The dependence of the maximal polarization on the parameter of Λ. Polarization was calculated at a distance one unit cell from the film surface.

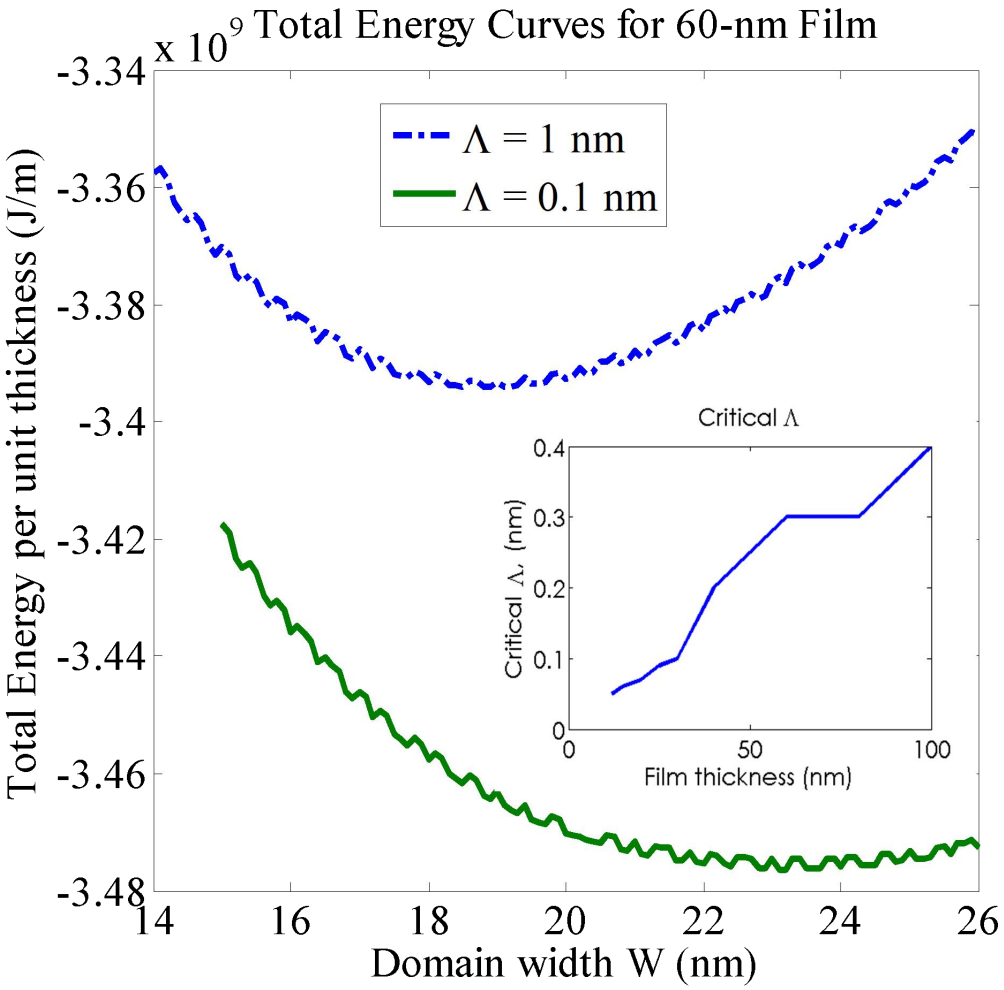

FIG. S4. Evaluation of the equilibrium domain width for 60-nm film through the minimum of total energy of the system at room temperature and Λ=1 nm (blue dash-dotted curve) and Λ=0.1 nm (green solid curve). It can be seen that the domain width with minimum energy for this film is estimated as 18.8 nm (Λ=1 nm) and 23.2 nm (Λ=0.1 nm).

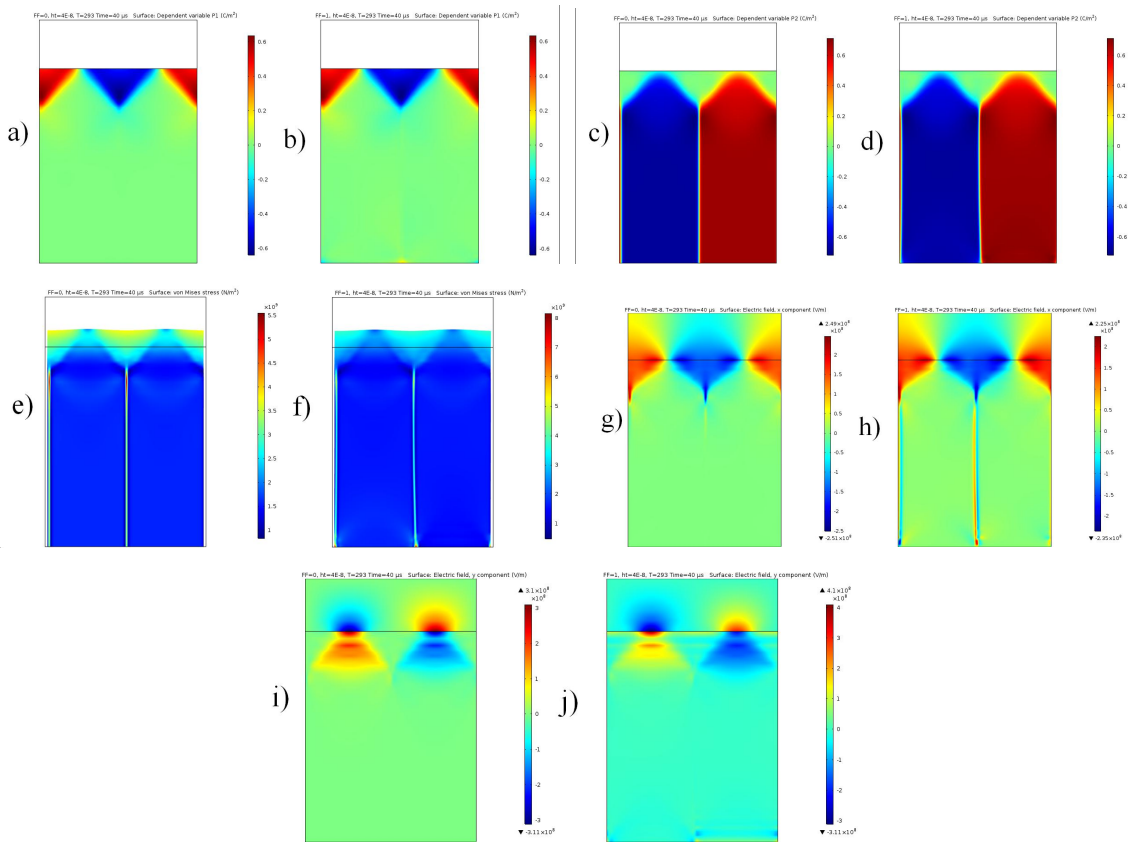

FIG. S5. Comparison between spatial distributions of horizontal (a, b) and vertical (c, d) spontaneous polarization components, elastic stress (e, f), horizontal (g, h) and vertical (i, j) electric field components in the 40-nm PT film without (a, c, e, g, i) and with (b, d, f, h, j) flexoelectric effect at the screening length Λ = 0.1 nm. Flexoelectricity creates and stabilizes tiny closure nanodomains near the film-electrode interface with an increased mechanical stress in these areas.

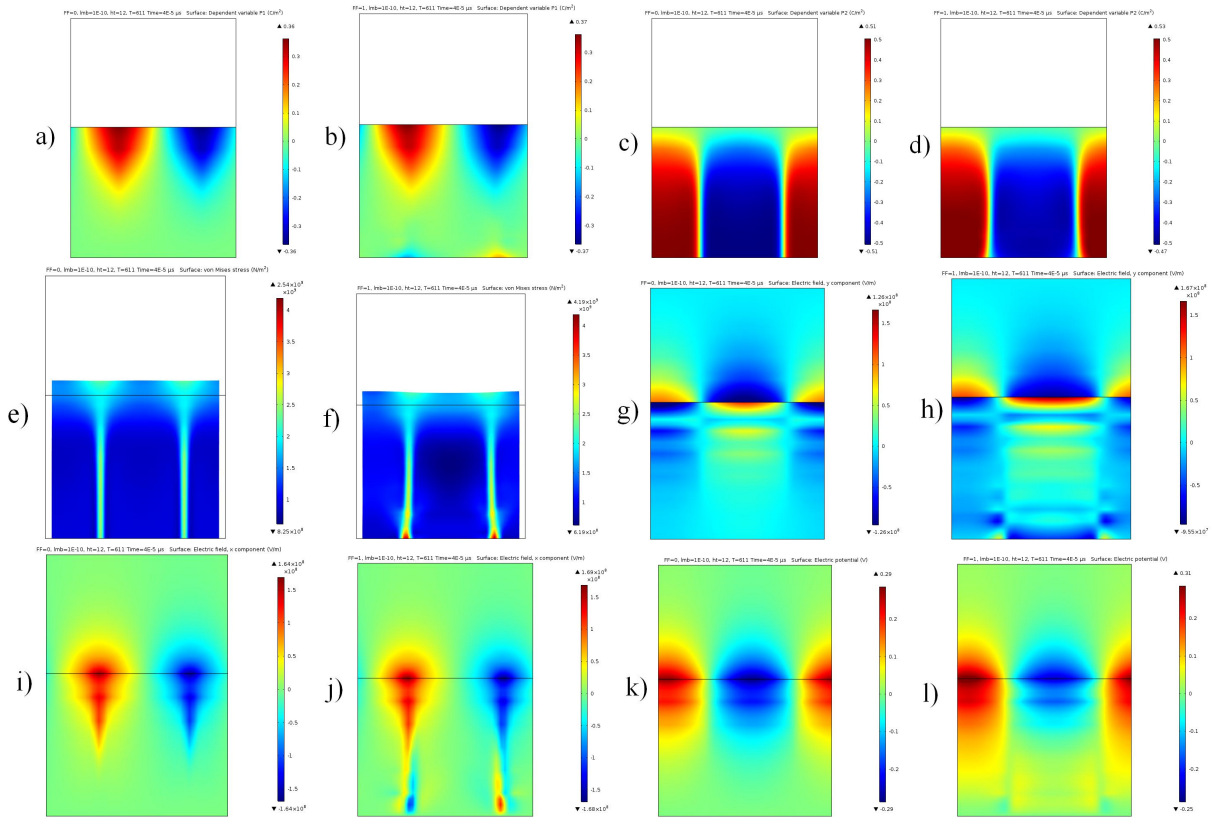

FIG. S6. Comparison between spatial distributions horizontal (a, b) and vertical (c, d) spontaneous polarization components, elastic stress (e, f), vertical (g, h) and horizontal (i, j) electric field components, and electrostatic potential (k, l) in the 12-nm PT film without (a, c, e, g, i, k) and with (b, d, f, h, j, l) flexoelectric effect at the screening length $\Lambda = 0.1$ nm and the temperature 611 K. Flexoelectricity creates and stabilizes tiny closure nanodomains near the film-electrode interface with an increased mechanical stress in these areas. Film thickness was chosen close to the critical value of the thickness induced phase transition for the ferroelectric film.

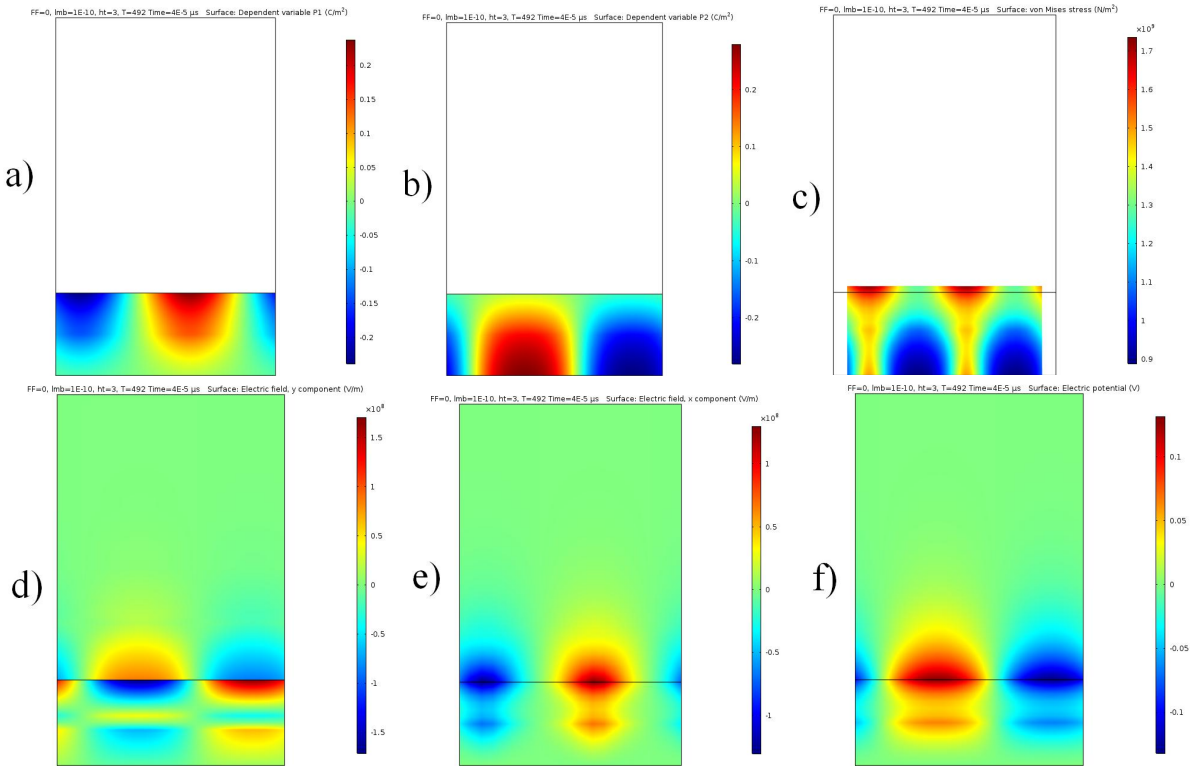

FIG. S7. Spatial distributions of horizontal and vertical polarization components P1 and P2 (a, b), mechanical stress (c), vertical and horizontal electric field components (d, e), and electrostatic potential (f) throughout a 3-nm thin film of PT at the temperature 492 K. Λ=0.1 nm, FA=0.

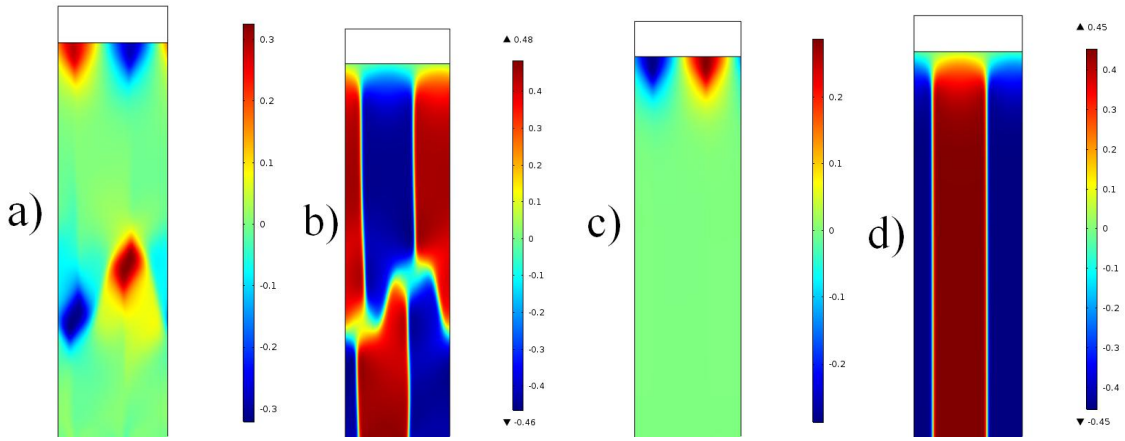

FIG. S8. Spatial distribution of the horizontal (a, c) and vertical (b, d) components of spontaneous polarization in the 110-nm-thick film with (a, b) and without (c, d) flexocoupling, featuring stabilized by flexoelectricity horizontal domains in the bulk with domain dimensions (≈10×20 nm) similar to those of polar nanoregions. Λ=0.1 nm.

REFERENCES

---

[i] Maxim Y. Gureev, Alexander K. Tagantsev, and Nava Setter. "Head-to-head and tail-to-tail 180 domain walls in an isolated ferroelectric." *Physical Review B* 83, 184104 (2011).

[ii] Note that we did not include the higher elastic gradient term, $\frac{1}{2} v_{ijklmn}\left(\partial \sigma_{ij}/\partial x_m\right)\left(\partial \sigma_{kl}/\partial x_n\right)$, in the functional (1), because its value and properties are still under debate. Therefore we are subjected to use only one half ($F_{ijkl}P_k\left(\partial \sigma_{ij}/\partial x_l\right)$) of the full Lifshitz invariant $F_{ijkl}\left(P_k\left(\partial \sigma_{ij}/\partial x_l\right)-\sigma_{ij}\left(\partial P_k/\partial x_l\right)\right)/2$. The higher elastic gradient term is required for the stability of the functional with full Lifshitz invariant included. The usage of either the term $F_{ijkl}P_k\left(\partial \sigma_{ij}/\partial x_l\right)$ or the term $F_{ijkl}\left(P_k\left(\partial \sigma_{ij}/\partial x_l\right)-\sigma_{ij}\left(\partial P_k/\partial x_l\right)\right)/2$ does not affect on the equations of state, but influences on the elastic boundary conditions.

[iii] J.F. Nye. Physical properties of crystals: their representation by tensors and matrices (Oxford: Clarendon Press, 1985).

[iv] E.A. Eliseev, A.V. Semchenko, Y.M. Fomichov, M.D. Glinchuk, V.V. Sidsky, V.V. Kolos, Yu.M. Pleskachevsky, M.V. Silibin, N.V. Morozovsky, A.N. Morozovska. “Surface and finite size effects impact on the phase diagrams, polar and dielectric properties of (Sr,Bi)Ta_2O_9 ferroelectric nanoparticles”. J. Appl. Phys. **119**, 204104 (2016).

[v] L.D. Landau and E.M. Lifshitz, Theory of Elasticity. Theoretical Physics, Vol. 7 (Butterworth-Heinemann, Oxford, 1976).

[vi] P. V. Yudin, R. Ahluwalia, A. K. Tagantsev. Upper bounds for flexocoupling coefficients in ferroelectrics, Appl.Phys.Lett. **104**(8), 082913 (2014)

[vii] Anna N. Morozovska, Eugene A. Eliseev, Christian M. Scherbakov, and Yulian M. Vysochanskii, The influence of elastic strain gradient on the upper limit of flexocoupling strength, spatially-modulated phases and soft phonon dispersion in ferroics. *Phys. Rev.* B 94, 174112 (2016)

3.6. Publication B2

Control of polarization hysteresis temperature behavior by interfacial screening in thin ferroelectric films

Anna N. Morozovska, Eugene A. Eliseev, Ivan S. Vorotiahin, Maxim V. Silibin, Sergei V. Kalinin, and Nicholas V. Morozovsky

Acta Materialia 160 (2018) 57-71. 15 pages.

Acta Materialia 160 (2018) 57–71

Contents lists available at ScienceDirect

Acta Materialia

journal homepage: www.elsevier.com/locate/actamat

Full length article

Control of polarization reversal temperature behavior by surface screening in thin ferroelectric films☆

Anna N. Morozovska [a, b, *], Eugene A. Eliseev [c], Ivan S. Vorotiahin [a, d], Maxim V. Silibin [e, f], Sergei V. Kalinin [g], Nicholas V. Morozovsky [a]

[a] Institute of Physics, National Academy of Sciences of Ukraine, pr. Nauky 46, 03028 Kyiv, Ukraine
[b] Bogolyubov Institute for Theoretical Physics, National Academy of Sciences of Ukraine, 14-b Metrolohichna str, 03680 Kyiv, Ukraine
[c] Institute for Problems of Materials Science, National Academy of Sciences of Ukraine, Krjijanovskogo 3, 03142, Kyiv, Ukraine
[d] Institut für Materialwissenschaft, Technische Universität Darmstadt, Jovanka-Bontschits-Str. 2, 64287 Darmstadt, Germany
[e] National Research University of Electronic Technology "MIET", Zelenograd, Moscow, Russia
[f] Institute for Bionic Technologies and Engineering, I.M. Sechenov First Moscow State Medical University, 2-4 Bolshaya Pirogovskaya st., Moscow, 119991, Russia
[g] The Center for Nanophase Materials Sciences, Oak Ridge National Laboratory, Oak Ridge, TN, 37831, USA

ARTICLE INFO

Article history:
Received 6 May 2018
Received in revised form
18 August 2018
Accepted 24 August 2018
Available online 27 August 2018

Keywords:
Ferroelectricity
Surfaces
Thin films
Screening charges
Absorbed ions
Temperature dependence

ABSTRACT

Ferroelectric surfaces and interfaces are unique physical objects for fundamental studies of various screening mechanisms of spontaneous polarization by free carriers and possible ion exchange between the polar surface and ambient media. The theory of the polarization charge compensation at ferroelectric surface by ambient screening charges requires a detailed comparison of different screening models. In the article, we study the free energy of a thin ferroelectric film covered by a screening charge layer of different nature and calculate hysteresis loops of polarization and screening charge in the system at different temperatures. The dependence of the screening charge density on electric potential was considered for three basic models, namely for the linear Bardeen-type surface states (BS) and nonlinear the Fermi-Dirac (FD) density of states describing two-dimensional electron gas at the film surface, and the strongly nonlinear electrochemical Stephenson-Highland (SH) model describing the surface charge density of absorbed ions. Among considered surface screening models, the most various behavior of polarization and screening charge hysteresis loops is inherent to SH model. Obtained results give new insight to the understanding of bound charge compensation at ferroelectric surfaces at different temperatures, as well as they open the way to control the polarization reversal in thin ferroelectric films by appropriate choice of the surface charge nature and screening mechanism.

1. Introduction

Free ferroelectric surfaces and interfaces are unique physical objects for fundamental studies of various screening mechanisms of spontaneous polarization by free carriers and possible ion exchange between the polar surface and ambient media [1,2]. Generally, existence of spontaneous polarization in thin ferroelectric films results from either complete screening of polarization by ideally conducting electrodes, or occurs from the emergence of the multidomain states in order to minimize the depolarization field energy [3–5]. Ferroelectric domains appears in the case of polarization incomplete screening by semiconducting electrodes, ultra-thin dead layers or physical gaps existence [6], leading to the non-zero spatial separation between polarization (i.e. bound) and

☆ **Notice:** This manuscript has been authored by UT-Battelle, LLC, under Contract No. DE-AC0500OR22725 with the U.S. Department of Energy. The United States Government retains and the publisher, by accepting the article for publication, acknowledges that the United States Government retains a non-exclusive, paid-up, irrevocable, world-wide license to publish or reproduce the published form of this manuscript, or allow others to do so, for the United States Government purposes. The Department of Energy will provide public access to these results of federally sponsored research in accordance with the DOE Public Access Plan (http://energy.gov/downloads/doe-public-access-plan).

* Corresponding author. Institute of Physics, National Academy of Sciences of Ukraine, pr. Nauky 46, 03028, Kyiv, Ukraine.
E-mail addresses: anna.n.morozovska@gmail.com, morozo@voliacable.com (A.N. Morozovska).

https://doi.org/10.1016/j.actamat.2018.08.041
1359-6454/

free screening charges [7–11]. The physical origin of natural dead layers and ultra-thin gaps is the unavoidable separation of the bound and free charges at electrically-open ferroelectric surface that becomes paraelectric and provides efficient electric screening of the bound charges [12,13].

Due to the long-range nature of depolarization field, the incomplete screening of ferroelectric polarization in the presence of ultra-thin dead layers or gaps leads to the nontrivial dynamics of domain structure [14]. These in turn causes unusual phenomena near the electrically opened ferroelectric surfaces and interfaces, such as correlated polarization switching, formation of flux-closure domains in multiaxial ferroelectrics [15–18], and domain wall broadening in uniaxial [19,20] and multiaxial ferroelectrics [17,18]. Further examples of these behaviours include the crossover between different screening regimes in ferroelectric films [21,22] and p-n junctions induced in two-dimensional (**2D**) semiconductors [23], separated by the ultra-thin gap from the moving ferroelectric domain walls. Notably the thickness of dead layer or gap should be small enough and its dielectric permittivity value should be high enough to prevent the dielectric breakdown when the voltage is applied between the film electrodes [24–26].

Most of the early papers, which consider the polar properties of ferroelectrics with electrically-open surfaces and interfaces, largely ignored nonlinear character of screening charges inherent to all self-screening mechanisms. Recent examples of linear screening consideration can be found in Refs. [17,18,27], where the authors studied the polar properties of thin ferroelectric films and nanoparticles covered by screening layer that's charge density $\sigma(\phi)$ is linearly proportional to the electric potential φ in the framework of Bardeen surface states (**BS**) model [28]. Electron density at the surface states is $\sigma(\phi) \sim \phi/L_S$, where L_S is the screening length. It was established that the critical thickness of the film and its transition temperature to a paraelectric phase strongly depend on the screening length L_S The joint action of the BS screening and flexoelectric coupling can remarkably modify polar and electromechanical properties of thin ferroelectric films. Effects similar to BS screening are expected for screening by electrodes with finite density of states [29].

Probably one of the most studied nonlinear models of the screening charge layer is the Fermi-Dirac (**FD**) density of states corresponding to the electron gas in a 2D semiconductor (see e.g. Refs. [30,31] for a single-layer graphene on a ferroelectric film). The FD charge density $\sigma(\phi) \sim \sinh(e\phi/k_BT)$. The impact of the FD screening charge on the domain structure dynamics in a ferroelectric film is considered theoretically in Refs. [23,32]. As a result of nonlinear screening nontrivial temperature behavior of the ferroelectric polarization and 2D-carrier concentration dynamics was revealed in the nanostructure “graphene channel on $Pb_{0.55}Zr_{0.48}TiO_3$ film with domain walls”. The transition from a ferroelectric-like polarization hysteresis loop to an antiferroelectric-like loop occurs in the system with the temperature increase. Notably, antiferroelectric-like polarization hysteresis loops exist in a wide temperature range (350–500) K.

A significantly more interesting example of the strongly nonlinear model describing surface charge is Stephenson and Highland (**SH**) model [1,33]. Stephenson and Highland considered an ultrathin ferroelectric film in equilibrium with a chemical environment that supplies at least two different charge species "i" (e.g. ions and vacancies) to compensate its polarization bound charge at the surface. The φ-dependence of absorbed positive and negative charges density is step-like, $\sigma_i(\phi) \sim \left(1 + q_i \exp\left(\frac{\Delta G_i^{00} + eZ_i\phi}{k_BT}\right)\right)^{-1}$, and it can be either odd or asymmetric depending on the relation between the ions formation energies ΔG_i^{00} in Langmuir adsorption isotherms. Within SH model the screening by ions is coupled to the electrochemical processes at the surface and thus the stabilization of ferroelectric state in ultrathin $PbTiO_3$ films occurs due to the chemical switching [34–36]. The coupling between the electric field of ions and polarization in the film has a non-trivial effect on the ferroelectric phase stability and phase diagrams [1,33]. In general case the polar state of ferroelectric film in contact with atmosphere is undefined due to the presence of mobile electrochemically active species at the surface [37,38].

Recently, we modified the SH approach [33] allowing for the presence of the gap between the ferroelectric surface covered by ions and the scanning probe microscope (**SPM**) tip [39–41]. We identified the **ferro-ionic, anti-ferroic** and **electret-like non-ferroelectric** states [39–41], which are the result of nonlinear electrostatic interaction between the single-domain ferroelectric polarization and absorbed ions. The properties of the ferro-ionic states were described by the system of coupled equations [40,41]. Further we studied the stability of the ferro-ionic states with respect to the domain structure formation and polarization reversal scenarios, and revealed unusual dependences of the film polar state and domain structure properties on the ion formation energies, their difference, and applied voltage [42]. Also we revealed that the electric field-induced phase transitions into ferro-ionic and antiferroionic states are possible in thin films covered with ion layer of electrochemically active nature.

Overall, the impact of ionic adsorption on polarization reversal in the ferroelectric with electrically-open surface had been investigated experimentally [1,33–36,39,43–46] and theoretically [1,33,39–42]; however its influence on the temperature behavior of polarization hysteresis remains unexplored. Furthermore, the comparative theoretical analysis of the peculiarities of ferroelectric hysteresis emerging in the case of linear and nonlinear screening of the polarization by electrons, with strongly nonlinear screening of the polarization by ions was absent.

To fill this gap, the paper studies the thermodynamics of a thin ferroelectric film covered by a screening charge layer of different nature with ultra-thin gap separating the film surface from the top biased electrode. We calculate hysteresis loops of polarization and screening charge at different temperatures. The dependence of the screening charge density on electric potential was considered for three basic models, namely for the linear BS density of electronic surface states, nonlinear FD density of states describing 2D electron gas at the film-gap interface, and strongly nonlinear SH model describing the surface charge density of absorbed ions.

The manuscript is structured as following. Basic equations with boundary conditions and analytical expressions for the BS, FD and SH charge densities are discussed in section II. Free energy of the system is considered in section III. The impact of the surface screening charge nature (on example of the basic screening models) on thermodynamics of the polar and charge states is analyzed in section IV.A. The influence of the screening model on the quasi-static hysteresis loops of polarization and screening charge at different temperatures is discussed in section IV.B. Section V is a brief discussion, section VI is conclusions. Electrostatic problem, description of physical variables and their numerical values are given in Appendixes A and B, respectively.

2. Basic equations and models of the screening charges

Here we consider the system consisting of electron conducting bottom electrode, ferroelectric film covered by a screening layer with 2D charge density $\sigma(\phi)$, ultra-thin gap (or dead layer) separating the electrically-open surface of the film from the top electrode (either ion

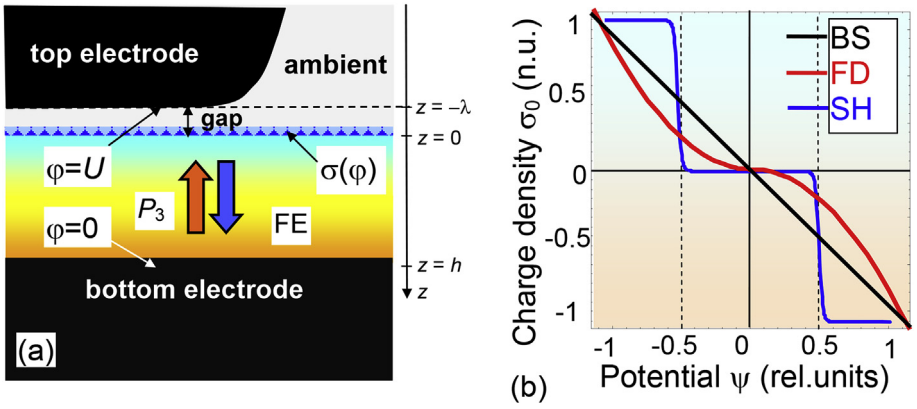

Fig. 1. **(a)** Layout of the considered system, consisting of electron conducting bottom electrode, ferroelectric (FE) film, screening layer with charge density $\sigma(\phi)$, and ultra-thin gap separating the film surface and the top electrode. **(b)** Schematic dependence of the normalized charge densities σ_0 vs. dimensionless electric potential ψ calculated for the models of Bardeen-type surface states (black line "BS") and Fermi-Dirac density of states (red curve "FD") describing 2D electron gas, in comparison with the Stephenson-Highland model describing the surface charge density of absorbed ions (blue step-like curve "SH"). (For interpretation of the references to colour in this figure legend, the reader is referred to the Web version of this article.)

conductive planar electrode or flatted apex of SPM tip), as shown in Fig.1(a). The direct exchange of screening charges with ambient media can take place at the film-gap interface. Mathematical statement of the problem is listed in Refs. [40–42], as well as in Appendix A.

The linear equation of state $\mathbf{D} = \varepsilon_0\varepsilon_d\mathbf{E}$ relates the electrical displacement $\mathbf{D}$ and electric field $\mathbf{E}$ in the gap. Here ε_0 is a universal dielectric constant and $\varepsilon_d \sim (1-100)$ is the relative permittivity of the physical gap or dead layer. A wide band-gap ferroelectric film can be considered dielectric. Quasi-static electric potential ϕ satisfies electrostatic equations for each layer. Namely, $\Delta\phi = 0$ in the gap and $\left(\varepsilon_b\frac{\partial^2}{\partial z^2} + \varepsilon_{11}^f\Delta_\perp\right)\phi = \frac{1}{\varepsilon_0}\frac{\partial P_3^f}{\partial z}$ in a ferroelectric film (see Appendix A).

The boundary conditions (**BCs**) for the system are the equivalence of the electric potential to the voltage U applied to the top electrode (or SPM tip apex) modeled by the flat region at $z = -\lambda$; the continuity of electric potential at the film-gap interface $z = 0$; and the equivalence of the normal components of electric displacement in ferroelectric ($D_3 = \varepsilon_0\varepsilon_b E_3 + P_3^f$) and in the gap ($D_3 = \varepsilon_0\varepsilon_d E_3$) to the screening charge density $\sigma[\phi]$ at $z = 0$; and zero potential at the bottom conducting electrode $z = h$ [see Fig. 1(a)].

The polarization components of uniaxial ferroelectric film depend on the inner electric field $\boldsymbol{E}$ as $P_1 = \varepsilon_0(\varepsilon_{11}^f - 1)E_1$, $P_2 = \varepsilon_0(\varepsilon_{11}^f - 1)E_2$ and $P_3 = P_3^f + \varepsilon_0(\varepsilon_b - 1)E_3$, where the isotropic background permittivity ε_b is introduced [12]. As a rule, $\varepsilon_b \leq 10$ [12]. The dielectric permittivity ε_{33}^f is related with the ferroelectric polarization P_3^f via the soft phonon mode. The evolution and spatial distribution of the ferroelectric polarization P_3^f is determined from the time-dependent Landau-Ginzburg-Devonshire (**LGD**) equation [40–42]:

$$\Gamma\frac{\partial P_3}{\partial t} + \alpha P_3 + \beta P_3^3 + \gamma P_3^5 - g_{33}\frac{\partial^2 P_3}{\partial z^2} = E_3, \qquad (1)$$

In what follows we will rename the $P_3^f \to P_3$ for brevity. In Eq. (1) Γ is a kinetic coefficient. The coefficient $\alpha = \alpha_T(T_C - T)$, where $\alpha_T > 0$, T is the absolute temperature and T_C is a Curie temperature. Constants β and γ are the coefficients of LGD potential $G(P_i, U)$ expansion on the higher polarization powers, at that $\gamma \geq 0$ for the $G(P_i, U)$ stability at high P_3 values [47]. The **BCs** for polarization are of the third kind, $\left(P_3 \mp \Lambda_\mp\frac{\partial P_3}{\partial z}\right)\Big|_{z=0,h} = 0$, and include extrapolation lengths $\Lambda_\pm$ [48,49], which can be different fort the film surfaces $z = 0$ and $z = h$.

To describe the screening charge dynamics, we propose a relaxation equation [40,41], $\tau\frac{\partial\sigma}{\partial t} + \sigma = \sigma_0[\phi]$, where τ is the relaxation time. Expression for **the equilibrium 2D charge density** $\sigma_0[\phi]$ is considered for three basic models.

I. Bardeen-type density of surface states (BS) for description of non-degenerated 2D electron gas. Using the Bardeen model [28] within the limits of its applicability, we consider a special case of screening charges, whose density linearly depends on the electric potential φ as follows,

$$\sigma_0[\phi] = -\varepsilon_0\phi/L_S, \qquad (2a)$$

where L_S is the effective screening length introduced in Refs. [17,18,27]. The schematic dependence of $\sigma_0[\phi]$ is shown by the black line in Fig. 1(b).

II. Fermi-Dirac (FD) density of states for general description of 2D electron gas. The electron gas is characterized by the charge density, $\sigma_0[\phi] = e(p_{2D}(\phi) - n_{2D}(\phi))$, that is the difference of 2D concentration of electrons in the conduction band $[n_{2D}(\phi) = \int_0^\infty d\varepsilon g_n(\varepsilon)f(\varepsilon - E_F - e\phi)\ ]$ and holes in the valence band $[p_{2D}(\phi) = \int_0^\infty d\varepsilon g_p(\varepsilon)f(\varepsilon + E_F + e\phi)]$, respectively. Electrons and holes density of states (**DOS**) are $g_n(\varepsilon)$ and $g_p(\varepsilon)$, E_F is the position of Fermi energy level. The expression for the gapless FD DOS is $g_n(\varepsilon) = g_p(\varepsilon) = 2\varepsilon/(\pi\hbar^2 v_F^2)$ (see e.g. Refs. [30,31]). Using the expressions for $g_n(\varepsilon)$ and $g_p(\varepsilon)$ (characteristic for e.g. graphene charge density) and their Pade-exponential approximation derived in Ref. [23], the FD screening charge density acquires the form:

$$\sigma_0[\psi] = \frac{4(k_BT)^2 e}{\pi\hbar^2 v_F^2}\sum_{m=1}^{\infty}\frac{(-1)^m}{m^2}\sinh(m\psi) \approx \frac{2(k_BT)^2 e}{\pi\hbar^2 v_F^2}\left(\frac{1}{\eta(\psi)} - \frac{1}{\eta(-\psi)}\right), \qquad (2b)$$

where v_F is the Fermi velocity of the charge carriers; the function $\eta(\psi) = \exp(\psi) + 2\left(\psi^2 + \frac{\psi}{2} + \frac{2\pi^2}{12-\pi^2}\right)^{-1}$ and $\psi = \frac{e\phi + E_F}{k_BT}$. The schematic dependence of the density (2b) on the dimensionless "acting" potential ψ is shown by the red curve in Fig. 1(b).

III. Stephenson-Highland (SH) model [33], that is analogous to the Langmuir adsorption isotherm used in surface electrochemistry for adsorption onto a conducting electrode exposed to ions in a solution [50]. The dependence of equilibrium charge density $\sigma_0[\phi]$ on electric potential φ is controlled by the concentration of surface ions $\theta_i(\phi)$ at the surface $z=0$ in a self-consistent manner:

$$\sigma_0[\phi] = \sum_i \frac{eZ_i\theta_i(\phi)}{A_i} \equiv \sum_i \frac{eZ_i}{A_i}\left(1 + q_i \exp\left(\frac{\Delta G_i^{00} + eZ_i\phi}{k_B T}\right)\right)^{-1}, \tag{2c}$$

where e is an elementary charge, Z_i is the ionization degree, $1/A_i$ is the saturation densities of the surface ions, at that $i \geq 2$ to reach the charge compensation for positive and negative surface ions (or vacancies). The factor $q_i = \left(\frac{p_{atm}}{p_{exc}}\right)^{1/n_i}$, where p_{exc} is the partial pressure of ambient gas relative to atmospheric pressure p_{atm}, n_i is the number of surface ions created per gas molecule, ΔG_i^{00} is the standard free energy of the surface ion formation at $p_{exc} = 1$ bar and $U = 0$. Below we consider the case $p_{exc} = p_{atm}$.

The step-like dependence of the screening charge density σ_0 on the dimensionless potential $\psi = \frac{e\phi}{k_B T}$ calculated at $\Delta G_1^{00} = \Delta G_2^{00}$ is shown schematically by the blue curve in Fig. 1(b). The screening charge is zero at $\psi = 0$, very small at $|\psi| < 0.4$ and abruptly increases at $|\psi| \approx 0.5$. Note that the abrupt step-like dependence is left-shifted with respect to $\psi = 0$ for $\Delta G_1^{00} < \Delta G_2^{00}$, symmetric for $\Delta G_1^{00} = \Delta G_2^{00}$ and right-shifted for $\Delta G_1^{00} > \Delta G_2^{00}$ (see Refs. [40–42]).

Noteworthy, the solutions of Eq. (1) are sensitive to the thermodynamic parameters of corresponding screening charges given by Eq. (2) [32,51].

3. Free energy of the system for different screening models

In thermodynamic equilibrium, the LGD free energy of the ferroelectric film is the sum of bulk (G_V) and surface (G_S) parts of Gibbs free energy, and the energy of the electric field outside the film (G_{ext}):

$$G = G_V + G_S + G_{ext}, \tag{3a}$$

$$G_V = \int_{V_{FE}} d^3r \left(\frac{\alpha}{2}P_3^2 + \frac{\beta}{4}P_3^4 + \frac{\gamma}{6}P^6 + \frac{g_{33ij}}{2}\left(\frac{\partial P_3}{\partial x_i}\frac{\partial P_3}{\partial x_j}\right) - P_3E_3 - \frac{\varepsilon_0\varepsilon_b}{2}E_iE_i\right), \tag{3b}$$

$$G_S = \int_S d^2r\left(\frac{\alpha_S}{2}P_3^2 - \frac{\phi}{2}\sigma_0[\phi]\right), G_{ext} = -\int_{\vec{r}\notin V_{FE}} d^3r \frac{\varepsilon_0\varepsilon_d}{2}E_iE_i. \tag{3c}$$

Coefficients α, β and γ are described after Eq. (1). Except for $\alpha = \alpha_T(T_C - T)$, all other coefficients included in the free energy (3) are assumed to be temperature independent. Positively defined tensor g_{ijkl} determines the magnitude of the gradient energy. E_i are the components of electric field. Extrapolation lengths $\Lambda_\pm = g_{33}/\alpha_S^\pm$ define the polarization derivative near the film surfaces.

Below we will develop simplified analytical model to get insight into numerically analyzed behaviors of different polarization states. Since the stabilization of single-domain polarization in ultrathin perovskite films takes place due to the chemical processes at the surface or in the near-surface regions (see e.g. Refs. [1,33–36]), we can assume that polarization distribution $P_3(x,y,z)$ is smooth. In this case, the behavior of the polarization averaged over film thickness $P = \langle P_3 \rangle$ and screening charge density $\sigma_0[\phi]$ can be described via the coupled nonlinear algebraic equations derived in Refs. [40,41]. For a given screening charge model, the equations for polarization P and overpotential Ψ are:

$$\alpha_R P + \beta P^3 + \gamma P^5 = \frac{\Psi}{h}, \tag{4a}$$

$$\Psi = \frac{\lambda(\sigma_0[\Psi] - P) + \varepsilon_0\varepsilon_d U}{\varepsilon_0(\varepsilon_d h + \lambda\varepsilon_{33}^b)}h. \tag{4b}$$

The physically justified free energy G, which formal minimization, $\frac{\partial G[P,\Psi]}{\partial P} = 0$ and $\frac{\partial G[P,\Psi]}{\partial \Psi} = 0$, gives the coupled equation (4) for polarization dynamics, has the form [42]:

$$\frac{G[P,\Psi]}{S} = h\left(\frac{\alpha_R}{2}P^2 + \frac{\beta}{4}P^4 + \frac{\gamma}{6}P^6\right) - \Psi P - \varepsilon_0\varepsilon_{33}^b\frac{\Psi^2}{2h} - \frac{\varepsilon_0\varepsilon_d}{2}\frac{(\Psi - U)^2}{\lambda} + \int_0^\Psi \sigma_0[\varphi]d\varphi. \tag{5}$$

The h-dependent function $\alpha_R(T,h) = \alpha_T(T_C - T) + \frac{g_{33}}{h}\left(\frac{1}{\Lambda_+} + \frac{1}{\Lambda_-}\right)$ is the coefficient α renormalized by "intrinsic" gradient-correlation and finite-size effects (the term $\sim g_{33}/h$). The first term in Eq. (5) is the polarization energy treated in the framework of LGD. The second term, ΨP, represents the interaction energy of polarization P with overpotential Ψ. The terms $\varepsilon_0\varepsilon_b\frac{\Psi^2}{2h}$ and $\frac{\varepsilon_0\varepsilon_d}{2}\frac{(\Psi-U)^2}{\lambda}$ are the energies of electric field in the ferroelectric film [where $\phi = (h-z)\frac{\Psi}{h}$] and in the gap [where $\phi = U - \frac{z+\lambda}{\lambda}(U - \Psi)$], correspondingly. The last term, $\int_0^\Psi \sigma_0[\varphi]d\varphi$, is the screening charge energy that's integration over Ψ for the considered models yields

$$\Sigma[\Psi] \equiv \int_0^\Psi \sigma_0[\varphi]d\varphi = \begin{cases} -\varepsilon_0\dfrac{\Psi^2}{2L_S}, & BS \\ \dfrac{4(k_BT)^2e}{\pi\hbar^2v_F^2}\displaystyle\sum_{m=1}^{\infty}\frac{(-1)^m}{m^3}(\cosh(m\Psi) - 1), & FD \\ \displaystyle\sum_i \frac{Z_i}{A_i}\left(e\Psi + k_BT\ln\left[\frac{1 + q_i\exp\left(\Delta G_i^{00}/k_BT\right)}{1 + q_i\exp\left(\left(\Delta G_i^{00} + eZ_i\Psi\right)/k_BT\right)}\right]\right), & SH \end{cases} \tag{6}$$

The energy given by Eq. (5) has an absolute minimum at high Ψ. According to the Biot's variational principle [52], we can further use the incomplete thermodynamic potential that's partial minimization of over P will give the coupled equations of state, and, at the same time, it has an absolute minimum at finite P values. For the considered BS, FD and SH models we will analyze graphically the relief of the energy (5)–(6) along with its extremals given by Eq (4).

For linear BS charge density described by Eq. (2a) the substitution of the extremal (4b) in expressions (5) and (6) yields

$$G[P,U]=\left(\begin{array}{l}\dfrac{\varepsilon_d U}{\varepsilon_d h+\lambda\varepsilon_b}P+\left(\dfrac{\lambda}{\varepsilon_0(\varepsilon_d h+\lambda\varepsilon_b)}+\alpha_R\left[1+\dfrac{\lambda}{(\varepsilon_d h+\lambda\varepsilon_b)}\dfrac{h}{L_S}\right]\right)\dfrac{P^2}{2}\\ +\beta\left(1+\dfrac{\lambda}{(\varepsilon_d h+\lambda\varepsilon_b)}\dfrac{h}{L_S}\right)\dfrac{P^4}{4}+\gamma\left(1+\dfrac{\lambda}{(\varepsilon_d h+\lambda\varepsilon_b)}\dfrac{h}{L_S}\right)\dfrac{P^6}{6}\end{array}\right) \tag{7}$$

As one can see the coefficients in Eq. (7) are renormalized by the terms proportional to $\frac{h}{L_S}$. Simple analytical expressions like (7) are hardly possible for FD density of states and SH model.

4. Polar and charge states for basic screening models

Below we will analyze graphically the surface relief of the free energy (5) along with its extremals given by Eq. (4) for BS, FD and SH models of the screening charges. Different screening charge mechanisms lead to the notable differences in the dependences of the overpotential and free energy on the polarization. Consequently the hysteresis loops of polarization reversal and screening charge density strongly depend on the model, as explained below.

4.1. Impact of the surface screening nature on the system thermodynamics

Since BS, FD and SH models are distinguished by the nature of screening charges, the expressions (2) for the charge densities $\sigma_0(\phi)$ corresponding to the models are distinguished by nonlinearity degree in the dependence of $\sigma_0(\phi)$ on electric potential φ. The results presented in Figs. 2–4, show that BS (Fig. 2), FD (Fig. 3) and SH (Fig. 4) models, and thereby corresponding screening mechanisms, determine the surface of the free energy relief in coordinates polarization “P”, overpotential "Ψ" and applied voltage "U", namely the free energy cross-sections at U and U-dependent free energy minima at certain P values. Difference in the densities $\sigma_0(\phi)$ [shown in Fig.B1] result in the noticeable difference of the free energy relief maps at zero voltage $U=0$ [compare Figs. 2(a), 3(a) and 4(a)], including the quantity and sharpness of free energy minima and character of their transformation under applied voltage increase [compare different curves in Figs. 2(b), 3(b) and 4(b)].

For BS model one of the symmetric minima of $G(P,U)$ with almost flat potential well at $U=0$ transforms to the asymmetric and smooth one shifted away from zero-polarization vertical line $P=0$ under U increase [compare black, red, magenta and blue curves in Fig. 2(b)]. For FD model one pronounced relatively sharp symmetric minimum of $G(P,U)$ with two inflection regions on it sides exists at $U=0$ [see the black curve in Fig. 3(b)]. Under the increase of U the dependence of $G(P,U)$ on polarization P at first transforms to the asymmetric curve with two minima of different

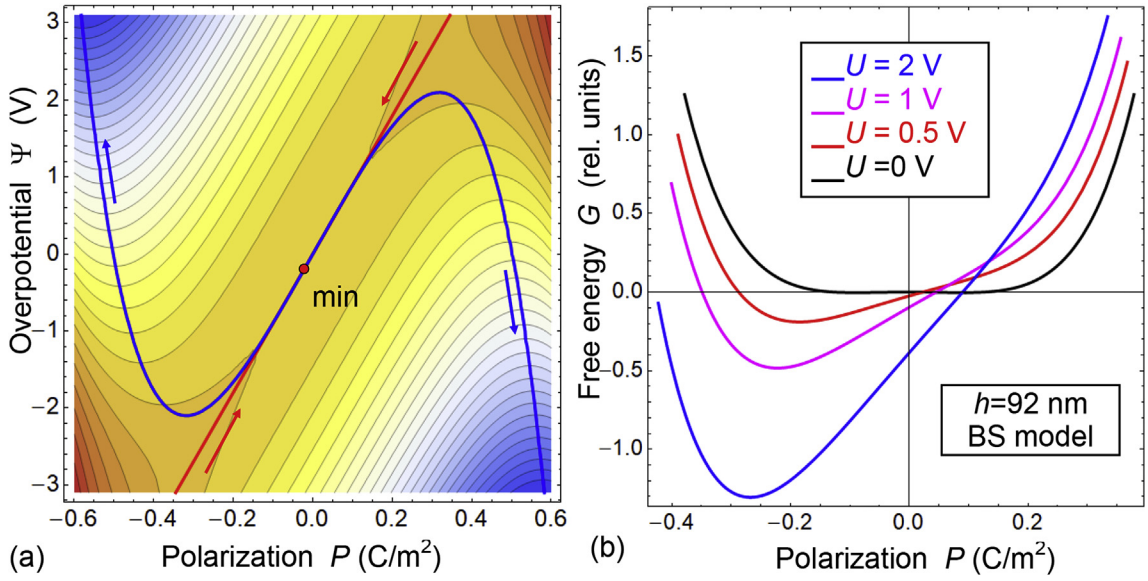

Fig. 2. Free energy relief for Bardeen model of screening charges. (a) Free energy relief map for $BaTiO_3$ film of thickness 92 nm at room temperature and zero applied voltage $U=0$. Blue and red curves, given by Eqs. (4a) and (4b), are extremals divergent and convergent towards the absolute minimum, respectively. **(b)** Free energy profile at $U=0$, 0.5, 1 and 2 V (black, red, magenta and blue curves). The screening length $L_S=0.1$ nm was chosen small enough to prevent the domains formation in the film. (For interpretation of the references to colour in this figure legend, the reader is referred to the Web version of this article.)

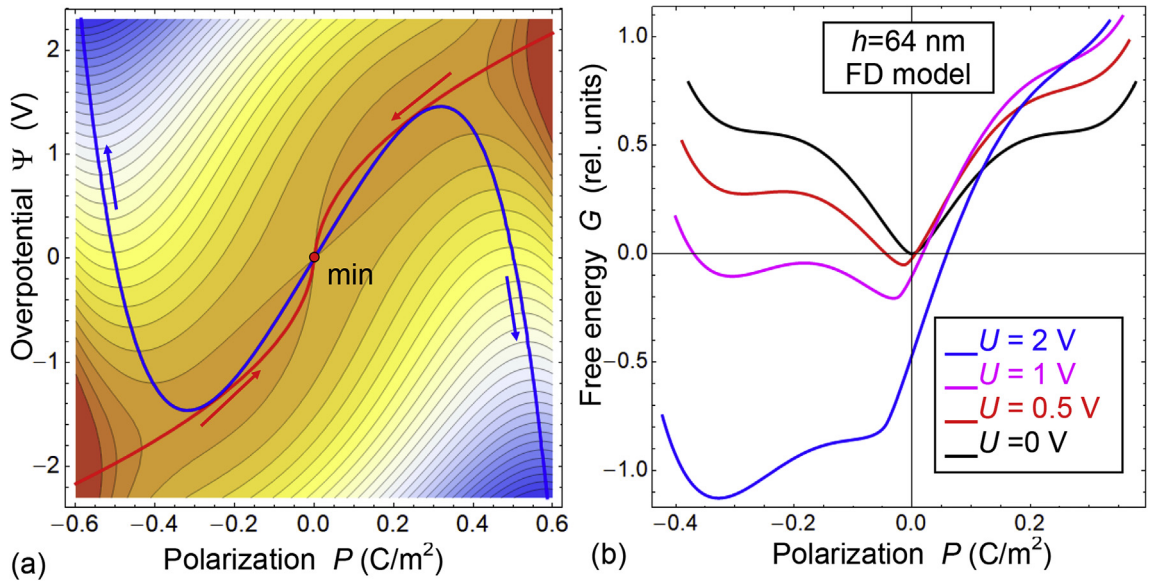

Fig. 3. Free energy relief for Fermi-Dirac model of screening charges. (a) Free energy relief map for $BaTiO_3$ film of thickness 64 nm at room temperature and zero applied voltage $U = 0$. Blue and red curves, given by Eqs. (4a) and (4b), are extremals divergent and convergent towards the absolute minimum, respectively. **(b)** Free energy profile at $U = 0$, 0.5, 1 and 2 V (black, red, magenta and blue curves). Fermi velocity $v_F = 10^6$ m/s. (For interpretation of the references to colour in this figure legend, the reader is referred to the Web version of this article.)

shape and one inflection region, and then, into the asymmetric curve with the side global minimum and two inflection regions located on the different sides from the line $P = 0$ [compare red, magenta and blue curves in Fig. 3(b)].

For SH screening by ions with equal and relatively small formation energies ($\Delta G_1^{00} = \Delta G_2^{00} = 0.1$ eV), a symmetric "horn"-like dependence of $G(P, U = 0)$ on polarization P has a smoothed shallow minimum at $P = 0$ [see Fig. 4(a) and (d)]. Under the voltage increase up to 0.5 V, the symmetric polarization dependence of $G(P, U)$ transforms into the asymmetric one with two shallow minima (the side and almost central ones) and one inflection region, which are located on different sides from the vertical line $P = 0$. Under further voltage increase up to 2 V, the small shift of the central minimum away from the line $P = 0$ takes place and pronouncedly nonlinear falling of $G(P, U)$ to negative values appears.

In the case of higher and equal ion formation energies ($\Delta G_1^{00} = \Delta G_2^{00} = 0.2$ eV) [see Fig. 4(b) and (e)], the voltage transformation of the symmetric dependence of $G(P, U)$ at $U = 0$ is similar to the one shown in Fig. 4(d). At that, however, the side inflection region transforms in a shallow minimum and the central shallow minimum transforms in the break with the voltage increase. The nonlinearity degree of voltage induced falling of the $G(P, U)$ dependence on polarization P is a bit higher than in the previous case, shown in Fig. 4(a) and (d).

In the case of different and high ion formation energies ($\Delta G_1^{00} = 0.2$ eV and $\Delta G_2^{00} = 0.4$ eV) the dependence of $G(P, U)$ on polarization P is asymmetric at $U = 0$ and has sharper minimum in the vicinity of $P = 0$, in contrast to the previous case [see Fig. 4(c) and (f) and compare them with Fig. 4(b) and (e)]. Under U increase, this minimum shifts away from the former position at $P = 0$. Similarly to the previous case, the side inflection region transforms in a shallow minimum and the central minimum transforms into the break. The nonlinearity degree of the voltage induced falling of $G(P, U)$ curve is almost the same as in the previous case.

Comparing Figs. 2–4 we should underline that the general tendency of $G(P, U)$ decreasing with the voltage increase is minimal for BS model (less than 0.5 rel. units at $P = 0$ at $U = 2$ V), a bit higher for FD model (about 0.5 rel. units at $P = 0$ at $U = 2$ V) and maximal for SH model (about 5 rel. units for at $P = 0$ at $U = 2$ V).

To resume the subsection, various nature of the screening charges (electrons, holes, adsorbed ions or vacancies) and thus the distinction of their localization and interaction with the film surface for the BS, FD and SH models leads to different dependence of their density σ_0 on the overpotential Ψ [see the dependences $\sigma_0(\psi)$ in Fig. 1(b) described by Eq. (2)]. The coupling between polarization $P(U)$ and screening charge $\sigma_0(U)$ through the overpotential Ψ described by Eq. (4) results in the hysteretic behavior of the both quantities, $P(U)$ and $\sigma_0(U)$, and therefore leads to the different peculiarities of their quasi-static hysteretic loops presented and analyzed in next subsection.

4.2. Effect of surface screening on the quasi-static polarization and charge hysteresis

First, we analyze the impact of the screening charges, localized at Bardeen surface states, on the quasi-static hysteresis of polarization and charge in a ferroelectric nanostructure shown in Fig. 1(a). The linear dependence of the BS charge density σ_0 on electric potential φ is shown by the black curve in Fig. 1(b) in relative units, and in Fig. B1 in C/m^2.

It is seen from Fig. 5, for temperatures below Curie temperature T_C, there is a hysteresis of ferroelectric type for $P(U)$ and the corresponding hysteresis of $\sigma_0(U)$ with quasi-linear parts outside the hysteresis region in a 100-nm $BaTiO_3$ film. The temperature increase leads to the simultaneous narrowing of the $P(U)$ and $\sigma_0(U)$ hysteresis loops up to their disappearance, since $P(U)$ and $\sigma_0(U)$ are strongly coupled via Eq. (4). Loops disappearance is accompanied by the decrease of remanent polarization $P(0)$ from 0.27 C/m^2 to 0, and by the expansion of $\sigma_0(U)$ maxima and their coming out from the hysteresis region, as well as by the maxima shift to higher voltages, while the maximal values of $\sigma_0(U)$ remains the same. The temperature behavior of $P(0)$ is similar to the behavior of the spontaneous polarization in the case of a second-order ferroelectric phase transition [53,54]. However, $P(0) \neq 0$ even for 450 K in a $BaTiO_3$ thin film, while $T_C = 381$ K for a bulk $BaTiO_3$ single-crystal. Therefore, the electric field of the screening charge unexpectedly

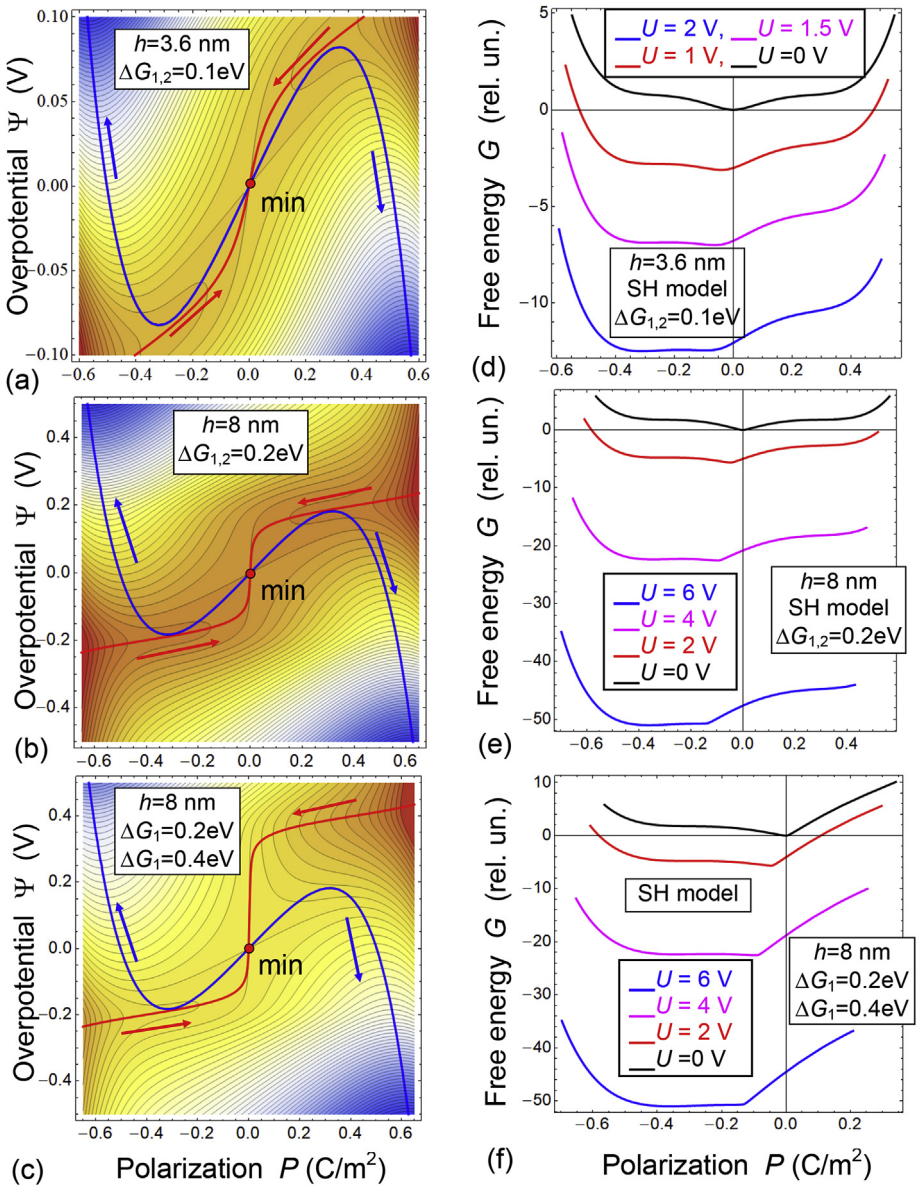

Fig. 4. Free energy relief for Stephenson-Highland model of ionic screening. (a, b, c) Free energy relief at room temperature, zero applied voltage $U = 0$, $BaTiO_3$ film thickness 3.6 nm **(a, d)**, and 8 nm **(b, c, e, f)**. Blue and red curves, given by Eqs. (4a) and (4b), respectively, are extremals divergent and convergent towards the absolute minimum. **(d, e, f)** Profiles of the free energy at different voltages U = 0, 2, 4 and 6 V (black, red, magenta and blue curves). Ion formation energies are $\Delta G_1^{00} = \Delta G_2^{00} = 0.1$ eV **(a, d)**; $\Delta G_1^{00} = \Delta G_2^{00} = 0.2$ eV **(b, e)**; $\Delta G_1^{00} = 0.2$ eV and $\Delta G_2^{00} = 0.4$ eV. **(c, f)**. Other parameters of SH model are listed in Table B1 in Appendix B. (For interpretation of the references to colour in this figure legend, the reader is referred to the Web version of this article.)

strongly supports ferroelectric-like remanent polarization $P(0)$ above T_C in the thin film. The behavior of $P(T)$ corresponds to the known scenario of the second-order ferroelectric phase transition, when an external electric field induces the polarization in a shallow paraelectric phase at temperatures somewhat higher than T_C [30]. Notably, that a bulk $BaTiO_3$ single-crystal undergoes the first-order phase transition.

Allowing for the relationship between $P(U)$ and $\sigma_0(U)$, described by Eq. (4), the behavior of the screening charge density $\sigma_0(U)$ for $T < T_C$ is determined by the ferroelectric-like hysteresis of $P(U)$, while the density $\sigma_0(U)$ for $T > T_C$ is governed by the nonlinear paraelectric-like dependence of $P(U)$. Therefore, the nonlinear dependence of $\sigma_0(U)$ on applied voltage U in the vicinity of T_C does not follow from the linear dependence of $\sigma_0(\phi)$ shown in Fig. 1(b) for the BS model. However, the dependence $\sigma_0(U)$ is also linear in the region of a quasi-linear variation of polarization $P(U)$ in the range $-1\,\mathrm{V} < U < 1\,\mathrm{V}$ for the temperature $T = 500$ K. It should be noted that the temperature changes of the $\sigma_0(U)$ loop width are smooth and correlate with the changes of the $P(U)$ loop width. Note that we did not reveal any polarization loops with a constriction or double hysteresis loops, speaking in favor of the second-order ferroelectric phase transition in thin $BaTiO_3$ film with BS screening of spontaneous polarization, while a bulk $BaTiO_3$ single-crystal undergoes the first-order phase transition. The physical origin of the change in the phase transition order is the joint action of BS screening and finite-size effect.

We further analyze the impact of the bound charge screening by 2D Fermi-Dirac electron gas on the quasi-static hysteresis of polarization and charge density in the system shown in Fig. 1(a). Super-linear dependence of the FD charge density σ_0 on acting

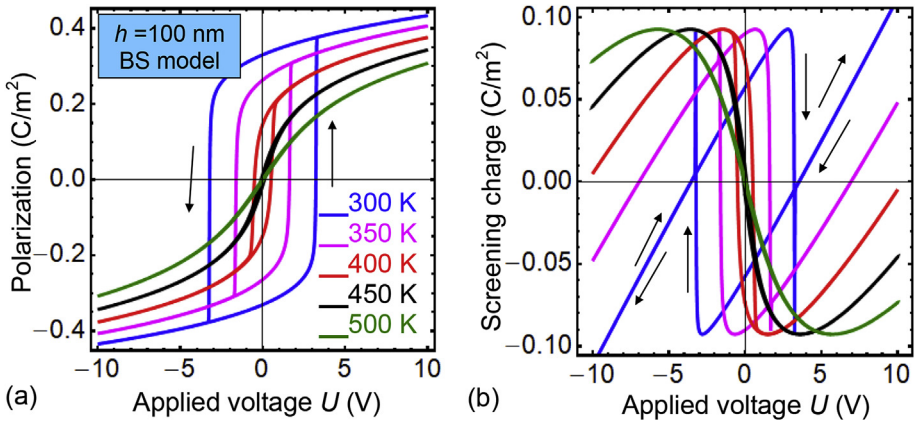

Fig. 5. Quasi-static hysteresis loops for Bardeen surface states model of the screening charge. Quasi-static hysteresis loops of the average ferroelectric polarization $P(U)$ **(a)** and screening charge density $\sigma_0(U)$ **(b)** calculated for different temperatures 300, 350, 400, 450 and 500 K (different curves) and $BaTiO_3$ film thicknesses $h = 100$ nm. Screening length $L_S = 0.1$ nm. Other parameters are listed in Table B1 in Appendix B.

potential ψ is shown by the red curve in Fig. 1(b) in relative units, and in Fig. B1 in C/m^2.

There is no hysteresis region on the $P(U)$ curve characteristic for the ferroelectric phase for a sufficiently thin 50-nm $BaTiO_3$ film with electrically open surface, since the ferroelectric state is not realized because of its suppression by finite-size effect [55]. Therefore, a very thin double hysteresis loop of $P(U)$, that occurs at 300 K in a 50-nm film covered by FD screening charge [shown by the blue curve in Fig. 6(a)], resembles the first order phase transition characteristic for the ferroelectrics in the presence of external electric field inducing polarization at $T > T_C$ [53]. A sufficiently high electric field increases the density of FD screening charge, that in turn compensates the size effect in a thin film and increases its thickness-dependent transition temperature $T_{CR}(h)$, and thereby induces a ferroelectric-like polarization. At that there is a transition through the state with zero polarization in a small electric field [53]. With the temperature increase up to 400 K the compensation of such kind occurs at much higher electric field and the hysteresis region shifts toward higher voltages. With further temperature increase from 400 K to 500 K the field-induced polarization disappears and the dependence $P(U)$ acquires a non-hysteretic form, characteristic of a shallow paraelectric phase, where the film behaves as a nonlinear paraelectric [53]. Allowing for the relationship between $P(U)$ and $\sigma_0(U)$ described by Eq. (4), the hysteresis behavior of $\sigma_0(U)$ at 300 K is related with the nonlinear hysteresis dependence of $P(U)$ at the same temperature. The hysteresis part of the dependences $\sigma_0(U)$ shifts toward higher voltages with increasing temperature [as shown in Fig. 6(d)]. The shift is accompanied by the expansion of the $\sigma_0(U)$ maxima region and their shift to the higher voltages, while the maximal value of $\sigma_0(U)$ remains constant. For higher temperatures (450–500) K the voltage dependence $\sigma_0(U)$ is nonlinear and hysteresis-less within the range $-5\ V < U < 5\ V$, while the dependence $P(U)$ is quasi-linear under the same voltages and temperatures.

For thicker 75 nm and 100 nm $BaTiO_3$ films a ferroelectric-like hysteresis of $P(U)$ appears at $T \leq 300$ K, which is typical for a ferroelectric phase [see Fig. 6(b) and (c)]. This happens because the ferroelectric state in thicker film with FD screening is not suppressed by a finite-size effect. The temperature increase causes the narrowing of the $P(U)$ hysteresis, followed by the appearance of constriction on the loop, and further transformation of the constricted loop into the double antiferroelectric-like hysteresis loop between 350 K and 450 K, and then to the nonlinear curve characteristic for a shallow paraelectric phase ($450\ K < T < 500\ K$), and eventually to the hysteresis-less curve characteristic for a deeper paraelectric phase ($T > 500$ K).

Allowing for the coupling between $P(U)$ and $\sigma_0(U)$ described by Eq. (4), the behavior of $\sigma_0(U)$ for $T < T_C$ is determined by the ferroelectric-like hysteresis of $P(U)$, and for $T > T_C$ it is determined by the double antiferroelectric-like hysteresis of $P(U)$ [compare Fig. 6(e) and (f) with 6(b), 6(c)]. Therefore, the dependence of $\sigma_0(U)$ on applied voltage U manifests hysteresis behavior and/or reveals other hysteresis-less features at the same voltages, for which $P(U)$ has corresponding peculiarities. The temperature increase leads to the narrowing of the $\sigma_0(U)$ hysteresis followed by its disappearance between 350 K and 400 K, which is accompanied by the expansion of the $\sigma_0(U)$ maxima and their shift into the region of higher voltages. For $T > T_C$ [namely for $T = (450–500)$ K] the dependence $\sigma_0(U)$ on applied voltage U is significantly nonlinear and almost hysteresis-less within the range $-5\ V < U < 5\ V$, while the dependence $P(U)$ is quasi-linear at the same voltages and temperatures.

Notably, the difference in coercive voltages (by a factor of 4) for 75 nm and 100 nm films is much higher that the ratio of their thicknesses (≈ 1.3 times) [compare Fig. 6(b), (e) and 6(c), 6(f)]. For the case we meet with the manifestation of a strongly nonlinear finite-size effect of coercive voltage. For a 100 nm film the gradual changes of the $P(U)$ loop widths does not correlate with the sharp changes of the $\sigma_0(U)$ loop widths in the temperature range between 300 K and 350 K [compare Fig. 6(c) with Fig. 6(f)].

For FD screening of polarization in $BaTiO_3$ thin films, we predict the transition from single ferroelectric-like hysteresis loops to double antiferroelectric-like loops of the polarization $P(U)$ and concentration $\sigma_0(U)$ above 320 K. The double loops exist in a wide temperature range (350–450) K, well beyond the vicinity of $BaTiO_3$ Curie temperature 381 K. It appeared that these double loops exist not only in $BaTiO_3$ film covered by 2D-semiconductor, but also in PZT film covered by a single-layer graphene [32]. Our calculations and results [32] prove that the double loops originate from the nonlinear screening of ferroelectric polarization by 2D-carriers at the film-gap interface, as well as their origin is conditioned by the temperature changes of the domain structure kinetics in a ferroelectric film.

We further analyze the impact of the Stephenson-Highland screening by ions on the quasi-static hysteresis of polarization and surface charge in the ferro-ionic system. Dependences of $P(U)$ and $\sigma_0(U)$ calculated in the case of equal formation energies $\Delta G_1^{00} = \Delta G_2^{00}$ in Langmuir absorption isotherms are shown in Fig. 7. Corresponding step-like dependence of the SH charge density σ_0 on

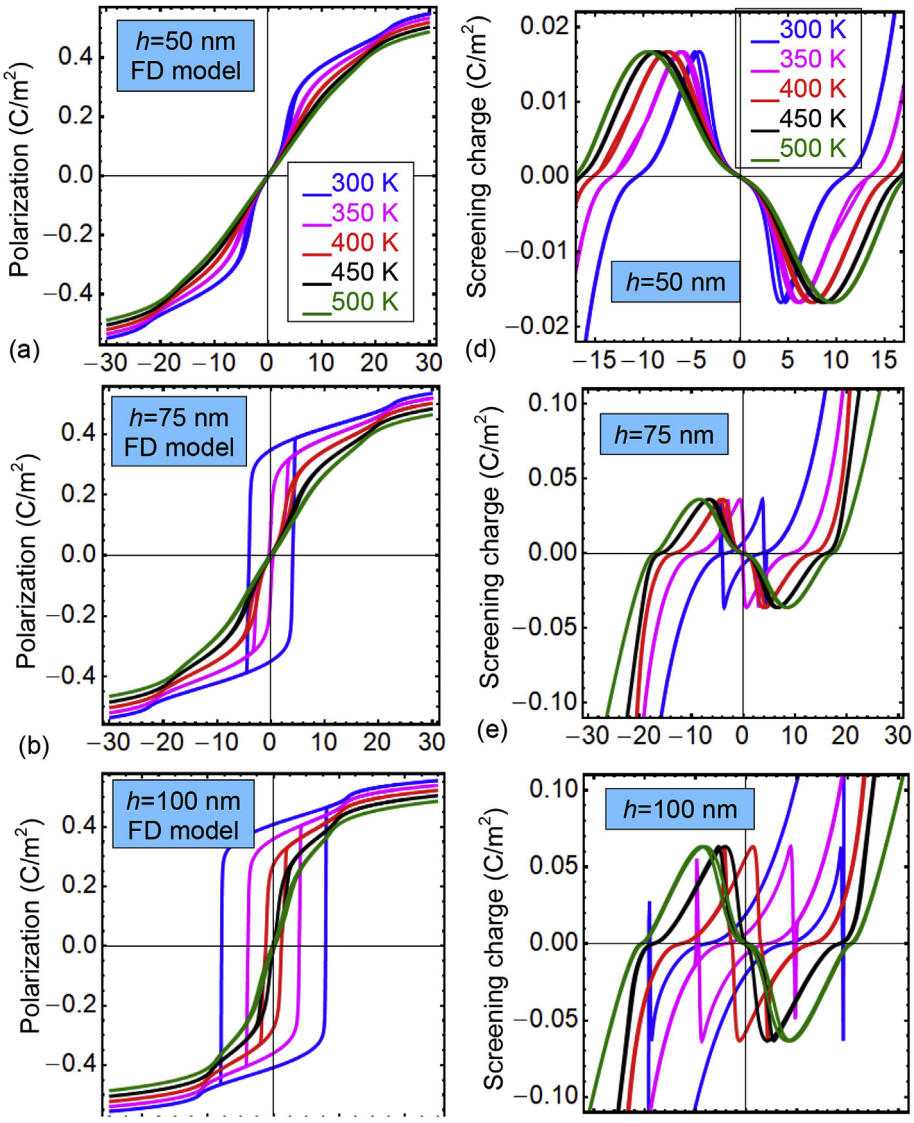

Fig. 6. Quasi-static hysteresis loops for Fermi-Dirac model of the surface screening charge. Quasi-static hysteresis loops of the average ferroelectric polarization $P(U)$ **(a, b, c)** and screening charge density $\sigma_0(U)$ **(d, e, f)** calculated for different temperatures 300, 350, 400, 450 and 500 K (blue, magenta, red, black and green curves) and different thicknesses $h = 50$ nm **(a, d)**, 75 nm **(b, e)** and 100 nm **(c, f)** of $BaTiO_3$ film. Fermi velocity $v_F = 10^6$ m/s. $BaTiO_3$ parameters are listed in Table B1 in Appendix B. (For interpretation of the references to colour in this figure legend, the reader is referred to the Web version of this article.)

the electric potential ψ is shown by the blue curve in Fig. 1(b) in relative units, and in Fig. B1 in C/m^2.

Symmetrical dependences of $P(U)$ and $\sigma_0(U)$ are related to the absence of the $\sigma_0(\phi)$ shift along φ-axis at $\Delta G_1^{00} = \Delta G_2^{00}$ [40,42]. The ferroelectric state is not realized in thin ferroelectric films at zero and small voltages U due to its suppression by finite-size effect. Meanwhile, antiferro-ionic state with double hysteresis loops is possible at voltages $|U| > U_{cr}$, since the behavior of $P(U)$ and $\sigma_0(U)$ are coupled through Eq. (4) (see Ref. [42] for details). The difference in the shape of the $P(U)$ and $\sigma_0(U)$ loops for $BaTiO_3$ films with thickness 8 nm, 10 nm, 15 nm and 20 nm are pronounced at different temperatures. For zero voltage ($U = 0$) and room (or lower) temperatures the thinnest 8-nm film is in the antiferro-ionic phase, the thicker 10-nm film is in the shallow ferroelectric phase, and the thickest 15-nm and 20-nm films are in a deeper ferroelectric phase. Notably, that the ferroelectric-like loop opening occurs for each of the film thickness at individual transition temperature varying in the range (300–500) K.

For a 8-nm film, the changes of $P(U)$ curves with the temperature increase from 300 K to 350 K are characteristic for the polarization of antiferro-ionic type induced by the electric field of ions in the paraelectric vicinity of the first-order ferroelectric phase transition [42,53].

For a 10-nm film the changes of $P(U)$ loops with the temperature increase from 300 K to 500 K are characteristic for the transition from a shallow ferroelectric phase with a relatively small coercive voltage to the antiferro-ionic phase at T > 350 K, which is characterized by a double hysteresis loop, and then to the deep paraelectric vicinity of the ferroelectric transition (T > 400 K), where the polarization becomes field-induced, decreases and eventually disappears by loosing its antiferro-ionic type hysteresis dependence.

For a 15-nm film, the changes of $P(U)$ loops with the temperature increase from 300 K to 450 K are characteristic for a transition from the ferroelectric phase with a single ferroelectric-type hysteresis loop with high coercive voltage to the antiferro-ionic state, where the double loops of anti-ferroionic type are field-induced. The anti-ferroionic hysteresis disappears in a paraelectric phase with temperature increase above 500 K. For a 20-nm film, the

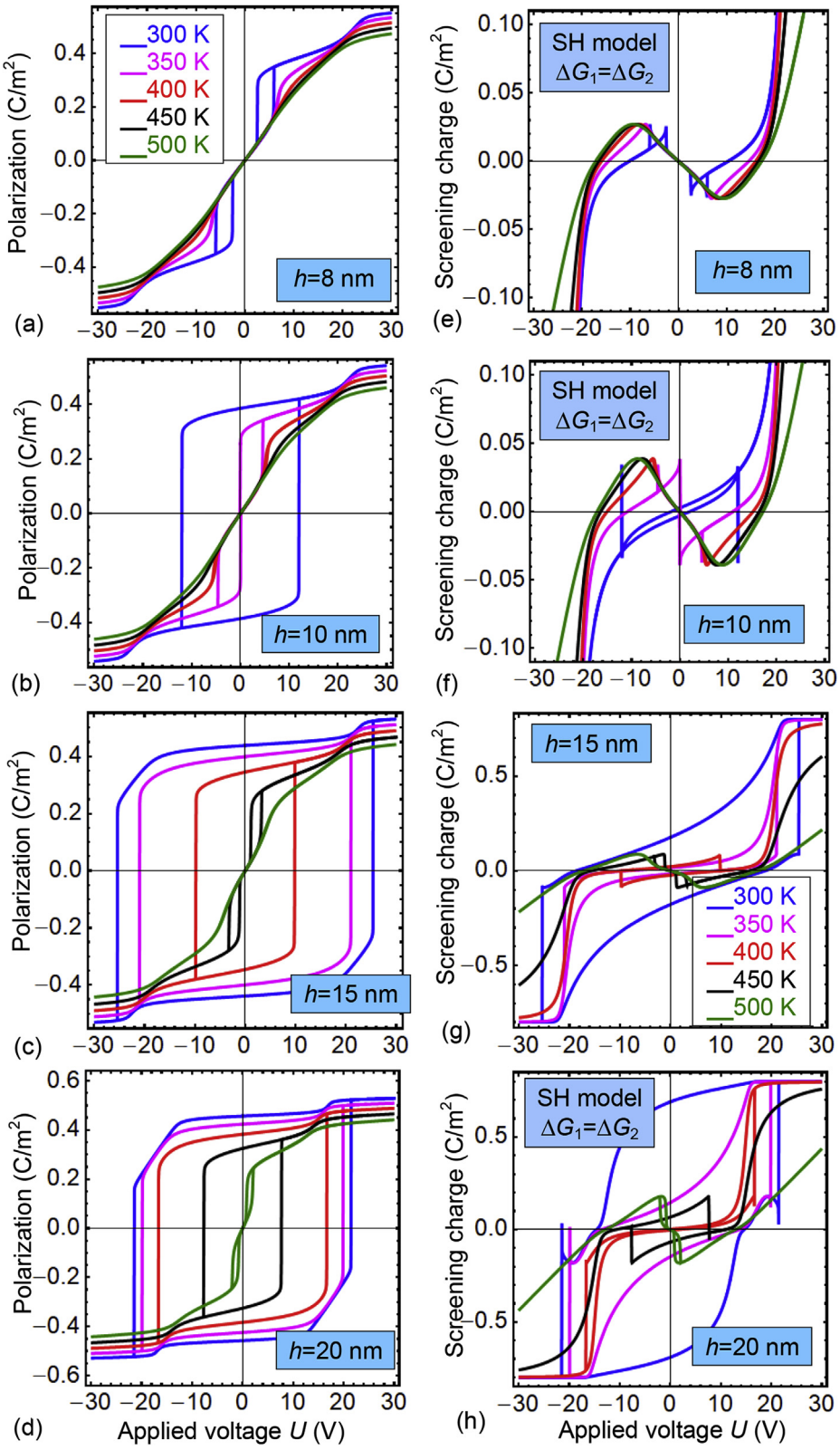

Fig. 7. Quasi-static hysteresis loops for Stephenson-Highland model of ionic screening with equal ion formation energies. Quasi-static hysteresis loops of the average ferroelectric polarization $P(U)$ **(a, b, c, d)** and screening charge density $\sigma_0(U)$ **(e, f, g, h)** calculated for different temperatures 300, 350, 400, 450 and 500 K (blue, magenta, red, black and green curves) and different thicknesses $h = 8$ nm **(a, e)**, 10 nm **(b, f)**, 15 nm **(c, g)** and 20 nm **(d, h)** of $BaTiO_3$ film. Ions formation energies are equal, $\Delta G_1^{00} = \Delta G_2^{00} = 0.2$ eV. Other parameters of SH model and $BaTiO_3$ are listed in Table B1 in Appendix B. (For interpretation of the references to colour in this figure legend, the reader is referred to the Web version of this article.)

changes of $P(U)$ loops with the temperature increase are characteristic for the gradual transition from a deep ferroelectric phase at 300 K to the antiferro-ionic state at 500 K.

The double hysteretic dependence of $P(U)$ with jumps at 300 K for 8 nm film [shown in Fig. 7(a)] correlates with the jump-like double features of the $\sigma_0(U)$ hysteresis shown in Fig. 7(e). Disappearance of the polarization loop with the temperature increase corresponds to the smoothing of $\sigma_0(U)$ dependences. For a 10-nm film the jump-like singularities of $\sigma_0(U)$ at 300 K correspond to the transition regions of the $P(U)$ hysteresis. As a result of the shape transition of $P(U)$ loop between 300 K and 350 K, the jump-like double singularities of $\sigma_0(U)$ appear and increase with the temperature increase. For 15 nm and 20 nm films, a single hysteresis loop of $\sigma_0(U)$ exists in the temperature range (300–450) K, a double hysteresis of $\sigma_0(U)$ exists in the range (400–450) K, and $\sigma_0(U)$ loops disappear with further temperature increase.

For 15 nm and 20 nm films, one should note the sharp character of the temperature changes in the shape and amplitude of the $\sigma_0(U)$ loop with a slight change in the shape and amplitude of the $P(U)$ loop between 300 K and 400 K. The sharp changes in $\sigma_0(U)$ are observed when the polarization changes its sign [compare the loops $P(U)$ and $\sigma_0(U)$ in Fig. 7(c)**-(h)** for 15 nm and 20 nm films]. Sharp anti-symmetric jumps within the hysteresis range of $\sigma_0(U)$ correspond to the temperature range of a deep ferroelectric phase. The sharp jump of $\sigma_0(U)$ gradually transforms into the smooth jumps out of hysteresis region for temperatures corresponding to the antiferro-ionic phase, and then, after a transition to the paraelectric phase, $\sigma_0(U)$ becomes a slightly sloping curve. Apparently, these effects are caused by the step-like dependence of the screening charge density inherent to the SH model [see Fig. 1(b) and Fig. B1].

Similarly to the case of FD model of the screening charge, we revealed the transition from the single ferroelectric-like to double antiferroelectric-like hysteresis loops of the polarization $P(U)$ and charge density $\sigma_0(U)$ voltage dependences for SH model with equal ion formation energies $\Delta G_1^{00} = \Delta G_2^{00}$ in the Langmuir adsorption isotherms. The transition occurs with the temperature increase above (300–450) K depending on the film thickness, while double loops exist in a temperature range of about 50 K in the vicinity of Curie temperature (that is a significantly more narrow range in comparison with FD model). These double loops originate from the nonlinear screening of ferroelectric polarization by absorbed ions.

Finally we analyze the dependences of $P(U)$ and $\sigma_0(U)$ calculated using SH model of surface screening in the case of different formation energies $\Delta G_1^{00} < \Delta G_2^{00}$ in Langmuir absorption isotherms. For the case $\Delta G_1^{00} \neq \Delta G_2^{00}$ the step of $\sigma_0(\phi)$ shifts along φ-axis [40–42]. In particular the dependence $\sigma_0(\phi)$ is shifted towards positive potentials φ for the case $\Delta G_1^{00} < \Delta G_2^{00}$ (see e.g. Fig. B1 and Fig. 4 in Ref. [42]). The asymmetric dependences of $P(U)$ and $\sigma_0(U)$ [shown in Fig. 8] are related with the shift of $\sigma_0(\phi)$.

Due to the asymmetry of the screening conditions for $\Delta G_1^{00} \neq \Delta G_2^{00}$, the polarization reversal in a ferroelectric film is facilitated for one polarity and is difficult for another polarity of applied voltage U, which leads to the shift of $P(U)$ and $\sigma_0(U)$ loops along U-axis and their shape deformation [40–42]. The ferroelectric state is not realized in ultra-thin films because of its suppression by finite-size effect at $\sigma_0 = 0$, but instead the ferro-ionic state can appear at $\sigma_0 \neq 0$ [40–42].

The 8 nm film is in the deep paraelectric phase at $\sigma_0 = 0$ due to the finite-size effect. For the film minor loops of $P(U)$ and $\sigma_0(U)$ occur at 300 K due to the electric field of ions at $U \neq 0$, at that the hysteresis region corresponds to the negative polarity of applied voltage. For the 10-nm film that is in a shallow paraelectric phase at $\sigma_0 = 0$, a truncated and shifted minor polarization loop of the ferro-ionic type opens at $T < 350$ K. As the temperature increases above 350 K, the loop gradually disappears and electret-like polarization decreases. For a 15-nm film the shifted and truncated polarization loops exist in a wider temperature range, $300\ \text{K} < T < 450$ K. After a transition to the paraelectric phase between 450 K and 500 K, the electret-like polarization induced by electric field gradually disappears. For the 20-nm film that is in a ferroelectric phase even at $\sigma_0 = 0$, the ferro-ionic loops of $P(U)$ have slightly deformed and shifted ferroelectric-like shape at 300 K. The narrowing, right shift, distortion and truncation of the loops occur with the temperature increase from 300 K to 500 K, at that the thinnest minor loop $P(U)$ of ferro-ionic type corresponds to 500 K. The ferroelectric-like and ferro-ionic polarization loops exist in a wider temperature range (300–500) K for the 20-nm film in comparison with the range (300–400) K for the 15 nm film, and the polarization induced by electric field of ions does not disappear in 20 nm film up to 500 K.

Notably, the jump-like singularities on $\sigma_0(U)$ dependences correspond to the transition regions of the hysteresis $P(U)$ for ferroelectric, ferro-ionic and electret-like field-induced polarization at different temperatures. Sharp changes of $\sigma_0(U)$ dependences are observed when the polarization changes its sign (compare the loops of $P(U)$ and $\sigma_0(U)$ for 15 nm and 20 nm films in Fig. 8). Apparently, these effects are induced by the asymmetric step-like dependence of the screening charge density $\sigma_0(U)$ inherent to the SH model at $\Delta G_1^{00} \neq \Delta G_2^{00}$.

5. Discussion

We considered the equilibrium states of polarization and screening charge and their hysteresis loops at different temperatures in the system consisting of electron conducting bottom electrode, ferroelectric film, screening charge layer and ultra-thin gap separating the film surface from the top electrode under the voltage U. The dependence of the screening charge density $\sigma(\phi)$ on electric potential φ was considered for three basic models, namely for the linear Bardeen-type surface states (BS) and nonlinear Fermi-Dirac (FD) models describing the density of states in 2D electron gas at the film surface, and strongly nonlinear Stephenson-Highland (SH) model describing the charge density of absorbed ions $\sigma(\phi)$ by Langmuir isotherms. The formation energies ΔG_i^{00}in Langmuir isotherms were considered equal or different for positively and negatively charged ions (or vacancies).

Using the analytical expressions we calculated and analyzed graphically the surface relief and profiles of the free energy $G(P,U)$ for $BaTiO_3$ thin films covered with BS, FD and SH screening charges. Appeared that the screening charge properties determine the shape of the free energy relief and corresponding free energy profiles, including the voltage-dependent position of free energy minima at certain polarization values.

For BS screening two symmetric minima of $G(P,U)$ with almost flat potential well exist at zero voltage $U = 0$. Under U increase one of the minima becomes smooth and shifts away from zero polarization line $P = 0$. For FD screening a pronounced symmetric minimum of $G(P,U)$ with two inflection regions exists at $U = 0$. The dependence of $G(P,U)$ on P becomes asymmetric with two non-equivalent minima and one inflection point with U increase.

For SH screening charges with equal and low ion formation energies ($\Delta G_1^{00} = \Delta G_2^{00} \leq 0.2$ eV), a symmetric horn-like $G(P,U)$ curve with smoothed shallow minimum at $P = 0$ corresponds to $U = 0$. The symmetric curve $G(P,U)$ transforms to the asymmetric one with two non-equivalent shallow minima and one inflection region with U increase. For different and high ion formation energies ($\left|\Delta G_1^{00} - \Delta G_2^{00}\right| \geq 0.2$ eV, $\Delta G_2^{00} \geq 0.4$ eV) the $G(P,U)$ curve is asymmetric at $U = 0$ and has relatively sharp minimum in the vicinity of $P = 0$. This minimum shifts away from the line $P = 0$ with U increase.

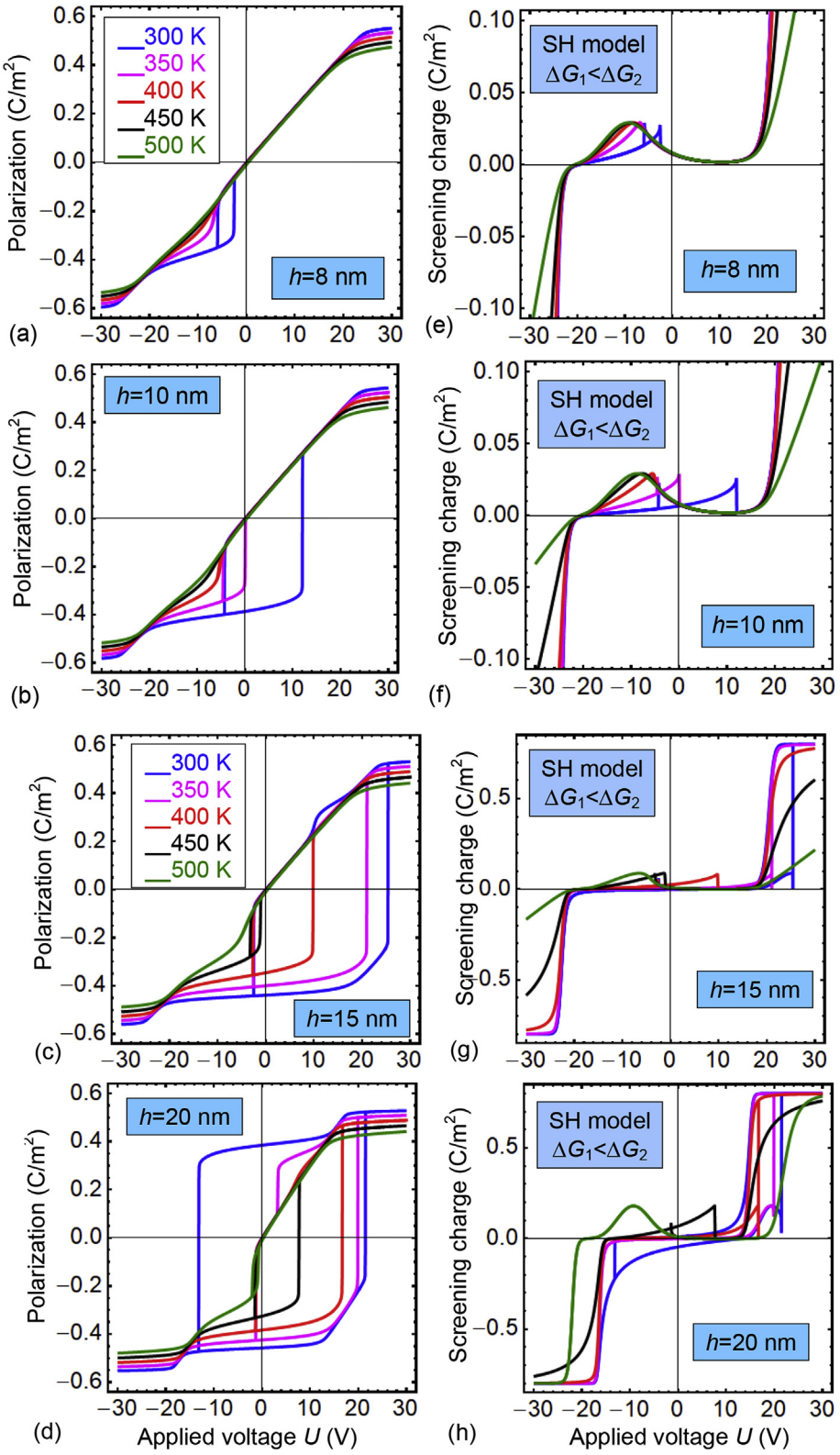

Fig. 8. Quasi-static hysteresis loops for Stephenson-Highland model of ionic screening with different ion formation energies. Quasi-static hysteresis loops of the average ferroelectric polarization $P(U)$ **(a, b, c, d)** and screening charge density $\sigma_0(U)$ **(e, f, g, h)** calculated for different temperatures 300, 350, 400, 450 and 500 K (blue, magenta, red, black and green curves) and different thicknesses $h = 8$ nm **(a, e)**, 10 nm **(b, f)**, 15 nm **(c, g)** and 20 nm **(d, h)** of $BaTiO_3$ film. Ions formation energies are different, $\Delta G_1^{00} = 0.2$ eV and $\Delta G_2^{00} = 0.4$ e V. Other parameters of SH model and $BaTiO_3$ are listed in Table B1 in Appendix B. (For interpretation of the references to colour in this figure legend, the reader is referred to the Web version of this article.)

We have established that the temperature behavior of quasi-static hysteresis loops of polarization depends on the density of the screening charge as follows. For BS screening we calculated that polarization loops have a conventional ferroelectric square-like shape and undergoes the classical second-order transition from the ferroelectric shape to paraelectric curves with the temperature increase. The temperature behavior of the loop shape speaks in favor of the second-order ferroelectric phase transition in the $BaTiO_3$ thin film covered by BS screening charges, in contrast to a bulk $BaTiO_3$ single-crystal that undergoes the first-order phase transition.

For FD screening we revealed the transition from the single ferroelectric-like to the double antiferroelectric-like hysteresis loops of the polarization $P(U)$ that happens with the temperature increase. Notably, double loops exist in a wide temperature range of about 100 K well beyond the vicinity of Curie temperature. Calculations performed for $BaTiO_3$ films in this work and for PZT films in Ref. [32] prove that the double loops originate from the nonlinear screening of ferroelectric polarization by charge carriers at ferroelectric surface.

Similarly to the case of FD screening charge, the transition from the single ferroelectric-like to double antiferroelectric-like hysteresis loops of the polarization $P(U)$ occurs for SH ionic screening at $\Delta G_1^{00} = \Delta G_2^{00}$. The transition occurs with the temperature increase above (300–450) K depending on the $BaTiO_3$ film thickness, while double loops exist in the temperature range of about 50 K near Curie temperature (that is the twice more narrow range in comparison with FD screening). These double loops originate from the nonlinear screening of spontaneous polarization by absorbed ions at the ferroelectric surface.

Due to the asymmetry of the screening conditions realized for the case $\Delta G_1^{00} \neq \Delta G_2^{00}$, polarization reversal in the film covered by SH screening charges is facilitated for one polarity and is difficult for another polarity of applied voltage U, which causes the shift of the polarization $P(U)$ and screening charge $\sigma_0(U)$ hysteresis loops along U-axis and their shape deformation. The ferroelectric state is not realized in ultra-thin $BaTiO_3$ films at $\sigma_0 = 0$ because of its suppression by finite-size effect, but the ferro-ionic minor hysteresis loops can appear at $\sigma_0 \neq 0$, and the hysteresis region corresponds to the definite polarity of applied voltage. For a thicker film a truncated and shifted minor polarization hysteresis loop of the ferro-ionic type opens at $T < 350$ K and $\left|\Delta G_1^{00} - \Delta G_2^{00}\right| \geq 0.2$ eV. As the temperature increases, the loop gradually disappears and electret-like polarization decreases. For thicker films, which are in a ferroelectric phase at $\sigma_0 = 0$, the $P(U)$ loops have slightly deformed and shifted ferroelectric shape at 300 K. The narrowing, horizontal shift, distortion and truncation of the loops occur with the temperature increase from 300 K to 500 K, and the thinnest minor loop of $P(U)$ is of ferro-ionic type up to 500 K. Apparently these effects are conditioned by the asymmetric step-like dependence of the ionic charge density inherent to the SH model at $\Delta G_1^{00} \neq \Delta G_2^{00}$.

6. Conclusions

Comparative analysis of the results obtained for BS, FD and SH screening charge models shows that the nonlinearity degree of the voltage dependences of the screening charge plays a decisive role in the ferroelectric charge compensation mechanism. As a consequence, the most varied and nontrivial temperature behavior of the hysteresis loop of polarization and the screening charge is inherent to the SH screening model. This variety is conditioned by either symmetric or asymmetric almost step-like dependence of the equilibrium charge density of absorbed ions on applied voltage, which is described by Langmuir absorption isotherms with equal or different formation energies for positive and negative ions, respectively. Obtained results open new possibilities for control of polarization reversal in thin ferroelectric films at different temperatures by appropriate choice of surface charge nature and screening mechanism.

Authors' contribution

A.N.M. generated the research idea, mathematically stated the problem and performed analytical calculations. E.A.E. and I.S.V. wrote the codes. E.A.E. performed numerical calculations and jointly with A.N.M. and M.V.S. presented the results of calculations in a graphical form. A.N.M. and N.V.M. interpret the obtained results and wrote the manuscript draft. S.V.K. worked on the results discussion and manuscript improvement.

Acknowledgements

S.V.K. acknowledges the Office of Basic Energy Sciences, U.S. Department of Energy. Part of the work was performed at the Center for Nanophase Materials Sciences, which is a DOE Office of Science User Facility. A.N.M. work was partially supported by the National Academy of Sciences of Ukraine (project No. 0118U003375 and No. 0117U002612). M.V.S. acknowledges RFBR grant 17-08-01374_a.

Appendix A. Electrostatic equations with boundary conditions

Quasi-static electric field inside the ferroelectric film is expressed via electric potential in a conventional manner, $E_3 = -\partial\phi_f/\partial x_3$. The potential ϕ_f satisfies electrostatic equations for each of the layer (i.e. for the gap and ferroelectric film), which have the form:

$$\Delta\phi_d = 0, \quad (-\lambda \leq z \leq 0 \text{ inside the gap}) \tag{A.1a}$$

$$\left(\varepsilon_b \frac{\partial^2}{\partial z^2} + \varepsilon_{11}^f \Delta_\perp\right)\phi_f = \frac{1}{\varepsilon_0}\frac{\partial P_3^f}{\partial z}, \quad (0 < z < h \text{ inside the ferroelectric film}) \tag{A.1b}$$

Here Δ is 3D-Laplace operator, $\Delta_\perp$ is 2D-Laplace operator.

Boundary conditions (**BCs**) for the system of equation (A.1) have the form:

$$\phi_d|_{z=-\lambda} = U, \quad \left(\phi_d - \phi_f\right)\Big|_{z=0} = 0, \quad \phi_f\Big|_{z=h} = 0, \tag{A.2a}$$

Table B.1
Description of physical variables and their numerical values

Description of the physical quantities used in Eqs. (1)–(3)	Designation and dimensionality	Value for a nanostructure $BaTiO_3$ film/ionic charge/gap/tip
Polarization of ferroelectric along polar axis Z	P_3 (C/m^2)	variable (0.26 for a bulk $BaTiO_3$)
Electric field	E_3 (V/m)	variable
Electrostatic potentials of dielectric gap and ferroelectric film	φ_d and φ_f (V)	variables
Electric voltage on the tip	U (V)	variable
The coefficient at P^2 in the LGD energy	$a_3 = \alpha_T(T - T_C)$ (C^{-2} J m)	T-dependent variable
Dielectric stiffness	α_T ($\times 10^5$ C^{-2} J m/K)	6.68
Curie temperature of a bulk $BaTiO_3$	T_C (K)	381 (about 10 K smaller than FE transition temperature)
The coefficient at P^4 in the LGD energy	β ($\times 10^9$ J C^{-4} m^5)	$-8.18 + 0.01876 \times T$
The coefficient at P^6 in the LGD energy	γ ($\times 10^{11}$ J C^{-6} m^9)	1.467–0.00331T
The coefficient at $(\nabla P)^2$ in the LGD energy	g ($\times 10^{-10}$ m/F)	(0.5–5)
Kinetic coefficient	Γ (s $\times$ C^{-2} J m)	rather small
Landau-Khalatnikov relaxation time	τ_K (s)	$10^{-11} - 10^{-13}$ (far from Tc)
Thickness of the ferroelectric layer	h (nm)	variable 3–500
Background permittivity of ferroelectric	ε_b (dimensionless)	10
Extrapolation lengths	Λ-, Λ_+ (angstroms)	$\Lambda_- = 1$ Å, $\Lambda_+ = 2$ Å
Surface charge density	$\sigma(\phi, t)$ (C/m^2)	variable
Equilibrium surface charge density	$\sigma_0(\phi)$ (C/m^2)	variable
Occupation degree of the surface ions	θ_i (dimensionless)	variable
Oxygen partial pressure	Po_2 (bar)	1 (atmospheric)
Surface charge relaxation time	τ (s)	$\gg$ Landau-Khalatnikov time
Thickness of the dielectric gap	λ (nm)	0.4
Permittivity of the dielectric gap	ε_d (dimensionless)	1–10
Universal dielectric constant	ε_0 (F/m)	8.85×10^{-12}
Electron charge	e (C)	1.6×10^{-19}
Ionization degree of the surface ion	Z_i (dimensionless)	$Z_1 = +2, Z_2 = -2$
Number of surface ions created per oxygen molecule	n_i (dimensionless)	$n_1 = 2, n_2 = -2$
Minimal area per the surface ion	A_i (m^2)	$A_1 = A_2 = 10^{-18}$–10^{-19}
Ion (or vacancy) formation energy	ΔG_i^{00} (eV)	0–1

$$\left(\varepsilon_0\varepsilon_d\frac{\partial\phi_d}{\partial z} + P_3^f - \varepsilon_0\varepsilon_b\frac{\partial\phi_f}{\partial z} - \sigma\right)\Big|_{z=0} = 0. \qquad \text{(A.2b)}$$

Appendix B. Description of physical variables and their numerical values

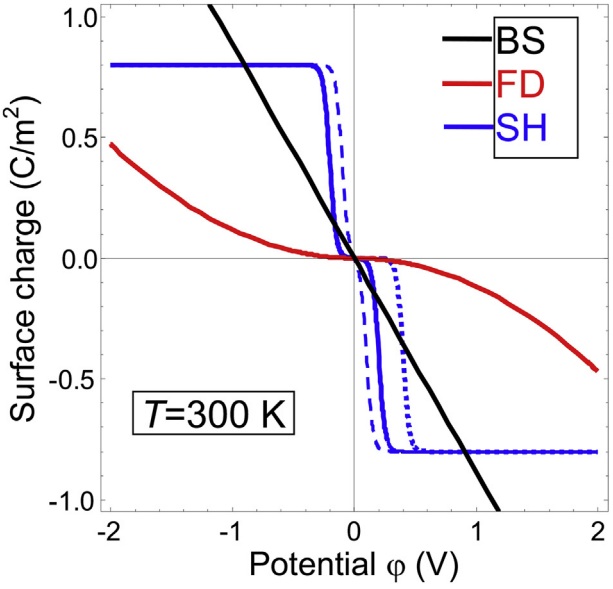

Fig. B1. Dependence of the surface charge densities σ_0 vs. the electric potential φ calculated for Bardeen-type surface states (black line "BS"), Fermi-Dirac electron gas (red curve "FD"), and Stephenson-Highland absorbed ions (solid and dashed blue step-like curves "SH" for $\Delta G_1^{00} = \Delta G_2^{00} = 0.2$eV and 0.1 eV, dotted curves for $\Delta G_1^{00} = 0.2$ eV and $\Delta G_2^{00} = 0.4$ eV) for parameters listed in Table B.1.

References

[1] M.J. Highland, T.T. Fister, D.D. Fong, P.H. Fuoss, Carol Thompson, J.A. Eastman, S.K. Streiffer, G.B. Stephenson, Equilibrium polarization of ultrathin PbTiO3 with surface compensation controlled by oxygen partial pressure, Phys. Rev. Lett. 107 (18) (2011) 187602.
[2] Sergei V. Kalinin, Yunseok Kim, Dillon Fong, Morozovska Anna, Surface-screening mechanisms in ferroelectric thin films and their effect on polarization dynamics and domain structures, Rep. Prog. Phys. 81 (2018) 036502.
[3] A.K. Tagantsev, L.E. Cross, J. Fousek, Domains in Ferroic Crystals and Thin Films, Springer, New York, 2010, https://doi.org/10.1007/978-1-4419-1417-0. ISBN 978-1-4419-1416-3, e-ISBN 978-1-4419-1417-0.
[4] A.M. Bratkovsky, A.P. Levanyuk, Continuous theory of ferroelectric states in ultrathin films with real electrodes, J. Comput. Theor. Nanosci. 6 (3) (2009) 465.
[5] A.M. Bratkovsky, A.P. Levanyuk, Effects of anisotropic elasticity in the problem of domain formation and stability of monodomain state in ferroelectric films, Phys. Rev. **B** 84 (4) (2011) 045401.
[6] E.V. Chensky, V.V. Tarasenko, Theory of phase transitions to inhomogeneous states in finite ferroelectrics in an external electric field, Sov. Phys. JETP 56 (1982) 618 [Zh. Eksp. Teor. Fiz. 83, (1982) 1089].
[7] S.V. Kalinin, D.A. Bonnell, Screening phenomena on oxide surfaces and its implications for local electrostatic and transport measurements, Nano Lett. 4 (2004) 555.
[8] S. Jesse, A.P. Baddorf, S.V. Kalinin, Switching spectroscopy piezoresponse force microscopy of ferroelectric materials, Appl. Phys. Lett. 88 (2006) 062908.
[9] A.N. Morozovska, S.V. Svechnikov, E.A. Eliseev, S. Jesse, B.J. Rodriguez, S.V. Kalinin, Piezoresponse force spectroscopy of ferroelectric-semiconductor materials, J. Appl. Phys. 102 (2007) 114108.
[10] A.V. Ievlev, S. Jesse, A.N. Morozovska, E. Strelcov, E.A. Eliseev, Y.V. Pershin, A. Kumar, V.Y. Shur, S.V. Kalinin, Intermittency, quasiperiodicity and chaos in probe-induced ferroelectric domain switching, Nat. Phys. 10 (2013) 59.
[11] A.V. Ievlev, A.N. Morozovska, V.Ya Shur, S.V. Kalinin, Humidity effects on tip-induced polarization switching in lithium niobate, Appl. Phys. Lett. 104 (2014), 092908.
[12] A.K. Tagantsev, G. Gerra, Interface-induced phenomena in polarization response of ferroelectric thin films, J. Appl. Phys. 100 (2006), 051607.
[13] A.K. Tagantsev, M. Landivar, E. Colla, N. Setter, Identification of passive layer in ferroelectric thin films from their switching parameters, J. Appl. Phys. 78 (1995) 2623.
[14] Vasudeva Rao Aravind, A.N. Morozovska, S. Bhattacharyya, D. Lee, S. Jesse, I. Grinberg, Y.L. Li, S. Choudhury, P. Wu, K. Seal, A.M. Rappe, S.V. Svechnikov, E.A. Eliseev, S.R. Phillpot, L.Q. Chen, Venkatraman Gopalan, S.V. Kalinin, Correlated polarization switching in the proximity of a 180° domain wall, Phys. Rev. B 82 (2010), 024111.
[15] Chun-Lin Jia, K.W. Urban, M. Alexe, D. Hesse, I. Vrejoiu, Direct observation of continuous electric dipole rotation in flux-closure domains in ferroelectric

Pb(Zr,Ti)O_3, Science 331 (2011) 1420.
[16] Y.L. Tang, Y.L. Zhu, X.L. Ma, A.Y. Borisevich, A.N. Morozovska, E.A. Eliseev, W.Y. Wang, Y.J. Wang, Y.B. Xu, Z.D. Zhang, S.J. Pennycook, Observation of a periodic array of flux-closure quadrants in strained ferroelectric $PbTiO_3$ films, Science 348 (6234) (2015) 547.
[17] I.S. Vorotiahin, E.A. Eliseev, Li Qian, S.V. Kalinin, Y.A. Genenko, A.N. Morozovska, Tuning the polar states of ferroelectric films via surface charges and flexoelectricity, Acta Mater. 137 (15) (2017) 85.
[18] E.A. Eliseev, I.S. Vorotiahin, Y.M. Fomichov, M.D. Glinchuk, S.V. Kalinin, Y.A. Genenko, A.N. Morozovska, Defect driven flexo-chemical coupling in thin ferroelectric films, Phys. Rev. B 97 (2018) 024102.
[19] B.M. Darinskii, A.P. Lazarev, A.S. Sidorkin, Fiz. Tverd. Tela. 31 (1989) 287 [Sov. Phys. Solid State, 31, (1989) 2003].
[20] E.A. Eliseev, A.N. Morozovska, S.V. Kalinin, Y.L. Li, Jie Shen, M.D. Glinchuk, L.Q. Chen, V. Gopalan, Surface effect on domain wall width in ferroelectrics, J. Appl. Phys. 106 (2009) 084102.
[21] V.Ya Shur, A.L. Gruverman, V.P. Kuminov, N.A. Tonkachyova, Ferroelectrics 111 (1990) 197.
[22] E.A. Eliseev, A.N. Morozovska, G.S. Svechnikov, E.L. Rumyantsev, E.I. Shishkin, V.Y. Shur, S.V. Kalinin, Screening and retardation effects on 180°-domain wall motion in ferroelectrics: wall velocity and nonlinear dynamics due to polarization-screening charge interaction, Phys. Rev. B 78 (24) (2008) 245409.
[23] A.I. Kurchak, E.A. Eliseev, S.V. Kalinin, M.V. Strikha, A.N. Morozovska, P-N junctions dynamics in graphene channel induced by ferroelectric domains motion, Appl. Phys. Rev. 8 (2017) 024027.
[24] S. Kim, Junghyo Nah, Insun Jo, Davood Shahrjerdi, L. Colombo, Zhen Yao, E. Tutuc, S.K. Banerjee, Realization of a high mobility dual-gated graphene field-effect transistor with Al_2O_3 dielectric, Appl. Phys. Lett. 94 (6) (2009) 062107.
[25] Ke Zou, Xia Hong, Derek Keefer, Jun Zhu, Deposition of high-quality HfO_2 on graphene and the effect of remote oxide phonon scattering, Phys. Rev. Lett. 105 (12) (2010) 126601.
[26] Hong Xia, Kaiqi Zou, A.M. DaSilva, C.H. Ahn, J. Zhu, Integrating functional oxides with graphene, Solid State Commun. 152 (15) (2012) 1365.
[27] E.A. Eliseev, A.V. Semchenko, Y.M. Fomichov, M.D. Glinchuk, V.V. Sidsky, V.V. Kolos, YuM. Pleskachevsky, M.V. Silibin, N.V. Morozovsky, A.N. Morozovska, Surface and finite size effects impact on the phase diagrams, polar and dielectric properties of (Sr,Bi)Ta_2O_9 ferroelectric nanoparticles, J. Appl. Phys. 119 (2016), 204104.
[28] J. Bardeen, Surface states and rectification at a metal semi-conductor contact, Phys. Rev. 71 (1947) 717.
[29] Yukio Watanabe, Theoretical stability of the polarization in a thin semi-conducting ferroelectric, Phys. Rev. B 57 (2) (1998) 789.
[30] P. Nemes-Incze, Z. Osváth, K. Kamarás, L.P. Biró, Anomalies in thickness measurements of graphene and few layer graphite crystals by tapping mode atomic force microscopy, Carbon 46 (11) (2008) 1435.
[31] E.J.G. Santos, Electric field effects on graphene materials, in: Exotic Properties of Carbon Nanomatter, Springer Netherlands, Dordrecht, 2015, pp. 383–391.
[32] A.I. Kurchak, A.N. Morozovska, E.A. Eliseev, S.V. Kalinin, M.V. Strikha, Nontrivial temperature behavior of the Carrier concentration in graphene on ferroelectric substrate with domain walls, Acta Mater. 155 (2018) 302.
[33] G.B. Stephenson, M.J. Highland, Equilibrium and stability of polarization in ultrathin ferroelectric films with ionic surface compensation, Phys. Rev. B 84 (6) (2011) 064107.
[34] R.V. Wang, D.D. Fong, F. Jiang, M.J. Highland, P.H. Fuoss, Carol Tompson, A.M. Kolpak, J.A. Eastman, S.K. Streiffer, A.M. Rappe, G.B. Stephenson, Reversible chemical switching of a ferroelectric film, Phys. Rev. Lett. 102 (2009) 047601.
[35] D.D. Fong, A.M. Kolpak, J.A. Eastman, S.K. Streiffer, P.H. Fuoss, G.B. Stephenson, Carol Thompson, D.M. Kim, K.J. Choi, C.B. Eom, I. Grinberg, A.M. Rappe, Stabilization of monodomain polarization in ultrathin $PbTiO_3$ films, Phys. Rev. Lett. 96 (2006) 127601.
[36] M.J. Highland, T.T. Fister, M.-I. Richard, D.D. Fong, P.H. Fuoss, C. Thompson, J.A. Eastman, S.K. Streiffer, G.B. Stephenson, Polarization switching without domain formation at the intrinsic coercive field in ultrathin ferroelectric $PbTiO_3$, Phys. Rev. Lett. 105 (2010) 167601.
[37] B.M.W. Trapnell, Chemisorption, Academic Press, New York, 1955.
[38] Ph Wolkenstein, Electronic Process on Semiconductor Surfaces during Chemisorptions, Consultants bureau, N.-Y, 1991.
[39] Sang Mo Yang, A.N. Morozovska, Rajeev Kumar, E.A. Eliseev, Ye Cao, L. Mazet, N. Balke, S. Jesse, Rama Vasudevan, C. Dubourdieu, S.V. Kalinin, Mixed electrochemical-ferroelectric states in nanoscale ferroelectrics, Nat. Phys. 13 (2017) 812, https://doi.org/10.1038/nphys4103.
[40] A.N. Morozovska, E.A. Eliseev, N.V. Morozovsky, S.V. Kalinin, Ferroionic states in ferroelectric thin films, Phys. Rev. B 95 (2017) 195413, https://doi.org/10.1103/PhysRevB.95.195413.
[41] A.N. Morozovska, E.A. Eliseev, N.V. Morozovsky, S.V. Kalinin, Piezoresponse of ferroelectric films in ferroionic states: time and voltage dynamics, Appl. Phys. Lett. 110 (2017) 182907, https://doi.org/10.1063/1.4979824.
[42] A.N. Morozovska, E.A. Eliseev, A.I. Kurchak, N.V. Morozovsky, R.K. Vasudevan, M.V. Strikha, S.V. Kalinin, Effect of surface ionic screening on polarization reversal scenario in ferroelectric thin films: crossover from ferroionic to antiferroionic states, Phys. Rev. B 96 (2017) 245405.
[43] V.V. Betsa, V.N. Zhikharev, Y.V. Popik, Mechanism of adsorption of oxygen and hydrogen on surface of solids, Sov. Phys. J. 20 (1977) 1188, https://doi.org/10.1007/BF00897126.
[44] Y.V. Popik, V.N. Zhikharev, V.V. Betsa, Adsorption impact on polarization processes in ferroelectric-semiconductors $BaTiO_3$ and SbSI, Solid State Phys. 24 (2) (1982) 486.
[45] Y.V. Popik, V.N. Zhikharev, Adsorption impact on polarization value of ferroelectrics, Poverkchnost' (Physics, Chemistry, Mechanics) (6) (1989) 33.
[46] I.D. Sejkovskij, V.N. Zhiharev, YuV. Popik, Calculation of adsorption and interaction mechanisms of O_2 and CO_2 molecules on $BaTiO_3$ surface, Condens. Matter Phys. 6 (2) (2003) 281 (34).
[47] E.A. Eliseev, A.N. Morozovska, General approach to the description of the size effect in ferroelectric nanosystems, J. Mater. Sci. 44 (19) (2009) 5149.
[48] R. Kretschmer, K. Binder, Surface effects on phase transitions in ferroelectrics and dipolar magnets, Phys. Rev. B 20 (1979) 1065.
[49] C.-L. Jia, Valanoor Nagarajan, Jia-Qing He, Lothar Houben, Zhao Tong, Ramamoorthy Ramesh, Knut Urban, Rainer Waser, Unit-cell scale mapping of ferroelectricity and tetragonality in epitaxial ultrathin ferroelectric films, Nat. Mater. 6 (2007) 64.
[50] K.Y. Foo, B.H. Hameed, Insights into the modeling of adsorption isotherm systems, Chem. Eng. J. 156 (1) (2010) 2.
[51] Ye Cao, S.V. Kalinin, Phase-field modeling of chemical control of polarization stability and switching dynamics in ferroelectric thin films, Phys. Rev. B 94 (2016) 235444.
[52] B.D. Vujanovic, S.E. Jones, Variational Methods in Nonconservative Phenomena, Academic Press, San Diego, 1989.
[53] W.J. Merz, Double hysteresis loop of BaTi O 3 at the Curie point, Phys. Rev. 91 (3) (1953) 513.
[54] J.C. Burfoot, G.W. Taylor, Polar Dielectrics and Their Applications, The Macmillan Press, London, 1979, 465.
[55] E.A. Eliseev, S.V. Kalinin, A.N. Morozovska, Finite size effects in ferroelectric-semiconductor thin films under open-circuited electric boundary conditions, J. Appl. Phys. 117 (2015) 034102.

3.7. Publication C1

Defect-driven flexochemical coupling in thin ferroelectric films
Eugene A. Eliseev, Ivan S. Vorotiahin, Yevhen M. Fomichov, Maya D. Glinchuk, Sergei V. Kalinin, Yuri A. Genenko, and Anna N. Morozovska
Physical Review B 97, 024102 (2018). 17 pages.

Defect-driven flexochemical coupling in thin ferroelectric films

Eugene A. Eliseev,[1] Ivan S. Vorotiahin,[2,3] Yevhen M. Fomichov,[1,4] Maya D. Glinchuk,[1] Sergei V. Kalinin,[5] Yuri A. Genenko,[3,*] and Anna N. Morozovska[2,†]

[1]*Institute for Problems of Materials Science, National Academy of Sciences of Ukraine, 3, Krjijanovskogo, 03142 Kyiv, Ukraine*
[2]*Institute of Physics, National Academy of Sciences of Ukraine, 46, Prospekt Nauky, 03028 Kyiv, Ukraine*
[3]*Institut für Materialwissenschaft, Technische Universität Darmstadt, Otto-Berndt-Str. 3, 64287 Darmstadt, Germany*
[4]*Faculty of Mathematics and Physics, Charles University, V Holesovickach 2, 18000 Prague 8, Czech Republic*
[5]*The Center for Nanophase Materials Sciences, Oak Ridge National Laboratory, Oak Ridge, Tennessee 37831, USA*

(Received 6 August 2017; revised manuscript received 11 December 2017; published 5 January 2018)

Using the Landau-Ginzburg-Devonshire theory, we considered the impact of the flexoelectrochemical coupling on the size effects in polar properties and phase transitions of thin ferroelectric films with a layer of elastic defects. We investigated a typical case, when defects fill a thin layer below the top film surface with a constant concentration creating an additional gradient of elastic fields. The defective surface of the film is not covered with an electrode, but instead with an ultrathin layer of ambient screening charges, characterized by a surface screening length. Obtained results revealed an unexpectedly strong effect of the joint action of Vegard stresses and flexoelectric effect (shortly flexochemical coupling) on the ferroelectric transition temperature, distribution of the spontaneous polarization and elastic fields, domain wall structure and period in thin $PbTiO_3$ films containing a layer of elastic defects. A nontrivial result is the persistence of ferroelectricity at film thicknesses below 4 nm, temperatures lower than 350 K, and relatively high surface screening length (∼0.1 nm). The origin of this phenomenon is the flexoelectric coupling leading to the rebuilding of the domain structure in the film (namely the cross-over from c-domain stripes to a-type closure domains) when its thickness decreases below 4 nm. The ferroelectricity persistence is facilitated by negative Vegard effect. For positive Vegard effect, thicker films exhibit the appearance of pronounced maxima on the thickness dependence of the transition temperature, whose position and height can be controlled by the defect type and concentration. The revealed features may have important implications for miniaturization of ferroelectric-based devices.

DOI: 10.1103/PhysRevB.97.024102

I. INTRODUCTION

Deep physical understanding and a possible control of the polar properties of thin ferroelectric films are important for both fundamental research and the most promising applications in memory elements as well as many other devices [1]. With a decreasing film thickness its ferroelectric properties usually decline until their complete disappearance at thicknesses smaller than the critical one [2]. Feasible ways to avoid the size-induced phase transition in thin epitaxial films are, for example, selecting of an appropriate substrate [3] or modification of their chemical composition [4]. Particularly it was shown that the retaining of ferroelectricity down to ultrathin films (3–5 lattice constants thick) is provided by the "self-polarizing" role of elastic strains arising in the film due to mismatching lattice constants of the film and the substrate [5]. Earlier it was shown by Roytburd *et al.* [6] that the change in the polarization is proportional to internal stresses due to film-substrate misfit strain, and, as an example, a significant recovery in the piezoelectric constant and susceptibility in $PbZr_{0.2}Ti_{0.8}O_3$ films on (001) $LaAlO_3$ substrate was revealed.

The presence of point elastic defects (such as uncharged impurities and vacancies, elastic dipoles, dilatation centers [7]) can strongly impact the electric polarization of films via electrostriction [8], flexoelectric effect (see, e.g., Refs. [9–13]) and "chemical" or Vegard strains (see, e.g., Refs. [14–19]). Actually, when the chemical heterogeneity is the actual mechanism for strain, the generalized Hooke's law relates the defect concentration excess δN, elastic stress tensor σ_{ij} and strain tensor u_{ij} in accordance with the Vegard law [16–19], $\sigma_{ij} = W_{ij}\,\delta N + c_{ijkl}u_{kl}$. Due to the gradient nature, the elastic defect influence is much more complex and less studied than the effect of homogeneous elastic strains arising in a film due to the film and substrate lattice mismatch [20]. A joint action of Vegard stresses and flexoelectric effect, named flexochemical effect [21], can explain some unusual phenomena caused by size effects, such as, e.g., reentrant ferroelectric phase with enhanced polarization at room temperature observed in $BaTiO_3$ nanoparticles with sizes less than 20 nm [22].

Flexoelectric effect, chemical composition gradient and/or defect impact on the polar properties of ferroelectric thin films were studied theoretically by several authors, but mostly these three different effects have been studied separately [see the columns "Flexoelectric effect" and "Composition gradient, defects" in Table I]. For instance, Marvan *et al.* [23] advanced the theory of compositionally graded ferroelectrics.

Roytburd and Slutsker [24] proposed a phenomenological model of a graded ferroelectric film taking into account approximate expressions for depolarization field containing

*genenko@mm.tu-darmstadt.de
†anna.n.morozovska@gmail.com

TABLE I. Flexoelectric, Vegard and size effects, compositional gradients, and domain structure formation considered "Yes" or "No" in ferroelectric thin films.

References examples	Flexoelectric, Vegard and size effects, compositional gradients, and domain structure formation considered ("Yes" or "No") in ferroelectric thin films						
	Flexoelectric effect	Composition gradient, defects	Compositional polariza-tion	Vegard stresses	Flexochemical effect	Domain formation	Size effects
Tilley [2]	No	No	No	No	No	No	Yes
Catalan *et al.* [38]	Yes	Yes	No	No	No	No	Yes
Marvan *et al.* [23]	No	Yes	Yes	No	No	No	No
Bratkovsky, and Levanyuk [32]	No	Yes	Yes	No	No	No	Yes
Ban *et al.* [33], Zhong *et al.* [34]	No	Yes	No	No	No	No	No
Karthik *et al.* [39]	Yes	Yes	No	No	No	No	No
Morozovska *et al.* [40]	No	Yes	No	Yes	No	Yes	No
Morozovska *et al.* [20]	Yes	Yes	No	Yes	No	No	Yes
Morozovska *et al.* [35]	Yes	Yes	No	Yes	No	No	Yes
Vorotiahin *et al.* [36]	Yes	No	No	No	No	No	Yes
Vorotiahin *et al.* [37]	Yes	No	No	No	No	Yes	Yes
This work	Yes	Yes	Yes	Yes	Yes	Yes	Yes

the term proportional to the average polarization, similar to the one proposed earlier by Kretschmer and Binder [25]. In the subsequent papers, they applied the same method to the ferroelectric films with domains [26,27]. Note that the approximation for the depolarization field being undoubtedly useful for derivation of analytical results in a single-domain case, becomes questionable in a poly-domain case. For the rigorous consideration of domains appearance one should solve numerically the coupled problem containing the Poisson equation for the electric field and a nonlinear equation for polarization dependence on the field [23]. The coupled problem is typically solved by a self-consistent phase field method allowing modeling of very complex domain structures such as flux-closure domains [28] and domain vortexes [29–31] in thin ferroelectric films and superlattices.

Bratkovsky and Levanyuk [32] theoretically studied the smearing of phase transition due to a surface effect or a bulk inhomogeneity in single-domain ferroelectric nanostructures. Ban *et al.* [33] and Zhong *et al.* [34] established the theoretical fundamentals of the piezoelectric and polar responses of graded ferroic materials. Morozovska *et al.* [35] studied theoretically the domain wall interaction with elastic defects in uniaxial ferroelectrics. The papers [23–35] considered chemical composition gradient only and ignored flexocoupling. Other authors considered only the impact of flexocoupling on the thermodynamics and kinetics of polarization reversal in thin ferroelectric films (see, e.g., Vorotiahin *et al.* [36,37]).

Remarkably the separate theoretical consideration of the flexoelectric coupling and inhomogeneous strains in thin ferroelectric films leads to results, which can be oversimplified for realistic applications, because flexocoupling is omnipresent and its relative contribution significantly increases with the film thickness decrease [13]. However, there are only a few theoretical studies considering both flexoelectric and chemical composition gradient effects, all of which are some particular cases [see Table I]. For instance, Catalan *et al.* [38] studied the effect of flexoelectricity on the polar and dielectric properties of inhomogeneously strained ferroelectric thin films. Karthik *et al.* [39] revealed giant built-in electric fields due to flexoelectricity in compositionally graded ferroelectric thin films. Morozovska *et al.* [40] studied the flexocoupling impact on size effects of piezoresponse and conductance in mixed-type ferroelectric semiconductors.

Notably the studies [20,21,38–40] analyze flexoelectric and compositional effects in linear approximation, and, the most important, the appearance of domains due to spatial inhomogeneities has not been considered [see the column "Domain formation" in Table I]. However, one can regard that even a tiny inhomogeneity leads to the splitting of the system into domains. This result was obtained by Bratkovsky and Levanyuk [41], who performed an analytical study of stability loss and evolution of domain structure in inhomogeneous ferroelectric (or ferroelastic) samples.

It is well-established that the spatial heterogeneity and incomplete screening of spontaneous polarization significantly influence domain structures in epitaxial thin films (see, e.g., the monograph by Tagansev *et al.* [42] and the recent review by Roytburd *et al.* [43] of theoretical approaches, phase field modeling and experimental studies of domain structures in epitaxial films). A classical result was obtained by Bratkovsky and Levanyuk [44], who studied theoretically the dielectric response of ferroelectric thin films with a "dead" dielectric layer at the interfaces with electrodes and obtained that the domain structure inevitably forms in a film in the presence of a dead layer.

While paying tribute to the previous theoretical results [20–40], the influence of incomplete screening, combined flexochemical and size effects on domain structures, polar, elastic, and electrophysical properties of thin ferroelectric films have not been considered so far in a self-consistent way. The main objective of our work is to propose a self-consistent approach describing the impact of the defect-driven flexochemical coupling on the film properties, domain structure evolution and size effects and analyze the outcomes towards optimization of the properties for advanced applications.

II. STATEMENT OF THE PROBLEM

The Landau-Ginzburg-Devonshire (LGD) expansion of bulk (G_V) and surface (G_S) parts of the Gibbs free energy of a ferroelectric film in powers of the polarization vector and stress tensor components P_i and σ_{ij} and the energy of the electric field outside the film (G_{ext}) have the form:

$$G = G_V + G_S + G_{\text{ext}}, \tag{1a}$$

$$G_V = \int_{V_{\text{FE}}} d^3r \left(\begin{array}{l} \frac{a_{ik}}{2} P_i P_k + \frac{a_{ijkl}}{4} P_i P_j P_k P_l + \frac{a_{ijklmn}}{6} P_i P_j P_k P_l P_m P_n + \frac{g_{ijkl}}{2} \left(\frac{\partial P_i}{\partial x_j} \frac{\partial P_k}{\partial x_l} \right) - P_i E_i \\ - \frac{\varepsilon_0 \varepsilon_b}{2} E_i E_i - \frac{s_{ijkl}}{2} \sigma_{ij} \sigma_{kl} - Q_{ijkl} \sigma_{ij} P_k P_l - F_{ijkl} \left(\sigma_{ij} \frac{\partial P_l}{\partial x_k} - P_l \frac{\partial \sigma_{ij}}{\partial x_k} \right) - W_{ij} \sigma_{ij} \delta N \end{array} \right), \tag{1b}$$

$$G_S = \int_S d^2r \left(\frac{a_{ij}^S}{2} P_i P_j - \frac{\varepsilon_0}{2\lambda} \varphi^2 \right), \quad G_{\text{ext}} = - \int_{\vec{r} \notin V_{\text{FE}}} d^3r \frac{\varepsilon_0 \varepsilon_e}{2} E_i E_i. \tag{1c}$$

The tensor a_{ij} is positively defined for linear dielectrics, and explicitly depends on temperature T for ferroelectrics and paraelectrics. Below we use an isotropic approximation for the tensor coefficients $a_{ij} = \alpha_T (T - T_c) \delta_{ij}$, where δ_{ij} is the Kroneker δ symbol, T is absolute temperature, and T_c is the Curie temperature. All other tensors included in the free-energy Eq. (1) are supposed to be temperature independent. Tensor a_{ijklmn} should be positively defined for the thermodynamic stability in paraelectrics and ferroelectrics. Tensor g_{ijkl} determines the magnitude of the gradient energy and is also regarded positively defined. ε_0 is the vacuum permittivity, ε_b is a relative background dielectric permittivity [45]. Coefficients Q_{ijkl} are the components of electrostriction tensor, s_{ijkl} are the components of elastic compliance tensor, F_{ijkl} is the flexoelectric strain coupling tensor. For most of the cases one can neglect the polarization relaxation and omit high order elastic strain gradient terms if the flexoelectric coefficients are below the critical values F_{ijkl}^{cr} [46,47]. W_{ij} is the elastic dipole (or Vegard strain) tensor, that is regarded diagonal hereinafter, i.e., $W_{ij} = W \delta_{ij}$. The quantity $\delta N = N(\vec{r}) - N_e$ is the difference between the concentration of defects N at the point $\mathbf{r}$ and their equilibrium (average) concentration N_e.

In the surface energy Eq. (1c), the tensor a_{ij}^S and the effective surface screening length λ are introduced [37,48]. In the isotropic approximation, $a_{ij}^S = \alpha_S \delta_{ij}$, used hereinafter, the constant α_S is related with a conventional extrapolation length Λ [2,25] as $\Lambda = g_{11}/\alpha_S$. Concerning the physical origin of λ, we regarded that the top surface of the film is covered with the surface screening charge of the specific nature, e.g., Bardeen-type surface states [49] and so λ can be associated with a Bardeen screening length. For the case the screening charges can be localized at surface states caused by the strong band-bending via depolarization field [50–54], at that the value of λ can be much smaller ($\leqslant 0.1$ nm) than a lattice constant ($\sim$0.5 nm) [55].

Also, we introduce electric field via electrostatic potential φ as $E_i = -\partial \varphi / \partial x_i$. Polarization is conjugated to the electric field E_i which can include external and depolarization contributions (if any exists).

Note that we neglected the higher elastic gradient term $\frac{1}{2} \upsilon_{ijklmn} (\partial \sigma_{ij}/\partial x_m)(\partial \sigma_{kl}/\partial x_n)$ in the functional Eq. (1b), because its magnitude and sign are still disputed [56]. Thus, we apply in the following only one half ($F_{ijkl} P_k (\partial \sigma_{ij}/\partial x_l)$) of the full Lifshitz invariant $F_{ijkl}(P_k(\partial \sigma_{ij}/\partial x_l) - \sigma_{ij}(\partial P_k/\partial x_l))/2$. The higher elastic gradient term is necessary for the stability of the thermodynamic potential if the full Lifshitz invariant is included. Application of either the term $F_{ijkl} P_k (\partial \sigma_{ij}/\partial x_l)$ or the term $F_{ijkl}(P_k(\partial \sigma_{ij}/\partial x_l) - \sigma_{ij}(\partial P_k/\partial x_l))/2$ results in the same equations of state. The full form, however, affects the boundary conditions [57–60]. The reason of using only the part of the Lifshitz invariant in Eq. (1) is that implementation of the full form causes poor convergence of the numerical code and impairs the quality and reliability of the obtained results. Using the truncated form in Eq. (1) can be justified by the smallness of the flexoelectric coupling strength as compared to the polarization gradient term. Thus, following Refs. [47,61,62] we assume that the used approximation is valid if $F_{klmn}^2 \ll g_{ijkl} s_{ijmn}$.

Polarization distribution can be found from the Euler-Lagrange equations obtained after variation of the free-energy Eq. (1):

$$a_{ik} P_k + a_{ijkl} P_j P_k P_l + a_{ijklmn} P_j P_k P_l P_m P_n - g_{ijkl} \frac{\partial^2 P_k}{\partial x_j \partial x_l} - Q_{ijkl} \sigma_{kl} P_j + F_{ijkl} \frac{\partial \sigma_{kl}}{\partial x_j} = E_i, \tag{2a}$$

along with the boundary conditions on the top surface of the film S at $x_3 = h$:

$$\left(g_{kjim} n_k \frac{\partial P_m}{\partial x_j} + a_{ij}^S P_j - F_{jkim} \sigma_{jk} n_m \right) \Big|_{x_3 = h} = 0. \tag{2b}$$

The most evident consequences of the flexocoupling are the inhomogeneous terms in the boundary conditions Eq. (2b).

Elastic stress tensor satisfies the mechanical equilibrium equation $\partial \sigma_{ij}/\partial x_j = 0$; elastic strains are $u_{ij} = -\delta G_V / \delta \sigma_{ij}$, resulting in

$$u_{ij} = s_{ijkl} \sigma_{kl} + Q_{ijkl} P_k P_l + F_{ijkl} \frac{\partial P_l}{\partial x_k} + W_{ij} \delta N. \tag{2c}$$

The boundary conditions at the mechanically free surface $x_3 = h$ can be obtained from the variation of the free-energy Eq. (1) with respect to the stresses:

$$\sigma_{ij} n_j |_S = 0. \tag{3a}$$

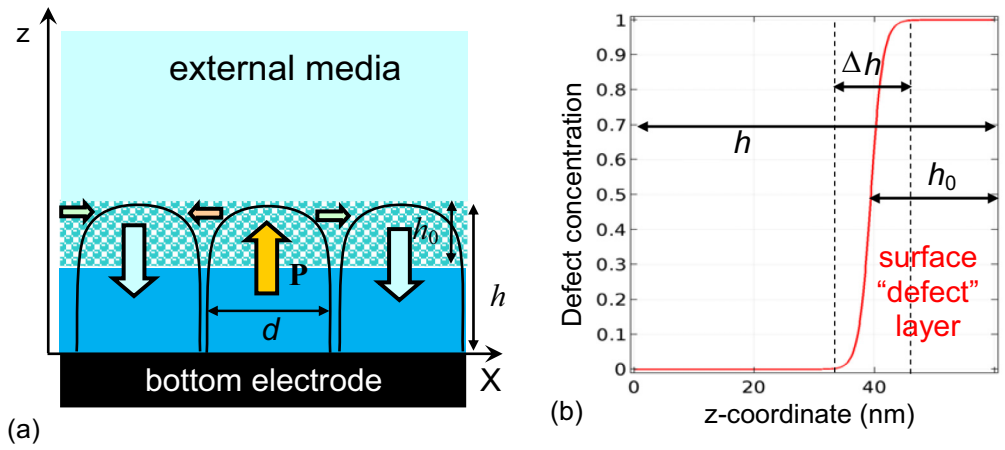

FIG. 1. (a) Scheme of a film with the thickness h and the layer of thickness h_0 where defects are accumulated. (b) Normalized concentration of defects inside the layer of thickness h_0 and transition layer depth Δh. Thick arrows point the direction of polarization z component and thin arrows point the direction of in-plane polarization components in the region of closure domains.

Here, n_j are components of the external normal to the film surface. Misfit strain u_m existing at the film-substrate interface ($x_3 = 0$) leads to the boundary conditions for mechanical displacement components U_i related to elastic strain as $u_{ij} = (\partial U_i/\partial x_j + \partial U_j/\partial x_i)/2$:

$$(U_1 - x_1 u_m)|_{x_3=0} = 0,\ U_3|_{x_3=0} = 0. \tag{3b}$$

The periodic conditions were imposed at the lateral sides, $U_1|_{x_1=-w/2} - U_1|_{x_1=w/2} = wu_m$, while the period w should be defined self-consistently.

The electric field $\mathbf{E}$ (being the sum of an external $\mathbf{E}^{\text{ext}}$ and a depolarization one $\mathbf{E}^d$) is determined self-consistently from the electrostatic problem for the electric potential φ,

$$\varepsilon_0\varepsilon_b \frac{\partial^2\varphi}{\partial x_i \partial x_i} = -\frac{\partial P_j}{\partial x_j}, \tag{4}$$

supplemented by the condition of potential continuity at the top surface of the film, $z - h$, using hereinafter also notations $x_1 \equiv x$, $x_2 \equiv y$, $x_3 \equiv z$. The difference of electric displacement components $D_n^{(i)} - D_n^{(e)}$ is conditioned by the surface screening produced by the ambient free charges at the film surface S:

$$(\phi^{(e)} - \varphi^{(i)})|_{x_3=h} = 0,\ \left(D_n^{(e)} - D_n^{(i)} + \varepsilon_0\frac{\varphi}{\lambda}\right)\Big|_{x_3=h} = 0. \tag{5}$$

Here, $\mathbf{n}$ is the outer normal to the film surface, electric displacement $\mathbf{D} = \varepsilon_0\varepsilon_b\mathbf{E} + \mathbf{P}$, the subscript "$i$" means the physical quantity inside the film, and "e" means outside the film. The conditions of zero potentials were imposed at the bottom electrode ($z = 0$) and a remote top electrode ($z = H + h$, $H \to \infty$), respectively [63] (see Fig. 1).

Note, that in the case of almost homogeneous polarization (or distributed along z-axis only) the internal electric field calculated on the basis of Eqs. (4) and (5) could be easily reduced to the well-known expressions, containing the difference of the polarization and its average, $-(P_3 - \bar{P}_3)$ (see, e.g., Refs [25,64,65].). However, in the case of pronounced domain structure the average polarization is zero and the internal electric field is usually localized in space, in contrast to the suppositions of some approximate models, used earlier (see, e.g., Refs. [26,27]).

Note that one can associate the elastic defects in Eq. (1b) with "random temperature" defects in some sense, but we do not use this terminology, because a classical random temperature defect only renormalizes the local Curie temperature, while the elastic defects we consider are incorporated in the elastic Eq. (2c) as well as in the mechanical equilibrium equation $\partial\sigma_{ij}/\partial x_j = 0$. Thus, the Vegard stresses and strains become coupled with flexoelecricity, leading to the appearance of the term dependent on δN in Eq. (2b) that originates from the term $F_{ijkl}\frac{\partial\sigma_{kl}}{\partial x_j}$. The defects also act as random temperature defects by renormalizing Curie temperature via electrostrictive coupling.

Further we suppose that most of defects are located in a thin top layer of thickness h_0 beyond which their concentration decreases exponentially towards the film bulk [66] (see Fig. 1):

$$\delta N(z) \approx \frac{N_0}{1 + \exp\left[-(z - h + h_0)/\Delta h\right]}. \tag{6}$$

We suppose that the interstitial point defects with maximal concentration $\sim 10^{26}\,\text{m}^{-3}$ [see Table I] can be introduced by inhomogeneous doping or implantation the PTO film with light ions, such as protons or Li, or oxygen vacancies, which may become electrically neutral inside the film due to the charge compensation by electronic carriers. It can either be "heavy" ions such as La or Bi. Also, standard chemical doping may introduce neutral lattice defects like Zr substitutions on Ti sites or Ca, Cu, Co, and Zn substitutions on Pb sites as first-principle-based calculations show [67]. A promising candidate for neutral chemical doping is Ba^{2+} substituting Pb^{2+} (see, e.g., Ref. [68]). This substitution has larger ionic radius (135 pm against 119 pm of Pb^{2+}), and thus $W > 0$. Experimentally it was proven to be possible at least in lead zirconate titanate; see Refs. [69] and [70]. All other mentioned substitutions have smaller radii than Pb^{2+} and likely provide $W < 0$. In fact, the maximal molar concentration of defects in our calculations does not exceed 1–2% (one defect per 50 unit cells or less), at that the volume of the cubic PTO unit cell is about $64 \times 10^{-30}\,\text{m}^3$. Such concentrations of

TABLE II. Description, dimension, and numerical values of material parameters.

Description	Symbol and dimension	Numerical value for $PbTiO_3$
Coefficient at P^2	$\alpha(T)(\times C^{-2}\,\mathrm{m\,J})$	$\alpha_T(T-T_C)$
Inverse Curie-Weiss constant	α_T $(\times 10^5\,\mathrm{C^{-2}\,m\,J/K})$	3.8
Curie temperature	T_C (K)	752
Background permittivity	ε_b	7
Surface energy coefficient	α_{S0} $(\times \mathrm{C^{-2}\,J})$	0
Electrostriction coefficient	Q_{ij} $(\times \mathrm{m^4/C^2})$	$Q_{11}=+0.89$, $Q_{12}=-0.026$, $Q_{44}=0.0675$
Elastic stiffness tensor	c_{ij} $(\times 10^{10}\,\mathrm{Pa})$	$c_{11}=17$, $c_{12}=8$, $c_{44}=11$
Elastic compliance tensor	s_{ij} $(\times 10^{-12}\,\mathrm{1/Pa})$	$s_{11}=8$, $s_{12}=-2.5$, $s_{44}=9$
Gradient coefficient	g_{ij} $(\times 10^{-10}\,\mathrm{C^{-2}\,m^3\,J})$	$g_{11}=4.0$, $g_{12}=-0.5$, $g_{44}=0.5$,
Flexoelectric stress tensor	f_{ij} (V)	$f_{11}=6.8$, $f_{12}=4.9$, $f_{44}=5.6$
Flexoelectric strain tensor	F_{ij} $(\times 10^{-11}\,\mathrm{m^3/C})$	F11 = 3, F12 = 1, F44 = 5[a]
Kinetic coefficient	Γ $(\times \mathrm{s\,m/F})$	100
LGD-coefficient at P^4	a_{11} $(\times 10^8\,\mathrm{JC^{-4}\,m^5})$	−0.73
LGD-coefficient at P^6	a_{111} $(\times 10^8\,\mathrm{JC^{-6}\,m^9})$	+2.60
Surface screening length	λ $(\times 10^{-10}\,\mathrm{m})$	1 (or vary within the range)
Vegard strain coefficient	W $(\times 10^{-30}\,\mathrm{m})$	± 10[b]
Misfit strain	u_m (%)	−1
Maximal defect concentration	N_0 $(\times 10^{26}\,\mathrm{m^{-3}})$	(0–3)
Defect layer thickness	h_0 (nm)	25
Transition layer depth	Δh (nm)	1

[a]The coefficients F_{ij} are still not available experimentally for PTO, but some components could be evaluated from the first principles for various perovskites [75–77] and their thin films [78]. On the other hand, the magnitudes of $F_{11}=3$, $F_{12}=1$ and $F_{44}=0.5$ (in $10^{-11}\,\mathrm{C^{-1}\,m^3}$ units) are of the same order as the microscopic estimations ($F\sim 10^{-11}\,\mathrm{m^3/C}$) by Kogan, and the values measured for $SrTiO_3$ by Zubko *et al.* [79,80]. The value $F_{44}=5\times 10^{-11}\,\mathrm{C^{-1}m^3}$ is higher than a conventional one, but its effect is only relevant for fine details of polarization and elastic field distributions close to the bottom electrode. We note also that all values we used are significantly smaller than the ones ($F\sim(5\text{–}10)10^{-10}\,\mathrm{m^3/C}$) measured for $PbZrTiO_3$ by Ma and Cross [81].

[b]The chosen values of Vegard coefficient, $W=\pm 10$ A are in agreement with *ab initio* calculations for perovskite $SrTiO_3$ [14] as well as with typical experimental values [16,17].

doping are quite realistic, for instance, doping with 0.5% and 1.0 mol% of Li of perovskite $Ca_xPb_{1-x}TiO_3$ was reported by Liu Jingbo *et al.* [71]. Perovskite $SrZrO_3$ doped with 0.3 mol% of protons was studied by Slodczyk *et al.* [72]. La doping up to 0.44 mol % of $PbTiO_3$ single crystal was reported by Wójcik [73]. Piezoelectric properties of PTO ceramics doped up to 5 mol% of Bi was studied by Ueda and Ikegami [74]. The defect layer can be also formed by, e.g., oxygen partial pressure conditioning during the film preparation; see, e.g., Refs. [3,5].

III. RESULTS AND DISCUSSION

Using COMSOL Multiphysics package we calculated ferroelectric polarization, electric fields, and elastic properties from Eqs. (2)–(5) for exemplarily chosen film thickness, temperature, misfit strain, the defect distribution given by Eq. (6) and $PbTiO_3$ (PTO) ferroelectric parameters listed in Table II. Results of FEM calculations are shown in Figs. 2–7.

A. Polarization, domain structure, and elastic field dependence on the sign of Vegard coefficient

Note that in most cases, a stable polydomain structure with prevailing out-of-plane polarization has been found for an applied negative misfit strain $u_m=-1\%$ and $\lambda>0.1$ nm [37], which support the out-of-plane polarization component [8] and a polydomain structures. The appearance of the closure domains [42] under the electrically open film surface depends strongly on the degree of screening, represented by the values of the surface screening length λ and temperature [37].

To illustrate the above-mentioned issues, Fig. 2 shows the spatial distributions of the in-plane and out-of-plane polarization components, P_x and P_z, respectively, corresponding elastic strains u_{xx} and u_{zz}, and von Mises stress [82],

$$\sigma_v=\sqrt{(\sigma_{xx}-\sigma_{yy})^2+(\sigma_{yy}-\sigma_{zz})^2+(\sigma_{zz}-\sigma_{xx})^2+6\sigma_{yz}^2+6\sigma_{zx}^2+6\sigma_{xy}^2}, \tag{7}$$

in the cross-section of a 50-nm-thick PTO film. The top and bottom rows are calculated for positive and negative Vegard coefficients, $W=+10$ Å and $W=-10$ Å, respectively. At elevated temperature $T=600$ K, which, however, is sufficiently far from the film's transition temperature to the paraelectric phase, shallow (up to 5 nm) closure a-domains appear near the electrically open surface. They have a form of rounded wedges and relatively diffuse domain walls [see Figs. 2(a) and 2(f) showing P_x distribution]. There are clearly visible stripe c-domains with relatively sharp domain walls in the

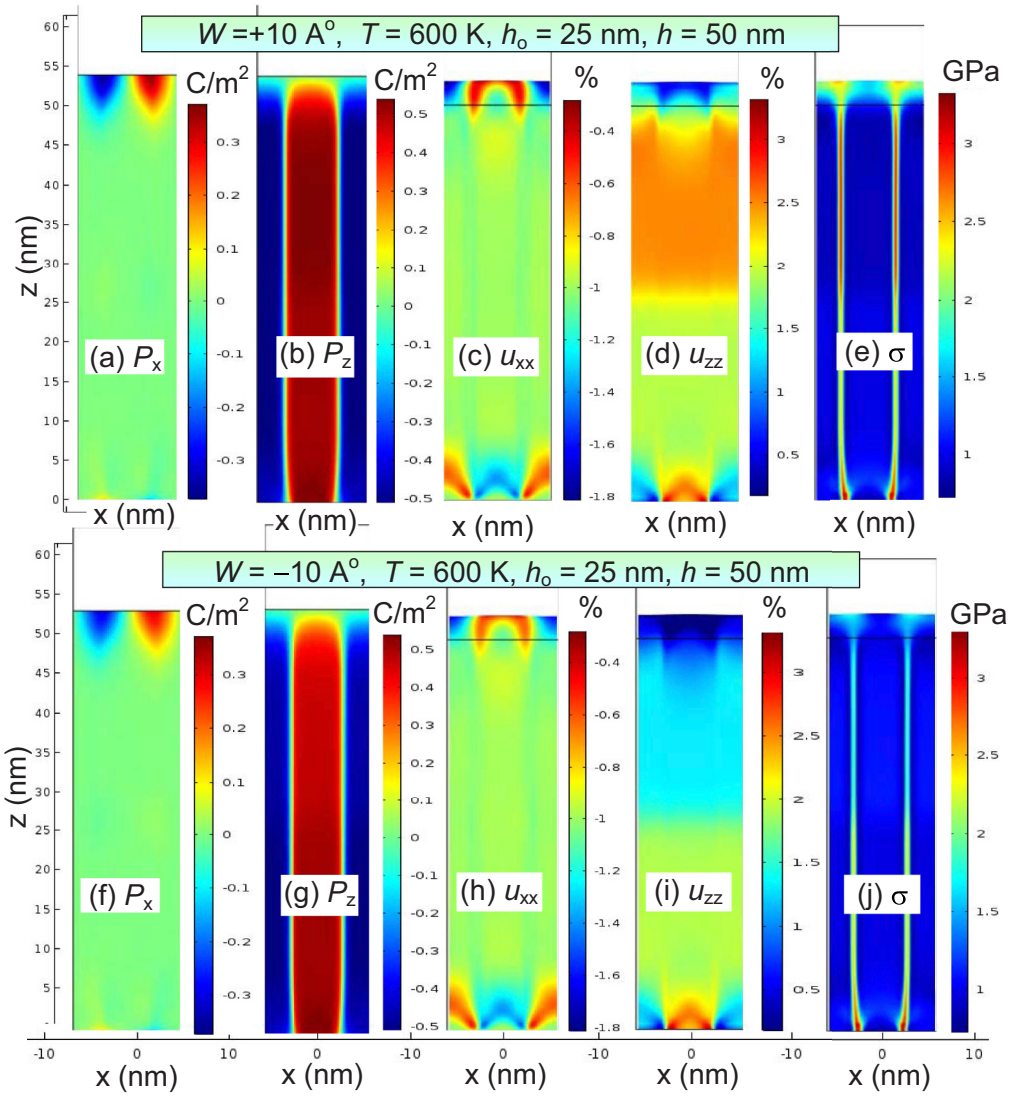

FIG. 2. Spatial distribution of the in-plane polarization component P_x (a), (f) and the out-of-plane component P_z (b), (g), elastic strains u_{xx} (c), (h) and u_{zz} (d), (i), and von Mises stress σ (e), (j) in the cross-section of the 50-nm PTO film calculated for positive [top row, plots (a)–(e)] and negative [bottom row, plots (f)–(j)] Vegard coefficients $W = \pm 10$ Å, temperature $T = 600$ K, screening length $\lambda = 0.1$ nm, depth of defect layer $h_0 = 25$ nm, $\Delta h = 1$ nm, and defect concentration $N_0 = 3 \times 10^{26}$ m^{-3}. Other parameters are listed in Table II.

middle of the film and near the bottom screening electrode for the normal component of the polarization. The stripe domain walls noticeably broaden and diffuse to the depth of about 5 nm near the top surface [see Figs. 2(b) and 2(g) showing P_z distribution]. The polarization in the middle of the closure and stripe domains is significantly larger for the Vegard coefficient $W = +10$ Å than it is for $W = -10$ Å, but all other characteristics of a- and c-domains depend weakly on the value of W [compare Figs. 2(a) and 2(f), Figs. 2(b) and 2(g)]. A 25-nm layer of elastic defects, the domain structure, and the misfit strain at the film-substrate interface determine the structure and spatial distribution of the elastic strain tensor in the film, whose diagonal components u_{xx} and u_{zz} are shown in Figs. 2(c), 2(d) and 2(h), 2(i), respectively**.** The main features on the lateral strain distribution are caused by the domain structure via the piezoelectric and flexoelectric effects, and so the distribution of u_{xx} is virtually independent on the sign of W [compare Figs. 2(c) and 2(h)]. The main features of the vertical strain distribution are conditioned not only by the domain structure, but also by an elastic field gradient in the defect layer. That is why a diffuse horizontal boundary is clearly visible on the edge of the defect layer in Figs. 2(d) and 2(i). The vertical strain in this layer is determined by a chemical pressure of defects and thus it changes sign when the sign of W is changed [compare Figs. 2(d) and 2(i)]. The distribution of von Mises dilatational stress σ reproduces the profile of the out-of-plane polarization component, namely, a stripe domain structure with broadened domain walls near the surface, while the value of σ, in a near-surface layer with a thickness of the order of 5 nm, is strongly dependent on the sign of W [see Figs. 2(e) and 2(j)]. We note that the pronounced features of the distributions of u_{xx}, u_{zz}, and σ near the bottom electrode do not depend on the sign of W, since they arise from the flexoelectric coupling.

Note that the value of the screening length λ strongly affects the polar properties of the film, determines its critical thickness at fixed temperature and the existence as well as the

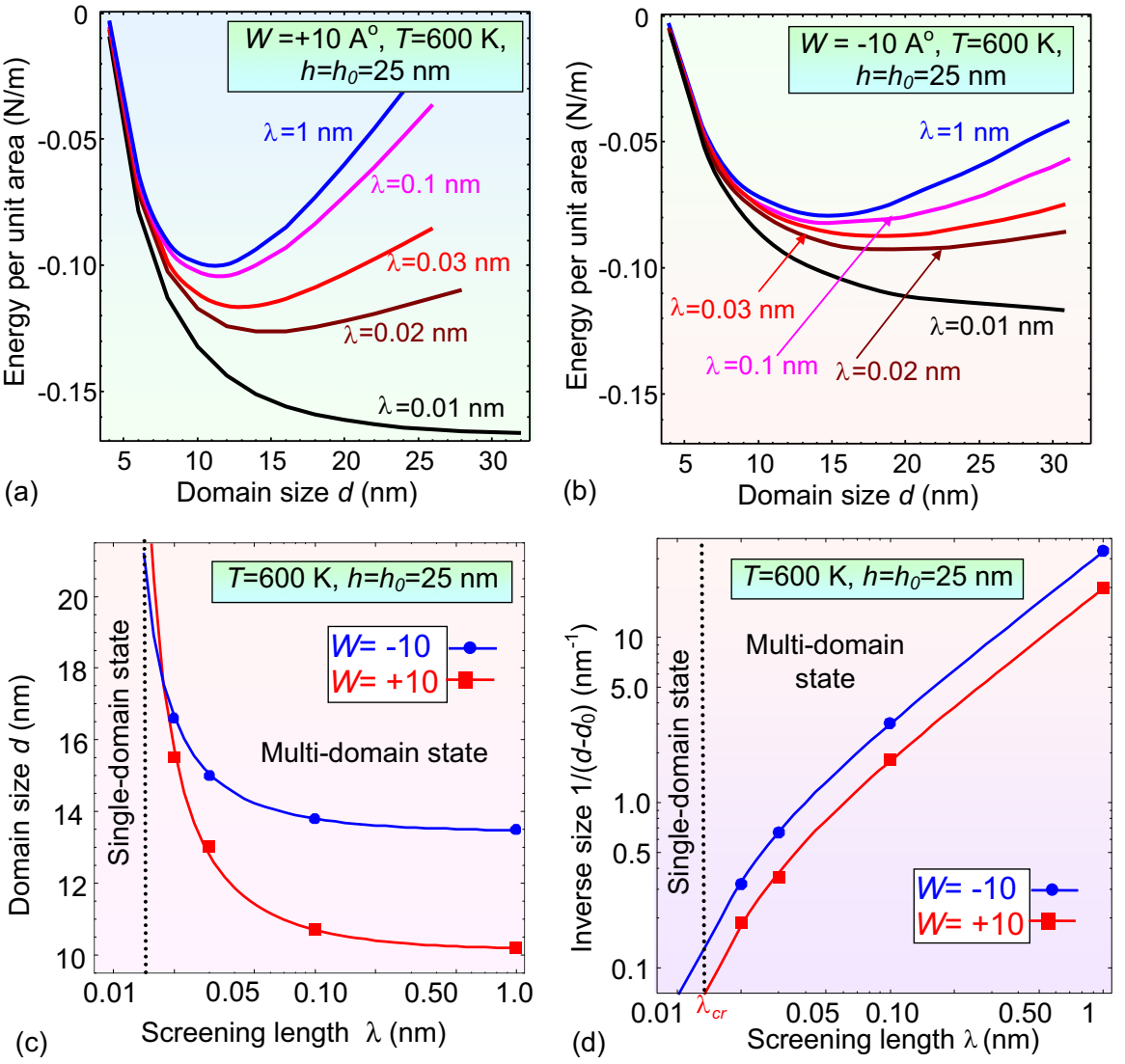

FIG. 3. (a) The dependence of the 25-nm-thick $PbTiO_3$ film total energy on the domain size (potential relief of wall-wall interaction) calculated for different values of surface screening length λ (shown near the curves), positive Vegard coefficient $W = +10$ Å (a) and negative Vegard coefficient $W = -10$ Å (b). Dependences of the equilibrium domain size d (c) and inverse value $1/(d - d_0)$ (d) on the surface screening length λ calculated numerically for $W = -10$ Å (circles) and $W = +10$ Å (squares). Solid curves are fitting to the formula $d = d_0 + \frac{D}{\lambda - \lambda_{cr}}$, where $d_0 = 13.5$ nm, $D = 0.03\,\text{nm}^2$, $\lambda_{cr} = 0.010$ nm for $W = -10$ Å; and $d_0 = 10.2$ nm, $D = 0.05\,\text{nm}^2$, and $\lambda_{cr} = 0.011$ nm for $W = +10$ Å. Temperature $T = 600$ K and defect concentration $N_0 = 3 \times 10^{26}\,\text{m}^{-3}$. Other parameters are listed in Table II.

type of the domain structure [37]. In addition, a pronounced minimum at a certain width, which depends on W, temperature and the film thickness, appears on the dependence of the system specific energy E on the domain lateral size d when λ increases [see Fig. 3]. The decreasing dependence $E(d)$ is steeper, and the minimum on it is much deeper for positive $W = +10$ Å than for negative $W = -10$ Å [compare Figs. 3(a) and 3(b)].

Notably, the expected Kittel-Mitsui-Furuichi (KMF) relation connecting the period d of the stripe domain structure, having infinitely thin walls, with the film thickness h, $d \sim \sqrt{h}$, is not confirmed in our calculations, since they naturally account for domain wall broadening near electrically open surfaces (via the polarization gradient [83]) and closure domains (via polarization rotation) [40]. Moreover, our results are λ- and W-dependent. To illustrate this, Fig. 3(c) shows the dependences of the equilibrium domain size d on the screening length λ. The dependence on the domain size on λ obeys an analytical formula, $d = d_0 + \frac{D}{\lambda - \lambda_{cr}}$ [see Fig. 3(d) showing the dependence of inverse value $1/(d - d_0)$ on λ], where the critical values λ_{cr} slightly differ for $W = +10$ Å and $W = -10$ Å, while the parameters d_0 and D depend on the W sign much more strongly (see caption to Fig. 3).

Notably the limit of "ideal metal" corresponds to $\lambda = 0$, while it was shown earlier that there is a finite non-zero value of λ below which the polydomain film transforms into monodomain state (see, e.g., Ref. [84] for uniaxial ferroelectric, when closure domains are absent, and Ref. [37] for multiaxial ferroelectrics).

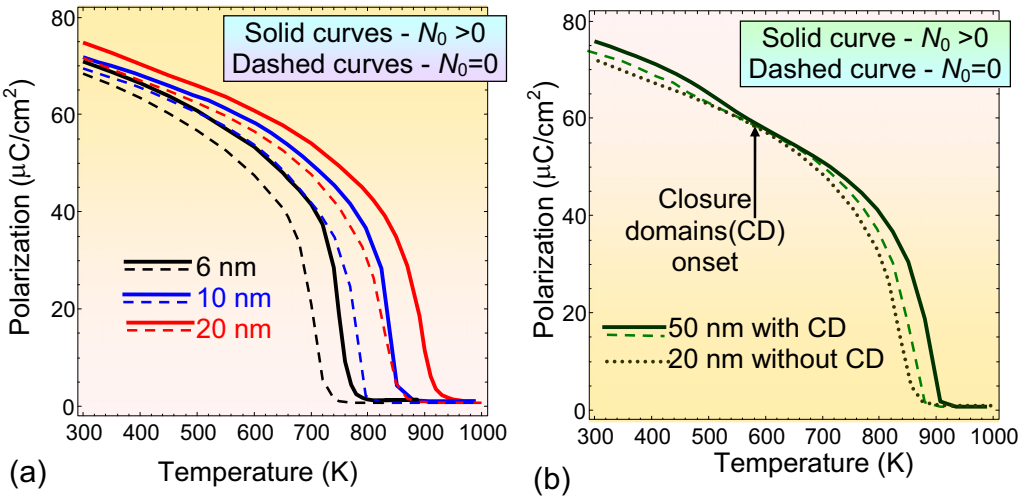

FIG. 4. Temperature dependence of the maximal spontaneous polarization calculated for different film thicknesses $h = (6,\ 10,\ 20)$ nm [plot (a)] and $h = (20,\ 50)$ nm [plot (b)], without defects ($N_0 = 0$, dashed curves) and with defect concentration $N_0 = 2 \times 10^{26}\,\mathrm{m}^{-3}$ and Vegard coefficient $W = +10$ Å, screening length $\lambda = 0.1$ nm. Other parameters are listed in Table II. The inflections at the curves for 50-nm-thick film indicate the appearance of the closure domains (CD) at temperatures lower than 550 K.

B. Temperature evolution of spontaneous polarization, domain structure, and elastic fields

Figure 4 shows the temperature dependencies of the maximum spontaneous polarization P_S at the center of the stripe domains, calculated for films of different thicknesses (6–50 nm) with a layer of elastic defects (solid curves) and without it (dashed curves). Note that the presence of defects noticeably enhances the value of switchable polarization $2P_S$ (dashed curves are always lower than solid ones) in PTO films with thickness less than 50 nm, but due to the stripe domain structure the average polarization is zero without applied electric field. Due to defects, corresponding switchable bound charge $\sigma_S = 2P_S$ increases significantly (up to 40–80 μC/cm^2) in the vicinity of phase transition temperature that varies in the range 750–950 K depending on the film thickness [compare the onset of solid and dashed curves in Fig. 4(a)]. At room temperature the increase of σ_S induced by defects is much smaller ($\sim$5 μC/cm^2).

Moreover, the temperature of the spontaneous polarization and domain structure appearance in a film with defects is much larger (by 50–70 K), than for films without them, and the polarization itself is somewhat larger for thin films with a thickness less than 25 nm, for which the defect layer occupies the whole film and the Vegard effect is positive ($W = +10$ Å) [compare solid and dashed curves in Fig. 4(a)]. When increasing the film thickness to 50 nm (with a thickness of the defect layer 25 nm), the temperature of the spontaneous polarization emergence becomes 20 K higher than the ferroelectric transition temperature of a 50-nm film without defects [compare solid and dashed curves in Fig. 4(b)]. Notably, the bending appears on the temperature dependence of the maximum polarization at the temperature 550 K, being related with the emergence of closure domains at lower temperatures. The temperature of polarization emergence decreases at negative $W = -10$ Å (this case is not shown in the figures, since we are primarily interested in the conditions of polar properties enhancement).

Spatial distributions of in-plane and out-of-plane polarization components and corresponding elastic strains in the cross-section of the 60-nm-thick PTO film calculated for positive Vegard coefficients $W = +10$ Å, elevated (850 K) and room (300 K) temperatures are shown in Fig. 5. It is evident that the closure domains, as well as a pronounced stripe domain structure, are absent at high temperatures near the phase transition of the film into the paraelectric phase [compare Figs. 5(a)–5(d) and 5(e)–5(h)]. On the contrary, small domains, which branch near the surface of the film, appear at 850 K. They gradually "freeze" and transform to stripe domain structure with closure domains as the temperature decreases.

C. Ferroelectric transition temperature dependence on the film thickness

Figure 6 shows the dependence of the ferroelectric transition temperature $T_C(h)$ on the film thickness h [Fig. 6(a)] and its inverse value $1/h$ [Fig. 6(b)], calculated for the positive, zero and negative Vegard coefficients W. At $W > 0$ the maximum appears on the dependence at a film thickness of 25 nm, virtually equal to the thickness of the defect layer h_0 [see red curve in Fig. 6(a)]. Temperature $T_C(h)$ decreases monotonically with decreasing h at $W \leqslant 0$. Notably, the inequality $T_C(h, W < 0) < T_C(h, W = 0) < T_C(h, W > 0)$ is valid for thicknesses more than 4 nm [compare red, magenta, and blue curves in Fig. 6(a)]. At a film thickness of about 3.5 nm, all three curves intersect, and the order of the curves corresponding to $W > 0$ and $W < 0$ changes with the further decrease of the film thickness. A maximum and a kink on dependencies $T_C(h)$ are observed at $h = h_0$, for positive and negative W, respectively [see red and blue curves in Fig. 6(a)].

From Fig. 6(a) we can see, that the critical thickness of the film below which the ferroelectric phase vanishes is absent for all W. It is true even until 2-nm thickness (that is about 5 lattice constants) for which the continual theory of LGD is still applicable at least qualitatively. Somewhat overstretching the LGD approach one can observe in Fig. 6(b) that T_C does not

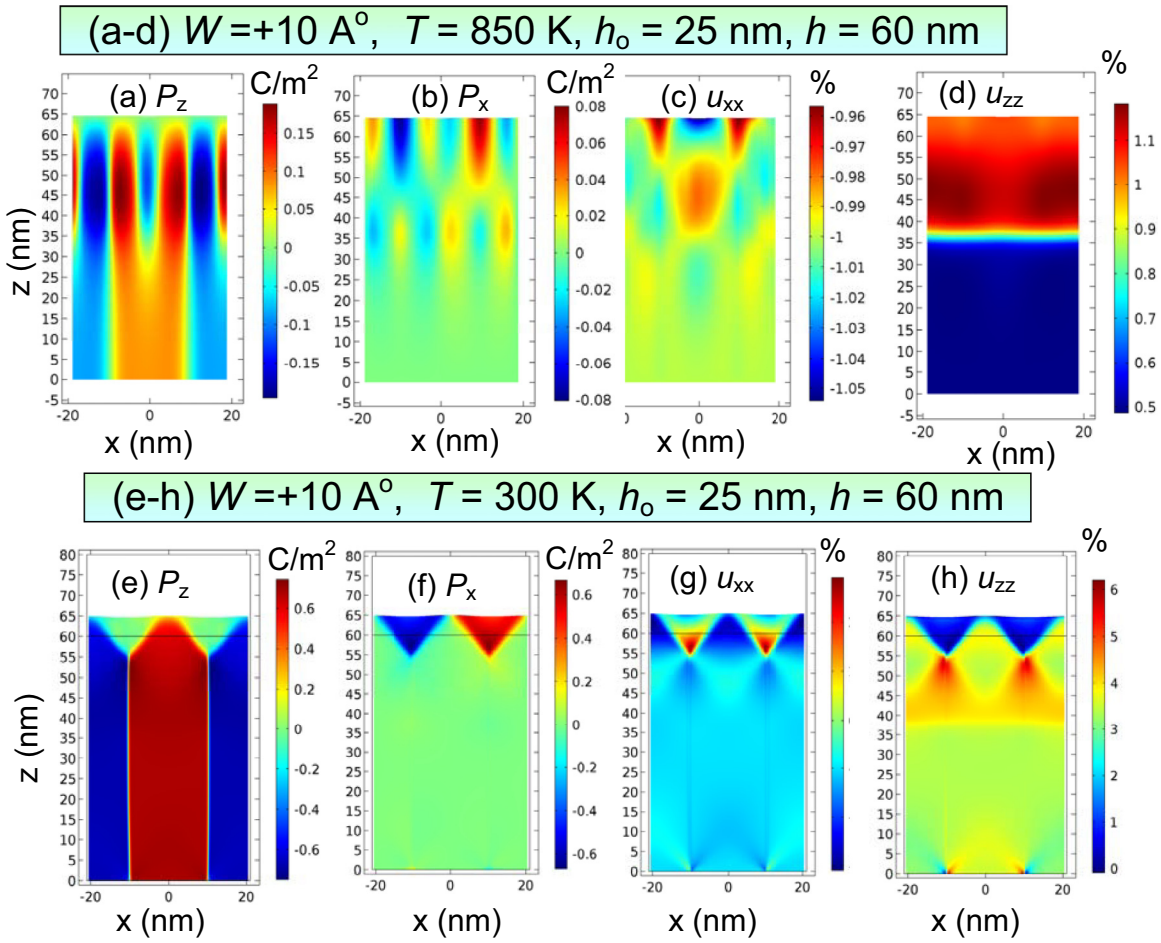

FIG. 5. Spatial distributions of polarization components P_z (a), (e) and P_x (b), (f), elastic strains u_{xx} (c), (g), and u_{zz} (d), (h) in the cross-section of the 60-nm-thick PTO film calculated for positive Vegard coefficients $W = +10$ Å, temperatures $T = 850$ K [plots (a)–(d)] and 300 K [plots (e)–(h)], screening length $\lambda = 0.1$ nm, and defect concentration $N_0 = 3 \times 10^{26}$ m^{-3}. Other parameters are listed in Table II.

decrease below room temperature for the films with thickness $h \geqslant 1$ nm or even less, its value varying within the range 350–450 K in dependence on the sign and value of W (compare red, magenta, and blue curves with symbols in Figs. 6). This effect can be explained only by the presence of relatively strong compressive strains (-1%) at the film-substrate interface, which effectively support spontaneous dipole displacements in ultathin films [3–5] due to the electrostriction [8] and flexoelectric effect [40]. The depolarization field in the film is minimal due to a developed domain structure [see Figs. 2 and 4]. Indeed, electrostrictive coupling between polarization and elastic stresses shifts the transition temperature significantly, in the order of $Q_{33ij}\sigma_{ij}/\alpha_T$ in a stressed film (see Ref. [8] for details), and the flexoelectric effect creates a built-in electric field proportional to the convolution of tensors $F_{jkim}\sigma_{jk}n_m$ in the boundary conditions Eq. (2b) (see Ref. [40] for details). The approximate part of the dependence $T_C(h)$ calculated analytically for small thicknesses without the flexoelectric effect and Vegard effect is shown in Fig. 6(b) by a dotted curve.

Room-temperature spontaneous polarization P_S in dependence on the film thickness is shown in Fig. 6(c). Since one can regard that $P_S(h) \sim \sqrt{T_C(h) - T}$ within LGD-approach, the value P_S becomes almost thickness-independent or even slightly increasing with thickness decrease below 2 nm for nonzero flexocoupling [see red, magenta, and blue curves with symbols in Fig. 6(c)]. Corresponding switchable bound charge σ_S is equal to $2P_S$.

Without flexocoupling and defects the spontaneous polarization sharply disappears with thickness decrease and the size-induced transition into a paraelectric phase occurs at $h = 3$ nm [see dotted curve in Fig. 6(c)]. At that the difference between the switchable polarization calculated for nonzero flexocoupling at positive and negative Vegard coefficients is about 12 μC/cm^2, leading to the difference of about 24 μC/cm^2 in the switchable bound charge. Hence, we can predict that the relatively high switchable polarization of order 50–60 μC/cm^2 and switchable bound charge σ_S about 100–120 μC/cm^2 can be induced in ultrathin PTO films due to the flexochemical effect. The predicted increase of $\sigma_S \sim 0.2$–1 C/m^2 in ultrathin perovskite films of thickness less than 5 nm is due to the flexochemical effect; and it can be important for applications in advanced memory devices opening the way for their further miniaturization.

Distributions for the 2-nm film calculated at temperature 300 K show the film in the state close to the phase transition (Fig. 7); that is why its polarization is severely weakened and domain walls are notably diffused. Also, a metastable domain state can be observed for the film at negative W. This illustrates

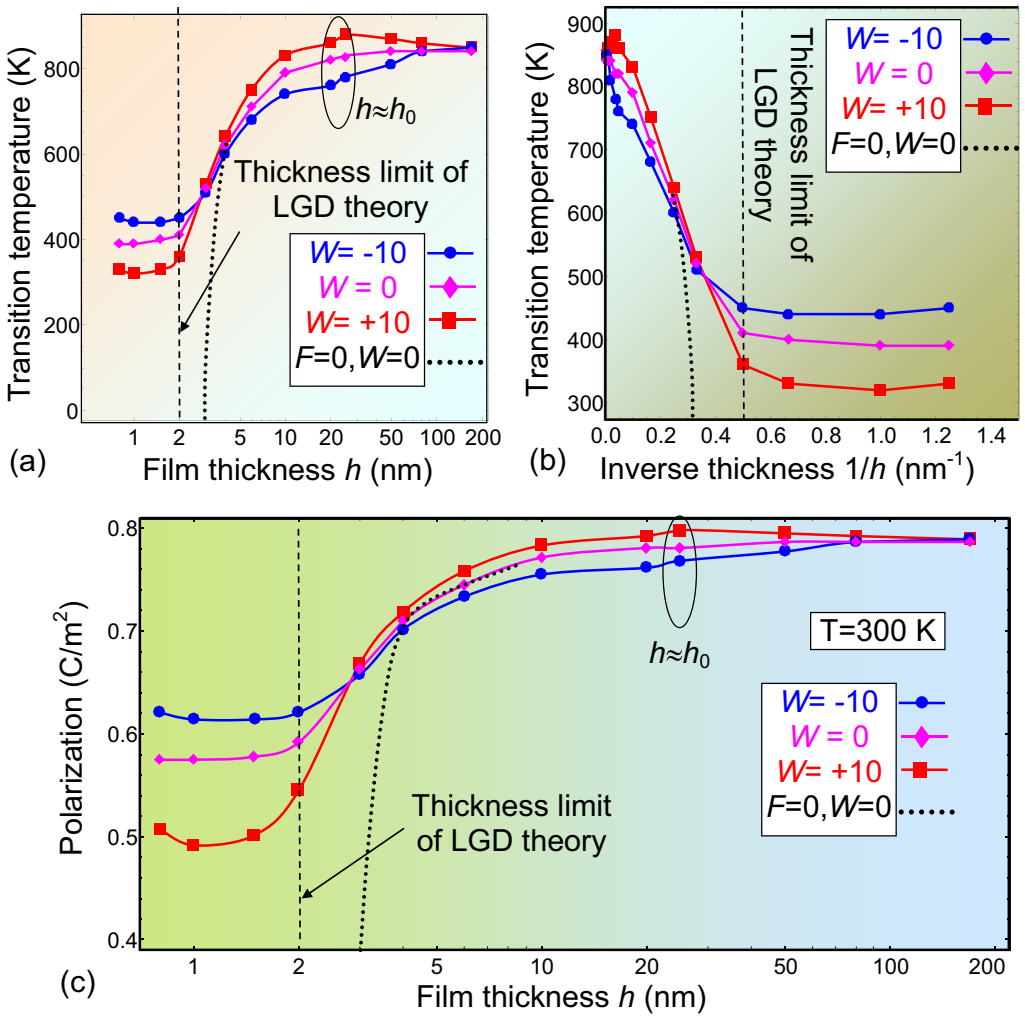

FIG. 6. Ferroelectric transition temperature vs. the film thickness h (a) and $1/h$ (b). The spontaneous polarization in dependence on the film thickness calculated at $T = 300$ K (c). Screening length $\lambda = 0.1$ nm, $N_0 = 3 \times 10^{26}$ m^{-3}, Vegard coefficient $W = +10$ Å (squares), $W = 0$ (diamonds), and $W = -10$ Å (circles), and nonzero flexocoupling. Dotted line in plots (b), (c) correspond to the simultaneous absence of the flexoelectric coupling and Vegard effect, $W = 0$, $F = 0$. Vertical dashed lines indicate the thickness limit of continuum LGD-theory applicability. Other parameters are listed in Table II.

sensitivity of thin films to lateral boundary conditions and flexoeffect that carry a major responsibility for the formation of such kinds of structures. Flexoelectric coupling, in particular, is also responsible for the very existence of the ferroelectric phase in thin films under 6 nm.

A possible explanation for an anomalous change in the phase-transition curve evolution at $h < 4$ nm [that is shown in Fig. 6(a)] could be a transition from the c-domain state of the film with polarization perpendicular to the surface in thick films (where a part of closure domains is relatively small because of their localization at approximately 5 nm below the surface, see Figs. 2 and 5) to the mainly a-domain state with the decrease of thickness, owing to the flexocoupling. Indeed, with the thickness decrease a-domains with the in-plane polarization direction become significant (see Fig. 7). This happens because it is well known that compressive misfit strains $u_m < 0$ support the c-domain formation, while the dilatation ones $u_m > 0$ support the a-domain formation. Respectively, $W > 0$ supports c-domain stability, while $W < 0$ supports the stability of a-domains. Therefore, for the case of thickness decrease below 4 nm in the film already having defects homogeneously occupying its whole bulk (because $h_0 = 25$ nm $\gg 4$ nm), it is energetically favorable to increase the fraction of a-domains, so that the ferroelectric phase transition temperature for this scenario is higher. This can be seen in Fig. 6; the detailed analysis of the corresponding domain structure and elastic fields for the film thicknesses below 5 nm is given in Fig. 7.

Polarization components change their behavior when the film thickness approaches 4 nm and less. The out-of-plane component that prevailed in thicker films gradually dims, giving the place for the in-plane polarization rising amplitude and growing area of closure domains. Three-nanometer film is already seen as such where the a-domains slightly exceed the c-domains in size. While the sign of the Vegard effect coefficient has an insignificant effect on the polarization amplitude and domain shapes, it can change mechanical strain and stress distributions. It can be seen in Fig. 7 that there are different elastic fields, specifically the out-of-plane component u_{zz}, changing significantly under positive and negative W, which can be consistently traced back to the thicker films (see Fig. 2), where such

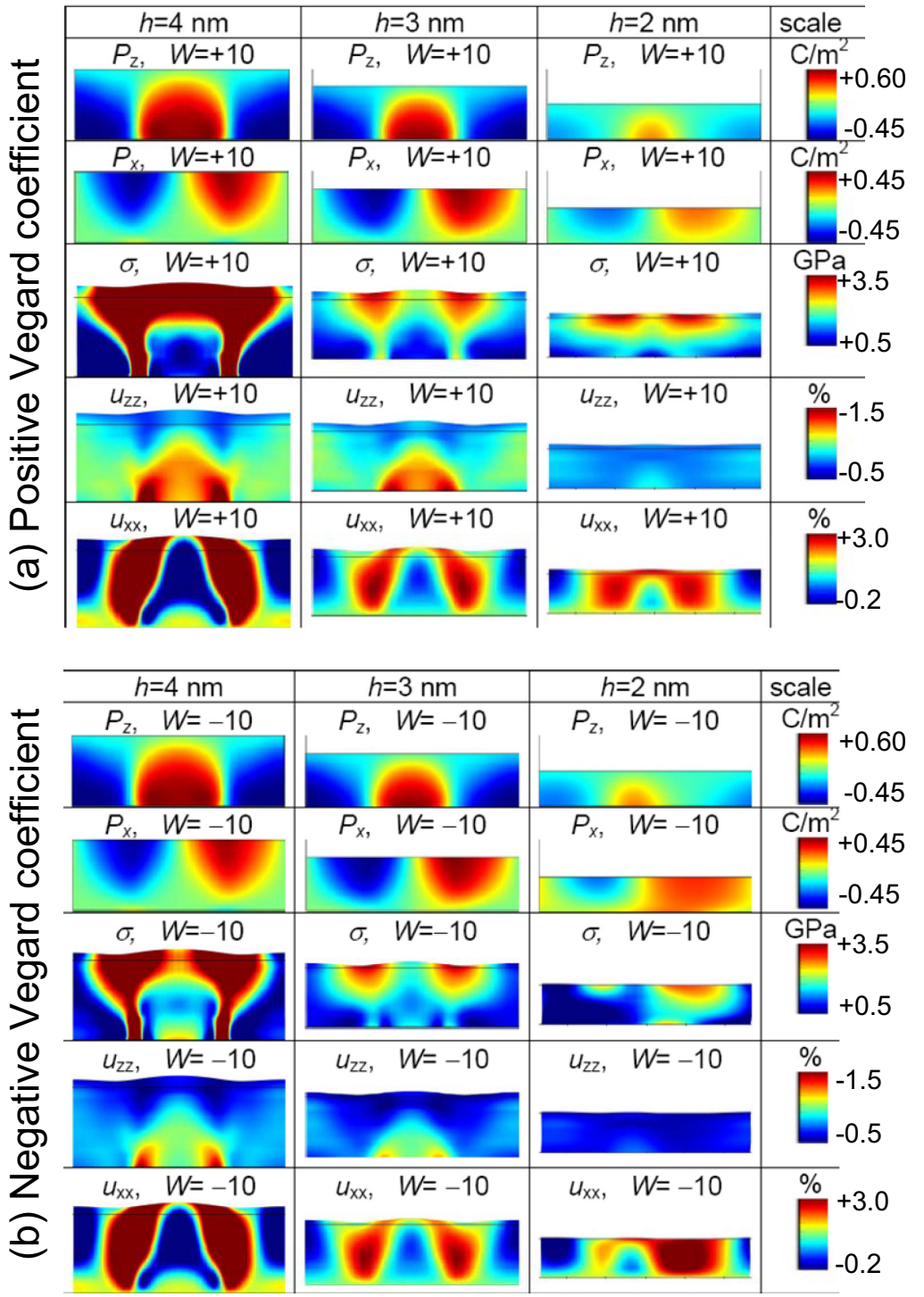

FIG. 7. Spatial distribution of the out-of-plane and in-plane polarization components P_x and P_z, von Mises stress σ and elastic strains u_{xx} and u_{zz} in the cross-sections of the 4, 3, and 2-nm PTO film calculated for positive [top part (a), $W = +10$ Å] and negative [bottom part (b), $W = -10$ Å] Vegard coefficients, room temperature $T = 300$ K, screening length $\lambda = 0.1$ nm, and defects filling the entire film with a concentration $N_0 = 3 \times 10^{26}$ m^{-3}. Other parameters are listed in Table II. Color gradient denotes scales of for the following physical parameters. In-plane polarization changes from -0.45 to 0.45 C/m^2; out-of-plane polarization changes from -0.45 to 0.6 C/m^2; Von Mises stress changes from 0.8 to 3.6 GPa; in-plane strain changes from -1.7% to -0.3%; out-of-plane strain changes from -0.2% to 3.1%.

dependencies occur in the defect-rich part of a ferroelectric bulk. Since defects are quasi-uniformly spread across the depth of the thin film ($h_0 \gg h$), Vegard stresses impact the whole film thickness. Note that the asymmetry of the out-of-plane polarization scale (from -0.45 to 0.6 C/m^2) at film thickness 2–3 nm originates from the built-in electric field induced by flexochemical coupling, and the asymmetry is absent for thicker films (compare Figs. 7 with Figs. 2 and 5). Temperature dependence of the total energy per unit area in the films of thickness 2–170 nm is presented in Fig. 10 in Appendix.

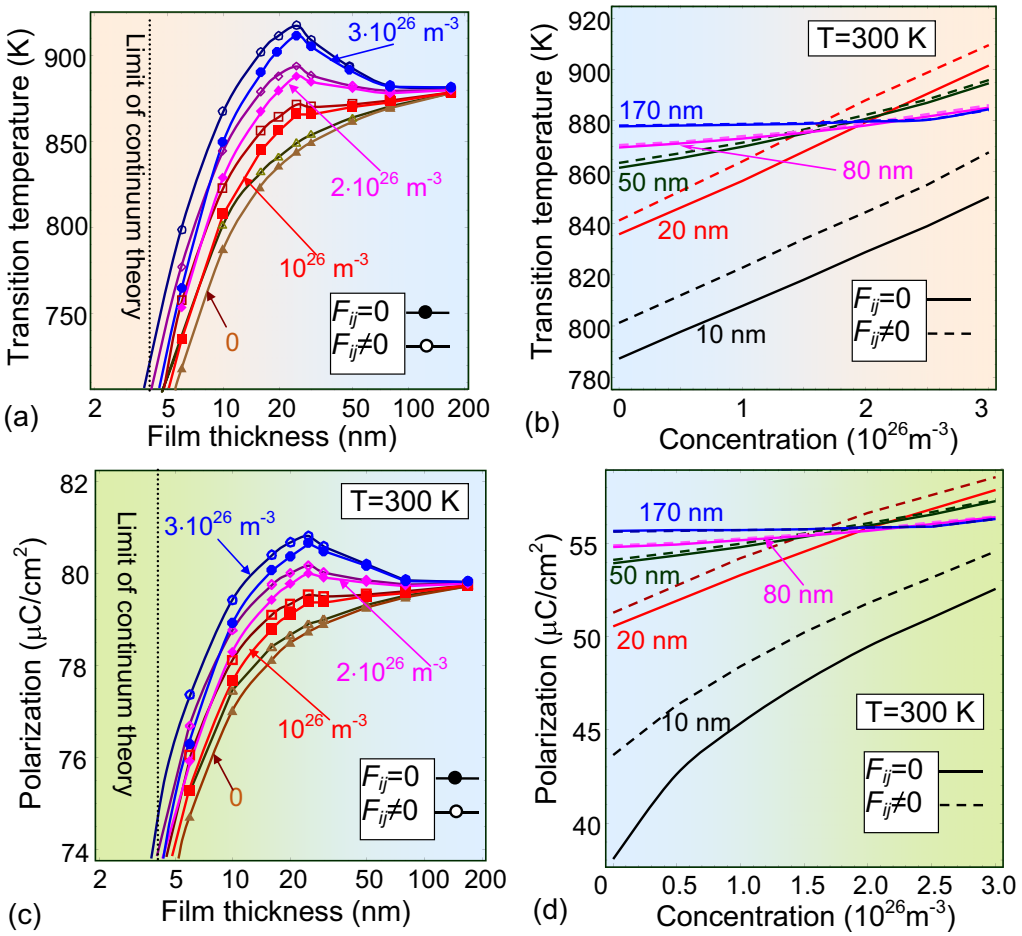

FIG. 8. Ferroelectric transition temperature dependence on the film thickness and defect concentration. (a) Dependence of the transition temperature on the film thickness calculated for different values of the defect concentration N_0 (shown near the curves) and zero (empty symbols) or nonzero (filled symbols) flexoelectric coefficients. (b) Dependence of the transition temperature on defect concentration calculated at 300 K for different values of the film thickness (shown near the curves) and zero (solid curves) or nonzero (dashed curves) flexoelectric coefficients. (c) Dependence of the spontaneous polarization on the film thickness calculated at $T = 300$ K and different values of the defect concentration N_0 (shown near the curves) and for zero (empty symbols) or nonzero (filled symbols) flexoelectric coefficients. (d) Dependence of the spontaneous polarization on defect concentration calculated at 300 K for different values of the film thickness (shown near the curves) and zero (solid curves) or nonzero (dashed curves) flexoelectric coefficients. Screening length $\lambda = 0.1$ nm, $W = +10$ Å, and the depth of the defect layer $h_0 = 25$ nm, $\Delta h = 1$ nm. Other parameters are listed in Table II.

Graphs in Figs. 6 and 7 are plotted for the fixed concentration of defects. Their detailed analysis, carried out for various defect concentrations in the temperature range of 600–900 K with a positive Vegard coefficient, shows that a pronounced maximum appears on the transition temperature dependence $T_C(h)$ at $h \approx h_0$ with the increase of the defect concentration [see Fig. 8(a) in a semilogarithmic graph]. At the maximum, the transition temperature of 20–30 nm film with a layer of defects near the surface exceeds by 50 K the transition temperature of a thick lead titanate film, which makes it possible to significantly improve the polar properties of thin films. The transition temperature of 20–30 nm film without defects is about 200 K lower than the one in the film with defect concentration 3×10^{26} m^{-3} and $W = +10$ Å. Note that we neglected the relaxation of the mismatch deformations in films with thickness $h > h_0$, and therefore the applied compressive strain (-1%) leads to renormalization of the Curie bulk temperature from 752 to 880 K in 100-nm films.

Dependence of transition temperature on the defect concentration N_0 increases quasilinearly at $W > 0$, and its slope increases with the film thickness decrease [Fig. 8(b)]. Solid curves with empty symbols in Fig. 8(a) and dashed curves in Fig. 8(b) calculated with account for the flexoelectric effect with flexoelectric coefficient $F_{ij} > 0$ listed in Table I correspond to a higher $T_C(h)$ than the curves calculated at $F_{ij} = 0$. The difference is most significant for the thinnest films [see the curves for $h = 10$ nm and 20 nm in Fig. 8(b)]; it decreases with the film thickness increase and is almost nondescript for the films with a thickness in the order of 100 nm and above [see the curves for $h = 80$ and 170 nm in Fig. 8(b)]. This is obviously related with the built-in electric field induced by the flexoelectric coupling of polarization with inhomogeneous elastic stresses, which is proportional to the product $F_{jkim}\sigma_{jk}n_m$ [see boundary conditions Eq. (2b)]. Note that the transition temperature substantially rises with defect concentration increase at positive Vegard coefficient (with

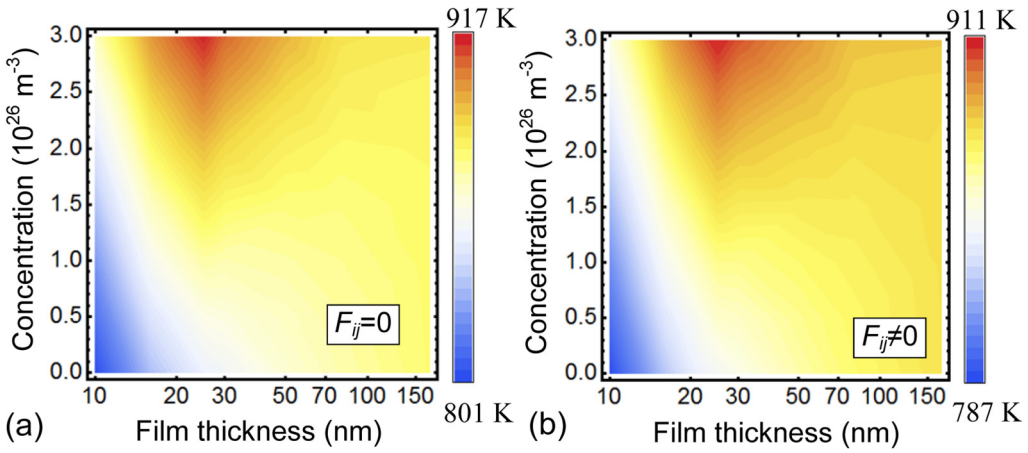

FIG. 9. Contour maps of the transition temperature in the coordinates "film thickness–defect concentration" for the two cases of zero (a) and nonzero (b) flexoelectric coefficients, screening length $\lambda = 0.1$ nm, $W = +10$ Å, and the depth of defect layer $h_0 = 25$ nm, $\Delta h = 1$ nm. Other parameters are listed in Table II.

the flexoeffect or without it), but the reentrant ferroelectric phase, observed experimentally in spherical nanoparticles with a radius $R < 5$ nm [22] and then explained theoretically by flexochemical coupling [21], has not been observed in thin films. In our opinion this is because there is no curved surface in the films that induces the ferroelectric phase due to a competition between the contributions of size effects and surface tension into the Curie temperature shift, which have different signs and are proportional to $1/R$ and $1/R^2$, respectively [21].

Room-temperature spontaneous polarization P_S in dependence on the film thickness is shown in Fig. 8(c) for various defect concentrations N_0 within the range $(0-3)10^{26}$ m^{-3} and positive Vegard coefficient $W = +10$ Å**.** Without defects P_S monotonically increases with the film thickness increase. Since $P_S(h) \sim \sqrt{T_C(h) - T}$ the polarization curves have maxima at $h \approx h_0$ with the increase of the defect concentration over about 10^{26} m^{-3} [see red, magenta, and blue curves with symbols in Fig. 8(c)]. However, a corresponding difference (0.03 C/m^2) of the maximal value 0.81 C/m^2 at $N_0 = 3 \times 10^{26}$ m^{-3} in comparison with 0.79 C/m^2 at $N_0 = 0$ is much smaller than the difference between the corresponding curves (∼0.79 C/m^2) for thin films [compare red, magenta, and blue curves in Fig. 8(c) with the corresponding ones in Fig. 6(c)].

Dependence of the spontaneous polarization on defect concentration N_0 calculated at 300 K for different film thicknesses (∼10–200 nm) is shown in Fig. 8(d). Polarization is increasing gradually with N_0 increase at positive Vegard coefficient, at that the slope essentially increases with the film thicknesses decrease [compare black, red, green, magenta, and blue curves in Fig. 8(d)]. Also, the difference between the curves calculated with and without flexoelectric coupling increases strongly with the film thickness decrease [compare solid and dashed curves in Fig. 8(d)]. In particular, the spontaneous polarization of 10-nm film substantially rises (from 0.35 to 0.45 C/m^2) with defect concentration increase from 0 to 3×10^{26} m^{-3}. At that the polarization curve calculated allowing for the flexocoupling in a 10-nm film is essentially higher (∼0.1 C/m^2) than the one calculated without it [compare solid and dashed black curves in Fig. 8(d)]. Corresponding switchable bound charge σ_S is approximately equal to 0.7 C/m^2 at $N_0 = 0$ and $F_{ij} = 0$ and can reach the value 0.98 C/m^2 at $F_{ij} > 0$ and $N_0 = 3 \times 10^{26}$ m^{-3}. The predicted increase of the switchable bound charge ∼0.28 C/m^2 due to the flexochemical effect can be important for thin films applications in memory devices.

The pronounced maximum on the transition temperature contour maps in the variables "film thickness-defect concentration" exists under the presence of flexoelectric coupling [see Fig. 9(a)] and without it [see Fig. 9(b)]; however, the flexoelectric effect significantly shifts the transition temperature (by up to 30 K for thin $PbTiO_3$ films).

Thus, the position and height of the maximum $T_C(h)$ can be controlled by the defect concentration in the layer and the surface screening length, which can be useful for advanced applications. Summarizing this section, we conclude that uncharged elastic defects have an unexpectedly strong impact on the polar and elastic properties of ferroelectric films due to Vegard stresses in the defective layer of the film and the flexoelectric effect.

Let us underline that polydomain states of ferroelectric films are used in several classical and advanced applications. There are a lot of applications of periodically poled ferroelectric layers of different compositions, for instance $LiNbO_3$ [85], $LiTaO_3$ [86], and $KTiOPO_4$ [87], for phase-matching of the second and higher harmonic generation in nonlinear optic devices. Two-dimensional (2D) semiconductors (e.g., graphene) placed on ferroelectric substrates with a domain structure are promising candidates in advanced memory cells, where each domain wall triggers the conductivity of the channel that is a 2D semiconductor (see, e.g., experimental works [88–90] and a recent theory [91,92]. Hence, the revealed polydomain state in ultrathin ferroelectric films induced by the flexochemical coupling can be of particular importance in advanced applications.

IV. CONCLUSIONS

Using the Landau-Ginzburg-Devonshire approach we established the effect of the flexoelectrochemical coupling on the polar properties and phase transitions in thin ferroelectric films with a surface layer of uncharged elastic point defects (vacancies or ions). We considered a typical case, when the defects are concentrated in a thin layer below the top film

surface creating a sharp gradient of elastic fields. The defective surface of the film is not covered with an electrode, but with an ultrathin layer of ambient screening charges, which are characterized by a surface screening length.

We obtained that the influence of the flexoelectrochemical coupling and surface screening length on the ferroelectric transition temperature of the film, distribution of the spontaneous polarization and elastic fields, domain wall structure and period is rather strong; namely, it turned out that

(1) The screening length strongly affects the polar properties and domain structure in the film. In particular, a pronounced minimum appears on the dependence of the system's specific energy on the domain size with an increase of the screening length, the depth of the minimum depending essentially on the magnitude of the Vegard coefficient.

(2) Due to the flexoelectric effect there is no size-induced transition to a paraelectric phase until 2–4 nm thickness of $PbTiO_3$ films with 1% of compressive misfit strain. The origin of this phenomenon is the re-building of the domain structure in the film (namely the crossover from *c*-domain stripes to *a*-type closure domains) emerging with its thickness decrease below 4 nm, conditioned by the flexoelectric coupling and facilitated by a negative Vegard coefficient. Though we observe no phase transition for smaller thickness, our results (as obtained in the continuum theory framework) can be inaccurate below the 2–4 nm size. Despite the said limitation the obtained results point at tempting opportunities for defect-strain engineering of the ultrathin perovskite film ferroelectric properties and domain structure tuning, which can be very promising for the ferroic film applications in nanoelectronics.

(3) Electric field induced by the defect layer has an unexpectedly strong influence on the polar and elastic properties of the strained films due to the coupling of inhomogeneous Vegard stresses and the flexoelectric effect (defect-driven flexochemical effect). Positive Vegard coefficients and high concentration of elastic defects effectively maintain the ferroelectric transition temperature above 350 K in the strained $PbTiO_3$ films due to the flexochemical effect. In contrast to the pure flexoelectric effect coefficients, which values are material-specific constants, the magnitude of the flexochemical effect can be controlled by the concentration of defects, their type, and distribution in the film, making the considered system much more suitable for tuning.

(4) The increase of defect concentration leads to a noticeable monotonic decrease in the ferroelectric transition temperature of the $PbTiO_3$ film with negative Vegard coefficients. In contrast, for positive Vegard coefficients, a pronounced maximum (with a height up to 200 K) appears on the thickness dependence of the transition temperature with increasing defect concentration. The film thickness corresponding to the maximum is approximately equal to the thickness of the defect layer and relatively weakly depends on the surface screening length. The latter property may have important implications for miniaturization of ferroelectric devices.

(5) The pronounced maximum on the dependence of the ferroelectric transition temperature on the film thickness exists even without the flexoelectric coupling in the film; however, the coupling strongly shifts the transition temperature (by up to 30 K for thin $PbTiO_3$ films). Since the maximum position and height can be controlled by modifying the defect concentration and Vegard coefficient, the obtained results are promising for advanced applications in ferroelectric memory devices and those applications in nanoelecronics, where introducing of different types and amounts of defects is conceivable.

ACKNOWLEDGMENTS

S.V.K. study was supported by the US DOE, Office of Basic Energy Sciences (BES), Materials Sciences and Engineering Division (MSED), under FWP Grant No. DE-AC0500OR22725. A portion of this research was conducted at the Center for Nanophase Materials Sciences, which is a DOE Office of Science User Facility. I.S.V. gratefully acknowledges support from the Deutsche Forschungsgemeinschaft (DFG) through the Grant No. GE 1171/7-1.

E.A.E. wrote the codes and, assisted by I.S.V. and Y.M.F., performed numerical calculations. A.N.M. stated the problem

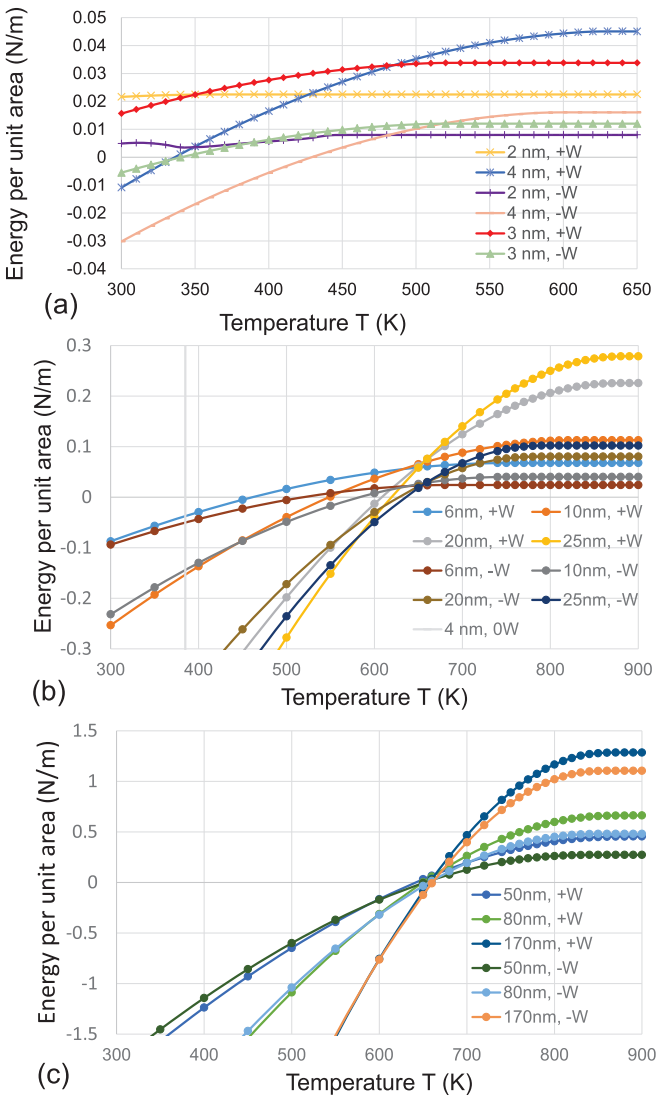

FIG. 10. Temperature-dependent energy diagram for the total energy in thin films of thicknesses 2, 3, and 4 nm (a), 6, 10, 20, and 25 nm (b), 50, 80, and 170 nm (c) with the defect concentration $N_0 = 3 \times 10^{26}\,1/\mathrm{m}^3$, $h_0 = 25\,\mathrm{nm}$, $\Delta h = 1\,\mathrm{nm}$, $\lambda = 0.1\,\mathrm{nm}$, at positive ($W = +10\,\text{Å}$) and negative ($W = -10\,\text{Å}$) Vegard coefficients.

and wrote the manuscript draft. E.A.E. and I.S.V. prepared the figures. Results analyses and manuscript improvement was performed by Y.A.G., M.D.G., and S.V.K.

APPENDIX: TEMPERATURE-DEPENDENT ENERGY DIAGRAM FOR THE TOTAL ENERGY

Temperature-dependent energy diagram for the total energy in thin films of thickness (2–170) nm have been calculated for the defect concentration $N_0 = 3 \times 10^{26}\ 1/\mathrm{m}^3$, positive ($W = +10$ Å) and negative ($W = -10$ Å) Vegard coefficients. Results are shown in Fig. 10. Saturation plateaus on the curves in the figure correspond to the paraelectric phase. Linear or parabolic-like dependencies correspond to the ferroelectric phase in the vicinity of the respectively first order and second order phase transitions. Note that the total energy of the system is positive because of its mechanical component modified by a misfit strain.

[1] J. F. Scott, *Ferroelectric Memories*, Springer Series in Advanced Microelectronics (Springer, Berlin, 2000), Vol. 3.

[2] D. R. Tilley, *Finite-size Effects on Phase Transitions in Ferroelectrics. Ferroelectic Thin Films*, edited by C. Paz de Araujo, J. F. Scott, and G. W. Teylor (Gordon and Breach, Amsterdam, 1996).

[3] M. J. Highland, T. T. Fister, D. D. Fong, P. H. Fuoss, C. Thompson, J. A. Eastman, S. K. Streiffer, and G. B. Stephenson, Equilibrium Polarization of Ultrathin $PbTiO_3$ with Surface Compensation Controlled by Oxygen Partial Pressure, Phys. Rev. Lett. **107**, 187602 (2011).

[4] I. Vrejoiu, G. Le Rhun, L. Pintilie, D. Hesse, M. Alexe, and U. Gösele, Intrinsic ferroelectric properties of strained tetragonal $PbZr_{0.2}Ti_{0.8}O_3$ obtained on layer-by-layer grown, defect-free single-crystalline films, Adv. Mater. **18**, 1657 (2006).

[5] D. D. Fong, G. B. Stephenson, S. K. Streiffer, J. A. Eastman, O. Auciello, P. H. Fuoss, and C. Thompson, Ferroelectricity in Ultrathin Perovskite Films, Science **304**, 1650 (2004).

[6] A. L. Roytburd, S. P. Alpay, V. Nagarajan, C. S. Ganpule, S. Aggarwal, E. D. Williams, and R. Ramesh, Measurement of Internal Stresses Via the Polarization in Epitaxial Ferroelectric Films, Phys. Rev. Lett. **85**, 190 (2000).

[7] J. S. Speck, A. Seifert, W. Pompe, and R. Ramesh, Domain configurations due to multiple misfit relaxation mechanisms in epitaxial ferroelectric thin films. II. Experimental verification and implications, J. Appl. Phys. **76**, 477 (1994).

[8] N. A. Pertsev, A. G. Zembilgotov, and A. K. Tagantsev, Effect of Mechanical Boundary Conditions on Phase Diagrams of Epitaxial Ferroelectric Thin Films, Phys. Rev. Lett. **80**, 1988 (1998).

[9] S. M. Kogan, Piezoelectric effect during inhomogeneous deformation and acoustic scattering of carriers in crystals, Sov. Phys. Solid State **5**, 2069 (1964).

[10] N. D. Sharma, C. M. Landis, and P. Sharma, Piezoelectric thin-film superlattices without using piezoelectric materials, J. Appl. Phys. **108**, 024304 (2010).

[11] P. Zubko, G. Catalan, and A. K. Tagantsev, Flexoelectric effect in solids, Annu. Rev. Mater. Res. **43**, 387 (2013).

[12] M. Stengel, Flexoelectricity from density-functional perturbation theory, Phys. Rev. B **88**, 174106 (2013).

[13] A. K. Tagantsev and P. V. Yudin editors, *Flexoelectricity in Solids: From Theory to Applications* (World Scientific, Singapore, 2016).

[14] D. A. Freedman, D. Roundy, and T. A. Arias, Elastic effects of vacancies in strontium titanate: Short-and long-range strain fields, elastic dipole tensors, and chemical strain, Phys. Rev. B **80**, 064108 (2009).

[15] G. Catalan and J. F. Scott, Physics and applications of bismuth ferrite, Adv. Mater. **21**, 1 (2009).

[16] X. Zhang, W. Shyy, and A. M. Sastry, Numerical simulation of intercalation-induced stress in Li-ion battery electrode particles, J. Electrochem. Soc., **154**, A910 (2007).

[17] X. Zhang, A. M. Sastry, and W. Shyy, Intercalation-induced stress and heat generation within single lithium-ion battery cathode particles, J. Electrochem. Soc. **155**, A542 (2008).

[18] A. N. Morozovska, E. A. Eliseev, A. K. Tagantsev, S. L. Bravina, Long-Qing Chen, and S. V. Kalinin, Thermodynamics of electromechanically coupled mixed ionic-electronic conductors: Deformation potential, Vegard strains, and flexoelectric effect, Phys. Rev. B **83**, 195313 (2011).

[19] A. N. Morozovska, I. S. Golovina, S. V. Lemishko, A. A. Andriiko, S. A. Khainakov, and E. A. Eliseev, Effect of Vegard strains on the extrinsic size effects in ferroelectric nanoparticles, Phys. Rev. B **90**, 214103 (2014).

[20] A. N. Morozovska, E. A. Eliseev, P. S. Sankara Rama Krishnan, A. Tselev, E. Strelkov, A. Borisevich, O. V. Varenyk, N. V. Morozovsky, P. Munroe, S. V. Kalinin, and V. Nagarajan, Defect thermodynamics and kinetics in thin strained ferroelectric films: The interplay of possible mechanisms, Phys. Rev. B **89**, 054102 (2014).

[21] A. N. Morozovska and M. D. Glinchuk, Flexo-chemo effect in nanoferroics as a source of critical size disappearance at size-induced phase transitions, J. Appl. Phys. **119**, 094109 (2016).

[22] J. Zhu, W. Han, H. Zhang, Z. Yuan, X.-H. Wang, L.-T. Li, and C-Q. Jin, Phase coexistence evolution of nano BaTiO3 as function of particle sizes and temperatures, J. Appl. Phys. **112**, 064110 (2012).

[23] M. Marvan, P. Chvosta, and J. Fousek, Theory of compositionally graded ferroelectrics and pyroelectricity, Appl. Phys. Lett. **86**, 221922 (2005).

[24] A. L. Roytburd and J. Slutsker, Thermodynamics of polydomain ferroelectric bilayers and graded multilayers, Appl. Phys. Lett. **89**, 042907 (2006).

[25] R. Kretschmer and K. Binder, Surface effects on phase transition in ferroelectrics and dipolar magnets, Phys. Rev. B **20**, 1065 (1979).

[26] A. L. Roytburd, V. Roytburd, and J. Slutsker, Domain structures in continuously graded ferroelectric films, Appl. Phys. Lett. **94**, 152904 (2009).

[27] A. Roytburd, and V. Roytburd, Domain evolution and polarization of continuously graded ferroelectric films, Philos. Mag. **90**, 61 (2010).

[28] Y. L. Tang, Y. L. Zhu, X. L. Ma, A. Y. Borisevich, A. N. Morozovska, E. A. Eliseev, W. Y. Wang, Y. J. Wang, Y. B. Xu, Z. D. Zhang, and S. J. Pennycook, Observation of a periodic array

of flux-closure quadrants in strained ferroelectric $PbTiO_3$ films, Science **348**, 547 (2015).

[29] N. Balke, B. Winchester, W. Ren, Y. H. Chu, A. N. Morozovska, E. A. Eliseev, M. Huijben, R. K. Vasudevan, P. Maksymovych, J. Britson, S. Jesse, I. Kornev, R. Ramesh, L. Bellaiche, L.-Q. Chen, and S. V. Kalinin, Enhanced electric conductivity at ferroelectric vortex cores in $BiFeO_3$, Nat. Phys. **8**, 81 (2012).

[30] B. Winchester, N. Balke, X. X. Cheng, A. N. Morozovska, S. Kalinin, and L. Q. Chen, Electroelastic fields in artificially created vortex cores in epitaxial $BiFeO_3$ thin films, Appl. Phys. Lett. **107**, 052903 (2015).

[31] A. R.Damodaran, J. D. Clarkson, Z. Hong, H. Liu, A. K. Yadav, C. T. Nelson, S.-L. Hsu *et al.*, Phase coexistence and electric-field control of toroidal order in oxide superlattices, Nat. Mater. **16**, 1003 (2017).

[32] A. M. Bratkovsky and A. P. Levanyuk, Smearing of Phase Transition Due to a Surface Effect or a Bulk Inhomogeneity in Ferroelectric Nanostructures, Phys. Rev. Lett **94**, 107601 (2005).

[33] Z.-G. Ban, S. P. Alpay, and J. V. Mantese, Fundamentals of graded ferroic materials and devices, Phys. Rev. B **67**, 184104 (2003).

[34] S. Zhong, Z.-G. Ban, S. P. Alpay, and J. V. Mantese, Large piezoelectric strains from polarization graded ferroelectrics, Appl. Phys. Lett. **89**, 142913 (2006).

[35] A. N. Morozovska, E. A. Eliseev, G. S. Svechnikov, and S.V. Kalinin, Mesoscopic mechanism of the domain wall interaction with elastic defects in uniaxial ferroelectrics, J. Appl. Phys. **113**, 187203 (2013).

[36] I. S. Vorotiahin, A. N. Morozovska, E. A. Eliseev, and Y. A. Genenko, Flexocoupling impact on the kinetics of polarization reversal, Phys. Rev. B **95**, 014104 (2017).

[37] I. S. Vorotiahin, E. A. Eliseev, Q. Li, S. V. Kalinin, Y. A. Genenko, and A. N. Morozovska, Tuning the Polar States of Ferroelectric Films via Surface Charges and Flexoelectricity, Acta Mater. **137**, 85 (2017).

[38] G. Catalan, L. J. Sinnamon, and J. M. Gregg, The effect of flexoelectricity on the dielectric properties of inhomogeneously strained ferroelectric thin films, J. Phys.: Condens. Matter **16**, 2253 (2004).

[39] J. Karthik, R. V. K. Mangalam, J. C. Agar, and L. W. Martin, Large built-in electric fields due to flexoelectricity in compositionally graded ferroelectric thin films, Phys. Rev. B **87**, 024111 (2013).

[40] A. N. Morozovska, E. A. Eliseev, Y. A. Genenko, I. S. Vorotiahin, M. V. Silibin, Y. Cao, Y. Kim, M. D. Glinchuk, and S. V. Kalinin, Flexocoupling impact on size effects of piezoresponse and conductance in mixed-type ferroelectric semiconductors under applied pressure, Phys. Rev. B **94**, 174101 (2016).

[41] A. M. Bratkovsky and A. P. Levanyuk, Formation and rapid evolution of domain structure at phase transitions in slightly inhomogeneous ferroelectrics and ferroelastics, Phys. Rev. B **66**, 184109 (2002).

[42] A. K. Tagantsev, L. E. Cross, and J. Fousek, *Domains in ferroic crystals and thin films* (Springer, New York, 2010).

[43] A. L. Roytburd, J. Ouyang, and A. Artemev, Polydomain structures in ferroelectric and ferroelastic epitaxial films, J. Phys.: Condens. Matter **29**, 163001 (2017).

[44] A. M. Bratkovsky and A. P. Levanyuk, Very large dielectric response of thin ferroelectric films with the dead layers, Phys. Rev. B **63**, 132103 (2001).

[45] A. K. Tagantsev and G. Gerra, Interface-induced phenomena in polarization response of ferroelectric thin films, J. Appl. Phys. **100**, 051607 (2006).

[46] E. A. Eliseev, A. N. Morozovska, M. D. Glinchuk, and R. Blinc, Spontaneous flexoelectric/flexomagnetic effect in nanoferroics, Phys. Rev. B **79**, 165433 (2009).

[47] P. V. Yudin, R. Ahluwalia, and A. K. Tagantsev, Upper bounds for flexocoupling coefficients in ferroelectrics, Appl. Phys. Lett. **104**, 082913 (2014).

[48] E. A. Eliseev, A. V. Semchenko, Y. M. Fomichov, M. D. Glinchuk, V. V. Sidsky, V. V. Kolos, Y. M. Pleskachevsky, M. V. Silibin, N. V. Morozovsky, and A. N. Morozovska, Surface and finite size effects impact on the phase diagrams, polar and dielectric properties of$(Sr,Bi)Ta_2O_9$ferroelectric nanoparticles, J. Appl. Phys. **119**, 204104 (2016).

[49] J. Bardeen, Surface states and rectification at a metal semiconductor contact, Phys. Rev. **71**, 717 (1947).

[50] V. M. Fridkin, *Ferroelectrics Semiconductors* (Consultant Bureau, New York/London, 1980), p. 119.

[51] M. A. Itskovsky, Some peculiarities of phase transition in thin layer ferroelectric, Fiz. Tv. Tela **16**, 2065 (1974).

[52] P. W. M. Blom, R. M. Wolf, J. F. M. Cillessen, and M. P. C. M. Krijn, Ferroelectric Schottky Diode, Phys. Rev. Lett. **73**, 2107 (1994).

[53] A. N. Morozovska, E. A. Eliseev, S. V. Svechnikov, A. D. Krutov, V. Y. Shur, A. Y. Borisevich, P. Maksymovych, and S. V. Kalinin, Finite size and intrinsic field effect on the polar-active properties of ferroelectric semiconductor heterostructures, Phys. Rev. B **81**, 205308 (2010).

[54] Y. A. Genenko, O. Hirsch, and P. Erhart, Surface potential at a ferroelectric grain due to asymmetric screening of depolarization fields, J. Appl. Phys. **115**, 104102 (2014).

[55] J. Wang, A. K. Tagantsev, and N. Setter, Size effect in ferroelectrics: Competition between geometrical and crystalline symmetries, Phys. Rev. B **83**, 014104 (2011).

[56] R. Maranganti and P. Sharma, A novel atomistic approach to determination of strain-gradient elasticity constants: Tabulation and comparison for various metals, semiconductors, silica, polymers and the (ir) relevance for nanotechnologies, J. Mech. Phys. Solids **55**, 1823 (2007).

[57] A. S. Yurkov, Elastic boundary conditions in the presence of the flexoelectric effect, JETP Lett. **94**, 455 (2011).

[58] *Flexoelectricity in Solids: From Theory to Applications*, edited by A. K. Tagantsev and P. V. Yudin (World Scientific, Singapore, 2016), and references therein.

[59] P. V. Yudin, A. K. Tagantsev, E. A. Eliseev, A. N. Morozovska, and N. Setter, Bichiral structure of ferroelectric domain walls driven by flexoelectricity, Phys. Rev. B **86**, 134102 (2012).

[60] E. A. Eliseev, P. V. Yudin, S. V. Kalinin, N. Setter, A. K. Tagantsev, and A. N. Morozovska, Structural phase transitions and electronic phenomena at 180-degree domain walls in rhombohedral BaTiO3, Phys. Rev. B **87**, 054111 (2013).

[61] A. N. Morozovska, Y. M. Vysochanskii, O. V. Varenik, M. V. Silibin, S. V. Kalinin, and E. A. Eliseev, Flexocoupling impact on the generalized susceptibility and soft phonon modes in the ordered phase of ferroics, Phys. Rev. B **92**, 094308 (2015).

[62] A. N. Morozovska, E. A. Eliseev, C. M. Scherbakov, and Y. M. Vysochanskii, The influence of elastic strain gradient on

the upper limit of flexocoupling strength, spatially-modulated phases and soft phonon dispersion in ferroics, Phys. Rev. B **94**, 174112 (2016).

[63] Exactly these conditions correspond to the minimum of the Gibbs potential, see Sec. 10 in L. D. Landau and E. M. Lifshitz, *Theoretical Physics, Electrodynamics of Continuous Media* (Pergamon, Oxford, 1963), Vol. VIII.

[64] E. A. Eliseev and A. N. Morozovska, General approach for the description of size effects in ferroelectric nanosystems, J. Mater. Sci. **44**, 5149 (2009).

[65] E. A. Eliseev, S. V. Kalinin, and A. N. Morozovska, Finite size effects in ferroelectric-semiconductor thin films under open-circuited electric boundary conditions, J. Appl. Phys. **117**, 034102 (2015).

[66] B. W. Sheldon, and V. B. Shenoy, Space Charge Induced Surface Stresses: Implications in Ceria and Other Ionic Solids, Phys. Rev. Lett. **106**, 216104 (2011).

[67] P. Erhart, and K. Albe, Dopants and dopant-vacancy complexes in tetragonal lead titanate: A systematic first principles study, Comput. Mater. Sci. **103**, 224 (2015).

[68] B. Jaffe, W. R. Cook, and H. Jaffe, *Piezoelectric Ceramics* (Academic Press, London/New York, 1971).

[69] J. K. Juneja, S. Singh, K. K. Raina, and C. Prakash, Study on structural, dielectric, ferroelectric and piezoelectric properties of Ba doped Lead Zirconate Titanate Ceramics, Physica B: Condensed Matter **431**, 109 (2013).

[70] D. M. Nguyen, T. Q. Trinh, J. M. Dekkers, E. P. Houwman, H. N. Vu, and A. J. H. M. Rijnders, Effect of dopants on ferroelectric and piezoelectric properties of lead zirconate titanate thin films on Si substrates, Ceram. Int. **40**, 1013 (2014).

[71] J.-B. Liu, W.-C. Li, Y.-X. Zhang, and Z.-M. Wang, Preparation and characterization of Li+-modified$Ca_xPb_{1-x}TiO_3$film for humidity sensor, Sens. Actuators B: Chem. **75**, 11 (2001).

[72] Aneta Slodczyk, Marie-Hélène Limage, Philippe Colomban, Oumaya Zaafrani, Frédéric Grasset, Johan Loricourt, and Béatrice Sala, Substitution and proton doping effect on $SrZrO_3$ behaviour: High-pressure Raman study, J. Raman Spectrosc. **42**, 2089 (2011).

[73] K. Wójcik, Electrical properties of $PbTiO_3$ single crystals doped with lanthanum, Ferroelectrics **99**, 5 (1989).

[74] I. Ueda and S. Ikegami, Piezoelectric properties of modified $PbTiO_3$ ceramics, Jpn. J. Appl. Phys. **7**, 236 (1968).

[75] R. Maranganti and P. Sharma, Atomistic determination of flexoelectric properties of crystalline dielectrics, Phys. Rev. B **80**, 054109 (2009).

[76] J. W. Hong and D. Vanderbilt, First-principles theory and calculation of flexoelectricity, Phys. Rev. B **88**, 174107 (2013).

[77] M. Stengel, Unified ab initio formulation of flexoelectricity and strain-gradient elasticity, Phys. Rev. B **93**, 245107 (2016).

[78] I. Ponomareva, A. K. Tagantsev, and L. Bellaiche, Finite-temperature flexoelectricity in ferroelectric thin films from first principles, Phys. Rev. B **85**, 104101 (2012).

[79] P. Zubko, G. Catalan, A. Buckley, P. R. L. Welche, and J. F. Scott, Strain-Gradient-Induced Polarization in $SrTiO_3$ Single Crystals, Phys. Rev. Lett. **99**, 167601 (2007).

[80] P. Zubko, G. Catalan, A. Buckley, P. R. L. Welche, and J. F. Scott, Erratum: Strain-Gradient-Induced Polarization in $SrTiO_3$ Single Crystals [Phys. Rev. Lett. **99**, 167601 (2007)], Phys. Rev. Lett. **100**, 199906 (2008).

[81] W. Ma and L. E. Cross, Flexoelectric effect in ceramic lead zirconate titanate, Appl. Phys. Lett. **86**, 072905 (2005).

[82] R. von Mises, *Mechanik der festen Körper im plastisch deformablen Zustand*, Göttin. Nachr. Math. Phys. **1**, 582. (1913), see also https://en.wikipedia.org/wiki/Von_Mises_yield_criterion.

[83] E. A. Eliseev, A. N. Morozovska, S. V. Kalinin, Y. L. Li, Jie Shen, M. D. Glinchuk, L. Q. Chen, and V. Gopalan, Surface Effect on Domain Wall Width in Ferroelectrics, J. Appl. Phys. **106**, 084102 (2009).

[84] A. S. Sidorkin, *Domain Structure in Ferroelectrics and Related Materials* (Cambridge International Science Publishing, Cambridge, 2006), p. 250.

[85] R. G. Batchko, M. M. Fejer, R. L. Byer, D. Woll, R. Wallenstein, V. Y. Shur, and L. Erman, Continuous-wave quasi-phase-matched generation of 60 mW at 465 nm by single-pass frequency doubling of a laser diode in backswitch-poled lithium niobate, Opt. Lett. **24**, 1293 (1999).

[86] H. Takaaki, K. Nakamura, T. Taniuchi, H. Ito, Y. Furukawa, and K. Kitamura, Quasi-phase-matched optical parametric oscillation with periodically poled stoichiometric$LiTaO_3$. Opt. Lett. **25**, 651 (2000).

[87] A. Garashi, A. Arie, A. Skliar, and G. Rosenman, Continuous-wave optical parametric oscillator based on periodically poled $KTiOPO_4$, Opt. Lett. **23**, 1739 (1998).

[88] J. H. Hinnefeld, R. J. Xu, S. Rogers, S. Pandya, M. Shim, L. W. Martin, and N. Mason, Single gate p-n junctions in graphene-ferroelectric devices, Appl. Phys. Lett. **108**, 203109 (2016).

[89] C. Baeumer, D. Saldana-Greco, J. M. P. Martirez, A. M. Rappe, M. Shim, and L. W. Martin, Ferroelectrically driven spatial carrier density modulation in graphene, Nat. Commun. **6**, 6136 (2015).

[90] W. Y. Kim, H.-D. Kim, T.-T. Kim, H.-S. Park, K. H. Lee, H. J. Choi, S. H. Lee, J.-H. Son, N.-K. Park, and B. K. Min, Graphene-ferroelectric metadevices for nonvolatile memory and reconfigurable logic-gate operations, Nat. Commun. **7**, 10429 (2016).

[91] A. I. Kurchak, E. A. Eliseev, S. V. Kalinin, M. V. Strikha, and A. N. Morozovska, P-N Junctions Dynamics in Graphene Channel Induced by Ferroelectric Domains Motion, Phys. Rev. Appl. **8**, 024027 (2017).

[92] A. N. Morozovska, A. I. Kurchak, and M. V. Strikha, Graphene Exfoliation at Ferroelectric Domain Wall Induced by Piezoeffect: Impact on the Conduction of Graphene Channel, Phys. Rev. Appl. **8**, 054004 (2017).

4. Discussion and Summary

The conducted studies have helped to understand the role of different physical effects, namely flexoelectricity, surface screening charges, and Vegard strains, on electromechanical, electrostatic and polar properties in ferroelectric films, ferroelectric phase diagrams, domain structures and parameters, and switching kinetics. Each effect has had the instances when its influence prevailed. It is possible to sum up the specific cases to attain a wholesome picture of the processes occurring in thin ferroelectric films. The discovered influences carry implications leading to new insights for better understanding of phenomena observed being of interest for applications. The already obtained answers can hint at how to control polar properties via surface preparations and defect incorporation, all features being electromechanically assisted.

4.1. Flexoelectric Effect

Compared to the two other investigated effects, flexoelectricity has the weakest quantitative influence on static ferroic properties of the film, however, they are still qualitatively remarkable. First of all, flexoelectricity manifests itself stronger the less the film thickness is. Domain-wall distortions and stressed nanodomain formation at the perfectly screened surface are all much more visible for thinner films. The increased stress at the domain walls can be explained by the nature of flexoelectricity, since the walls are exactly the regions of small linear sizes and high gradients. The flexoelectric-induced shift of the critical thickness of the ferroelectric phase is also a well-known implication of the effect, although, contrary to expectations, phase transition temperature has not changed dramatically due to the flexoelectric impact. One of the most remarkable effects on the domain structure due to flexoeffect issues at higher film thickness is supporting of metastable states with ribbon structures and changed domain periods. Ribbon-structured states are especially reminiscent of polar nanoregions (PNR) in the bulk of relaxor ferroelectrics. Existence of PNR in non-relaxor and non-solid-solution perovskite ferroelectrics has been also recently predicted [211] by using an atomistic toy model as the result of flexoelectricity, so that the appearance of the metastable structures confirms this peculiar workout of the flexoelectricity. In the defected films, flexoelectricity relaxes stresses induced by elastic defects and slightly lowers their influence, with the effect being stronger at smaller thicknesses.

Perhaps the most significant flexoelectric impact was that upon the switching dynamics of a ferroelectric film. Flexoeffect basically facilitates the switching process, lowering the critical switching fields and boosting the switching to be carried out faster, and this boost depends on the field applied to the film. With this in mind, it is safe to conclude that it is necessary to take flexoelectricity into account when calculating the properties of thin ferroelectric films.

4.2. Surface Screening

The influence of different types of the surface screening might be the most significant both on the static distributions and on the ferroelectric switching. Since the screening, at least small, exists on every surface, it is important to take this fact into account. Concerning the domain structure, we have learnt that the strong surface screening, caused by a perfect or imperfect electrode, essentially shatters the domain structure and introduces the single-domain state. In this state some other quantities lost their parametric dependencies. Particularly, the phase transition temperature of a strongly screened film got significantly higher and lost its thickness dependence.

There is a range of the medium screening charge densities that are still strong but exhibit additional effects. In this range, while the Curie point is already significantly elevated, the thickness dependence remains. Most notably, there are two states of a domain structure available at this screening strength: the first is a stable one at a global energy minimum, with a single domain, *i.e.* correspondent to the strong screening, and the second is a metastable one at a local energy minimum, where differently oriented out-of-plane domains exist. With a decrease of the screening the latter structure obtains closure domains at the surface, the area of which is inversely proportional to the screening charge. Domain sizes

in a defected film, dependent at the low screening on the Vegard coefficient, gradually lose their dependence with an increase of the screening, with the most significant loss registered at the intermediate screening range. Finally, at the low screening, a closure Kittel-type stripe domain structure is stable, and all size effects are the strongest.

The surface screening dependence of ferroelectric switching is another interesting topic. Different screening mechanisms have resulted in different shapes of the hysteresis curve, changing the relief of the Gibbs free energy.

The linear Bardeen screening, which has been assumed in the domain structures study, strives to flatten the free energy profile. It influences the switching process by narrowing the hysteresis loop until it closes making it a reversible curve at lower temperatures.

The Fermi-Dirac screening model creates a pointy minimum in the middle of the Gibbs free energy versus polarization profile. This minimum becomes global at lower thicknesses and higher temperatures, effectively narrowing the hysteresis curve. There is a well-known state of an antiferroelectric-like double loop at increased temperatures and lower thicknesses. The end point of the loop narrowing is closing the hysteresis loop into a simple curve.

The Stephenson-Highland model works out similarly to the Fermi-Dirac model, creating a minimum in the free energy profile that narrows the hysteresis loop. Antiferroelectric-like double loops are even more noticeable. But the most prominent effect of the SH-model is caused by the asymmetry of the surface ion-formation conditions. Under unequal formation energies there is a charge imbalance created on the surface that shifts the energy minima aside, deforming the shapes of hysteresis loops asymmetrically. At such conditions, one of the polarization values can be much harder to obtain than another that makes up different coercive fields for each part of the hysteresis.

It is obvious that the surface screening plays a significant role both in static and dynamic properties of the thin ferroelectric films and should be considered in both theoretical and experimental studies. In the experiment, surface screening is controlled by surface treatment techniques and atmospheric conditions.

4.3. Elastic Point Defects

As follows from the studies consisting this work, Vegard strains can significantly modify properties of thin ferroelectric films. Though it is shown for defect densities of about 10^{26} m^{-3}, this concentration is reasonable and corresponds to ordinary semiconductor doping rates. The electrostatic implications of the defect introduction were set aside to focus upon the mechanical properties. First of all, two types of defects were studied with opposite properties, and their influences upon the film properties proven to be also opposite.

When considering the defects with positive Vegard coefficients, *i.e.* those repulsing neighbouring ions in the lattice, we see the increase of polarization and phase transition temperature caused by increased strains inside the defected layer. This layer has greater polarization, and when it fades elsewhere near the phase transition point, it remains stronger within the layer, prolonging the existence of the polar phase. The most favourable energetically domain size is decreased when the film is filled with repulsing defects.

Attracting defects, with the negative Vegard tensor coefficient, on the other hand, decrease both polarization and phase transition temperature. The defected layer is less strained which is reflected in weaker polarization that fades at lower temperatures and makes the whole film follow into the paraelectric phase. Domains of the film filled with attracting defects have greater energetically favourable size than those in the non-defected films.

The influence of defects, both positive and negative ones, can be increased. If the defected layer has the same thickness as the film, *i.e.* if the whole film is stuffed with defects, it produces a local maximum or a local minimum (dependent on the Vegard coefficient sign) of the phase transition temperature that means that the defect impact is stronger if no part of the film pulls the system towards the undefected values of polarization and phase transition temperature. Also, it is intuitively clear that defect concentrations affect the strength of their effect. Indeed, increasing their concentration two- or threefold for the positive Vegard coefficient makes polarization and Curie point higher with a maximum becoming especially pronounced.

From this point it can be said that defect-driven processes may significantly influence functionality of thin ferroelectric films by creating Vegard strains contributing to distributions of polar and mechanical properties. Choosing a doping profile and defect concentration may effectively tailor properties of such a film.

5. Prospects

The above listed results, though covering a range of different physical mechanisms, by far do not exhaust the opportunities of the FEM simulations of ferroics. However, they pave the way to further possible researches concerning the influence of various physical phenomena and their combinations on the ferroelectric properties. Being further refined, the suggested models can potentially take into account a vast range of electromechanical and semiconductor properties, electrostatics and electrodynamics and many others.

The most obvious candidate for further research would be studying of point defects that combine elastic properties with the effect of their charge. Through many years of investigation, the role of defect charges was established to be defining in the processes of ferroelectric aging and fatigue, that influences, often direly, the switching process and is one of the factors defining longevity of FeRAM devices [212, 213]. The influence is notable, for example, when defects create charged clusters that contribute to the internal electric field and provoke charge imbalance, making poling easier or harder depending on the sign of the field applied. On the other hand, mechanical and electromechanical effect of defects can also mess with polarization switching. Defect-driven electromechanical fields can as well introduce asymmetry to the poling and even prevent the film from switching at all [214]. From this point, the study of interest would be defining the role of chemical strains in the ferroelectric aging and fatigue processes. Depending on the defect concentration, the role it may play may be crucial. One of the exciting and important part of such a work would be defining realistic Vegard coefficients for defects in studied BT or PT perovskites. Even if reliable measurements are still lacking, to find them one may assess and transform data from the first-principle simulations [215].

Another direction of studies comes from the properties of electrodes attached to the ferroelectric surfaces. We already know that the type of electrode impacts most of ferroic properties. But additionally, it can be considered as a medium that injects or extracts charge carriers from the bulk it is attached to. The same can be said about charged defects. Properties of electrodes as a medium derived from the semiconductor zone structure, being intensively studied, may provide necessary accurate information about boundary conditions which should be imposed on the metal/ferroelectric interface. An interplay between polar properties of ferroelectrics and injection from and in electrodes would be another interesting topic of studies. Such process was studied with respect to semiconductors or linear dielectrics in the system conductor/insulator/(semi)conductor and with electrode parameters being precalculated analytically [216, 217, 218, 219]. Self-consistent numerical simulation of all media in the system can reveal a nature of interaction between the subsystems.

This was an assessment of only a couple of potential researches in the future. Others may include similar FEM studies of additional materials like KNN or bismuth ferrite ($BiFeO_3$) influenced by the same effects, development of knowledge about flexoelectricity and chemical strains to obtain more accurate data for

a wide range of materials, changing dimensionality of problems and modelling more complex structures with ferroelectric films, modelling devices on ferroic films *etc*. It would primarily help to refine the working principles of FeRAM and piezoelectric devices, giving hints on how to improve their functionality.

List of Figures

List of Tables

List of Abbreviations

BCT-BZT	Barium-calcium titanate-barium zirconate-titanate
BNT-BT	Bismuth-sodium titanate-barium titanate
BS	Bardeen linear screening model
BST	Barium-strontium titanate
BT	Barium Titanate
FD	Fermi-Dirac screening model

FEM	Finite-element method
FeRAM	Ferroelectric random access memory
KDP	Potassium dihydrogenphosphate
KNN	Potassium-sodium niobate
LGD	Landau-Ginsburg-Devonshire
LNO	Lithium niobate
MPB	Morphotropic boundary condition
ODE	Ordinary differential equations
PDE	Partial-differential equation
PT	Lead Titanate
PVDF	Polyvinylidenfluoride
PZT	Lead Zirconate-Titanate
SH	Stephenson-Highland screening model
SPM	Scanning-probe microscopy
XRD	X-ray diffraction
CMOS	Complementary metal-oxide-semiconductor
e.g.	*exempli gratia*, for example
et al.	*et alii*, and others
etc.	*et cetera*, and other
i.a.	*inter alia*, among others
i.e.	*id est*, that is

List of Symbols

F	Helmholz free energy
G	Gibbs free energy
G_V	Free energy of the ferroelectric bulk
G_S	Free energy of the top surface
G_{ext}	Free energy of the external medium (ambience)
a	Temperature-independent first Landau coefficient
α_{ik}	First Landau coefficient
β_{ijkl}	Second Landau coefficient
γ_{ijklmn}	Third Landau coefficient
g_{ijkl}	Gradient term
s_{ijkl}	Elastic stiffness
c_{ijkl}	Elastic compliance
Q_{ijkl}	Electrostriction tensor
F_{ijkl}	Flexoelectric tensor
W_{ij}	Vegard coefficient
φ	Electrostatic potential
P_i	Spontaneous polarization
E_i	Electric field
D_i	Electric displacement
e	Electron charge

σ_{ij}	Elastic stress
u_{ij}	Elastic strain
ε_0	Dielectric permittivity of vacuum
ε_b	Background dielectric permittivity
ε_e	Dead-layer dielectric permittivity
n	Electron concentration
p	Hole concentration
N_d^+	Donor concentration
N_a^-	Acceptor concentration
N_C	Density of states in conduction band
N_V	Density of states in valence band
S_d	Entropy of ionized donors
S_a	Entropy of ionized acceptors
S_{el}	Entropy of electrons
S_h	Entropy of holes
δN	Difference between non-equilibrium and equilibrium concentrations.
d_{jkl}	Piezoelectric coefficient
A_{jk}^m	Surface energy coefficient
T	Temperature
E_g	Band gap
E_C	Bottom of conduction band
E_V	Top of valence band
E_f	Fermi level
k_B	Boltzmann constant
x_k	Spatial coordinate
t	Time
$F_k(\xi)$	Fermi integral of order k
Γ	Khalatnikov constant
χ	Dielectric susceptibility
c_p	Heat capacity

List of Publications

A1

Flexocoupling impact on size effects of piezoresponse and conductance in mixed-type ferroelectric semiconductors under applied pressure

Anna N. Morozovska, Eugene A. Eliseev, Yuri A, Genenko, Ivan S. Vorotiahin, Maxim V. Silibin, Ye Cao, Yunseok Kim, Maya D. Glinchuk, and Sergei V. Kalinin

Physical Review B 94, 174101 (2016). 10 pages, with Supplementary materials, 10 pages.

A2

Flexocoupling impact on the kinetics of polarization reversal

Ivan S. Vorotiahin, Anna N. Morozovska, Eugene A. Eliseev, and Yuri A. Genenko
Physical Review B 95, 014104 (2017). 9 pages, with Supplementary materials, 6 pages.

B1

Tuning the polar states of ferroelectric films via surface charges and flexoelectricity

Ivan S. Vorotiahin, Eugene A. Eliseev, Qian Li, Sergei V. Kalinin, Yuri A. Genenko, Anna N. Morozovska
Acta Materialia 137 (2017) 85-92. 8 pages, with Supplementary materials, 15 pages.

B2

Control of polarization hysteresis temperature behavior by interfacial screening in thin ferroelectric films

Anna N. Morozovska, Eugene A. Eliseev, Ivan S. Vorotiahin, Maxim V. Silibin, Sergei V. Kalinin, and Nicholas V. Morozovsky
Acta Materialia 160 (2018) 57-71. 15 pages.

C1

Defect-driven flexochemical coupling in thin ferroelectric films

Eugene A. Eliseev, Ivan S. Vorotiahin, Yevhen M. Fomichov, Maya D. Glinchuk, Sergei V. Kalinin, Yuri A. Genenko, and Anna N. Morozovska
Physical Review B 97, 024102 (2018). 17 pages.

Bibliography

[1] Courtesy of Wikimedia Commons https://commons.wikimedia.org/wiki/File:Perovskite.svg
[2] A.K. Tagantsev, P.V. Yudin (Eds.), Flexoelectricity in Solids: from Theory to Applications, World Scientific, (2016).
[3] A.N. Morozovska, E.A. Eliseev, A.K. Tagantsev, S.L. Bravina, L.-Q. Chen, and S.V. Kalinin, Thermodynamics of electromechanically coupled mixed ionic-electronic conductors: Deformation potential, Vegard strains, and flexoelectric effect, Phys. Rev. B 83, 195313 (2011).
[4] R. Landauer, Electrostatic Considerations in $BaTiO_3$ Domain Formation during Polarization Reversal, J. Appl. Phys., 28 p. 227-234 (1957).
[5] M. Molotskii, Generation of ferroelectric domains in films using atomic force microscope , J. Appl. Phys. Vol.97, №1, 014109-8 (2005).
[6] M. Molotskii, Generation of ferroelectric domains in atomic force microscope, J. Appl. Phys. Vol.93, №10, 6234-6237 (2003).
[7] M.A. Abplanalp, Piezoresponse Scanning Force Microscopy of Ferroelectric Domains: A dissertation submitted to the Swiss Federal Institute of Technology for the degree of Doctor of Natural Sciences, Zurich, 208 p (2001).
[8] S.V. Kalinin, D.A. Bonnell, Local potential and polarization screening on ferroelectric surfaces, Phys. Rev. B 63, №12, 125411-13 (2001).
[9] A.Yu. Emelyanov, Coherent ferroelectric switching by atomic force microscopy, Phys. Rev. B. - 2005. - Vol.71, №13. - P. 132102.
[10] S. Liu, I. Grinberg & A. Rappe, Intrinsic ferroelectric switching from first principles, Nature 534, 360-363 (2016).
[11] R.C. Miller, & G. Weinreich, Mechanism for the sidewise motion of 180° domain walls in barium titanate. Phys. Rev. 117, 1460–1466 (1960).
[12] L.E. Cross and R.E. Newnham, History of Ferroelectrics, Ceramics and Civilization Vol. III (1987).
[13] M. Acosta, N. Novak, V. Rojas, S. Patel, R. Vaish, J. Koruza, G. A. Rossetti, and J. Rödel, BaTiO3-based piezoelectrics: Fundamentals, current status, and perspectives, Applied Physics Reviews 4, 041305 (2017).
[14] P. Debye, Physik. Einige Resultate einer kinetischen Theorie der Isolatoren (Vorläufige Mitteilung), Zeitschr. XIII, 97-100 (1912).
[15] A. Lüker, Sol-Gel derived Ferroelectric Thin Films for Voltage Tunable Applications, Ph.D. thesis, Cranfield/Holstein (2009).
[16] J. Curie et P. Curie, Développement par pression de l'électricité polaire dans des crystaux hémiédriques à faces inclinées, Compt. rend. 91, 294-295, 383-387 (1880).
[17] J.A. Anderson, Rep. Nat. Res. Council, March and April 1918.
[18] W.G. Cady, Rep. Nat. Res. Council May 1918.
[19] David Brewster, Observation on the Pyro-Electricity in Minerals, Edinbg. J. of Science, Vol. 1, No. II. 208-218 (1824).
[20] G. Busch, Vom „Sel Polychreste" zur Ferroelektrizität: Ein Rückblick, Helvetica Physica Acta 59 (1986) 1-20.
[21] E. Schrödinger, Aus den Sitzungsberichten der Kaiserl. Akademie der Wissenschaften in Wien. Mathem.-Naturw. Klasse; Bd. CXXI, Abt. Iia, November 1912. Studien üder Kinetik der Dielektrika, dam Schmelzpunkt, Pyro-und Piezoelekrizität.
[22] J. Valasek, Piezoelectric and allied phenomena in Rochelle salt, Phys. Rev. 15, 537 (1920); 17, 475-481 (1920).
[23] J. Valasek, Piezo-electric activity of Rochelle salt under various conditions, Phys. Rev. 19, 478-491 (1922).
[24] G. Steulmann, Die Dielektrizitätskonstante einer Anzahl von Kaliumsalzen und Alkalihalogeniden, Z. Phys. 77, 114-116 (1932).
[25] J. West, A quantitative X-Ray Analysis of the Structure of Potassium-Dihydrogen-Phasphate (KH_2PO_4), Z. Krist. 74, 306 (1930).

[26] G. Busch, P. Scherrer, Eine neue Seignetteelektrische Substanz, Naturwiss. 2_3_, 737 (1935).
[27] G. Busch, Neue Seignetteelektrika, Helv, Phys. Acta 11., 269-298 (1938).
[28] H. Thurnaurer and J. Deaderick, U.S. Patent 2,429,588, Oct. 21, 1947, filed Oct. 2 1941.
[29] R. B. Gray, Transducer and Method of Making Same, U.S. Pat. No. 2486 560.
[30] W. Känzig, Röntgenuntersuchungen über die Segneitteelektrizität von Bariumtitanat, Helv. Phys. Acta 24, 175 (1951).
[31] A. von Hippel, R.G. Breckenbridge, F.G. Chesley, and L. Tisza, High dielectric constant ceramics, Ind. Eng. Chem. 38, 1097 (1946).
[32] B. Wul and J.M. Goldman, Ferroelectric switching in BaTiO3 ceramics, C.R. Acad. Sci. URSS 51, 21 (1946).
[33] L.D. Landau, Theory of Phase Transformations I, II, JETP, 7, 19, 627 (1937). Phys. Zs. Soviet Union, 11, 26, 545 (1937).
[34] L.D. Landau, E.M. Lifshitz, Theory of the dispersion of magnetic permeability in ferromagnetic bodies, Phys. Z. Sowjetunion. 8, 153 (1935).
[35] V. L. Ginzburg, On the dielectric properties of ferroelectric (seignetteelectric) crystals and barium titanate, JETP (Zhur. Exper. Teor. Fiz.), 15, 739 (1945). Journ. Phys. USSR, 10, 107 (1946).
[36] A.F. Devonshire, Theory of barium titanate: Part I, Phil. Mag. 40, 1040 (1949).
[37] A.F. Devonshire, Theory of barium titanate: Part II, Phil. Mag. 42, 1065 (1951).
[38] A.F. Devonshire, Theory of Ferroelectrics, Adv. Phys. 3, 85 (1954).
[39] L.E. Cross and R.E. Newnham, History of Ferroelectrics, Ceramics and Civilization Vol. III (1987).
[40] E. Sawaguchi, Ferroelectricity vs. Antiferroelectricity in the Solid Solutions of $PbZrO_3$:$PbTiO_3$, J. Phys. Soc. Jpn., 8 [5] 615-29 (1953).
[41] G. Shirane and A. Takeda, Phase Transitions in Solid Solutions of $PbZrO_3$ and $PbTiO_3$. I. Small Concentrations of $PbTiO_3$, J. Phys. Soc. Jpn., 7[1] 5-11 (1952).
[42] G. Shirane, K. Suzuki, and A. Takeda, Phase Transitions in Solid Solutions of $PbZrO_3$. II. X-ray Study, J. Phys. Soc. Jpn., 7[1] 12-17 (1952).
[43] B. Jaffe, R.S. Roth, and S. Marzullo, Piezoelectric Properties of Lead Zirconate-Lead Titanate Solid Solution Ceramics, J. Appl. Phys., 25 [6] 809-10 (1954).
[44] B. Jaffe, R.S. Roth, and S. Marzullo, Properties of Piezoelectric Ceramics in the Solid Solution Series Lead Titanate-Lead Zirconate-Lead Oxide-Tin Oxide and Lead Titanate-Lead Hafnate, J. Res. Natl. Bur. Stand., 55, 239-43 (1955).
[45] H. Jaffe, Titanate Ceramics for Electro-Mecanical Purposes, Ind. Eng. Chem., 2, 264-68 (1950).
[46] B. Malič, J. Koruza, J. Hreščak, J. Bernard, K. Wang, J.G. Fisher and A. Benčan, Sintering of Lead-Free Sodium Potassium Niobate Ceramics, Materials 8, 8117-8146 (2015).
[47] S.L.A. Lang, Conversation with Professor W. G.Cady, Ferroelectrics, 9 [3/4]141-49 (1975).
[48] A.M. Nicholson, Piezophony. U.S. Patent 1, 495, 429. Filed April 10, 1918. Patentd May 27, 1924. A.M. Nicholson, Generating and Transmitting electric Currents , U.S. Patent 2, 212, 845. Filed April 10, 1918. Patented August 27, 1940.
[49] P. Langevin, Procédé et appareils d'émission et de réception des ondes élastiques sous-marines à l'aide des propriétés piézoélectriques du quartz. Brevet d'Invention No. 505,703. Demandé le 17 septembre 1918. Délivré le 14 mai 1920.
[50] K. Uchino, private communication.
[51] T. Xu, V. Leppanen, Analysing emerging memory technologies for big data and signal processing applications, Digital Information Processing and Communications (ICDIPC) Fifth International Conference on, pp. 104-109, (2015).
[52] J. Junquera and P. Ghosez, Critical thickness for ferroelectricity in perovskite ultrathin films, Nature 422, 506-509 (2003).
[53] J.E. Spanier, A.M. Kolpak, J.J. Urban, I. Grinberg, L. Ouyang, W.S. Yun, A.M. Rappe, H. Park, Ferroelectric Phase Transition in Individual Single-Crystalline BaTiO3 Nanowires, Nano Lett. April;6(4) 735-9 (2006).
[54] J. Garra, J.M. Vohs, D.A. Bonnell, The effect of ferroelectric polarization on the interaction of water and methanol with the surface of LiNbO3 (0 0 0 1), Surface Science, Vol.603(8), 1106-1114 (2009).

[55] T. Coughlin, Crossing the Chasm to New Solid-State Strorage Architectures, IEEE Consumer Electronics Magazine, vol. 5, no. 1, pp. 133-142 (2016).
[56] S. Thakoor, A. P. Thakoor, Optically Adressed Ferroelectric Memory With Non-Destructive Read-Out. Sarita Thakoor, Anil Thakoor. Applied Optics IP, vol. 34, Issue 17, p.3136 (1995).
[57] A. N. Kalinkin, A. E. Polyakov, and V. M. Skorikov, Dipole Skyrmion Vortices in Multiferroic $BiFeO_3$, Inorganic Materials, Vol. 49, No. 3, pp. 315–318 (2013).
[58] M. Lawrence, Lithium niobate integrated optics, Rep. Prog. Phys. 363-429 (1993).
[59] R.S. Ponomarev, Channel waveguides on lithium niobate. Optical properties dependence on external electric field applying, International Symposium on Ferroic Domains and Micro-to Nanoscopic Structures and Russian/CIS/Baltic/Japan Symposium on Ferroelectricity (ISFD-11th-RCBJSF), P. 218 (2012).
[60] В.В. Павлов, В.В. Семашко, Оптический параметрический генератор, Казанский (приволжский) федеральный университет, p.68. (2014)
[61] M. Marangoni, R. Ramponi, Nonlinear Optical Waveguides in Stoichiometric Lithium Tantalate, in: Ferroelectric crystals for Photonic Applications, ed. By: P. Ferraro, S. Grilli, P. De Natale, Springer (2009).
[62] В.В. Щербина, М.В. Бородин, С.А. Смычков, Формирование и исследование планарных волноводных и периодических доменных структур в кристаллах ниобата лития, Известия Самарского научного центра Российской академии наук, vol. 14, №4 (2012), УДК 535.015.
[63] R.S. Ponomarev, A.A. Zhuravlev, A.V. Kichanov, Relaxation processes of mobile charges in integrated optics Mach–Zehnder interferometer, International conference on micro/nanotechnologies and electron devices, Erlagol, P.336–338 (2011).
[64] E.V Bursian and N.N. Trunov, Nonlocal piezoelectric effect, Sov. Phys.—Solid State 10, 760–2 (1974).
[65] V.L. Indenbom, E.B. Loginov and M.A. Osipov, Flexoelectric effect and the structure of crystals, Kristalografija 26, 1157 (1981).
[66] P.V. Yudin and A.K. Tagantsev, Fundamentals of flexoelectricity in solids, Nanotechnology 24, 432001 (2013).
[67] P. Zubko, G. Catalan, A.K. Tagantsev, Flexoelectric Effect in Solids, Ann. Rev. Mat. Res. (2013).
[68] S.V Kalinin, V. Meunier, Electronic flexoelectricity in low-dimensional systems, Phys. Rev. B 77, 033403 (2008).
[69] V.S. Mashkevich and K.B. Tolpygo, Electrical, optical and elastic properties of diamond type crystals, J. Sov. Phys.—JETP 5 435–9 (1957).
[70] K.B. Tolpygo, Long wavelength oscillations of diamond-type crystals including long range forces, Sov. Phys.—Solid State 4 1297–305(1963).
[71] S.M. Kogan, Piezoelectric effect during inhomogeneous deformation and acoustic scattering of carriers in crystals, Sov. Phys. Solid State 5 2069–70 (1964).
[72] E.V. Bursian and O.I. Zaikovskii, Changes in the curvature of a ferroelectric film due to polarization, Sov. Phys.—Solid State 10 1121–4 (1968).
[73] E.V. Bursian, O.I. Zaikovskii and K.V. Makarov, Ferroelectric plate polarization by bending, Izv. Akad. Nauk, SSSR Ser. Fiz. 33 1098–102 (1969).
[74] R.D. Mindlin, Polarization gradient in elastic dielectrics, Int. J. Solids Struct. 4 637–42 (1968).
[75] A. Ashkar, P.C.Y. Lee and A.S. Cakmak, Lattice-dynamics approach to the theory of elastic dielectrics with polarization gradient, Phys. Rev. B 1 3525 (1970).
[76] J.D. Axe, J. Harada and G. Shirane, Anomalous acoustic dispersion in centrosymmetric crystals with soft optic phonons, Phys. Rev. B 1 1227–34 (1970).
[77] A.K. Tagantsev, Theory of flexoelectric effects in crystals, Zh. Eksp. Teor. Fiz. 88 2108–22 (1985).
[78] A.K. Tagantsev, Piezoelectricity and flexoelectricity in crystalline dielectrics, Phys. Rev. B 34 5883–9 (1986).
[79] L. Cross Flexoelectric effects: charge separation in insulating solids subjected to elastic strain gradients, J. Mater. Sci. 41 53–63 (2006).
[80] W. Ma and L. E. Cross, Observation of the flexoelectric effect in relaxor $Pb(Mg_{1/3}Nb_{2/3})O_3$ ceramics, Appl. Phys. Lett. 78 2920–1 (2001).

[81] W. Ma W and L. E. Cross Large flexoelectric polarization in ceramic lead magnesium niobate, Appl. Phys. Lett. 79 4420–2 (2001).
[82] W. Ma and L. E. Cross, Flexoelectric polarization of barium strontium titanate in the paraelectric state, Appl. Phys. Lett. 81 3440–2 (2002).
[83] W. Ma and L. E. Cross Strain-gradient-induced electric polarization in lead zirconate titanate ceramics, Appl. Phys. Lett. 82 3293–5 (2003).
[84] W. Ma and L. E. Cross, Flexoelectricity of barium titanate, Appl. Phys. Lett. 88 232902 (2006).
[85] J.Y. Fu, W. Zhu, N. Li and L. E. Cross, Experimental studies of the converse flexoelectric effect induced by inhomogeneous electric field in a barium strontium titanate composition, J. Appl. Phys. 100 024112 (2006).
[86] W. Huang, K. Kim, S. Zhang, F.-G. Yuan and X. Jiang, Scaling effect of flexoelectric (Ba, Sr)TiO_3 microcantilevers, Phys. Status Solidi (RRL) 5 350–2 (2011).
[87] P. Hana, Study of flexoelectric phenomenon from direct and from inverse flexoelectric behavior of pmnt ceramic, Ferroelectrics 351 196–203 (2007).
[88] W. Ma and L. E. Cross, Flexoelectric effect in ceramic lead zirconate titanate, Appl. Phys. Lett. 86 072905 (2005).
[89] V.G. Vaks, Introduction to the Microscopic Theory of Ferroelectrics, Moscow: Nauka (1973).
[90] J. Harada, J. Axe and G. Shirane, Neutron-scattering study of soft modes in cubic $BaTiO_3$, Phys. Rev. B 4 155 (1971).
[91] R.A. Cowley, Lattice dynamics and phase transitions of strontium titanate, Phys. Rev. 134 A981–97, (1964).
[92] B. Hehlen, L. Arzel, A.K. Tagantsev, E. Courtens, Y. Inaba, A. Yamanaka and K. Inoue, Brillouin-scattering observation of the Ta–To coupling in $SrTiO_3$, Phys. Rev. B 57 R13989 (1998).
[93] E. Farhi, A.K. Tagantsev, R. Currat, B. Hehlen, E. Courtens and L. A. Boatner, Low energy phonon spectrum and its parameterization in pure $KTaO_3$ below 80 K, Eur. Phys. J. B 15 615–23 (2000).
[94] S.M. Shandarov, S.S. Shmakov, N.I. Burimov, O.S. Syuvaeva, Y.F. Kargin and V.M. Petrov, Detection of the contribution of the inverse flexoelectric effect to the photorefractive response in a bismuth titanium oxide single crystal JETP Lett. 95 618–21 (2012).
[95] E.V. Bursian, and N.N. Trunov, Nonlocal piezoelectric effect, Sov. Phys.—Solid State 10 760–2 (1974).
[96] A.K. Tagantsev and A.S. Yurkov, Flexoelectric effect in finite samples, J. Appl. Phys. 112 044103 (2012).
[97] E.A. Eliseev, A.N. Morozovska, M.D. Glinchuk and R. Blinc, Spontaneous flexoelectric/flexomagnetic effect in nanoferroics, Phys. Rev. B 79 165433 (2009).
[98] A.S. Yurkov, Elastic boundary conditions in the presence of the flexoelectric effect, JETP Lett. 94 455–8 (2011).
[99] R. Maranganti and P. Sharma, Atomistic determination of flexoelectric properties of crystalline dielectrics, Phys. Rev. B 80 054109 (2009).
[100] J. Hong, G. Catalan, J.F. Scott and E. Artacho, The flexoelectricity of barium and strontium titanates from first principles, J. Phys.: Condens. Matter 22 112201 (2010).
[101] I. Ponomareva I, A.K. Tagantsev and L. Bellaiche, Finite-temperature flexoelectricity in ferroelectric thin films from first principles, Phys. Rev. B 85 104101 (2012).
[102] J. Hong and D. Vanderbilt, First-principles theory of frozen-ion flexoelectricity, Phys. Rev. B 84 180101 (2011).
[103] T. Dumitrica, C.M. Landis and B.I. Yakobson, Curvature-induced polarization in carbon nanoshells, Chem. Phys. Lett. 360 182–8 (2002).
[104] S.V. Kalinin and V. Meunier, Electronic flexoelectricity in low-dimensional systems, Phys. Rev. B 77 033403 (2008).
[105] A.K. Tagantsev, Piezoelectricity and flexoelectricity in crystalline dielectrics, Phys. Rev. B 34 5883–9 (1986).
[106] M. Stengel, Unified ab initio formulation of flexoelectricity and strain-gradient elasticity, Phys. Rev. B 93, 245107 (2016).
[107] R.M. Martin, Piezoelectricity, Phys. Rev. B 5 1607 (1972).

[108] A.N. Morozovska, E.A. Eliseev, M.D. Glinchuk, L.-Q. Chen and V. Gopalan, Interfacial polarization and pyroelectricity in antiferrodistortive structures induced by a flexoelectric effect and rotostriction. Phys. Rev. B 85 094107 (2012).
[109] A.Y. Borisevich, E.A. Eliseev, A.N. Morozovska, C.-J. Cheng, J.-Y. Lin, Y. H. Chu, D. Kan, I. Takeuchi, V. Nagarajan and S.V. Kalinin, Atomic-scale evolution of modulated phases at the ferroelectric—antiferroelectric morphotropic phase boundary controlled by flexoelectric interaction, Nature Commun. 3 775 (2012).
[110] P.V. Yudin, A.K. Tagantsev, E.A. Eliseev, A.N. Morozovska and N. Setter, Bichiral structure of ferroelectric domain walls driven by flexoelectricity, Phys. Rev. B 86 134102 (2012).
[111] A.N. Morozovska, E.A. Eliseev, A.K. Tagantsev, S.L. Bravina, L.-Q. Chen and S.V. Kalinin, Thermodynamics of electromechanically coupled mixed ionic-electronic conductors: deformation potential, Vegard strains, and flexoelectric effect, Phys. Rev. B 83 195313 (2011).
[112] K. Abe, S. Komatsu, N. Yanase, K. Sano and T. Kawakubo, Asymmetric ferroelectricity and anomalous current conduction in heteroepitaxial $BaTiO_3$ thin films, Japan. J. Appl. Phys. 36 5846–53 (1997).
[113] K. Abe, N. Yanase, T. Yasumoto and T. Kawakubo, Voltage shift phenomena in a heteroepitaxial BaTiO3 thin film capacitor, J. Appl. Phys. 91 323–30 (2002).
[114] A.K. Tagantsev, L.E. Cross and J. Fousek, Domains in Ferroic Crystals and Thin Films, New York: Springer (2010).
[115] M. Gharbi, Z.H. Sun, P. Sharma and K. White, The origins of electromechanical indentation size effect in ferroelectrics, Appl. Phys. Lett. 95 142901 (2009).
[116] M. Gharbi, Z.H. Sun, P. Sharma, K. White and S. El-Borgi, Flexoelectric properties of ferroelectrics and the nanoindentation size-effect Int. J. Solids Struct. 48 249–56 (2011).
[117] C.R. Robinson, K.W. White and P. Sharma, Elucidating the mechanism for indentation size-effect in dielectrics Appl. Phys. Lett. 101 122901 (2012).
[118] S. M. Park, B. Wang, S. Das, S. C. Chae, J.-S. Chung, J.-G. Yoon, L.-Q. Chen, S. M. Yang and T. W. Noh, Selective control of multiple ferroelectric switching pathways using a trailing flexoelectric field, Nature Nanotechnology Vol. 13, 366–370 (2018).
[119] M.S. Majdoub, R. Maranganti and P. Sharma, Understanding the origins of the intrinsic dead layer effect in nanocapacitors, Phys. Rev. B 79 115412 (2009).
[120] H. Zhou, J. Hong, Y. Zhang, F. Li, Y. Pei and D. Fang, Flexoelectricity induced increase of critical thickness in epitaxial ferroelectric thin films, Physica B 407 3377–81 (2012).
[121] J. Y. Fu, W. Zhu, N. Li, N. Smith and L. E. Cross, Gradient scaling phenomenon in microsize flexoelectric piezoelectric composites Appl. Phys. Lett. 91 182910 (2007).
[122] W. Zhu, J.Y. Fu, N. Li and L. Cross, Piezoelectric composite based on the enhanced flexoelectric effects Appl. Phys. Lett. 89 192904 (2006).
[123] B. Chu, W. Zhu, N. Li and L.E. Cross, Flexure mode flexoelectric piezoelectric composites, J. Appl. Phys. 106 104109 (2009).
[124] J. Fousek, L.E. Cross and D.B. Litvin, Possible piezoelectric composites based on the flexoelectric effect, Mater. Lett. 39 287–91 (1999).
[125] N.D. Sharma, R. Maranganti and P. Sharma, On the possibility of piezoelectric nanocomposites without using piezoelectric materials J. Mech. Phys. Solids 55 2328–50 (2007).
[126] N.D. Sharma, C.M. Landis and P. Sharma, Piezoelectric thin-film superlattices without using piezoelectric materials, J. Appl. Phys. 108 024304 (2010).
[127] S. Chandratre and P. Sharma, Coaxing graphene to be piezoelectric, Appl. Phys. Lett. 100 023114 (2012).
[128] A. Gruverman, B.J. Rodriguez, A.I. Kingon, R.J. Nemanich, A.K. Tagantsev, J.S. Cross and M. Tsukada, Mechanical stress effect on imprint behavior of integrated ferroelectric capacitors, Appl. Phys. Lett. 83 728–30 (2003).
[129] H. Lu, C.-W. Bark, D. Esque de los Ojos, J. Alcala J, C. B. Eom, G. Catalan and A. Gruverman, Mechanical writing of ferroelectric polarization, Science 336 59–61 (2012).
[130] D. Lee, A. Yoon, S.Y. Jang, J.-G. Yoon, J.-S. Chung, M. Kim, J.F. Scott and T. W. Noh, Giant flexoelectric effect in ferroelectric epitaxial thin films, Phys. Rev. Lett. 107 057602 (2011).

[131] G. Catalan, L.J. Sinnamon and J.M. Gregg, The effect of flexoelectricity on the dielectric properties of inhomogeneously strained ferroelectric thin films J. Phys.: Condens. Matter 16 2253 (2004).
[132] V. Lyahovitskaya, Y. Feldman, I. Zon, E. Wachtel, K. Gartsman, A.K. Tagantsev and I. Lubomirsky, Formation and thermal stability of quasi-amorphous thin films, Phys. Rev. B 71 094205 (2005).
[133] P. Zubko, G. Catalan, A. Buckley, P.R.L. Welche, & J.F. Scott, Strain-Gradient-Induced Polarization in $SrTiO_3$ Single Crystals, Phys. Rev. Lett. 99, 167601 (2007).
[134] W. Ma, & L.E. Cross, Strain-gradient-induced electric polarization in lead zirconate titanate ceramics, Appl. Phys. Lett. 82, 3293–3295 (2003).
[135] S.M. Kogan, Solid State Phys. 5, 2829 (1963).
[136] I. Ponomareva, A.K. Tagantsev, & L. Bellaiche, Finite-temperature flexoelectricity in ferroelectric thin films from first principles, Phys. Rev. B 85, 104101 (2012).
[137] J. Hong & D. Vanderbilt, First-principle theory of frozen-ion flexoelectricity, Phys. Rev. B 84, 180101(R) (2011).
[138] S.V. Kalinin, A.N. Morozovska, Focusing light on flexoelectricity, Nature Nanotechnology Vol 10, pp.916-917 (2015).
[139] J.W. Matthews, A.E. Blakeslee, Defects in epitaxial multilayers. I. Misfit dislocations, J. Cryst. Growth 27, 118–25 (1974).
[140] G. Catalan, L.J. Sinnamon, J.M. Gregg, The effect of flexoelectricity on the dielectric properties of inhomogeneously strained ferroelectric thin films, J. Phys. Condens. Matter 16(13), 2253 (2004).
[141] G. Catalan, B. Noheda, J. McAneney, L.J. Sinnamon, J.M. Gregg, Strain gradients in epitaxial ferroelectrics, Phys. Rev. B 72, 020102 (2005).
[142] H.J. Kim, S. Hoon Oh, H.M. Jang, Thermodynamic theory of stress distribution in epitaxial Pb(Zr, Ti)O_3 thin films, Appl. Phys. Lett. 75(20), 3195–97 (1999).
[143] M.S. Majdoub, R. Maranganti, P. Sharma, Understanding the origins of the intrinsic dead layer effect in nanocapacitors. Phys. Rev. B 79, 115412 (2009).
[144] L.J. Sinnamon, R.W. Bowman, J.M. Gregg, Investigation of dead-layer thickness in $SrRuO_3/Ba_{0.5}Sr_{0.5}TiO_3$/Au thin-film capacitors, Appl. Phys. Lett. 78(12):1724–26 (2001).
[145] H. Zhou, J. Hong, Y. Zhang, F. Li, Y. Pei, D. Fang, Flexoelectricity induced increase of critical thickness in epitaxial ferroelectric thin films, J. Phys. Condens. Matter 407(17):3377–81 (2012).
[146] V. Lyahovitskaya, Y. Feldman, I. Zon, E. Wachtel, K. Gartsman, A.K. Tagantsev, I. Lyubomirsky. Formation and thermal stability of quasi-amorphous thin films, Phys. Rev. B 71, 094205 (2005).
[147] A.K. Tagantsev, G. Gerra G, Interface-induced phenomena in polarization response of ferroelectric thin films, J. Appl. Phys. 100, 051607 (2006).
[148] H.X. Cao, V.C. Lo, Z.-Y. Li, Simulation of flexoelectricity effect on imprint behaviour of ferroelectric thin films, Solid State Commun. 138, 404–8 (2006).
[149] D. Lee, A. Yoon, S.Y. Jang, J.-G. Yoon, J.-S. Chung, M. Kim, J.F. Scott, and T.W. Noh, Giant flexoelectric effect in ferroelectric epitaxial thin films, Phys. Rev. Lett. 107, 057602 (2011).
[150] A.K. Tagantsev, L.E. Cross, J. Fousek, Domains in Ferroic Crystals and Thin Films, New York: Springer (2010).
[151] E.V. Bursian, Z. Oi, K.V. Makarov, Ferroelectric plate polarization by bending, Izv. Akad. Nauk SSSR Ser. Fiz. 33(7), 1098–102 (1969).
[152] H. Lu, C.-W. Bark, D. Esque de los Ojos, J. Alcala, C.B. Eom, G. Catalan, A. Gruverman, Mechanical writing of ferroelectric polarization. Science 336(6077), 59–61 (2012).
[153] A. Gruverman,B.J. Rodriguez, A.I. Kingon, R.J. Nemanich, A.K. Tagantsev, J.S. Cross, M. Tsukada, Mechanical stress effect on imprint behavior of integrated ferroelectric capacitors. Appl. Phys. Lett. 83(4), 728–30 (2003).
[154] A.N. Morozovska, E.A. Eliseev, A.K. Tagantsev, S.L. Bravina, L.-Q. Chen, S.V. Kalinin, Thermodynamics of electromechanically coupled mixed ionic-electronic conductors: deformation potential, Vegard strains, and flexoelectric effect, Phys. Rev. B 83, 195313 (2011).
[155] J.F. Scott, Lattice perturbations in $CaWO_4$ and $CaMoO_4$, J. Chem. Phys. 48, 874 (1968).
[156] A. Kholkin, I. Bdikin, T. Ostapchuk, J. Petzelt, Room temperature surface piezoelectricity in $SrTiO_3$ ceramics via piezoresponse force microscopy. Appl. Phys. Lett. 93(22), 222905 (2008).

[157] E.V. Bursian, O.I. Zaikovskii, Changes in the curvature of a ferroelectric film due to polarization, Sov. Phys. Solid State 10(5), 1121–24 (1968).
[158] J.D. Axe, J. Harada, G. Shirane, Anomalous acoustic dispersion in centrosymmetric crystals with soft optic phonons, Phys. Rev. B 1, 1227–34 (1970).
[159] W. Cao, G.R. Barsch, Landau-Ginzburg model of interphase boundaries in improper ferroelastic perovskites of d418 h symmetry, Phys. Rev. B 41, 4334–48 (1990).
[160] A.N. Morozovska, E.A. Eliseev, M.D. Glinchuk, L.-Q. Chen, V. Gopalan, Interfacial polarization and pyroelectricity in antiferrodistortive structures induced by a flexoelectric effect and rotostriction, Phys. Rev. B 85, 094107 (2012).
[161] G. Catalan, J. Seidel, R. Ramesh, J.F. Scott, Domain wall nanoelectronics. Rev. Mod. Phys. 84, 119–56 (2012).
[162] J. Seidel, L.W. Martin, Q. He, Q. Zhan, Y.H. Chu, A. Rother, M.E. Hawkridge, P. Maksymovych, P. Yu, M. Gajek, N. Balke, S.V. Kalinin, S. Gemming, F. Wang, G. Catalan, J.F. Scott, N.A. Spaldin, J. Orenstein, R. Ramesh, Conduction at domain walls in oxide multiferroics, Nat. Mater. 8, 229–34 (2009).
[163] P. Zubko, G. Catalan, A.K. Tagantsev, Flexoelectric Effect in Solids, Ann. Rev. Mat. Res. (2013).
[164] A.S. Sidorkin, Domain Structure in Ferroelectrics and Related Materials, Cambridge international science publishing, Cambridge, (2006).
[165] A.K. Tagantsev, L.E. Cross, J. Fousek, Domains in Ferroic Crystals and Thin Films, Springer, New York, (2010).
[166] B.V. Selyuk, Charged domain boundaries in ferroelectric crystals, Ferroelectrics 6, 37 (1973).
[167] E.A. Eliseev, A.N. Morozovska, G.S. Svechnikov, V. Gopalan, V.Ya Shur, Static conductivity of charged domain walls in uniaxial ferroelectric semiconductors, Phys. Rev. B 83, 235313 (2011).
[168] Y.A. Genenko, O. Hirsch, P. Erhart, Surface potential at a ferroelectric grain due to asymmetric screening of depolarization fields, J. Appl. Phys. 115, 104102 (2014).
[169] D.D. Fong, A.M. Kolpak, J.A. Eastman, S.K. Streiffer, P.H. Fuoss, G.B. Stephenson, C. Thompson, D.M. Kim, K.J. Choi, C.B. Eom, I. Grinberg, A.M. Rappe, Stabilization of monodomain polarization in ultrathin $PbTiO_3$ films, Phys. Rev. Lett. 96, 127601 (2006).
[170] R.V. Wang, D.D. Fong, F. Jiang, M.J. Highland, P.H. Fuoss, C. Tompson, A.M. Kolpak, J.A. Eastman, S.K. Streiffer, A.M. Rappe, G.B. Stephenson, Reversible chemical switching of a ferroelectric film, Phys. Rev. Lett. 102, 047601 (2009).
[171] G.B. Stephenson, M.J. Highland, Equilibrium and stability of polarization in ultrathin ferroelectric films with ionic surface compensation, Phys. Rev. B 84, 064107 (2011).
[172] M.J. Highland, T.T. Fister, D.D. Fong, P.H. Fuoss, C. Thompson, J.A. Eastman, S.K. Streiffer, G.B. Stephenson, Equilibrium polarization of ultrathin $PbTiO_3$ with surface compensation controlled by oxygen partial pressure, Phys. Rev. Lett. 107, 187602 (2011).
[173] S.M. Yang, A.N. Morozovska, R. Kumar, E.A. Eliseev, Y. Cao, L. Mazet, N. Balke, S. Jesse, R. Vasudevan, C. Dubourdieu, and S.V. Kalinin, Mixed Electrochemicalferroelectric States in Nanoscale Ferroelectrics, Nature Physics volume 13, pages 812–818 (2017).
[174] A.N. Morozovska, E.A. Eliseev, N.V. Morozovsky, and S.V. Kalinin. Ferroionic states in ferroelectric thin films, Phys. Rev. B 95, 195413 (2017).
[175] E.A. Eliseev, S.V. Kalinin, A.N. Morozovska, Finite size effects in ferroelectric-semiconductor thin films under open-circuit electric boundary conditions, J. Appl. Phys. 117, 034102 (2015).
[176] A.M. Bratkovsky, A.P. Levanyuk, Continuous theory of ferroelectric states in ultrathin films with real electrodes, J. Comput. Theor. Nanosci. 6, 465 (2009).
[177] A.M. Bratkovsky, A.P. Levanyuk, "Effects of anisotropic elasticity in the problem of domain formation and stability of monodomain state in ferroelectric films, Phys. Rev. B 84 (2011), 045401.
[178] E.V. Chensky, V.V. Tarasenko, Theory of phase transitions to inhomogeneous states in finite ferroelectrics in an external electric field, Sov. Phys. JETP 56, 618 (1982) [Zh. Eksp. Teor. Fiz. 83, 1089 (1982)].
[179] C.-L. Jia, K.W. Urban, M. Alexe, D. Hesse, I. Vrejoiu, Direct observation of continuous electric dipole rotation in flux-closure domains in ferroelectric Pb(Zr,Ti)O3, Science 331, 1420 (2011).

[180] Y.L. Tang, Y.L. Zhu, X.L. Ma, A.Y. Borisevich, A.N. Morozovska, E.A. Eliseev, W.Y. Wang, Y.J. Wang, Y.B. Xu, Z.D. Zhang, S.J. Pennycook, Observation of a periodic array of flux-closure quadrants in strained ferroelectric PbTiO3 films, Science 348 547 (2015).
[181] G. Catalan, A. Lubk, A.H.G. Vlooswijk, E. Snoeck, C. Magen, A. Janssens, G. Rispens, G. Rijnders, D.H.A. Blank, B. Noheda, Flexoelectric rotation of polarization in ferroelectric thin films, Nat. Mater 10, 963 (2011).
[182] B.M. Darinskii, A.P. Lazarev, A.S. Sidorkin, Domain-wall structure near the surface of a ferroelectric, Fiz. Tverd. Tela. 31, 287 (1989) [Sov. Phys. Solid State, 31, 2003 (1989)].
[183] E.A. Eliseev, A.N. Morozovska, S.V. Kalinin, Y.L. Li, J. Shen, M.D. Glinchuk, L.Q. Chen, V. Gopalan, Surface effect on domain wall width in ferroelectrics, J. Appl. Phys. 106, 084102 (2009).
[184] V.Ya Shur, A.L. Gruverman, V.P. Kuminov, N.A. Tonkachyova, Dynamics of plane domain-walls in lead germanite and gadolinium molybdate, Ferroelectrics 111, 197 (1990).
[185] E.A. Eliseev, A.N. Morozovska, G.S. Svechnikov, E.L. Rumyantsev, E.I. Shishkin, V.Y. Shur, S.V. Kalinin, Screening and retardation effects on 180-domain wall motion in ferroelectrics: wall velocity and nonlinear dynamics due to polarization-screening charge interaction, Phys. Rev. B 78, 245409 (2008).
[186] S.K. Streiffer, J.A. Eastman, D.D. Fong, C. Thompson, A. Munkholm, M.V. Ramana Murty, O. Auciello, G.R. Bai, G.B. Stephenson, Observation of Nanoscale 180 stripe domains in ferroelectric PbTiO3 thin films, Phys. Rev. Let. 89, 067601 (2002).
[187] D.D. Fong, G.B. Stephenson, S.K. Streiffer, J.A. Eastman, O. Auciello, P.H. Fuoss, C. Thompson, Ferroelectricity in ultrathin perovskite films, Science 304, 1650 (2004).
[188] V.M. Fridkin, Ferroelectrics Semiconductors, Consultant Bureau, New-York and London, 1980, p. 119.
[189] A.N. Morozovska, I.S. Golovina, S.V. Lemishko, A.A. Andriiko, S.A. Khainakov, and E.A. Eliseev, Effect of Vegard strains on the extrinsic size effects in ferroelectric nanoparticles, Phys. Rev. B 90, 214103 (2014).
[190] G. Liebfried, N. Breuer, Point Defects in Metals I: Introduction to the Theory, Springer-Verlag, Berlin Heidelberg New York (1978).
[191] Stuart B. Adler, Chemical Expansivity of Electrochemical Ceramics, J. Am. Ceram. Soc., 84 [9] 2117–19 (2001).
[192] X.Y. Chen, J.S. Yu, and S. B. Adler, Thermal and Chemical Expansion of Sr-Doped Lanthanum Cobalt Oxide ($La_{1-x}Sr_xCoO_{3-\delta}$), Chem. Mater., 17, 4537-4546 (2005).
[193] S.R. Bishop, K.L. Duncan, E.D. Wachsman, Defect equilibria and chemical expansion in non-stoichiometric undoped and gadolinium-doped cerium oxide, Electrochimica Acta 54 (2009) 1436–1443.
[194] D.A. Freedman, D. Roundy, and T. A. Arias, Elastic effects of vacancies in strontium titanate: Short- and long-range strain fields, elastic dipole tensors, and chemical strain, Phys. Rev. B 80, 064108 (2009).
[195] J.C. Slater, The Lorentz Correction in Barium Titanate, Phys. Rev. 78, 748 (1950).
[196] B. Meyer and D. Vanderbilt, Ab initio study of ferroelectric domain walls in $PbTiO_3$, Phys. Rev. B 65, 104111 (2002).
[197] W.P. Mason, B.T. Matthias, Phys. Rev. 74, 1622 (1948).
[198] J.B. Neaton, C. Ederer, UV Waghmare, N.A. Spaldin, K.M. Rabe, First-principles study of spontaneous polarization in multiferroic $BiFeO_3$, Phys. Re. B 71 (1), 014113 (2005).
[199] T. Krajewski, Zagadnienia Fizyki Dielektryków, ch. 4: Własności ferroelektryczne krzyształów, Wydawnictwa Komunikacji i Łączności, Warszawa (1970).
[200] Y. Genenko, K. Albe, Theoretical Methods in Materials Science: Collection of Slides 2017-2018.
[201] P. Chandra, P.B. Littlewood, A Landau Primer for Ferroelectrics, in Physics of Ferroelectrics: Modern Perspective, ed. By: K. Rabe, Ch.H. Ahn, J.-M. Triscone, Springer Berlin Heidelberg New York (2007).
[202] B.-X. Xu, D. Schrade, R. Müller, D. Gross, T. Granzow, J. Rödel, Phase field simulations and experimental investigation of the electro-mechanical behavior of ferroelectrics, Z. Angew. Math. Mech. 90, 623-632 (2010).

[203] D. Schrade, R. Mueller, B.X. Xu, D. Gross, Domain evolution in ferroelectric materials: A continuum phase field model and finite element implementation, Comput. Methods Appl. Mech. Engrg. 196, 4365-4374 (2007).
[204] Y. Zuo, Y.A. Genenko, A. Klein, P. Stein, B.-X. Xu, Domain wall stability in ferroelectrics with space charges, J. Appl. Phys. 115, 084110 (2014).
[205] A.S. Yurkov, Elastic boundary conditions in the presence of the flexoelectric effect, JETP Lett. 94 (6) (2011) 455.
[206] P.V. Yudin, A.K. Tagantsev, E.A. Eliseev, A.N. Morozovska, N. Setter, Bichiral structure of ferroelectric domain walls driven by flexoelectricity, Phys. Rev. B 86, 134102 (2012).
[207] E.A. Eliseev, P.V. Yudin, S.V. Kalinin, N. Setter, A.K. Tagantsev, A.N. Morozovska, Structural phase transitions and electronic phenomena at 180-degree domain walls in rhombohedral $BaTiO_3$, Phys. Rev. B 87, 054111 (2013).
[208] R. Courant, Variational methods for the solution of problems of equilibrium and vibrations. Bulletin of the American Mathematical Society. 49, 1–23 (1943).
[209] A. Hrennikoff, Solution of Problems of Elasticity by the Frame-Work Method. ASME J. Appl. Mech. 8, A619–A715 (1941).
[210] The Finite Element Method (FEM), Multiphysics Cyclopedia, Comsol (2016). https://www.comsol.de/multiphysics/finite-element-method.
[211] E.K.H. Salje, S. Li, M. Stengel, P. Gumbsch, and X.D. Ding, Flexoelectricity and the polarity of complex ferroelastic twin patterns, Phys Rev. B 94, 024114 (2016).
[212] A. K. Tagantsev, I. Stolichnov, E. L. Colla, and N. Setter, Polarization fatigue in ferroelectric films: Basic experimental findings, phenomenological scenarios, and microscopic features, J. Appl. Phys., 90 No.3, 1387-1402 (2001).
[213] Y.A. Genenko, J. Glaum, M.J. Hoffmann, K. Albe, Mechanisms of aging and fatigue in ferroelectrics, Materials Science and Engineering B 192 (2015) 52–82.
[214] E.-M. Anton, R. E. García, T. S. Key, J. E. Blendell, and K. J. Bowman, Domain switching mechanisms in polycrystalline ferroelectrics with asymmetric hysteretic behavior, J. Appl. Phys., 105, 024107 (2009).
[215] P. Erhart, K. Albe, Dopants and dopant–vacancy complexes in tetragonal lead titanate: A systematic first principles study, Comp. Mater. Science, 103, 224-230 (2015).
[216] F. Neumann, Y. A. Genenko, C. Melzer, and H. von Seggern, Self-consistent theory of unipolar charge-carrier injection in metal/insulator/metal systems, J. Appl. Phys. 100, 084511 (2006).
[217] F. Neumann, Y. A. Genenko, C. Melzer, S. V. Yampolskii, and H. von Seggern, Self-consistent analytical solution of a problem of charge-carrier injection at a conductor/insulator interface, Phys. Rev. B 75, 205322 (2007).
[218] S. V. Yampolskii, Yu. A. Genenko, C. Melzer, K. Stegmaier, and H. von Seggern, Bipolar charge-carrier injection in semiconductor/insulator/conductor heterostructures: Self-consistent consideration, J. Appl. Phys. 104, 073719 (2008).
[219] Yu. A. Genenko, S. V. Yampolskii, C. Melzer, K. Stegmaier, and H. von Seggern, Charge carrier injection into insulating media: Single-particle versus mean-field approach, Phys. Rev. B 81, 125310 (2010).

Curriculum Vitae

M.Sc. Ivan Vorotiahin,
Born on the August 15, 1992 in Kyiv, Ukraine

Education

Mar 2016 - Jan 2019	Doctoral studies in Materials Science **Technische Universität Darmstadt, Germany** **Doctoral thesis:** Domain formation and switching kinetics of polarization domains in thin ferroelectric films conditioned by flexoelectricity, surface screening and chemical strains
Sep 2013 - Jun 2015	Master studies: “Micro- and nanoelectronic devices” **National Technical University of Ukraine “Kyiv Polytechnic Institute”, Kyiv, Ukraine** **Master thesis:** A Model of Artificial Nanodomain in Ferroelectric
Sep 2009 - Jun 2013	Bachelor studies: “Micro- and nanoelectronics” **National Technical University of Ukraine “Kyiv Polytechnic Institute”, Kyiv, Ukraine** **Bachelor thesis:** A Dielectric Nonlinearity in Paraelectrics
Sep 1999 - Jun 2009	Basic and Secondary Education **Vasyl Symonenko Specialized School No. 252 of Kyiv, Ukraine**

Peer-reviewed Publications

1. A.N. Morozovska, E.A. Eliseev, I.S. Vorotiahin, M.V. Silibin, S.V. Kalinin, N.V. Morozovsky, *Control of polarization reversal temperature behavior by surface screening in thin ferroelectric films*, Acta Mater. 160 (2018) 57-71

2. E.A. Eliseev, I.S. Vorotiahin, Y.M. Fomichov, M.D. Glinchuk, S.V. Kalinin, Y.A. Genenko, and A.N. Morozovska, *Defect-driven flexochemical coupling in thin ferroelectric films*, Phys. Rev. B 97, 024102 (2018)

3. I.S. Vorotiahin, E.A. Eliseev, Q. Li, S.V. Kalinin, Y.A. Genenko, A.N. Morozovska, *Tuning the polar states of ferroelectric films via surface charges and flexoelectricity*, Acta. Mater. 137 (2017) 85-92

4. I.S. Vorotiahin, A.N. Morozovska, E.A. Eliseev, Y.A. Genenko, *Flexoelectric impact on the kinetics of polarization reversal*, Phys. Rev. B 95, 014104 (2017)

5. A.N. Morozovska, E.A. Eliseev, Y.A. Genenko, I.S. Vorotiahin, M.V. Silibin, Y. Cao, Y. Kim, M.D. Glinchuk, and S.V. Kalinin, *Flexocoupling impact on the size effects of piezo-response and conductance in mixed-type ferroelectrics-semiconductors under applied pressure*, Phys. Rev. B 94, 174101 (2016)

6. I.S. Vorotiahin, Y.M. Poplavko, Y.M. Fomichov, *Features of Dielectric Nonlinearity in Paraelectrics*, Ukr. J. Phys. 2015. Vol. 60, No. 4.

Oral and Poster Presentations on International Conferences

1. 18-20 September 2018. I.S. Vorotiahin, E.A. Eliseev, Y.A. Genenko, A.N. Morozovska, M.D. Glinchuk, Q. Li4, S.V. Kalinin, Y.M. Fomichov, *An Interplay Between Electromechanical Effects, Surface Charges and Chemical Strains in Thin Ferroelectric Films*, V Ukrainian-Polish-Lithuanian Meeting on Physics of Ferroelectrics, Uzhhorod (talk)

2. 18-20 September 2018. N.V. Morozovsky, A.N. Morozovska, I.S. Vorotiahin1, E.A. Eliseev, A.I. Kurchak, R.K. Vasudevan, M.V. Strikha, S.V. Kalinin, *Surface ion screening impact on polarization reversal in ferroelectric nanoscale films: nonlinear electrostatic interaction and unusual polar states characterization*, V Ukrainian-Polish-Lithuanian Meeting on Physics of Ferroelectrics, Uzhhorod (poster)

3. 9-12 June 2018. E.A. Eliseev, I.S. Vorotiahin, Y.M. Fomichov, M.D. Glinchuk, S.V. Kalinin, Y.A. Genenko, and A.N. Morozovska, *Effects of Flexoelectrochemical Coupling in Thin Ferroelectric Films*, ECerS Electroceramics XVI, Hasselt (talk)

4. 27 May - 1 June 2018. E.A. Eliseev, I.S. Vorotiahin, Y.M. Fomichov, M.D. Glinchuk, S.V. Kalinin, Y.A. Genenko, and A.N. Morozovska, *Flexoelectrochemical Coupling in Thin Ferroelectric Films*, 2018 ISAF-FMA-AFM-AMEC-PFM Joint Conference (IFAAP 2018), Hiroshima (poster)

5. 11-16 March 2018. E.A. Eliseev, I.S. Vorotiahin, Y.M. Fomichov, M.D. Glinchuk, S.V. Kalinin, Q. Li, Y.A. Genenko, A.N. Morozovska, *Domain Properties in Thin Ferroelectric Films Related to Flexoelectrochemical Coupling*, 2018 DPG Frühjahrstagung, Berlin (talk)

6. 7-11 May 2017. I.S. Vorotiahin, E.A. Eliseev, Q. Li, S.V. Kalinin, A.N. Morozovska, Y.A. Genenko, *Flexoelectric Impact on Spontaneous Formation and Properties of Domain Structures in Thin Ferroelectric Films*, IEEE International Symposium on Applications of Ferroelectrics (ISAF-2017), Atlanta (poster)

7. 6 October 2017. I.S. Vorotiahin, *Flexoelectric Influence on Static and Dynamic Properties of Ferroelectric Films or How Influential are Tiny Things?*, PhD Thesis Presentation Contest, The First Annual Meeting of German-Ukrainian Academic Society 2017, Augsburg (talk).

8. 4-8 September 2017. I.S. Vorotiahin, A.N. Morozovska, E.A. Eliseev, Q. Li, S.V. Kalinin, Y.A. Genenko, *Impact of Flexoelectricity and Surface Charges on the Formation and Properties of Domain Structures in Thin Ferroelectric Films*, 14th International Meeting on Ferroelectrics (IMF-2017), San Antonio (talk)

9. 19-24 March 2017. I.S. Vorotiahin, A.N. Morozovska, E.A. Eliseev, Q. Li, S.V. Kalinin, Y.A. Genenko, *Flexoelectric Impact on the Formation of Domain Structures and the Polarization Switching in Thin Ferroelectric Films*, 2017 DPG Frühjahrstagung, Dresden (talk)

10. 21-25 August 2016. A.N. Morozovska, E.A. Eliseev, Y.A. Genenko, I.S. Vorotiahin, M.V. Silibin, Y. Cao, Y.S. Kim, M.D. Glinchuk, and S.V. Kalinin, *Flexocoupling impact on the size effects of piezo-response in ferroelectrics mixed-type semiconductors*, Joint ISAF-ECAPD-PFM Conference, Darmstadt, (Poster)

11. 21-25 August 2016. I.S. Vorotiahin, A.N. Morozovska, Y.A. Genenko, *Effects of electrostriction and flexoelectricity on polarization switching kinetics in thin ferroelectric films*, Joint ISAF-ECAPD-PFM Conference, Darmstadt, (Poster and talk)